RHENIUM COMPLEXES WITH MULTIDENTATE BENZAZOLES AND RELATED N,X-DONOR (X = N, O, S) LIGANDS

K.C. Potgieter

2012

RHENIUM COMPLEXES WITH MULTIDENTATE BENZAZOLES AND RELATED N,X-DONOR (X = N, O, S) LIGANDS

by

Kim Carey Potgieter

Submitted in fulfilment
of the requirements for the degree of
Philosophiae Doctor
in the Faculty of Science at the
Nelson Mandela Metropolitan University

November 2012

Promoter: Prof T.I.A. Gerber

DECLARATION

I, *Kim Carey Potgieter(205002102)* hereby declare that the *thesis* for *Philosophiae Doctor* is my own work and that it has not previously been submitted for assessment or completion of any postgraduate qualification to another University or for another qualification.

Kim Carey Potgieter

Official use:

In accordance with Rule G4.6.3,

4.6.3 A treatise/dissertation/thesis must be accompanied by a written declaration on the part of the candidate to the effect that it is his/her own work and that it has not previously been submitted for assessment to another University or for another qualification. However, material from publications by the candidate may be embodied in a treatise/dissertation/thesis.

Table of Contents

Chapter 3

Coordination Modes of 4-Aminoantipyrine and its Schiff Base Derivatives towards Rhenium

Chapter 4

Coordination of Bidentate Aniline Derivatives to the fac-$[Re(CO)_3]^+$ core

Chapter 5

Isolation of tris(bidentate) Complexes of Rhenium(III) from the cis-$[ReO_2]^+$ Core and Benzenethiol Derivatives

Chapter 6

Coordination of Bidentate Heterocyclic Derivatives to the $[ReO]^{3+}$ core

Chapter 7

Rhenium Complexes with Multidentate Benzo(thiazole/imidazole) Ligands

Chapter 8

Acknowledgements

I would like to express my sincere gratitude to my promoter, Prof T.I.A. Gerber, for giving me the opportunity to conduct my research under his supervision as well as for his time and guidance given during the project.

I am also grateful to Dr P. Mayer, Dr E. Hosten and Dr R. Betz for assistance with the crystallographic analysis.

I would like to acknowledge H. Schalekemp, P. Gaika and V. Maqoko for technical assistance.

I would also like to thank my colleagues Charmelle, Nonzaliseko, Nadia and Bonell in the Chemistry Department for their friendship and encouragement, as well as the Rhenium Chemistry Group, past and present.

I am grateful towards the Nelson Mandela Metropolitan University and the National Research Foundation for funding.

I would like to express my appreciation towards my family, especially my parents Faith and Keith, for their love, encouragement and inspiration. To my loving fiancé, Irvin, thank you for the endless support and motivation you have constantly provided.

Many thanks to God for being my protector, guide and strength.

List of Publications

The following publications emanated from this thesis:

1. Rhenium(I) tricarbonyl complexes with multidentate nitrogen-donor derivatives, K. Potgieter, P. Mayer, T. Gerber, N. Yumata, E. Hosten, I. Booysen, R. Betz, M. Ismail, B. van Brecht, *Polyhedron*, 2013, **49**, 67.

2. Dimers of the *fac*-$[Re(CO)_3]^+$ core with benzothiazole derivatives of thiourea, K.C. Potgieter, T.I.A. Gerber, E. Hosten, *Inorganic Chemistry Communications*, 2012, **24**, 231.

3. Coordination of Tridentate Schiff Base Derivatives of 4-Aminoantipyrine to Rhenium(V), K.C. Potgieter, T.I.A. Gerber, P. Mayer, *South African Journal of Chemistry*, 2011, **64**, 179.

4. Coordination of bidentate aniline derivatives to the *fac*-$[Re(CO)_3]^+$ core, T.I.A. Gerber, R. Betz, I.N. Booysen, K.C. Potgieter, P. Mayer , *Polyhedron*, 2011, **30**, 1739.

5. The reaction of a potentially N_2S-donor *bis*[benzo(thiazole/imidazole)] with the *fac*-$[Re(CO)_3]^+$ and *cis*-$[ReO_2]^+$ cores, T.I.A. Gerber, K.C. Potgieter, P. Mayer, *Inorganic Chemistry Communications*, 2011, **14**, 1115.

6. Coordination of 4-Aminoantipyrine to Rhenium(V), P. Mayer, E. Hosten, K.C. Potgieter, T.I.A. Gerber, *Journal of Chemical Crystallography*, 2010, **40**, 1146.

Abstract

The coordination behaviour of 4-aminoantipyrine (H_2pap) and its Schiff base derivatives with the oxorhenium(V) and tricarbonyl rhenium(I) cores are reported. The reactions of *trans*-[$ReOX_3(PPh_3)_2$] (X = Cl, Br) with H_2pap were studied, and the complexes *cis*-[ReX_2(pap)(H_2pap)(PPh_3)](ReO_4) were isolated. The ligand pap is coordinated monodentately through the doubly deprotonated amino nitrogen as an imide, and H_2pap acts as a neutral bidentate chelate, with coordination through the neutral amino nitrogen and the ketonic oxygen. The reactions of *trans*-[$ReOBr_3(PPh_3)_2$] and *cis*-[$ReO_2I(PPh_3)_2$] with 4-(2-aminobenzylideneamino)-1,2-dihydro-2,3-dimethyl-1-phenylpyrazol-5-one (H_2nap) and 4-(2-hydroxybenzylideneamino)-1,2-dihydro-2,3-dimethyl-1-phenylpyrazol-5-one (Hoap) are also reported. The complexes *cis*-[Re(nap)$Br_2(PPh_3)$]Br, [ReO(OEt)(Hnap)(PPh_3)]I and [ReO(OMe)(oap)(PPh_3)]I were isolated and structurally characterized. The reactions of the Schiff base derivatives 1,2-(diimino-4'-antipyrinyl)ethane (dae) and 2,6-*bis*(4-amino-1,2-dihydro-2,3-dimethyl-1-phenylpyrazol-5-one)pyridine (bap) with [$Re(CO)_5X$] (X = Br or Cl) produced *fac*-[$Re(CO)_3$(dae)Cl] and *fac*-[$Re(CO)_3$(bap)Br] respectively.

A series of rhenium(I) tricarbonyl complexes containing bidentate derivatives of aniline was synthesized and structurally characterized. With 1,2-diaminobenzene (Hpda) the '2+1' complex salt *fac*-[$Re(CO)_3(\kappa^1$-Hpda)(κ^2-Hpda)]Br was isolated, but with 2-mercaptophenol (Hspo) the bridged dimer [$Re_2(CO)_7(spo)_2$] was found. The neutral complex [$Re(CO)_3$(ons)(Hno)] was isolated from the reaction of [$Re(CO)_5$Br] with 2-[(2-methylthio)benzylideneimino]phenol (Hons; Hno = 2-aminophenol), with ons coordinated as a bidentate chelate with a free SCH_3 group. In the complex [$Re(CO)_3$(Htpn)Br] (Htpn = *N*-(2-(methylthio)benzylidene)benzene-1,2-diamine) the potentially tridentate ligand Htpn is coordinated *via* the methylthiol sulfur and imino nitrogen atoms only, with a free amino group. These rhenium(I) complexes, with the exception of [$Re_2(CO)_7(spo)_2$], revealed broad emissions centred around 535 nm.

The reactions of the rhenium(V) complex *cis*-$[ReO_2I(PPh_3)_2]$ with 2-aminothiophenol (H_2atp), benzene-1,2-dithiol (H_2tdt) and 2-hydroxybenzenethiol (H_2otp) led to the formation of the rhenium(III) compounds $[Re(Hatp)(ibsq)_2].OPPh_3$, $[Re(sbsq)_3].OPPh_3$ and $[Re(obsq)_3].OPPh_3$ (ibsq = 2-iminothiobenzosemiquinonate, sbsq = 1,2-dithiobenzosemiquinonate, obsq = 2-hydroxothiobenzosemiquinonate) respectively. The complexes adopt a trigonal prismatic geometry around the rhenium centre with average twists angles between 3.20-26.10˚. The $E_{1/2}$ values for the Re(III)/Re(IV) redox couple were found to be 0.022, 0.142 and 0.126 V for $[Re(Hatp)(ibsq)_2].OPPh_3$, $[Re(sbsq)_3].OPPh_3$ and $[Re(obsq)_3].OPPh_3$ respectively.

The reactions of the benzoxazole ligands, 3-(benzoxazol-2-yl)pyridin-2-ol (Hbop) and 5-amino-2-(benzoxazol-2-yl)phenol (Habo) with a $[ReO]^{3+}$ precursor led to the rhenium(III) complex, $[ReCl_2(bop)(PPh_3)_2]$, and the complex salt, $[ReO(abo)I(PPh_3)_2]ReO_4$, respectively. A variety of benzothiazole and benzimidazole derivatives were reacted with $[Re(CO)_5Br]$. In the case of *bis*(benzothiazol-2-ylethyl)sulfide (bts), the neutral complex *fac*-$[Re(CO)_3(bts)Br]$ was obtained. The dimeric complexes $(\mu\text{-dbt})_2[Re(CO)_3]_2$ and $(\mu\text{-mbt})_2[Re(CO)_3]_2$ were formed when 1,3-*bis*(benzothiazol-2-yl)thiourea (Hdbt) and 1-(benzothiazol-2-ylidene)-3-methylthiourea (Hmbt) were used as ligands. The reaction of 2,2'-(oxy*bis*(methylene))*bis*(benzimidazole) (bmb) with $[Re(CO)_5Cl]$ resulted in the rhenium(I) complex salt *fac*-$[Re(CO)_3(bmb)]^+$, with the *tri*-μ-chlorohexacarbonyl dirhenate $[Re_2(CO)_6Cl_3]^-$ as the counter anion. The neutral complex *fac*-$[Re(CO)_3(btp)Cl]$ was isolated from the reaction of the 2,9-*bis*(benzothiazol-2-yl)-1,10-phenanthroline (btp) ligand and $[Re(CO)_5Cl]$. The reactions of *trans*-$[ReOCl_3(PPh_3)_2]$ with *bis*(benzimidazol-2-ylethyl)sulfide (btn) and 1-(benzothiazol-2-ylidene)-3-methylthiourea (Hmbt) led to the formation of the cationic compounds $(\mu\text{-O})_2[Re_2O_2(btn)_2]I_2$ and $[ReCl_2(bte)(PPh_3)_2]Cl$ (bte = (benzothiazole-2-yl)-*N*-ethylidenemethanamine) respectively.

Keywords: Rhenium, bidentate, tridentate, 4-aminoantipyrine, benzothiazole, benzoxazole, benzimidazole, oxo, crystal structure

Crystallographic Data

Supplementary data for all the crystal structures that were determined in this study are stored on the compact disk that is included in this dissertation (attached to the inside back cover).

These data include the:

- Final crystal data and details of the structure determinations;
- Final coordinates and equivalent isotropic displacement parameters of the non-hydrogen atoms;
- Hydrogen atom positions;
- Isotropic displacement parameters;
- All bond distances and bond angles;
- Torsion angles;
- Contact distances;
- Hydrogen-bonds.

Chapter 1

Introduction

1.1 General Background

Coordination chemistry is crucial in the design of new radiopharmaceuticals, since it will determine the stability and geometry of the radiopharmaceutical, which are important in the biodistribution of the potential radiopharmaceutical [1]. Rhenium has significance in nuclear medicine as a therapeutic agent due to the favourable nuclear characteristics of the ^{186}Re and ^{188}Re radionuclides, and an understanding of its coordination chemistry is therefore essential [1-4].

Rhenium is also often used as a model to imitate the reactivity of ^{99m}Tc radiopharmaceuticals (E_γ = 140 keV, $t_{1/2}$ = 6.02 h) which dominate the field of diagnostic nuclear medicine [2]. The physical properties of these group VII congeners are similar; however rhenium complexes are more kinetically inert and are more prone to oxidation [1].

Rhenium has a rich redox chemistry, exhibiting a wide range of oxidation states ranging from -I to +VII. The complexity to control the oxidation state of the metal provides research impetus to manipulate the structural, magnetic, redox and ultimately the biodistribution of rhenium complexes with the use of a variety of donor atoms, chelators and the inclusion of non-coordinating functional groups [1].

The coordination chemistry of rhenium is characterized by a variety of metal cores, particularly in oxidation states +I and +V, such as the mono-oxo $[Re^{V}O]^{3+}$ [5], *cis*- and

trans-dioxo $[Re^{V}O_2]^{+}$ [6,7], dinuclear oxobridged $[Re^{V}{}_2O_3]^{4+}$ [8], nitrido $[Re^{V}N]^{2+}$ [9], imido $[Re^{V}NR]^{3+}$ [10], amido $[Re^{V}NHR]^{4+}$ [11] and the *facial* tricarbonyl core *fac*-$[Re^{I}(CO)_3]^{+}$ [12].

1.2 Aim and Motivation of Study

Rhenium(I) complexes containing the tricarbonyl core have the advantage of being kinetically and thermodynamically inert. This chemically robust core possesses ideal properties, such as a low-spin d^6 electron configuration and a high stability in aqueous solutions, making it ideal for radiopharmaceutical applications. However, even though rhenium(I) complexes fulfill the conditions for therapeutic applications, their effectiveness is restricted either by high toxicity or by the development of drug resistance of tumour cells to chemotherapeutic agents [13]. Therefore, further development of rhenium(I) complexes containing biologically relevant ligands is vital for the discovery of new therapeutic agents of reduced cytotoxicity and enhanced susceptibility towards cancer cells.

Rhenium(V) complexes are predominantly unstable in aqueous systems and readily undergo reduction [to Re(III) or Re(IV)], or easily convert back to perrhenate by *in vivo* oxidation. This limitation can be overcome with the use of aromatic ligands having a large steric bulk which provides shielding of the metal centre and can potentially induce the metal core to be less prone to oxidation. In addition, coordination of aromatic multidentate ligands to rhenium can result in the formation of chelate rings which render additional stability to the metal complex [14].

The design of novel chelating systems is of great importance in the development of target specific radiopharmaceuticals. In this study the reactions of rhenium precursors containing the *fac*-$[Re^{I}(CO)_3]^{+}$ and $[Re^{V}O]^{3+}$ cores with various aromatic and heterocyclic ligands (Figure 1.1) were investigated. By investigating the coordination chemistry of various chelators towards rhenium, the chemical properties (*e.g.* charge, size, lipophilicity, *etc*.) of the resultant complexes can be fine-tuned.

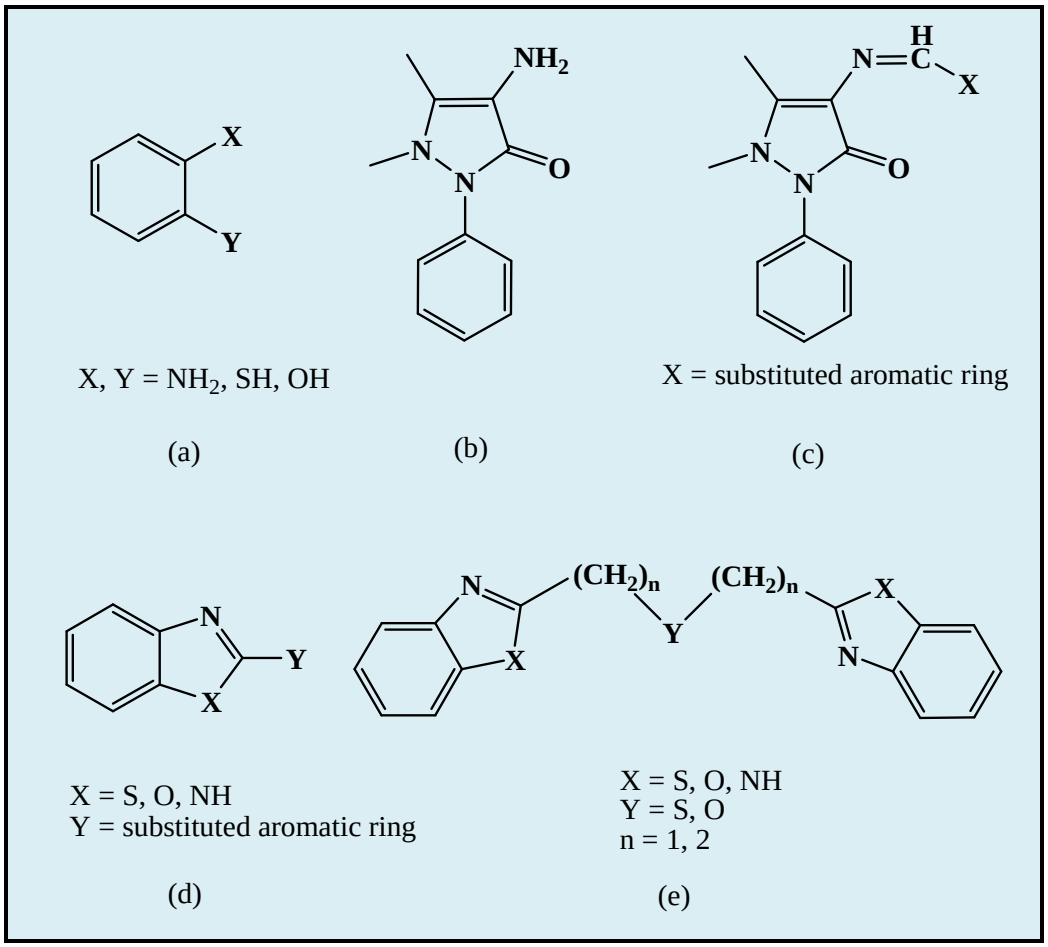

Figure 1.1: Ligands used in study: (a) bidentate aromatic derivatives, (b) 4-aminoantipyrine, (c) derivatives of 4-aminoantipyrine, (d) heterocyclic derivatives, (e) alkyl bridged heterocyclics.

Bidentate ligands containing an aromatic backbone (Figure 1.1(a)) are able to coordinate as neutral, monoanionic or dianionic chelates resulting in the formation of rigid rhenium complexes [15,16]. The systematic variation of the donor atoms situated at the ortho positions on the aromatic ring, results in the formation of metal complexes with different structural configurations. The results obtained from the study of various bidentate rhenium complexes would lead to a greater understanding of the coordination capabilities of the *fac*-$[Re^{I}(CO)_3]^+$ and $[Re^{V}O]^{3+}$ cores. These bidentate ligands are capable of being derivatized to incorporate amine and carboxylic acid fragments which are able to act as a bifunctional chelator to the metal centre. Thus the development of rhenium complexes containing this class of ligand systems has synthetic significance in radiopharmacy.

The considerable research interest in 4-aminoantipyrine (Figure 1.1(b)) and its derivatives results from their potential biological activities [17]. 4-Aminoantipyrine is a pyrazolone derivative and has been extensively used as an antipyretic, analgesic and anti-inflammatory agent [18]. The derivatization of 4-aminoantipyrine through Schiff base formation to produce multidentate ligand systems (Figure 1.1(c)), provides a variety of donor atoms, flexibility and multidenticity to the metal centre [19]. Coordination of multidentate, 4-aminoantipyrine Schiff base ligands to rhenium can result in several chelate rings being formed which may be useful in the stabilization of rhenium complexes. It is thought that the discovery of rhenium complexes containing 4-aminoantipyrine and derivatives thereof would have promise in radiopharmaceutical applications.

Benzothiazoles, benzimidazoles and benzoxazoles (Figure 1.1(d)) and their metal complexes are relevant in a number of medicinal applications and have shown to possess anticancer, antimicrobial, anti-inflammatory and antioxidant activities [20]. In particular, a derivative of benzothiazole, 2-(4'-methylaminophenyl)-6-hydroxy benzothiazole (also known as *Pittsburg Compound B*; *PIB*) have proved to be a promising compound for the *in vivo* visualization of amyloid plaques in patients with Alzheimer's disease [21]. Benzothiazoles and the related oxazoles and imidazoles (Figure 1.1(e)) have the ideal combination of donor/functional groups for metal coordination and are attractive ligands for derivatization, which will assist in enhancing the biological effects of these compounds [22]. The complexation of this class of ligand systems to rhenium is of interest towards the discovery of potential radiopharmaceuticals which target specific biological receptors.

Thus the main aims of this study were:

- To study the reactions of bidentate aromatic derivatives towards the *fac*-$[Re^{I}(CO)_3]^+$ and $[Re^{V}O]^{3+}$ cores.
- To investigate the coordination modes of 4-aminoantipyrine and derivatives towards rhenium.

- To design, synthesize and characterize a variety of 1,3-benzothiazole, benzimidazole and benzoxazole derivatives, and to study their coordination behaviour towards rhenium(I) and (V).

1.3 Applications of Rhenium

1.3.1 Rhenium radiopharmaceuticals

(a) Rhenium radionuclides

Rhenium occurs naturally as a combination of the two non-radioactive isotopes ^{185}Re and ^{187} Re with abundances of 37.4% and 62.6% respectively. The radionuclides ^{186}Re and ^{188}Re are of interest in nuclear medicine [3]. ^{186}Re is a reactor-produced radionuclide, formed by the irradiation of ^{185}Re with neutrons by the nuclear reaction ^{185}Re + n → ^{186}Re. The specific activity is from low to medium and it is impossible to achieve a carrier-free product. ^{188}Re can be obtained either from the nuclear reaction ^{187}Re + n → ^{188}Re, or from the ^{188}W/^{188}Re generator. The generator-created ^{188}Re has an exceptionally superior specific activity and is carrier-free [1].

The similar chemistry between technetium and rhenium facilitates the development of $^{186/188}$Re in nuclear medicine [23]. While technetium has found extensive use in diagnostic nuclear medicine [24], $^{186/188}$Re has been found to be suitable for use in radiotherapy [1,25]. This is due to the nuclear properties tabulated in Table 1.1 [26].

Both β^- emitters possess optimum energies and half-lives which allow an effective energy transfer to cancer tissue [27]. The photon emission of the rhenium radionuclides are similar to that of technetium which allows the rhenium radiopharmaceuticals biodistribution to be monitored by the same gamma-ray camera. ^{186}Re can be used for small tumours due to its tissue range of 5 mm and ^{188}Re, with a larger 11 mm range, can be used for larger tumours [3].

Table 1.1: Properties of the rhenium radionuclides.

Isotope	Half-life (h)	Decay mode* (%)	β_{max} (MeV)	E_γ (keV)	Tissue range (mm)
^{186}Re	90	β^- (92), EC (8)	1.07	137	5
^{188}Re	17	β^- (100)	2.12	155	11

* β^- = beta emission, EC = electron capture

(b) Design approach to rhenium radiopharmaceuticals

Earlier rhenium radiopharmaceuticals were designed analogous to its group VII congener technetium through the "match-pair" approach. For example, Tc-HEDP and Re-HEDP (HEDP = 1-hydroxyethylidene-1,1-diphosphonate) (Figure 1.2) are both excellent bone seekers with Re-HEDP used for pain relief from bone metastases [28]. However, this approach failed due to subtle differences in the chemistry of rhenium and technetium, since rhenium is more easily oxidized, which means that *in vivo* oxidation to $[ReO_4]^-$ is common [3].

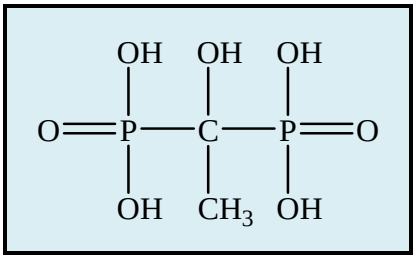

Figure 1.2: Structure of HEDP.

Modern radiopharmaceutical design approaches have focused on the use of a biologically active molecule (BAM) which has a high affinity for a receptor site. There are three approaches towards the design of rhenium radiopharmaceuticals [1]:

- The first generation "metal design" in which the biodistribution and targeting capability of the nuclear agent depends on their lipophilicity, size and charge;

- The integrated approach which involves the manipulation of the metal complex structure to suit the topology of the BAM for successful tagging of it;

- The bifunctional approach which makes use of a high affinity receptor compound as the targeting biomolecule, a bifunctional chelator for attachment of the receptor compound and coordination of the radiometal, and a linker to manipulate the biodistribution, absorption and metabolism of the radiopharmaceutical.

Recently, dual-modality molecular probes has been developed which combines multiple molecular imaging techniques [29]. The dinuclear Re(I)/Tc(I) complex, $[Re(CO)_3(bipy)\{(4\text{-}PyrIDA)Tc(CO)_3\}]$ (bipy = bipyridine, 4-PyrIDA = 2,2'-[(pyridin-4-ylmethyl)imino]diacetic acid) (Figure 1.3) incorporates the nuclear features of Tc(I) with the fluorescence properties of Re(I) and has potential for use as a radioimaging and optical imaging agent [30]. It is thought that the combination of two or more detection techniques could enhance visualization of biological materials and provide greater reliability of collected data.

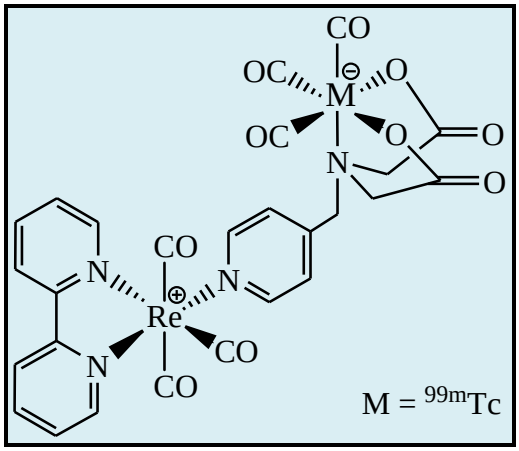

Figure 1.3: Structure of *fac*-$[Re(CO)_3(bipy)\{(4\text{-}PyrIDA)Tc(CO)_3\}]$.

(c) Applications of rhenium radiopharmaceuticals

Clinical studies have shown that although ^{186}Re-HEDP is effective for the relief of pain associated with metastatic bone cancer, it causes unnecessary radiation to occur in the bone marrow. This led to the development of ^{186}Re-labelled biphosphonate derivatives based on the concept of bifunctional radiopharmaceuticals, such as ^{186}Re-MAMA-HBP (Figure 1.4). This radiopharmaceutical has been proved to have a higher affinity for bone than ^{186}Re-HEDP [23,31].

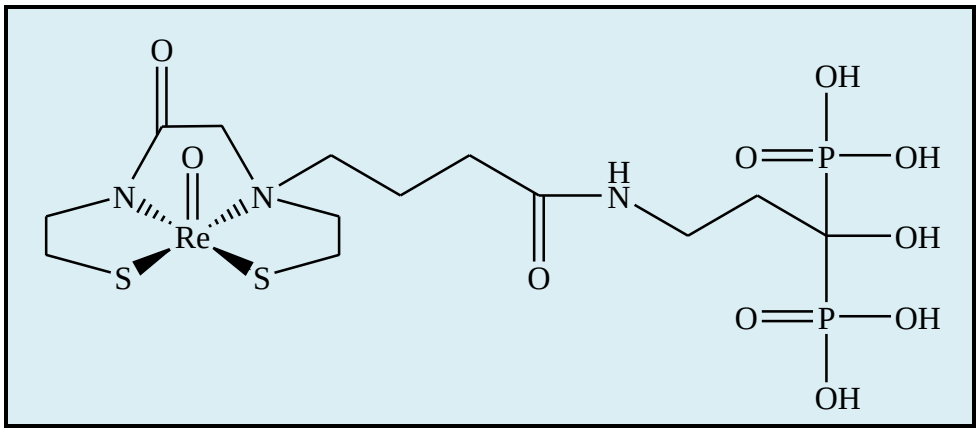

Figure 1.4: Structure of Re-MAMA-HBP.

Studies have shown that ^{188}Re-SOCTA-trastuzumab (Figure 1.5) could be a suitable radioimmunoagent for breast cancer treatment. The trastuzumab antibody is labeled with ^{188}Re through the use of a N_2S_2 ligand SOCTA, which is a useful bifunctional chelator for protein conjugation [32].

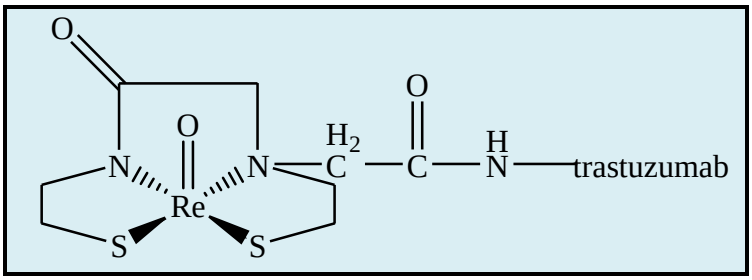

Figure 1.5: Structure of ^{188}Re-SOCTA-trastuzumab.

A facile synthetic approach has been developed for a tridentate bifunctional chelator offering a primary amine or a carboxylic acid group for modification of peptides and proteins for labeling with the *fac*-$[M(CO)_3]^+$ core (M = Tc, Re). The corresponding ^{99m}Tc complex, $[^{99m}Tc(APPA)(CO)_3]$ (APPA = [(5-amino-pentyl)-pyridin-2-yl-methylamino]-acetic acid) (Figure 1.6) showed good clearance characteristics from all organs and tissues which are of importance for potential use in radiopharmacy [33].

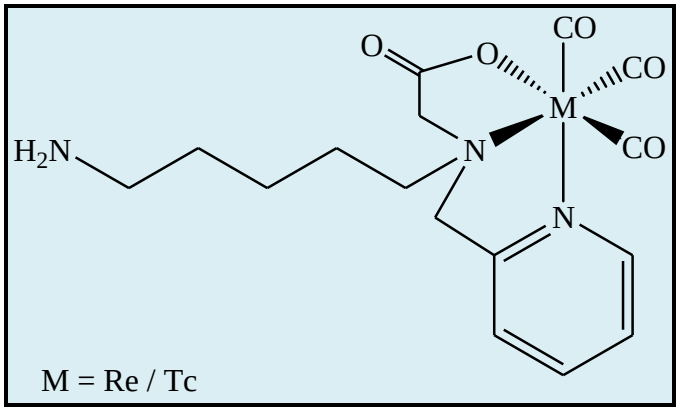

Figure 1.6: Structure of *fac*-$[M(APPA)(CO)_3]$.

(d) Potential therapeutic agents for Alzheimer's disease

The extracellular deposition of amyloid β plaques are thought to be the key contribution to the parthenogenesis and progression of Alzheimer's disease (AD). Non-invasive imaging and quantification of amyloid β deposition in living human brain has been made possible by the recent advancement of amyloid β plaque targeting radiotracers [34]. Aminophenyl-benzothiazole derivatives are known to have possible applications as tracer agents for the *in vivo* visualization of amyloid plaques in AD patients. Thus far, the most favourable and clinically relevant outcomes have been observed with the ^{11}C radiolabelled *Pittsburg Compound B* (^{11}C-PIB) (Figure 1.7). It has been shown that ^{11}C-PIB has substantial uptake in beta-amyloid plaques in neuronal tissue and generates images *via* Positron Emission Tomography (PET) [21].

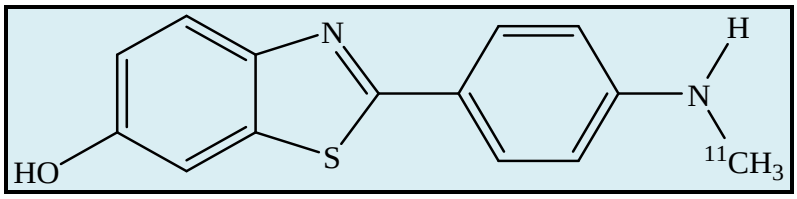

Figure 1.7: Structure of ^{11}C-PIB.

Thus far a series of neutral complexes of rhenium-2-phenylbenzothiazoles (Figure 1.8) were developed and has shown to have good binding affinity to aggregated amyloid β fibres. It is believed that the corresponding ^{99m}Tc analogues would hold great potential for imaging amyloid β deposition with Single-Photon Emission Computed Tomography (SPECT) [34].

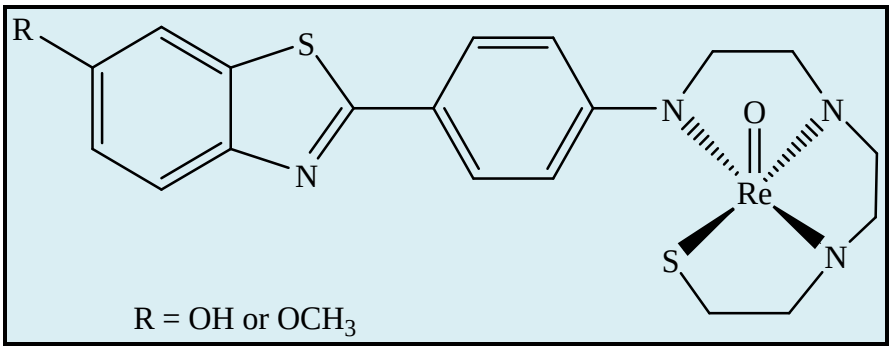

Figure 1.8: Structure of rhenium-2-phenylbenzothiazoles.

1.3.2 Electrochemistry

The redox properties of radiopharmaceuticals have a significant influence on their biological activity. Biodistribution studies of rhenium agents have shown that there is a link between the redox reactivity and the rate of clearance of a therapeutic agent from a specific organ [35]. In addition, a study of the redox behaviour of rhenium complexes provides an indication of the radiopharmaceuticals specificity towards particular organs and determines its resistance towards *in vivo* oxidation [36]. The redox properties of the complexes can be manipulated by changing the rhenium core used, the oxidation state of the metal and by varying the donor properties of the coordinated ligand [35].

For example, it has been shown that electrochemical techniques can be employed in the evaluation of the protein binding capacity of cationic rhenium complexes. The *trans*-$[ReO_2(en)_2]^+$ (en = 1,2 ethanediamine) cation interacts with the plasmatic protein albumin at neutral pH, due to the functional groups in the protein being mostly negatively charged. This method provides insight to the mechanism of the protein interaction, which would prove invaluable in the understanding of the biodistribution and activity of potential radiopharmaceuticals [37].

1.3.3 Photochemistry

The reactions of $[Re(CO)_5X]$ (X = Cl, Br) with bidentate diimine ligands like 1,10-phenanthroline and 2,2'-bipyridine, result in the substitution of two carbonyl ligands forming stable *fac*-$[Re(CO)_3(diimine)X]$ complexes. It was found that the *fac*-$[Re(CO)_3(diimine)X]$ complexes exhibited remarkable photochemical properties [38]. The diimine ligand can be modified to allow the systematic tuning of the electronic characteristics of the Re(I) complexes [39].

For example, the photochemical behaviours of *fac*-$[Re(CO)_3(MebpyTTF)X]$ (MebpyTTF = 4,5-*bis*(methyloxycarbonyl)-4′,5′-(4′-methyl-2,2′-dipyrid-4-ylethylenedi-thio)tetrathiafulvalene; X = Cl, Br) (Figure 1.9) were extensively studied [40]. Photoexcitation of the complexes in CH_2Cl_2 at 460 nm resulted in intense luminescence at room temperature, with emission maxima between 600 and 620 nm. These emissions were ascribed to the metal to ligand charge transfer (MLCT) excited state.

The exceptional photochemical characteristics of diimine rhenium(I) tricarbonyl complexes has brought about their various applications as sensors, light emitting materials, non-linear optical materials and as photoluminescent metal-based probes for the study of DNA binding [41]. This has provided huge impetus for the discovery of novel rhenium(I) complexes containing diimine chelates.

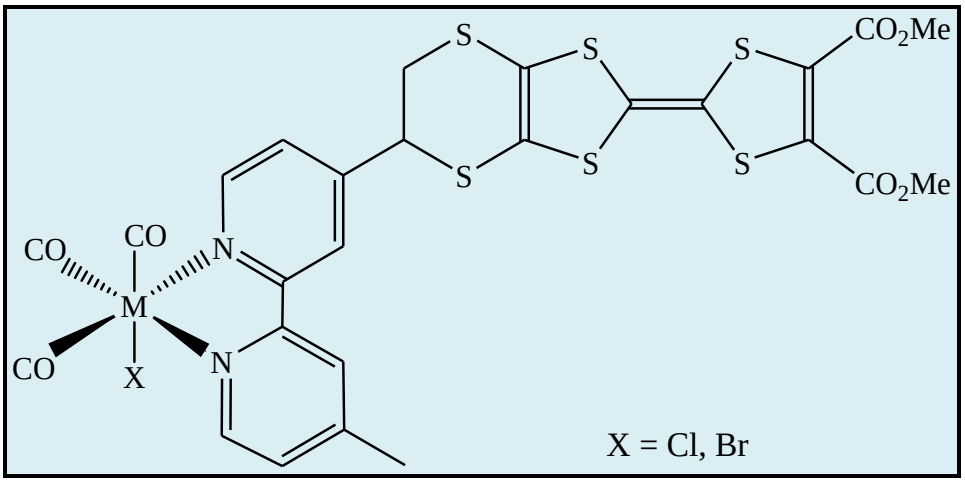

Figure 1.9: Structure of *fac*-[Re(CO)$_3$(MebpyTTF)X].

1.4. The General Chemistry of Rhenium(I)

Rhenium(I) has a d^6 electronic configuration in an octahedral field and complexes in this oxidation state display kinetic and thermodynamic stability [27]. Monodentate ligands such as phosphines, diphosphines, isonitriles, nitrosyls and carbonyls are required to stabilize rhenium in oxidation state +I.

1.4.1 Rhenium(I) tricarbonyl core, *fac*-[Re(CO)$_3$]$^+$

Alberto and coworkers first reported the one step synthesis of the rhenium(I) complex [Re(H$_2$O)$_3$(CO)$_3$]$^+$, by direct reduction of perrhenate with sodium borohydride in aqueous solution in the presence of carbon monoxide [12]. This complex serves as a synthon for the formation of *fac*-[Re(CO)$_3$]$^+$ complexes since the labile solvent molecules are easily replaced by a variety of functional groups, including amines, thioethers, imines, thiols, carboxylates and phosphines [27].

The *fac*-[M(CO)$_3$]$^+$ (M = Tc, Re) moiety has been found to be of value due to its favourable properties [12,27,42]:

- The *fac*-$[M(CO)_3]^+$ precursor complexes can be readily prepared in high yield from the permetalates in aqueous-based kit formulations.
- The small size of the $[M(CO)_3]^+$ core allows flexibility in the labeling of various molecular weight biomolecules.
- The *fac*-$[M(CO)_3]^+$ core has a large affinity for a variety of donor atoms due to the fact that the stability of these complexes is purely kinetic.
- Potential radiopharmaceuticals containing the *fac*-$[M(CO)_3]^+$ moiety have a high stability in water compared to radiopharmaceuticals containing the oxorhenium(V) core which is prone to oxidation by water.

1.4.2 Coordination chemistry of rhenium(I)

(a) Rhenium(I) complexes with NN-donor ligands

A novel Re(I) diimine complex was designed by introducing the carrier-transporting carbazole moiety (Figure 1.10) into the diimine ligand. The single crystal X-ray diffraction results for the *fac*-$[Re(CO)_3(cpb)Cl]$ complex (cpb = *N*-(4-carbazolylphenyl)-2,2'-dipyridylamine) displays a distorted octahedral geometry with the N-Re-N bond angle much less than 90˚ due to the steric requirement of the bidentate coordination of the cpb ligand. The photoluminescent properties of the complex in the solid state were found to be superior to that of the corresponding diimine complex without the functional carbazole group [43].

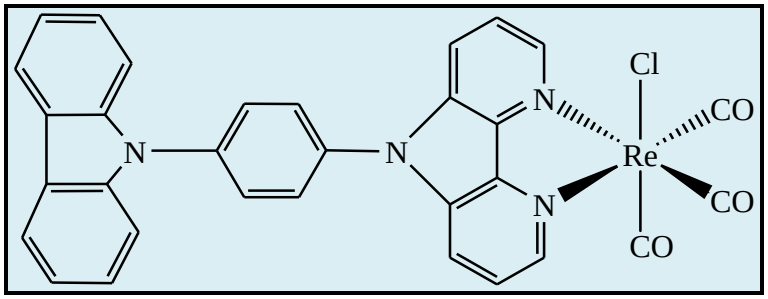

Figure 1.10: Structure of *fac*-$[Re(CO)_3(cpb)Cl]$.

The "2+1" *fac*-[$Re(CO)_3$(phen)(app)](BF_4) complex (Figure 1.11) (phen = 1,10-phenanthroline, app = 3-amino-*N*-phthalimido-pyridine) was formed from the reaction of [$Re(CO)_3$(phen)(CH_3CN)](BF_4)] and app in chloroform. The lipophilic planar phthalimide moiety coordinates through the pyridyl nitrogen, while the phen unit acts as a neutral bidentate chelate. Photophysical analysis of this compound showed that the complex has useful emission properties and, in addition, the phthalimide unit provides a useful basis for biological application in confocal fluorescent microscopy [44].

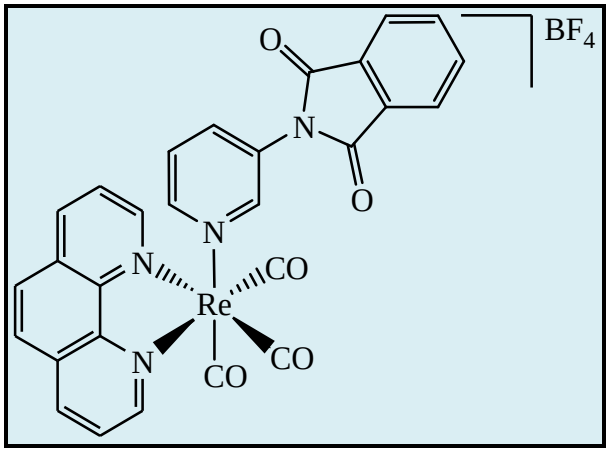

Figure 1.11: Structure of *fac*-[$Re(CO)_3$(phen)(app)](BF_4).

(b) Rhenium(I) complexes with heterocyclic ligands

The reaction of [$Re(CO)_5Br$] with 2,6-*bis*(1'-methylbenzimidazol-2'-yl)pyridine (btmbip) formed the stable octahedral complex *fac*-[$Re(CO)_3$(btmbip)Br] (Figure 1.12). The btmbip acts as a neutral bidentate chelate with coordination through the pyridyl nitrogen and the imidazoyl nitrogen [45].

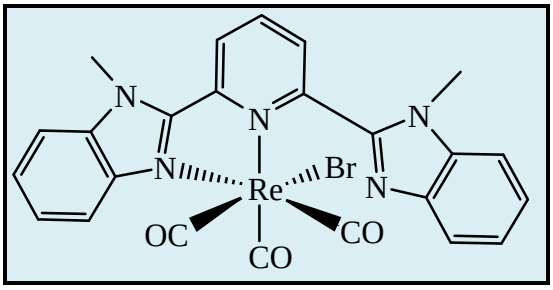

Figure 1.12: Structure of *fac*-[$Re(CO)_3$(btmbip)Br].

Coordination of the heterocyclic ligand 2,3-*bis*(methylthio)pyrrolo[1,2-*a*]benzimidazol-1-one (mpbo) with *fac*-$[Re(CO)_3(THF)_2Br]$ in refluxing toluene gave the *fac*-$[Re(CO)_3(mpbo)Br]$ (Figure 1.13) complex. The ancillary heterocyclic mpbo ligand exhibits an *N,S* chelation mode with the ketonic oxygen and methyl sulfur on the exterior pyrrol-1-one ring remaining uncoordinated [46].

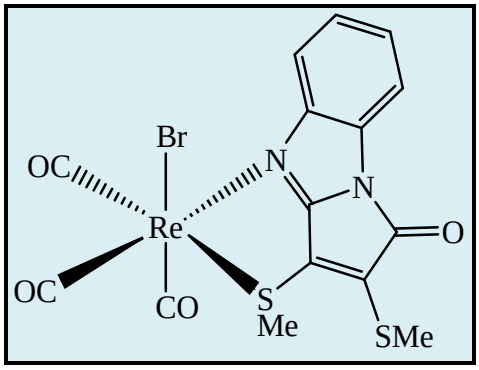

Figure 1.13: Structure of *fac*-$[Re(CO)_3(mpbo)Br]$.

(c) Rhenium(I) complexes with nitrogen, oxygen and/or sulfur donor ligands

Complexes of *fac*-$[Re(CO)_3L]^+$ (where L is a facially coordinating tridentate ligand) are stable in aqueous media and there is a possibility for such compounds to be of use in nuclear medicine. The coordinated tridentate ligand can serve as a bifunctional chelator for the labeling of bioactive molecules [26]. An example of this is the 4-(benzimidazol-2-yl)-3-thiabutanoic acid (Hbtb) ligand which acts as a NSO tridentate chelate towards the *fac*-$[Re(CO)_3Br_3]^{2-}$ precursor by replacing the bromide atoms.

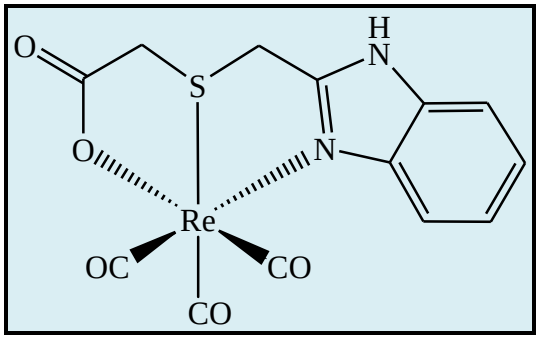

Figure 1.14: Structure of *fac*-$[Re(CO)_3(btb)]$.

The tridentate ligand coordinates through the pyridine nitrogen of the benzimidazole, the thioether sulfur and the carboxylate oxygen, forming the neutral lipophillic *fac*-[$Re(CO)_3$(btb)] complex (Figure 1.14). The NH group of the benzimidazole moiety can be modified to serve as an anchoring point for the bridging of a receptor targeting molecule of biological interest [47].

Dimeric $[Re(CO)_3(NX)]_2$ (NX = 8-thioquinoline or 8-hydroxyquinoline) complexes were isolated from the reaction of $[Re(CO)_5Cl]$ and the substituted quinoline ligands. The dimeric rhenium molecules consists of two *fac*-$[Re(CO)_3(NX)]$ sub-units connected *via* sulfur or oxygen atoms of 8-thioquinoline and 8-hydroxyquinoline respectively. Upon further reaction in a strongly coordinating solvent (pyridine), the $[Re(CO)_3(NX)]_2$ complexes underwent dissociative solvolysis to produce the *fac*-$[Re(CO)_3(NX)(py)]$ complexes (Scheme 1.1) [48].

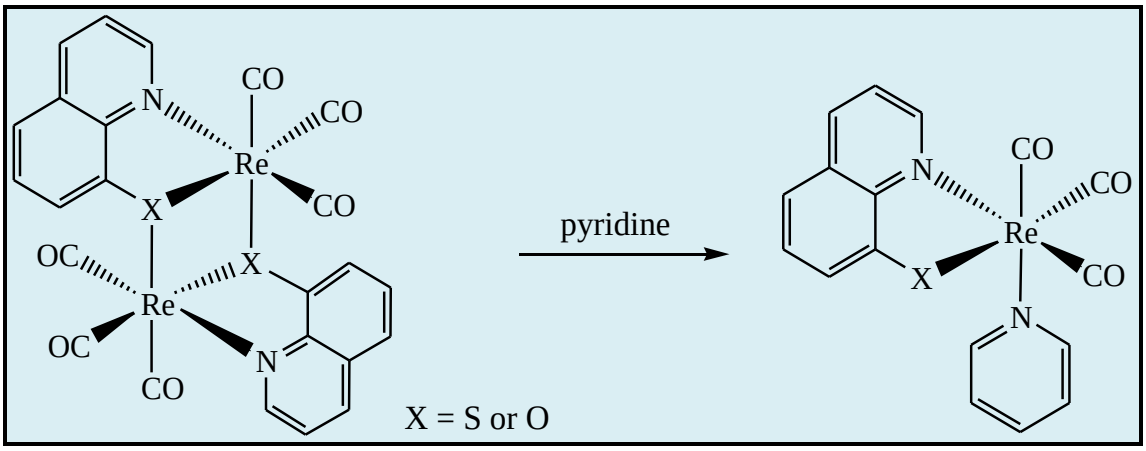

Scheme 1.1: Formation of *fac*-$[Re(CO)_3(NX)(py)]$ from $[Re(CO)_3(NX)]_2$.

1.5 The General Chemistry of Rhenium(V)

The oxidation state +V of rhenium has the largest number of structurally characterized complexes for this metal. This is due to the easily accessibility of rhenium(V) *via* the reduction of $[ReO_4]^-$ with reducing agents (*e.g.* $SnCl_2$) and by the coordination of the central metal atom with a large variety of donor atoms. Rhenium(V) complexes generally exhibits an octahedral geometry with a diamagnetic d^2 configuration. The common cores

for rhenium in oxidation state +V are the oxo, imido and amido, with the former dominating the coordination chemistry of rhenium.

1.5.1 Rhenium(V) oxo core, $[ReO]^{3+}$

The oxorhenium(V) complexes predominates and undergoes various reactions such as given below.

(a) Oxidation

Oxorhenium(V) complexes are oxidized by strong oxidants which usually result in the formation of perrhenate. The oxo-hydrazido $[Re^{VII}OCl(NNMePh)(PPh_3)_2]^{2+}$ cationic complex was formed by the oxidation of *trans*-$[Re^{V}OCl_3(PPh_3)_2]$ with an excess of the unsymmetrically disubstituted organohydrazine $MePhNNH_2$ in boiling methanol by the following reaction [49]:

$$\textit{trans}\text{-}[ReOCl_3(PPh_3)_2] + MePhNNH_2 \rightarrow [ReOCl(NNMePh)(PPh_3)_2]^{2+} + 2Cl^- + H_2O$$

(b) Reduction

The common route to rhenium(III) complexes is the reduction of monooxorhenium(V) by triphenylphosphine *via* the removal of the terminal oxide, as shown by the following reaction [50]:

$$\textit{trans}\text{-}[ReOCl_3(PPh_3)_2] + CNC(CH_3)_3 + PPh_3 \rightarrow [ReCl_3(CNC(CH_3)_3)(PPh_3)_2] + OPPh_3$$

(c) Disproportionation

Oxorhenium(V) complexes can also undergo disproportionation to Re(IV)/Re(III) and Re(VII). The disproportionation of rhenium(V) to rhenium(III) and rhenium(VII) was noted in the reaction [51]:

trans-$[ReOCl_3(PPh_3)_2]$ + phen ⟶ $[ReCl_2(phen)(PPh_3)_2]^+$ + $[ReO_4]^-$

(d) Ligand Substitution

Ligand substitution is readily affected in the cold or by gentle warming in a suitable solvent. An example is shown in the following reactions where different solvents produce different products [52]:

fac-$[ReOCl_3(Dppen)]$ + $OPPh_3$ + SMe_2

fac-$[ReOCl_3(OPPh_3)(SMe_2)]$ + Dppen ⇄ (THF / EtOH)

fac-$[ReOCl_2(OEt)(Dppen)]$ + $OPPh_3$ + SMe_2 + HCl

1.5.2 Rhenium(V) imido core, $[ReNR]^{3+}$

The dianionic ligand $[NR]^{2-}$ is isoelectronic with the oxo ligand and is also able to stabilize metals in their high oxidation states [53]. The organoimido core, M = N – R, is of synthetic value in radiopharmacology since different organic substituents can be included into a stable nitrogen core. The biological properties can then be adjusted by variation of the imido core's R substituent [54]. The bonding between the metal and imido ligands consists of one sigma and two pi bonds, and it can adopt different geometries as shown in Figure 1.9.

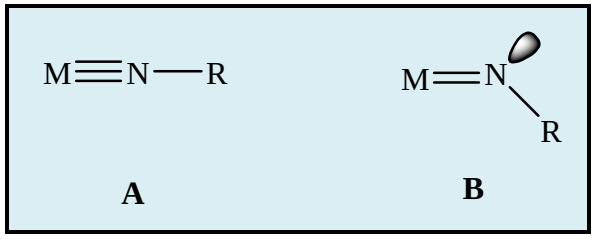

Figure 1.15: Representations of the bonding in imido complexes.

When the imido ligand is bonded to the metal in a linear fashion (structure **A** in Figure 1.15), the bond can be regarded as a triple bond and the N-atom considered to be sp

hybridized. The bent imido (structure **B**) results in a double bond between the metal and the nitrogen atom with the lone pair centered on a sp^2 hybridized nitrogen [55].

It was previously shown that the imido moiety can be obtained from oxo complexes through the use of a condensation reaction with aniline derivatives [10]:

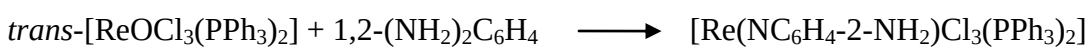

trans-$[ReOCl_3(PPh_3)_2]$ + 1,2-$(NH_2)_2C_6H_4$ ⟶ $[Re(NC_6H_4\text{-}2\text{-}NH_2)Cl_3(PPh_3)_2]$

In addition, the nitrido core can also produce imido rhenium(V) complexes through alkylation or acylation with carbanions and anhydrides [56]:

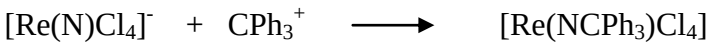

$[Re(N)Cl_4]^-$ + CPh_3^+ ⟶ $[Re(NCPh_3)Cl_4]$

Ligand substitution reactions with the $[Re(NPh)Cl_3(PPh_3)_2]$ and $[Re(NMe)Cl_3(PPh_3)_2]$ precursors have also been shown to be a versatile method to produce imido complexes with different ligands attached to the rhenium(V) imido core [55].

1.5.3 Coordination chemistry of rhenium(V)

(a) Rhenium(V) complexes with heterocyclic ligands

The tridentate NNO ligand Hbp (*N*-(2-hydroxybenzyl)-2-picolylamine) was used to generate $[ReO(bp)Cl_2]$ (Scheme 1.2) from (*n*-Bu_4N)$[ReOCl_4]$. The deprotonated Schiff base binds in a *facially* tridentate fashion with the phenoxide oxygen atom occupying the *trans* position to the oxo group. The tetradentate ONNO donating ligand H_2bbp (N^1,N^2-*bis*(2-hydroxybenzyl)-2-picolylamine) reacted with (*n*-Bu_4N)$[ReOCl_4]$ to form the monochloro complex [ReO(bbp)Cl] (Scheme 1.2). The pyridyl nitrogen, amine nitrogen and one phenoxide oxygen of the doubly deprotonated bbp^{2-} moiety coordinated meridonally, with the other phenoxide oxygen being *trans* to the terminal oxo group [58].

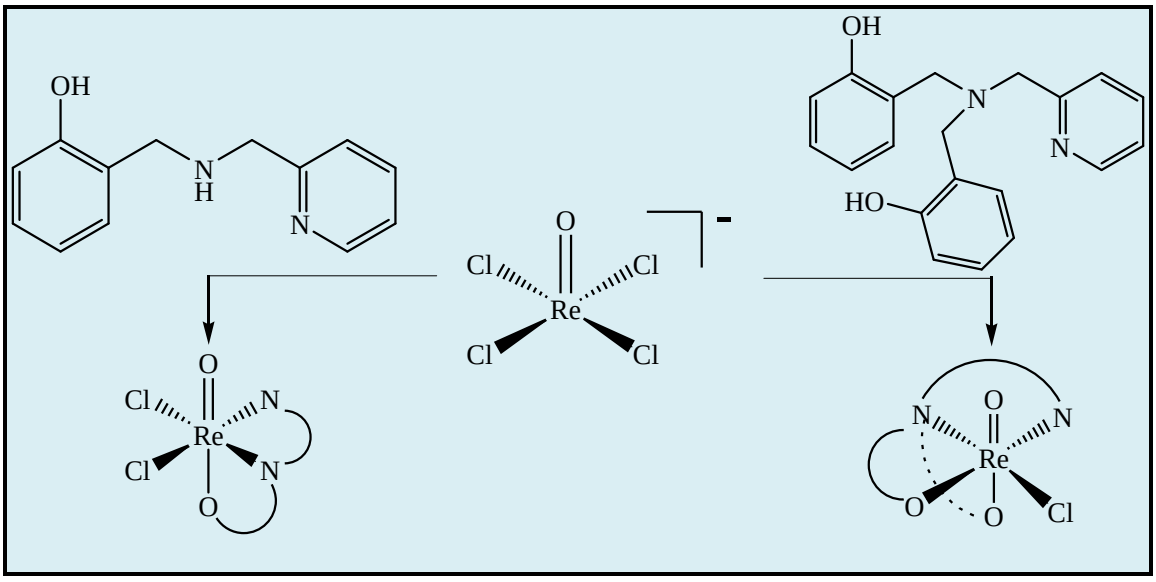

Scheme 1.2: Reaction pathway for the formation of $[ReO(bp)Cl_2]$ and [ReO(bbp)Cl].

The reaction of *trans*-$[ReOBr_3(PPh_3)_2]$ with *bis*(3,5-dimethylpyrazol-1-yl)methane (bdmpzm) in ethanol produced the cationic dioxorhenium(V) *trans*-$[ReO_2(bdmpzm)_2]^+$ complex salt (Figure 1.16). The two bidentate bdmpzm ligands coordinated through the nitrogens of the pyrazole rings to form 6 membered chelate rings [6].

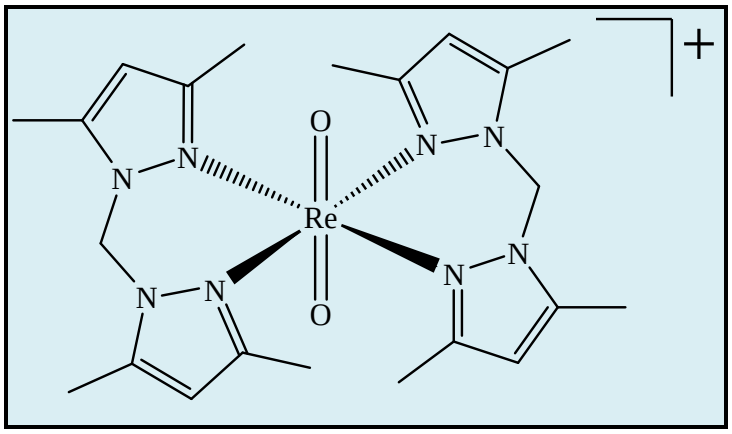

Figure 1.16: Structure of $[ReO_2(bdmpzm)_2]^+$.

(b) Rhenium(V) complexes with nitrogen, oxygen and sulfur donor ligands

The mixed-ligand Re(V) complex (Figure 1.17) containing the tridentate thiocarbamoylbenzamide (H_2tcb) and the bidentate *N,N'*-dialkyl-*N'*-benzoylthioureato

(HR_2btu) ligands was formed upon reaction of (n-Bu_4N)[$ReOCl_4$] with H_2tcb and HR_2btu in the presence of a supporting base triethylamine. The benzoylic oxygen of the R_2btu^- ligand occupies the position *trans* to the rhenium oxo moiety and the tridenate tcb^{2-} is coordinated meridionally [59].

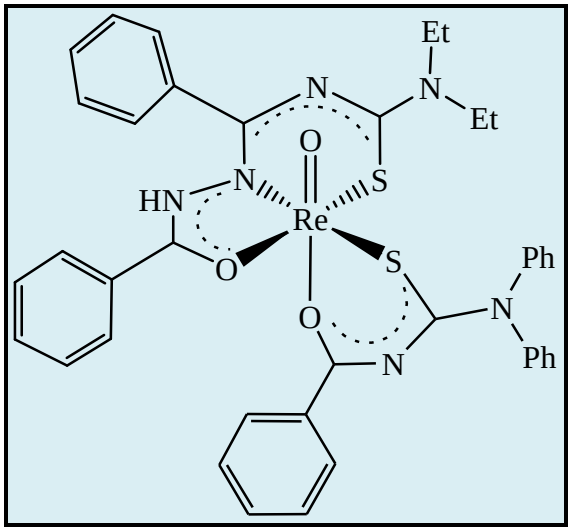

Figure 1.17: Structure of [$ReO(R_2btu)(tcb)$].

The neutral [ReO(mcg)(bipy)] complex (H_3mcg =2-mercaptoethyl-*N*-glycine, bipy = 2,2'-bipyridine) (Figure 1.18) was formed from *trans*-[$ReOCl_3(PPh_3)_2$] upon treatment with a mixture of H_3mcg and bipy in methanol. This '3+2' complex consists of a neutral bidentate NN chelate as well as a SNO tridentate trianionic ligand leading to the stable oxorhenium complex [60].

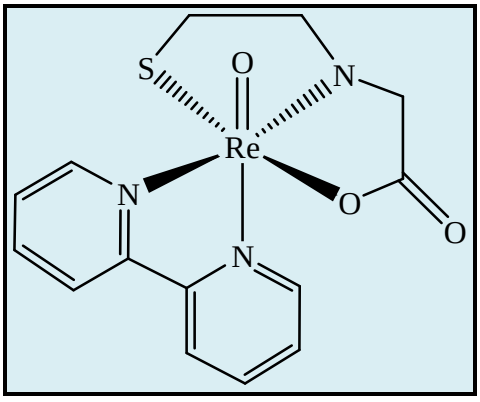

Figure 1.18: Structure of [ReO(mcg)(bipy)].

1.6. References

[1] S. Liu, *Chem. Soc. Rev*., 2004, **33**, 445.

[2] D.E. Reichert, J.S. Lewis, C.J. Anderson, *Coord. Chem. Rev*., 1999, **184**, 3.

[3] J.R. Dilworth, S. Parrott, *Chem. Soc. Rev*., 1998, **27**, 43.

[4] U. Abram, R. Alberto, *J. Braz. Chem. Soc*., 2006, **17**, 1486.

[5] M. Videira, F. Silva, A. Paulo, I.C. Santos, I. Santos, *Inorg. Chim. Acta*, 2009, **362**, 2807.

[6] B. Machura, R. Kruszynski, R. Penczek, J. Mroziński, J. Kusz, *Polyhedron*, 2008, **27,** 797; C. Kremer, E. Kremer, *Polyhedron*, 1996, **15**, 4341.

[7] G. Bandoli, A. Dolmella, T.I.A. Gerber, D. Luzipo, J.G.H. du Preez, *Inorg. Chim. Acta*, 2001, **325**, 215; P. Bouziotis, D. Papagiannopoulou, I. Pirmettis, M. Pelecanou, C.P. Raptopoulou, C.I. Stassinopoulou, A. Terzis, M. Friebe, H. Spies, M. Papadopoulos, E. Chiotellis, *Inorg. Chim. Acta*, 2001, **320**, 174.

[8] H. Sugimoto, T. Takahira, T. Yoshimura, M. Shiro, M. Yamasaki, H. Miyake, K. Umakoshi, Y. Sasaki, *Inorg. Chim. Acta*, 2002, **337**, 203; B. Machura, *Coord. Chem. Rev*., 2005, **249**, 591.

[9] V. Yam, Y. Pui, K. Wong, K. Cheung, *Inorg. Chim. Acta*, 2000, **300–302,** 721; C. Bolzati, F. Tisato, F. Refosco, M. Porchia, G. Bondoli, *Inorg. Chim. Acta*, 2010, **363**, 1289.

[10] T.I.A. Gerber, J. Perils, J.G.H. du Preez, *Inorg. Chim. Acta*, 1998, **278**, 96.

[11] T.I.A. Gerber, D. Luzipo, P. Mayer, *J. Coord. Chem*., 2005, **58**, 637.

[12] R. Alberto, R. Schibli, A. Egli, A.P. Schubiger, *J. Am. Chem. Soc*., 1998, **120**, 7987.

[13] P. Kozminski, E. Gniazdowska, L. Fuks, S. Kowalska, *Appl. Radiat. Isotopes*, 2011, **69**, 436.

[14] H. Luo, S. Liu, S.J. Rettig, C. Orvig, *Can. J. Chem*., 1995, **73**, 2272.

[15] X. Chen, F.J. Femia, J.W. Babich, J. Zubieta, *Inorg. Chim. Acta*, 2001, **315**, 147; T.I.A. Gerber, D. Luzipo, P. Mayer, *Inorg. Chim. Acta,* 2004, **357**, 429; T.I.A. Gerber, P. Mayer, *J. Nucl. Radiochem. Sci*., 2005, **6**, 165.

[16] G. Bandoli, A. Dolmella, T.I.A. Gerber, D. Mpinda, J. Perils, J.G.H. Du Preez, *J. Coord. Chem*., 2002, **55**, 823.

[17] G. Turan-Zitouni, M Sivaci, F.S. Kilic, K. Erol, *Eur. J. Med. Chem*., 2001, **36**, 685.

[18] J.S. Casas, M.S. Garcia-Tasend, A. Sanchez, J. Sordo, A. Touceda, *Coord. Chem. Rev*., 2007, **251**, 1561.

[19] N. Raman, L. Mitu, A. Sakthivel, M.S.S. Pandi, *J. Iran. Chem. Soc*., 2009, **6**, 738.

[20] S. Huang, I. Hsei, C. Chen, *Bioorg. Med. Chem*., 2006, **14**, 6106; B. Soni, M. Ranawat, R. Sharma, A. Bhandari, S. Sharma, *Eur. J. Med. Chem.*, 2010, **45**, 2938; S. Hibi, Y. Okamoto, K. Tagami, H. Numata, N. Kobayashi, M. Shinoda, T. Kawahara, M. Murakami, K. Oketani, T. Inoue, H. Shibata, and I. Yamatsu, *J. Med. Chem*., 1994, **37**, 3062; H.M. Refaat, O.M. Khalil, S.M. Abuel-Maaty, *J. Chem. Res*., 2009, **7**, 448; R.V. Satyendra, K.A. Vishnumurthy, H.M. Vagdevi, K.P. Rajesh, H. Manjunatha, A. Shruthi, *Eur. J. Med. Chem.*, 2011, **46**, 3078.

[21] K. Serdons, T. Verduyckt, D. Vanderghinste, P. Borghgraef, J. Cleynhens, F. Van Leuven, H. Kung, G. Bormans, A. Verbruggen, *Eur. J. Med. Chem.*, 2009, **44**, 1415.

[22] M. Boca, R.F. Jameson, W. Linert, *Coord. Chem. Rev*., 2011, **255**, 290.

[23] T. Uehara, Z. Jin, K. Ogawa, H. Akizawa, K. Hashimoto, M. Nakayama, Y. Arano, *Nucl. Med. Biol*., 2007, **34**, 79.

[24] S.R. Banerjee, K.P. Maresca, L. Francesconi, J. Valliant, J.W. Babich, J. Zubieta, *Nucl. Med. Biol*., 2005, **32**, 1.

[25] N. Iznaga-Escobar, *Appl. Radiat. Isotopes*, 2001, **54**, 399.

[26] *Table of Isotopes*, 7th edn., Vol. 7, Wiley, New York (1978).

[27] R. Alberto, R. Schibli, R. Waibel, U. Abram, A.P. Schubiger, *Coord. Chem. Rev*., 1999, **190**, 901.

[28] S.W. Falen, R.J. Kowalsky, *Radiopharmaceuticals in Nuclear Pharmacy and Nuclear Medicine,* American Pharmacists Association, Washington DC (2004).

[29] L.E. Jennings, N.J. Long, *Chem. Commun*., 2009, 3511.

[30] A. Boulay, M. Artigau, Y. Coulais, C. Picard, B. Mestre-Voegtle, E. Benoist, *Dalton Trans*., 2011, **40**, 6206.

[31] K. Ogawa, T. Mukai, Y. Arano, A. Otaka, M. Ueda, T. Uehara, Y. Magata, K. Hashimoto, H. Saji, *Nucl. Med. Biol*., 2006, **33**, 513.

[32] T. Luo, I. Tang, Y. Wu, K. Hsu, S. Liu, H. Kung, P. Lai, W. Lin, *Nucl. Med. Biol*., 2009, **36,** 81.

[33] A. Stichelberger, R. Waibel, C. Dumas, P.A. Schubiger, R. Schibli, *Nucl. Med. Biol*., 2003, **30**, 465.

[34] K. Lin, M.L. Debnath, C.A. Mathis, W.E. Klunk, *Bioorg. Med. Chem. Lett.*, 2009, **19**, 2258.

[35] G.N. Holder, L.A. Bottomley, *Transition Met. Chem.*, 1991, **16**, 579.

[36] M.F. Cerda, E. Mendez, L. Malacrida, C.F. Zinola, C. Melian, M.E. Martins, A.M.C Luna, C. Kremer, *J. Colloid Interface Sci*., 2002, **249**, 366.

[37] M.F. Cerda, E. Mendez, G. Obal, C. Kremer, J.S. Gancheff, A.M.C. Luna, *J. Inorg. Biochem*., 2004, **98,** 238.

[38] A. Kumar, S. Sun, A.J. Lees, *Top. Organomet. Chem*., 2010, **29**, 1.

[39] D.J. Stufkens, A. Vlcek, *Coord. Chem. Rev*., 1998, **177**, 127.

[40] Y. Chen, W. Liu, J. Jin, B. Liu, Z. Zou, J. Zuo, X. You, *J. Organomet. Chem*., 2009, **694**, 763.

[41] A. Kumar, S. Sun, A.J. Lees, *Coord. Chem. Rev*., 2008, **252**, 922; Z. Si, J. Li, B. Li, F. Zhao, S. Liu, W. Li, *Inorg. Chem*., 2007, **46**, 6155; J. Zhang, B.W. Chu, N. Zhu, V.W. Yam, *Organometallics*, 2007, **26**, 5423; D.L. Ma, C. Che, F. Siu, M. Yang, K. Wong, *Inorg. Chem*., 2007, **46**, 740.

[42] U. Abram, S. Abram, R. Schibli, R. Alberto, J.R. Dilworth, *Polyhedron*, 1998, **17**, 1303.

[43] J. Wu, H. Li, L. Kang, D. Li, H. Li, X. Zhou, Y. Sui, Y. Zheng, J. Zuo, X. You, *J. Photochem. Photobiol. A–Chem*., 2010, **211**, 135.

[44] F.L. Greenwood, M.P. Coogan, A.J. Hallett, R.H. Laye, S.J.A. Pope, *J. Organomet. Chem*., 2009, **694**, 1400.

[45] A. Gelling, K.G. Orrell, A.G. Osborne, V. Sik, M.B. Hursthouse, D.E. Hibbs, K.M.A. Malik, *Polyhedron*, 1998, **17**, 2141.

[46] G. Wu, D.R. Glass, D. May, W.H. Watson, D. Wiedenfeld, M.G. Richmond, *J. Organomet. Chem*., 2005, **690**, 4993.

[47] T. Tsotakos, C. Tsoukalas, G. Patsis, A. Panagiotopoulou, N. Nikolic, D. Jankovic, D. Djokic, C.P. Raptopoulou, A. Terzis, D. Papagiannopoulou, M. Pelecanou, M. Papadopoulos, I. Pirmettis, *Inorg. Chim. Acta*, 2011, **377**, 62.

[48] R. Czerwieniec, A. Kapturkiewicz, J. Nowacki, *Inorg. Chem. Commun*., 2005, **8**, 34.

[49] J.C. Vites, M.M. Lynam, *Coord. Chem. Rev*., 1995, **142**, 1.

[50] H. Spies, M. Glaser, F.E. Hahn, T. Lugger, D. Scheller, *Inorg. Chim. Acta*, 1995, **232**, 235.

[51] B. Machura, R. Kruszynski, M. Jaworska, J. Klak, J. Mrozinski, *Polyhedron*, 2006, **25**, 2537.

[52] O. Signouin, A. Beauchamp, *Inorg. Chim. Acta*, 2005, **358**, 4489.

[53] H. Braband, T.I. Kuckmann, U. Abram, *J. Organomet. Chem*., 2005, **690**, 5421.

[54] M.T. Ahmet, B. Coutinho, J.R. Dilworth, J.R. Miller, S.J. Parrott, Y. Zheng, *Polyhedron*, 1996, **15**, 2041.

[55] R.A. Eikey, M.M. Abu-Omar, *Coord. Chem. Rev*., 2003, **243**, 83.

[56] A. Voigt, U. Abram, R. Kirmse, *Inorg. Chem. Commun*., 1998, **1**, 203.

[58] A. Mondal, S. Sarkar, D. Chopra, T.N. Guru Row, K.K. Rajak, *Dalton Trans*., 2004, 3244.

[59] H.H. Nguyen, U. Abram, *Polyhedron*, 2009, **28**, 3945.

[60] D. Papagiannopoulou, I. Pirmettis, M. Pelecanou, D. Komiotis, M. Sagnou, D. Benaki, C.P. Raptopoulou, A. Terzis, M.S. Papadopoulos, *Inorg. Chim. Acta*, 2007, **360**, 3597.

Chapter 2

Experimental

2.1 Handling of Rhenium

Rhenium occurs naturally with two non-radioactive isotopes, ^{185}Re and ^{187}Re, with a natural abundance of 37.4 % and 62.6 % respectively. The radioactive isotopes ^{186}Re and ^{188}Re are generated from the non-radioactive isotopes ^{185}Re and ^{187}Re respectively. The non-radioactive isotopes were used in this study and no special precautions were taken in the handling of rhenium.

2.2 Materials

2.2.1 Precursor compounds

(a) Ammonium perrhenate

The ammonium perrhentate $(NH_4)[ReO_4]$ was obtained from Sigma-Aldrich in +99 % purity and required no further purification.

(b) Rheniumpentacarbonyl halide

The rheniumpentacarbonyl halides $[Re(CO)_5X]$ (X = Cl or Br), were obtained from Sigma-Aldrich in 98 % purity and were used without further purification.

(c) *trans*-[$ReOCl_3(PPh_3)_2$] [1]

To a mixture of 0.9 g of $(NH_4)[ReO_4]$ in 3 cm^3 of conc. hydrochloric acid was added 5.0 g of triphenylphosphine in 50 cm^3 glacial acetic acid under nitrogen. A bright green precipitate formed, which was filtered, washed with glacial acetic acid and diethyl ether, and dried under vacuum. Yield = 95 %. Anal. Calcd. for $C_{36}H_{30}P_2OCl_3Re$ (mol. wt. = 833.09 g/mol) (%): C, 51.90; H, 3.63; Cl, 12.95. Found: C, 51.92; H, 3.61; Cl, 12.87.

(d) *trans*-[$ReOBr_3(PPh_3)_2$] [1]

To a solution of 1.0 g of $(NH_4)[ReO_4]$ in 3 cm^3 conc. hydrobromic acid was added 5.0 g of triphenylphosphine in 50 cm^3 glacial acetic acid under nitrogen. A yellow precipitate formed, which was filtered, washed with glacial acetic acid and diethyl ether, and dried under vacuum. Yield = 90 %. Anal. Calcd. for $C_{36}H_{30}P_2OBr_3Re$ (mol. wt. = 966.49 g/mol) (%): C, 44.74; H, 3.13; Br, 24.80. Found: C, 44.40; H, 3.11; Br, 24.20.

(e) *trans*-[$ReOI_2(OEt)(PPh_3)_2$]

A mass of 5.0 g of triphenylphosphine in 30 cm^3 ethanol was added to 1.0 g of $(NH_4)[ReO_4]$ in 5 cm^3 hydroiodic acid (56%), and the mixture was heated under reflux for 15 minutes. The solution was allowed to cool to room temperature, and the resultant green precipitate was filtered, washed with ethanol and diethyl ether, and dried under vacuum. Yield = 85 %. Anal. Calcd. for $C_{38}H_{35}I_2O_2P_2Re$ (mol.wt. = 1142.8 g/mol) (%): C, 44.50; H, 3.43; I, 24.75. Found: C, 44.72; H, 3.91; I, 25.17.

(f) *cis*-[$ReO_2I(PPh_3)_2$] [2]

A mixture of 1.0 g of *trans*-[$ReOI_2(OEt)(PPh_3)_2$] in 50 cm^3 of acetone and 2 cm^3 of water was stirred at ambient temperature for an hour. The purple crystalline product which formed was filtered, washed with acetone and diethyl ether and dried under vacuum.

Yield = 80 %. Anal. Calcd. for $C_{36}H_{30}IO_2P_2Re$ (mol.wt. = 869.68 g/mol) (%): C, 49.72; H, 3.48; I, 14.59. Found: C, 49.72; H, 3.46; I, 14.41.

(g) *trans*-$[ReO_2(py)_4]Cl$ [3]

A mixture of 3 cm^3 pyridine and 0.5 cm^3 water was added to a solution of 0.50 g of *trans*-$[ReOCl_3(PPh_3)_2]$ in 10 cm^3 of acetone. The resultant mixture was refluxed for 90 minutes and then cooled in ice water for 30 minutes, to give an orange precipitate which was washed with toluene (2 x 3 cm^3) and diethyl ether (3 x 2 cm^3), and dried under vacuum. Yield = 90 %. Anal. Calcd. for $C_{20}H_{20}ClN_4O_2Re$ (mol.wt. = 570.06 g/mol) (%): C, 42.14; H, 3.54; Cl, 14.16; N, 9.83. Found: C, 42.72; H, 3.46; Cl, 14.41; N, 9.87.

2.2.2 General laboratory chemicals

All solvents used were of analytical grade, and were purified by standard methods [4]. All common laboratory chemicals were of analytical grade and were used without further purification.

The following chemicals were commercially obtained and used as received:

4-Aminoantipyrine	Aldrich (98.5 %)
2-Aminobenzaldehyde	Aldrich
Salicylaldehyde	Fluka (> 98.5 %)
2,6-Pyridinedicarboxaldehyde	Aldrich (97 %)
2-Mercaptobenzoic acid	Aldrich (97 %)
2-Aminothiophenol	Aldrich (99 %)
Phthalaldehyde	Fluka (≥ 98.5 %)
3,3'-Thiodipropionic acid	Aldrich (97 %)
2-Aminophenol	Aldrich (99 %)

1,2-Diaminobenzene	Aldrich (98 %)
Benzene-1,2-dithiol	Fluka (≥ 95 %)
Glyoxal (40% solution)	Riedel de Haën
4-Amino-2-hydroxybenzoic acid	Aldrich (99 %)
Neocuproine hydrate	Aldrich (99 %)
Selenium dioxide	Fluka (≥ 98 %)
Diglycolic acid	Aldrich (98 %)
Carbon disulfide	Holpro Analytics
Methyl iodide	Fluka (≥ 99 %)
2-Mercaptophenol	Aldrich (95 %)
2-Amino-benzothiazole	Aldrich (97 %)

2.3 Instrumentation

The ^{1}H NMR spectra were obtained at 300 K using a Bruker Avance III 400 MHz spectrometer. Deuterated dimethyl sulfoxide or deuterated chloroform was used as the solvent and the peak positions were obtained relative to $SiMe_4$. The infrared spectra were recorded on Bruker Tensor 27 FT-IR spectrophotometer in the 4000-200 cm^{-1} range.

The paramagnetism was measured by the Evans' method using a Bruker Avance III 400 MHz spectrometer and a 5 mm Wilmad NMR tube in $CDCl_3$. Diamagnetic corrections were calculated from Pascal constants [5].

UV-Vis spectra were obtained using a Perkin-Elmer 330 spectrophotometer. The extinction coefficients (ε) are given in $dm^3mol^{-1}cm^{-1}$. Emission spectra were recorded at room temperature with a Perkin-Elmer LS45 Flourescence Spectrometer.

Melting points were determined using an Electrothermal 9100 melting point apparatus with a benzoic acid standard used as a melting point test. The elemental analyses for carbon, hydrogen, nitrogen and sulfur were carried out on a Vario EL cube (Elementar Analysensysteme GmbH) instrument.

An Oxford Xcalibur, Nonius Kappa CCD or a Bruker Kappa Apex II diffractometer in the conventional ω-2θ scan mode and monochromatic Mo-Kα radiation (λ = 0.71073 Å) was used for the X-ray crystallographic analysis.

Conductivity measurements were carried out at 293K on a Phillips PW 9509 digital conductometer. The measurements were compared to the expected ranges of the different electrolyte types [Table 2.1] [6].

Table 2.1: Expected conductivity values ($ohm^{-1}cm^2mole^{-1}$) at 10^{-3} M.

	Electrolyte type	
Solvent	**1:1**	**2:1**
Acetonitrile	120 - 160	220 - 300
Dimethylformamide	65 - 90	130 - 170
Methanol	80 - 115	160 - 220

The cyclic voltammetry (CV) studies were carried out using a Bas Epsilon Version 1.30.64 system. A three electrode system was used which consisted of a platinum wire as the auxillary electrode, a glassy carbon working electrode and a non-aqueous $Ag/AgNO_3$ reference electrode in acetonitrile. Measurements were done in CH_2Cl_2, DMF or CH_3CN solutions with 0.1 M tetrabutylammonium perchlorate (TBAP) as supporting electrolyte. Before each run the sample solutions were first deoxygenated by bubbling nitrogen through the sample solutions. Under these conditions, ferrocene displays a reversible one electron process (Figure 2.1) with ΔE = 105 mV and $I_c/I_a \sim 1$ for the Fe(II)/Fe(III) couple.

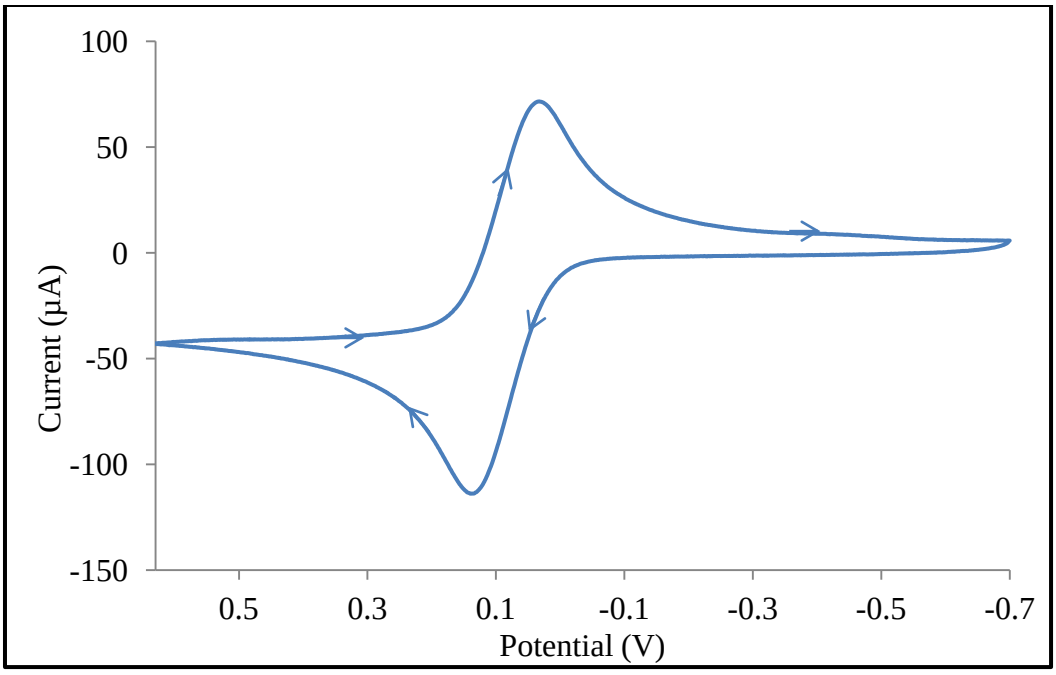

Figure 2.1: Cyclic voltammogram of ferrocene in the -0.7 to 0.6 V potential range at a scan rate of 50 mV/s.

2.4 References

[1] N.P. Johnson, C.J.L. Lock, G. Wilkinson, *Inorg. Synth.*, 1967, **9**, 145.

[2] G. Ciani, G.D. Alfonso, P. Romiti, A. Sironi, M. Freni, *Inorg. Chim. Acta*, 1983, **72**, 29.

[3] M.S. Ram, J.T. Hupp, *Inorg. Chem.*, 1991, **30**, 130.

[4] B.S. Furniss, A.J. Hannaford, P.W.G. Smith, A.R. Tatchell, *Vogel's textbook of Practical Organic Chemistry, Longman Scientific and Technical*, England (5th Ed), 1989.

[5] G.A. Bain, J.F. Berry, *J. Chem. Educ.*, 2008, **85**, 532.

[6] W.J. Geary, *Coord. Chem. Rev.*, 1971, **7**, 81.

Chapter 3

Coordination Modes of 4-Aminoantipyrine and its Schiff Base Derivatives towards Rhenium

3.1 Introduction

Pyrazolones is a class of organic compounds that have been studied extensively due to their pharmaceutical properties. Pyrazolone is a five-membered lactam ring which contains two nitrogen atoms and a ketone group in the same molecule (refer to Scheme 3.1), and it is an active moiety in pharmacological activity, such as anti-inflammatory agents [1], for the treatment of arthritis [2] and as analgesics [3]. Anticancer activity has also been reported [4]. Pyrazolones have also found applications outside the pharmaceutical field, such as in solvent extraction of metal ions [5], for analytical purposes [6] and as ligands in complexes with catalytic activity [7].

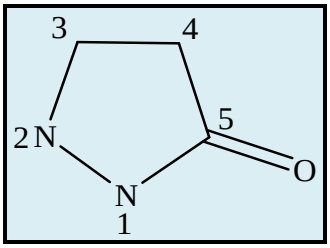

Scheme 3.1: Skeletal structure and numbering system for the pyrazolone ring.

From a coordination chemistry viewpoint, the only atoms available for coordination are the nitrogen atoms of the pyrazole ring and the oxygen atom of the carbonyl group (see Scheme 3.1). If the nitrogens are blocked by substitution, such as in antipyrine (Scheme 3.2), coordination can only be achieved through the oxygen atom.

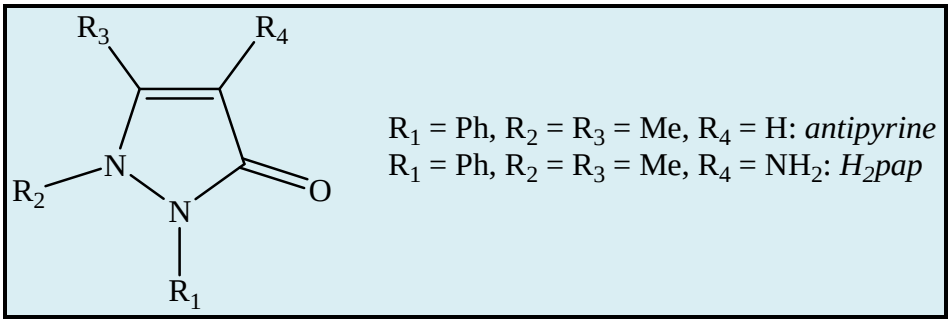

Scheme 3.2: Derivatives of pyrazole.

Transition metal complexes of 4-amino-2,3-dimethyl-1-phenyl-5-pyrazoline (4-aminoantipyrine, H_2pap) and its derivatives have been extensively studied due to their wide applications in the biological and therapeutical fields [8, 9]. Most of this research was done on the 3d transition metals, and in all of these H_2pap coordinated as a neutral ligand: as a bidentate in $[M(H_2pap)_2X_2]$ (M = Co, Ni; X^- = Cl^-, NO_3^-, SCN^-) or as a monodentate through the neutral amino nitrogen in $[M(H_2pap)_4]Br_2$ (M = Co, Ni) [10].

In this chapter, the coordination behaviour of 4-aminoantipyrine (H_2pap) and its Schiff base derivatives (Scheme 3.3) with the oxorhenium(V) and tricarbonyl rhenium(I) cores are reported. The reactions of *trans*-$[ReOX_3(PPh_3)_2]$ (X = Cl, Br) with H_2pap were studied, and the complexes *cis*-$[ReX_2(pap)(H_2pap)(PPh_3)](ReO_4)$ (X = Cl (**1**), Br (**2**)) were isolated. The ligand pap is coordinated monodentately through the doubly deprotonated amino nitrogen as an imide, and H_2pap is coordinated bidentately *via* the neutral amino nitrogen and neutral ketonic oxygen. The reactions of *trans*-$[ReOBr_3(PPh_3)_2]$ and *cis*-$[ReO_2I(PPh_3)_2]$ with 4-(2-aminobenzylideneamino)-1,2-dihydro-2,3-dimethyl-1-phenylpyrazol-5-one (H_2nap) and 4-(2-hydroxybenzylidene amino)-1,2-dihydro-2,3-dimethyl-1-phenylpyrazol-5-one (Hoap) are also reported. The complexes *cis*-$[Re(nap)Br_2(PPh_3)]Br$ (**3**), $[ReO(OEt)(Hnap)(PPh_3)]I$ (**4**) and $[ReO(OMe)(oap)(PPh_3)]I$ (**5**) were isolated and structurally characterized. The reactions of the Schiff base derivatives 1,2-(diimino-4'-antipyrinyl)ethane (dae) and 2,6-*bis*(4-amino-1,2-dihydro-2,3-dimethyl-1-phenylpyrazol-5-one)pyridine (bap) with $[Re(CO)_5X]$ (X = Br or Cl) produced *fac*-$[Re(CO)_3(dae)Cl]$ (**6**) and *fac*-$[Re(CO)_3(bap)Br]$ (**7**) respectively.

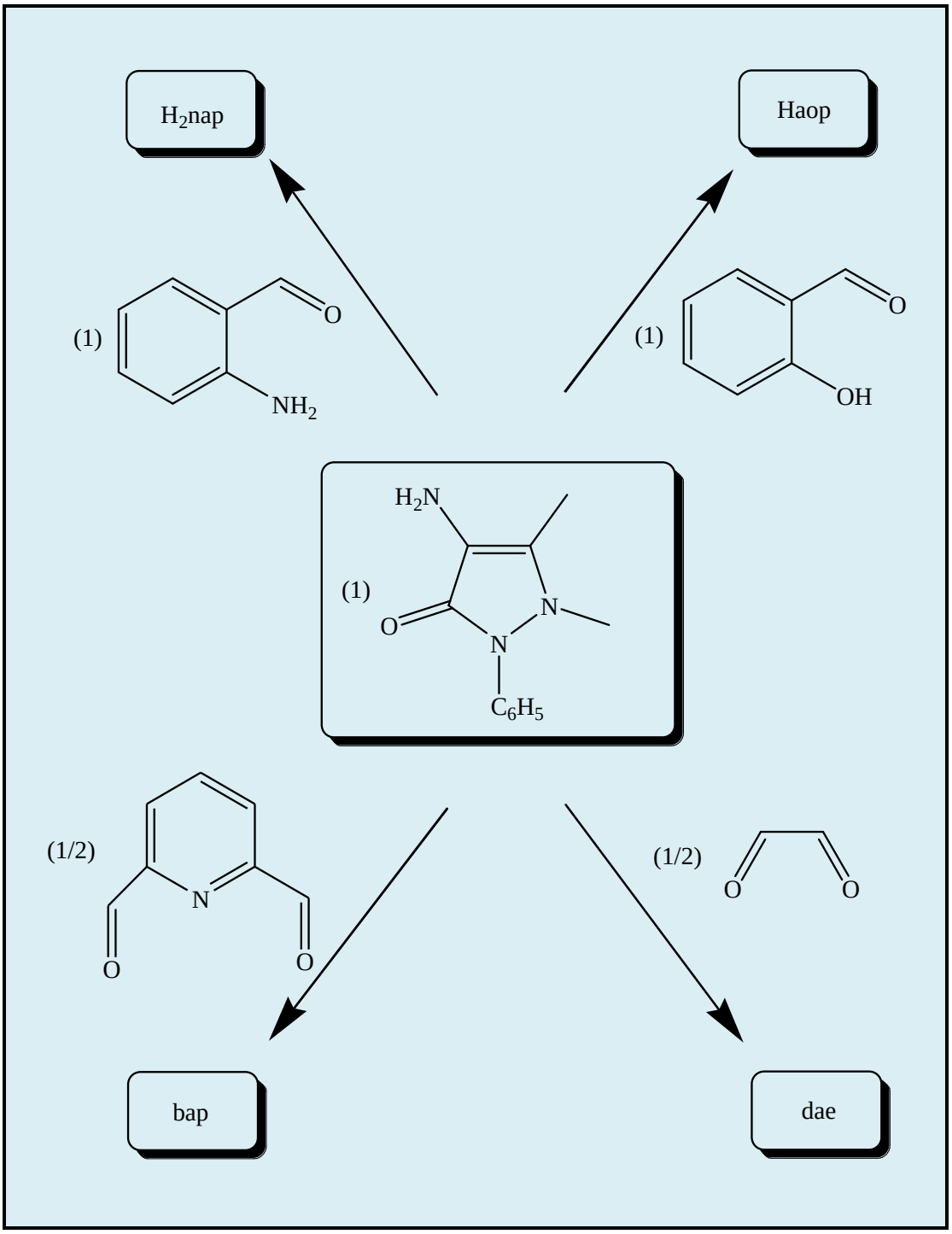

Scheme 3.3: Reaction pathway for the formation of Schiff base derivatives of 4-aminoantipyrine.

3.2 Experimental

3.2.1 Synthesis of (4*Z*)-4-(2-aminobenzylideneamino)-1,2-dihydro-2,3-dimethyl-1-phenylpyrazol-5-one (H_2nap)

A solution of 0.840 g of 4-aminoantipyrine (4.13 mmol) in 20 cm^3 of methanol was added dropwise to a solution of 0.505 g of 2-aminobenzaldehyde (4.17 mmol) in 30 cm^3 of toluene, which was kept at –18 °C (with a sludge bath of liquid nitrogen/1,2-dichlorobenzene). The reaction mixture was allowed to warm to room temperature, and then heated under refluxed for three hours. On cooling the solution to room temperature, a yellow precipitate separated which was removed by filtration and dried under vacuum. Yield = 87 %, m.p. = 168 °C. Anal. Calcd. (%) for $C_{18}H_{18}N_4O$: C, 70.6; H, 5.9; N, 18.3. Found: C, 70.5; H, 6.1; N, 18.4. IR (ν_{max}/cm^{-1}): *v*(N-H) 3039(m), 3050(m); *v*(C=O) 1646(s); *v*(C=N) 1612(s). ^{1}H NMR (295K, ppm): 9.62 (s, 1H, *H*(7)); 7.52 (t, 2H, *H*(15), *H*(17)); 7.36 (m, 3H, *H*(14), *H*(16), *H*(18)); 7.23 (s, 2H, NH_2); 7.18 (d, 1H, *H*(2)); 7.09 (t, 1H, *H*(3)); 6.73 (d, 1H, *H*(5)); 6.57 (t, 1H, *H*(4)); 3.11 (s, 3H, C(12)H_3); 2.36 (s, 3H, C(11)H_3).

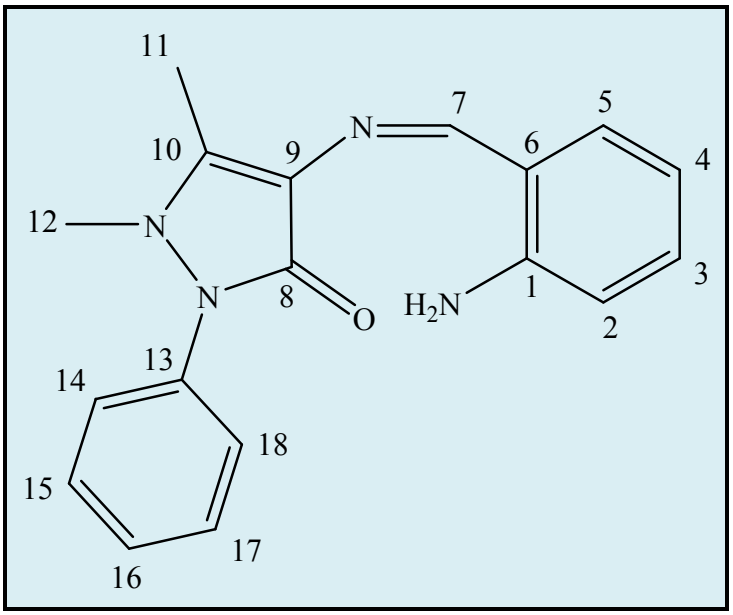

Figure 3.1: Structure of H_2nap.

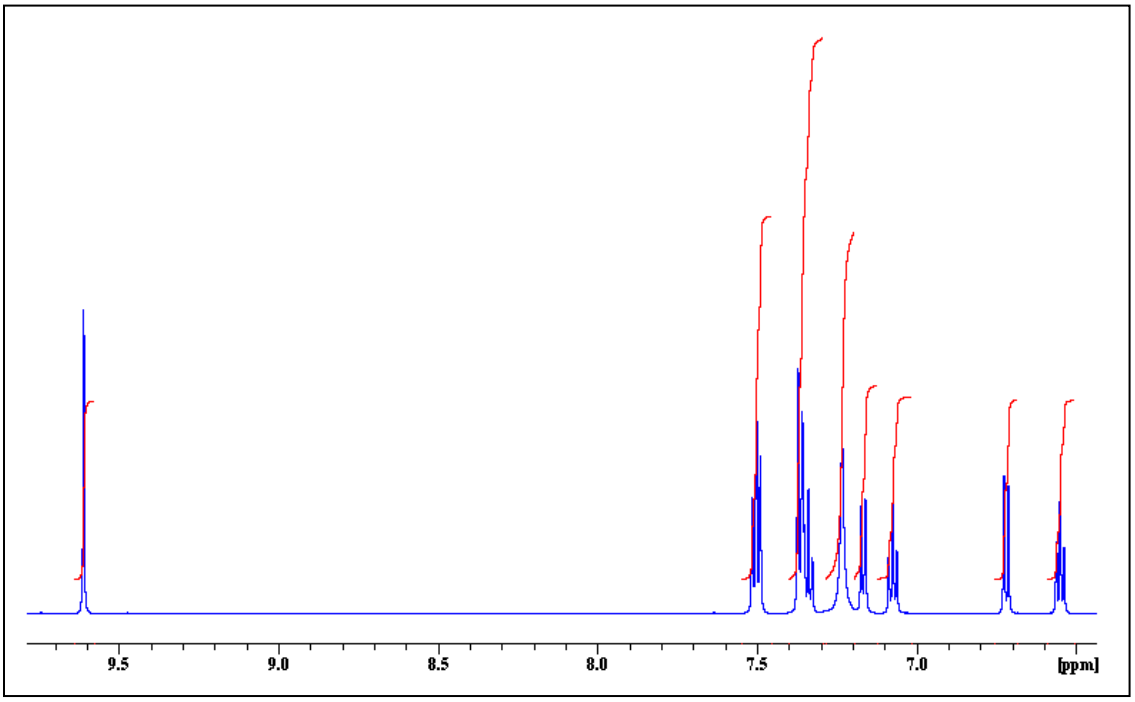

Figure 3.2: ^{1}H NMR spectrum of H_2nap in the range 6.50-9.80 ppm.

3.2.2 Synthesis of (4*Z*)-4-(2-hydroxybenzylideneamino)-1,2-dihydro-2,3-dimethyl-1-phenylpyrazol-5-one (Hoap)

A mass of 3.038 g of 4-aminoantipyrine (149 mmol) and 1.776 g of salicylaldehyde (145 mmol) were dissolved in 50 cm^3 of methanol. The resultant solution was heated to reflux under nitrogen for three hours to give a yellow solution, which was cooled to room temperature and filtered. The filtrate was placed in a cold room (0 °C) overnight to produce yellow crystals, which was collected by filtration and dried under vacuum. Yield = 96 %, m.p. = 199 °C. Anal. Calcd. (%) for $C_{18}H_{17}N_3O_2$: C, 70.3; H, 5.6; N, 13.7. Found: C, 70.3; H, 5.5; N, 13.7. IR (ν_{max}/cm^{-1}): ν(C=O) 1653(s); ν(C=N) 1594(s). ^{1}H NMR (295K, ppm): 9.68 (s, 1H, *H*(7)); 7.54 (t, 2H, *H*(15), *H*(17)); 7.45 (d, 1H, *H*(16)); 7.38 (m, 3H, *H*(14), *H*(18), *H*(5)); 7.30 (t, 1H, *H*(3)); 6.91 (m, 2H, *H*(2), *H*(4)); 3.19 (s, 3H, C(12)H_3); 2.47 (s, 1H, O*H*); 2.39 (s, 3H, C(11)H_3). UV-Vis (CH_2Cl_2, λ_{max} (ε, M^{-1}cm^{-1})): 305 (13815), 320 (16964), 350 (27711), 366 (23155).

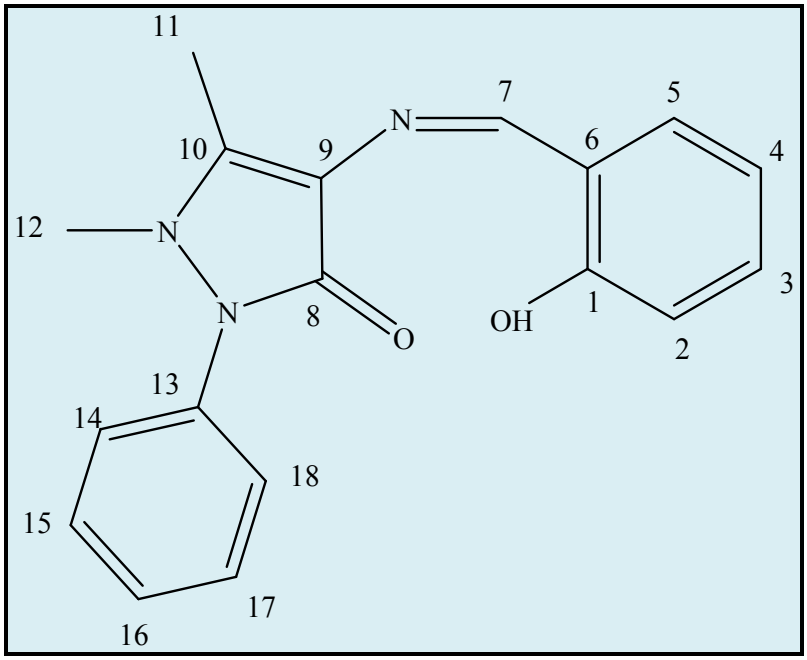

Figure 3.3: Structure of Hoap.

3.2.3 Synthesis of 1,2-(diimino-4'-antipyrinyl)ethane (dae)

A mixture of glyoxal (0.20 g, 3.44 mmol) and 4-aminoantipyrine (1.40 g, 6.88 mmol) was dissolved in 50 cm^3 of ethanol and heated under reflux for 3 hours. The solution was allowed to cool to room temperature and the resultant yellow precipitate was collected by filtration and washed with acetone. Yield = 87 %, m.p. > 300 °C. Anal. Calcd. (%) for $C_{24}H_{24}N_6O_2$: C, 67.3; H, 5.7; N, 19.6. Found: C, 67.4; H, 5.8; N, 19.3. IR (ν_{max}/cm^{-1}): ν(C=O) 1649; ν(C=N) 1578. ^{1}H NMR (295K, ppm): 9.22 (s, 2H, *H*(1), *H*(2)); 7.46 (t, 4H, *H*(10), *H*(12), *H*(21), *H*(23)); 7.43-7.50 (m, 6H, *H*(9), *H*(11), *H*(13), *H*(20), *H*(22), *H*(24)); 3.21 (s, 6H, C(7)H_3, C(18)H_3); 2.42 (s, 6H, C(6)H_3, C(17)H_3). UV-Vis (CH_2Cl_2, λ_{max} (ε, $M^{-1}cm^{-1}$)): 378 (60800), 400 (50000).

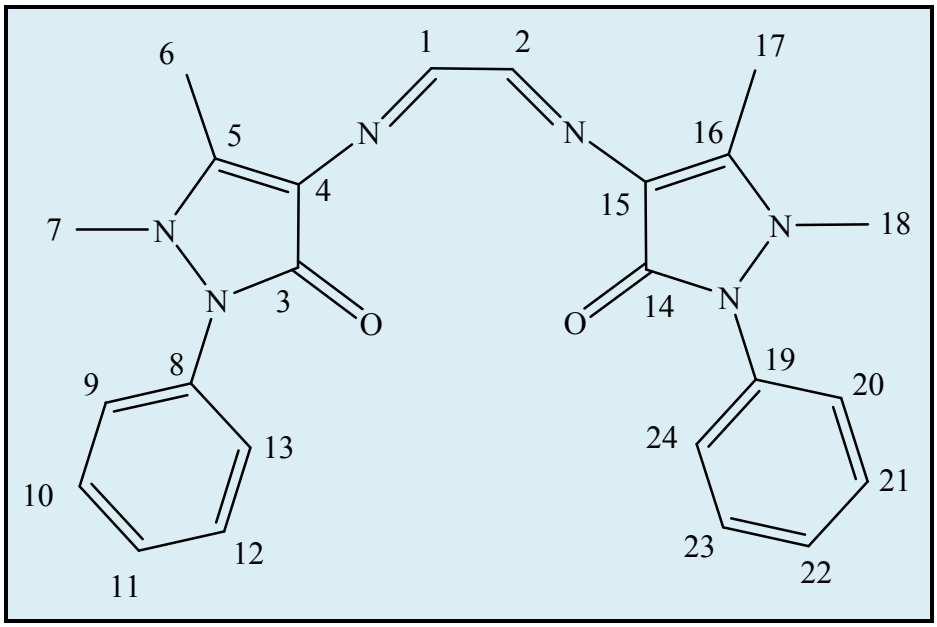

Figure 3.4: Structure of dae.

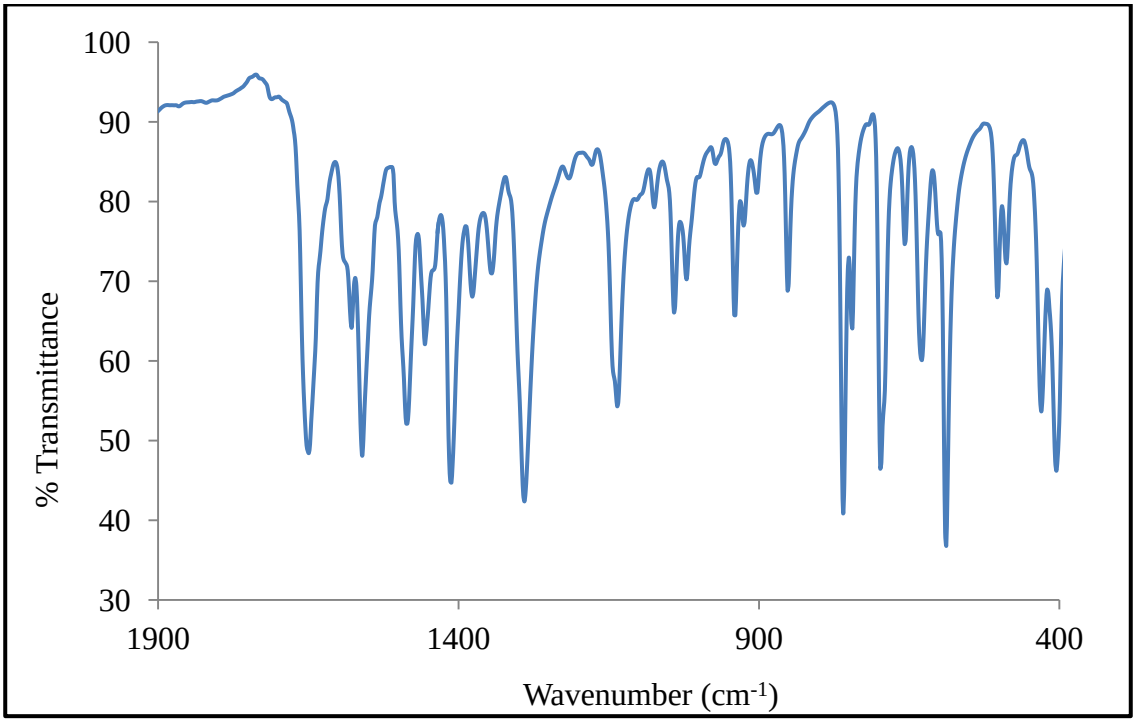

Figure 3.5: IR spectrum of dae in the 400-1900 cm^{-1} range.

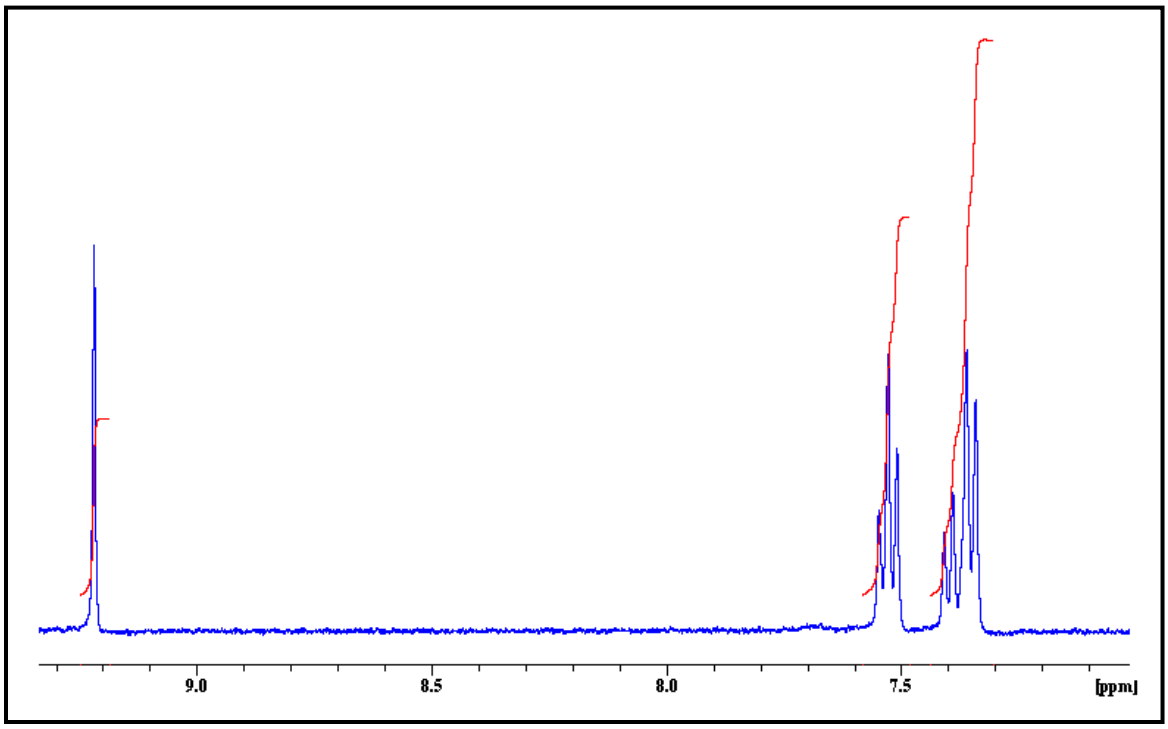

Figure 3.6: ^{1}H NMR spectrum of dae in the 7.0-9.3 ppm range.

3.2.4 Synthesis of 2,6-*bis*(4-amino-1,2-dihydro-2,3-dimethyl-1-phenyl-pyrazol-5-one)pyridine (bap)

A solution of 0.067 g (5.0 mmol) of 2,6-pyridinedicarbaldehyde in 20 $cm^3$of methanol was added dropwise to a solution of 2.00 g (9.8 mmol) of 4-aminoantipyrine in 30 cm^3 of methanol. The solution was allowed to boil under reflux under nitrogen. After three hours the solution was cooled to room temperature and a yellow precipitate was filtered off and dried under vacuum. The product was recrystallized from methanol to produce yellow crystals. Yield = 78 %, m.p. = 262 °C. Anal. Calcd. (%) for $C_{29}H_{27}N_7O_2$: C, 68.9; H, 5.4; N, 19.4. Found: C, 68.7; H, 5.5; N, 19.1. IR (ν_{max}/cm^{-1}): *v*(C=O) 1639(s); *v*(C=N) 1581(m). ^{1}H NMR (295K, ppm): 9.57 (s, 2H, *H*(1), *H*(7)); 8.09 (d, 2H, *H*(3), *H*(5)); 7.94 (t, 1H, *H*(4)); 7.54 (t, 4H, *H*(15), *H*(17), *H*(26), *H*(28)); 7.35-7.43 (m, 6H, *H*(14), *H*(16), *H*(18), *H*(25), *H*(27), *H*(29)); 3.25 (s, 6H, C(12)H_3, C(23)H_3); 2.48 (s, 6H, C(11)H_3, C(22)H_3). UV-Vis (CH_2Cl_2, λ_{max} (ε, $M^{-1}cm^{-1}$)): 355 (61400).

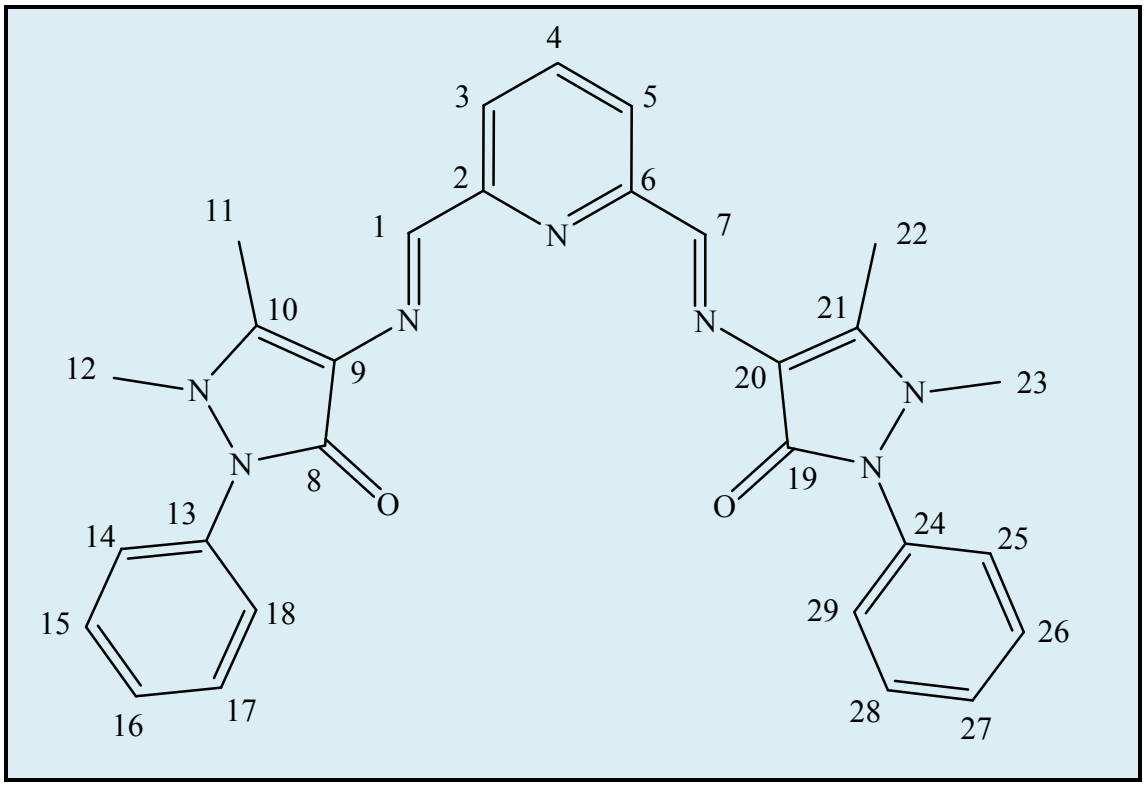

Figure 3.7: Structure of bap.

3.2.5 Synthesis of $[ReX_2(pap)(H_2pap)(PPh_3)](ReO_4)$ (X = Cl (1), Br (2))

Trans-$[ReOX_3(PPh_3)_2]$ (120 μmol) and H_2pap (55 mg, 270 μmol) were dissolved in dry ethanol, and the mixture was heated under reflux for two hours. After heating was stopped, the resulting green solution was allowed to cool to room temperature. For compound **1**, a green precipitate was collected by filtration. It was washed with diethyl ether, dried under vacuum, and recrystallized from a 1:2 (v/v) ethanol/dichloromethane mixture to give green needles. For **2**, no precipitate formed. However, the slow evaporation of the mother liquor over a period of two days gave green crystals, which were suitable for X-ray diffraction analysis.

*Analysis of **1***: Yield = 71 %, m.p. > 300˚C. Anal. Calcd. (%): C, 40.9; H, 3.4; N, 7.2. Found: C, 41.0; H, 3.4; N, 7.3. IR (ν_{max}/cm^{-1}): ν(NH_2) 3060(w); ν(C=O) 1655(s), 1614(m); ν(Re-N) 528(m); ν(Re=N) 1070(m); ν(Re-O) 428(m); ν(Re^{VII}=O) 907(s). ^{1}H NMR (295K, ppm): 7.60-7.90 (m, 15H, PP*h*$_3$); 7.58 (d, 2H, *H*(11), *H*(18)); 7.55 (t, 4H, *H*(8), *H*(10), *H*(19), *H*(21)); 7.50 (d, 2H, *H*(7), *H*(22)); 7.46 (dd, 2H, *H*(9), *H*(20)); 2.21

(s, 3H, C(15)H_3); 2.55 (s, 3H, C(4)H_3); 3.25 (s, 3H, C(16)H_3); 3.61 (s, 3H, C(5)H_3). Conductivity (10^{-3} M, DMF): 69 $ohm^{-1}cm^2mol^{-1}$. UV-Vis (MeOH, λ_{max} (ε, $M^{-1}cm^{-1}$)): 374 (11798).

Analysis of ***2***: Yield = 68 %, m.p. > 300˚C. Anal. Calcd. (%): C, 38.0; H, 3.10; N, 6.7. Found: C, 38.2; H, 3.3; N, 6.6. IR (ν_{max}/cm^{-1}): $\nu(NH_2)$ 3054(w); ν(C=O) 1666(s), 1608(m); ν(Re-N) 511(m); ν(Re=N) 1074(m); ν(Re-O) 398(m); $\nu(Re^{VII}=O)$ 910(s). ^{1}H NMR (295K, ppm): 7.62-7.89 (m, 15H, PPh_3); 7.59 (d, 2H, *H*(11), *H*(18)); 7.56 (t, 4H, *H*(8), *H*(10), *H*(19), *H*(21)); 7.50 (d, 2H, *H*(7), *H*(22)); 7.46 (dd, 2H, *H*(9), *H*(20)); 2.23 (s, 3H, C(15)H_3); 2.58 (s, 3H, C(4)H_3); 3.29 (s, 3H, C(16)H_3); 3.68 (s, 3H, C(5)H_3). Conductivity (10^{-3} M, DMF): 71 $ohm^{-1}cm^2mol^{-1}$. UV-Vis (MeOH, λ_{max} (ε, $M^{-1}cm^{-1}$)): 374 (13174).

3.2.6 Synthesis of *cis*-[Re(nap)Br_2(PPh_3)]Br (3)

Solid *trans*-[$ReOBr_3(PPh_3)_2$] of mass 105 mg (109 μmol) was added to a solution of 67 mg of H_2nap (219 μmol) in 20 cm^3 ethanol, and the mixture was heated under reflux for 3 h. After cooling to room temperature, the solution was filtered and the filtrate was allowed to evaporate slowly at room temperature. After two days brown crystals were collected. Yield = 52 %, m.p. = 192 °C. Anal. Calc. (%): C, 43.6; H, 3.2; N, 5.6. Found: C, 43.8; H, 3.4; N, 5.6. IR (ν_{max}/cm^{-1}): ν(C=O) 1593(m); ν(C=N) 1575(s); ν(Re=N) 1095(m); ν(Re-O) 512(m); ν(Re-N) 440(m). ^{1}H NMR (295K, ppm): 9.64 (s, 1H, *H*(7)); 7.50-7.70 (m, 24H, PPh_3, *H*(2), *H*(3), *H*(4), *H*(5), *H*(14), *H*(15), *H*(16), *H*(17), *H*(18)); 3.18 (s, 3H, C(12)H_3); 2.32 (s, 3H, C(11)H_3). Conductivity (10^{-3} M, DMF): 83 $ohm^{-1}cm^2mol^{-1}$. UV-Vis (MeOH, λ_{max} (ε, $M^{-1}cm^{-1}$)): 313 (10450), 370 (5110).

3.2.7 Synthesis of [ReO(OEt)(Hnap)(PPh_3)]I (4)

A mass 104 mg of *cis*-[$ReO_2I(PPh_3)_2$] (120 μmol) and 72 mg of H_2nap (235 μmol) were dissolved in 20 cm^3 ethanol, and the mixture was heated under reflux for 3 h. After cooling to room temperature, the solution was filtered and the filtrate was left to evaporate at room temperature. After 3 days red crystals were collected. Yield = 61 %,

m.p. = 183 °C. Anal. Calc. (%) for **4**.½EtOH.½H_2O: C, 48.1; H, 4.2; N, 6.6. Found: C, 48.2; H, 4.4; N, 6.8. IR (ν_{max}/cm^{-1}): *ν*(N-H) 3049(w); *ν*(C=O) 1600(s); *ν*(C=N) 1578(s); *ν*(Re=O) 940(m); *δ*(OCH_2) 907(s); *ν*(Re-O) 510(m); *ν*(Re-NH) 440(m). ^{1}H NMR (295K, ppm): 9.62 (s, 1H, *H*(12)); 7.50-7.70 (m, 6H, *H*(2), *H*(3), *H*(5), *H*(6), *H*(15), *H*(18)); 7.35-7.48 (m, 15H, PP*h*$_3$); 7.22-7.32 (m, 3H, *H*(4), *H*(16), *H*(17)); 3.18 (s, 3H, C(11)*H*$_3$); 2.68 (t, 2H, C(37)*H*$_2$); 2.34 (s, 3H, C(10)*H*$_3$); 2.35 (d, 3H, C(38)*H*$_3$). Conductivity (10^{-3} M, MeOH): 116 $ohm^{-1}cm^2mol^{-1}$. UV-Vis (MeOH, λ_{max} (ε, $M^{-1}cm^{-1}$)): 317 (13250), 370 (12300), 491(420).

3.2.8 Synthesis of [ReO(OMe)(oap)(PPh$_3$)]I (5)

A mixture of *cis*-[$ReO_2I(PPh_3)_2$] (102 mg, 117 μmol) and Hoap (73 mg, 237 μmol) in 20 cm^3 of methanol was heated under reflux for 2 h. After cooling to room temperature, the solution was filtered, and the filtrate was evaporated slowly, yielding brown crystals after 3 days. Recrystallization from MeOH/CH_2Cl_2 produced brown crystals suitable for X-ray diffraction analysis. Yield = 58 %, m.p. = 179 °C. Anal. Calc. (%) for **5**.CH_2Cl_2: C, 45.0; H, 3.6; N, 4.1. Found: C, 44.8; H, 3.8; N 4.4. IR (ν_{max}/cm^{-1}): *ν*(C=O) 1599(s); *ν*(C=N) 1569(s); *ν*(Re=O) 940(s); *ν*(Re-O) 530(m), 510(m).^{1}H NMR (295K, ppm): 9.10 (s, 1H, *H*(7)); 7.92 (d, 1H, *H*(2)); 7.74-7.88 (m, 4H, *H*(3), *H*(4), *H*(152), *H*(172)); 7.69 (d, 2H, *H*(142), *H*(182)); 7.42-7.66 (m, 15H, PP*h*$_3$); 7.04 (t, 1H, *H*(162)); 6.75 (d, 1H, *H*(5)); 3.63 (s, 3H, C(122)*H*$_3$); 2.94 (s, 3H, C(37)*H*$_3$); 2.86 (s, 3H, C(11)*H*$_3$). Conductivity (10^{-3} M, MeOH): 106 $ohm^{-1}cm^2mol^{-1}$. UV-Vis (MeOH, λ_{max} (ε, $M^{-1}cm^{-1}$)): 316 (12400), 370 (12250), 481(350).

3.2.9 Synthesis of *fac*-[Re(CO)$_3$(bap)Br] (6)

A mass of 249 mg (493 μmol) of bap and 100 mg (246 μmol) of *fac*-[$Re(CO)_5Br$] were dissolved in 20 cm^3 of toluene. The solution was heated with stirring under nitrogen for three hours. The red solution was allowed to cool to room temperature and the resultant orange precipitate was filtered and washed with diethyl ether. Orange crystals were obtained by recrystallization from dichloromethane. Yield = 63 %, m.p. = 278-280 °C.

Anal. Calcd. (%) for $C_{32}H_{27}BrN_7O_5Re$: C, 44.9; H, 3.2; H, 11.5. Found: C, 44.6; H, 3.3; N, 11.3. IR (ν_{max}/cm^{-1}): $\nu(CO)_{fac}$ 2020(vs), 1920(vs), 1902(vs); ν(C=O) 1658(s); ν(C=N) 1586(m); ν(Re-N) 456(m), 475(m). ^{1}H NMR (295K, ppm): 10.14 (s, 1H, *H*(7)); 9.33 (s, 1H, *H*(6)); 8.32 (m, 2H, P*h*); 8.10 (d, 2H, *H*(2), *H*(4)); 7.95 (t, 1H, *H*(3)); 7.55 (m, 3H, P*h*); 7.37 (m, 5H, P*h*); 3.24 (s, 3H, C(15)H_3); 3.22 (s, 3H, C(25)H_3); 2.58 (s, 3H, C(14)H_3); 2.54 (s, 3H, C(24)H_3). Conductivity (10^{-3}M, CH_3CN): 5 $ohm^{-1}cm^2mol^{-1}$. UV-Vis (CH_3CN, λ_{max} (ε, $M^{-1}cm^{-1}$)): 371 (140800), 446 (82140).

3.2.10 Synthesis of *fac*-[Re(CO)$_3$(dae)Cl] (7)

A solution of 173 mg (404 μmol) of dae was dissolved in 10 cm^3 of methanol. To this was added 101 mg (277 μmol) of *fac*-[$Re(CO)_5Cl$] in 10 cm^3 of methanol. The combined solution was heated to refluxed under nitrogen for two hours. The resultant deep red solution was allowed to cool and the red precipitate which formed was washed with diethyl ether. Red crystals were obtained by the slow evaporation of the mother liquor which were filtered and dried under vacuum. Yield = 69 %, m.p. = 231 °C. Anal. Calcd. (%) for **7**.H_2O: C, 43.1; H, 3.5; N, 11.2. Found: C, 43.0; H, 3.7; N, 10.9. IR (ν_{max}/cm^{-1}): $\nu(CO)_{fac}$ 2017(vs), 1905(vs); ν(C=O) 1654(s); ν(C=N) 1562(s); ν(Re-N) 467(m). ^{1}H NMR (295K, ppm): 8.88 (s, 2H, *H*(1), *H*(2)); 7.32-7.64 (m, 10H, P*h*); 3.28 (s, 6H, C(15)H_3, C(35)H_3); 2.32 (s, 6H, C(14)H_3, C(34)H_3). Conductivity (10^{-3} M, CH_3CN): 21 $ohm^{-1}cm^2mol^{-1}$. UV-Vis (CH_3CN, λ_{max} (ε, M^{-1} cm^{-1})): 385 (15020), 402(sh) (14320), 510 (9410).

3.2.11 X-ray Crystallography

X-ray diffraction studies were performed at 200(2) K using a Nonius Kappa CCD (for Hoap, H_2nap, **1**, **2** an **3**), an Oxford Xcalibur (for **4** and **5)** and a Bruker Kappa Apex II (for **6** and **7**) diffractometers with graphite monochromated Mo Kα radiation (λ = 0.71073 Å). The structures were solved by direct methods applying SIR97 [11] and refined by least-squares procedures using SHELXL-97 [12]. All non-hydrogen atoms were refined anisotropically, and the hydrogen atoms were calculated in idealized

geometrical positions. The data were corrected by a numerical absorption correction [13] after optimizing the crystal shape with XShape [14]. In **3,** the Br^- counter-ion is highly disordered, with a lot of remaining electron density present around it which could not be described properly. However, connectivity and other general features of the structure were confidently determined, and the molecular positional parameters of the atoms in the 'inner core' are well defined. In **4,** the hydrogen atoms in the water molecule have not been considered in the refinement, with all the other hydrogens constrained. In **5,** a split model has been applied to describe the disorder in N(2), N(3), C(13)–C(18). Crystal and structure refinement data are given in Tables 3.5-3.9 with selected bond distances and angles in Tables 3.10-3.17. Complete data are stored on the CD pasted onto the back of this thesis.

3.3 Results and Discussion

3.3.1 Synthesis and characterization of Hoap

The reaction of 4-aminoantipyrine and salicylaldehyde in methanol produced the potentially tridentate Schiff base ligand Hoap. Crystals of the compound were obtained from a methanol solution of Haop left at 0˚C overnight. It is soluble in dichloromethane and insoluble in alcohols and acetonitrile.

Two absorptions at 1653 and 1594 $cm^{-1}$are observed in the IR spectrum of Hoap (Figure 3.8) due to the ketone [ν(C=O)] and imine [ν(C=N)] stretching frequencies respectively. The ^{1}H NMR spectrum (Figure 3.9) shows the signal of the imine proton as a one-proton singlet at 9.68 ppm. Five signals appear in the aromatic region in the form of a triplet, doublet, multiplet, triplet and triplet integrating for two, one, three, one and two protons respectively. Two singlets for the methyl protons of the pyrazole ring are found at 2.39 and 3.19 ppm. The OH protons' signal appears as a broad singlet at 2.47 ppm.

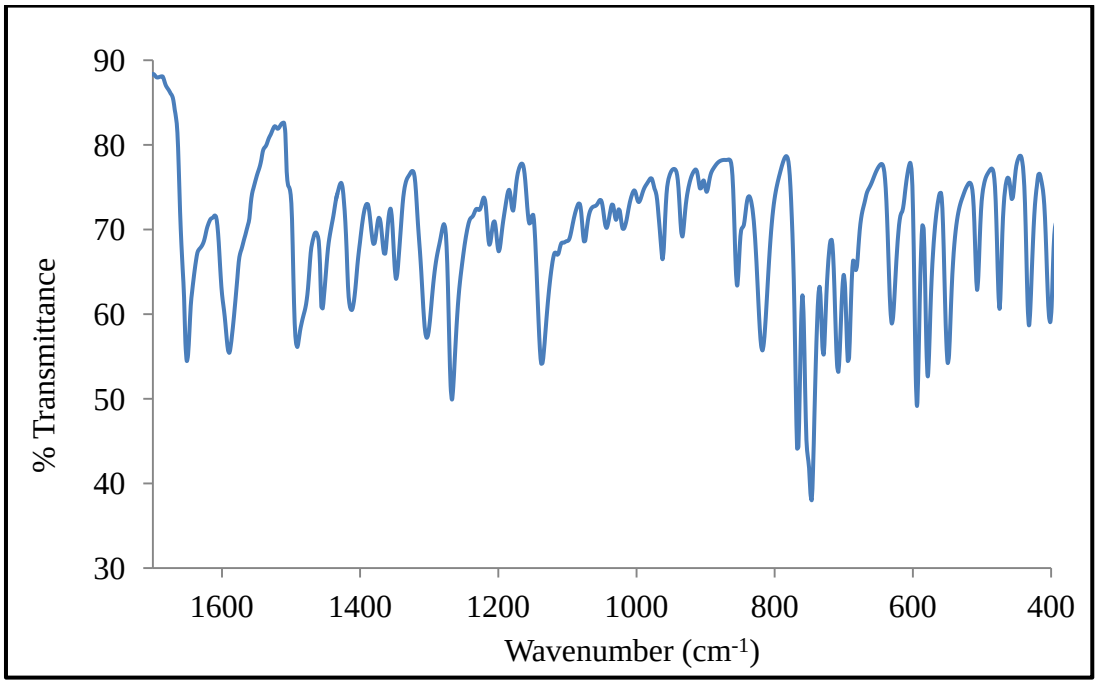

Figure 3.8: IR spectrum of Hoap.

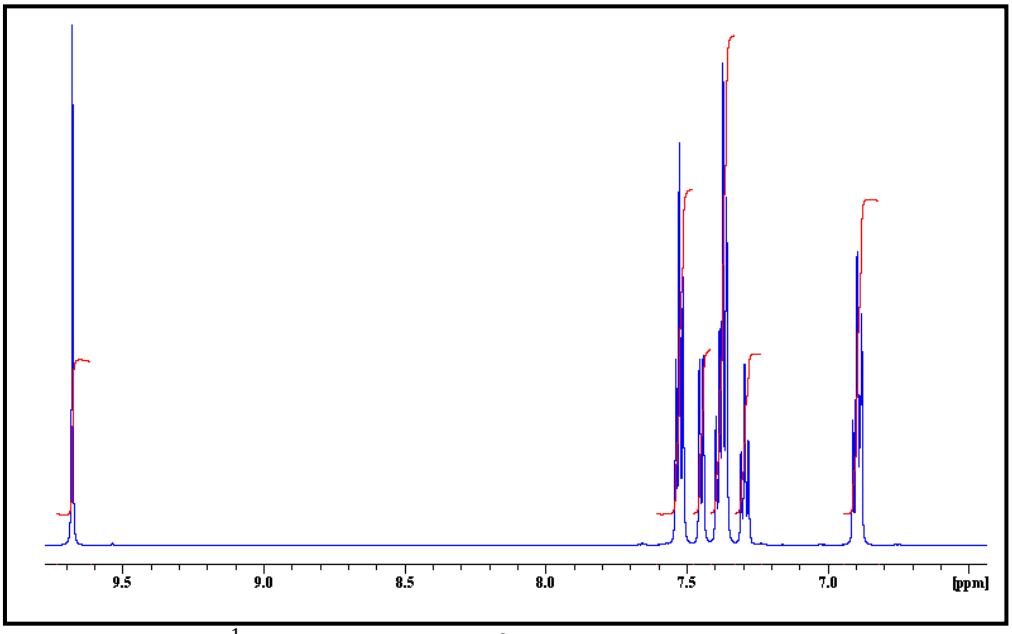

Figure 3.9: ^{1}H NMR spectrum of Hoap in the 6.5-9.7 ppm range.

An ORTEP view of the asymmetric unit of Hoap is shown in Figure 3.10. It consists of a nitrogen-bonded phenyl ring, a five-membered pyrazole ring and a phenol ring. The phenol and pyrazole rings are almost coplanar with a dihedral angel of 5.82˚, while the

nitrogen-bonded phenyl ring has a dihedral angle of 48.22˚ with the phenol ring. The nitrogen-bonded phenyl moiety adopts a staggered conformation relative to the pyrazole ring, with the least-squares planes intersecting at an angle of 43.09˚ (Figure 3.12).

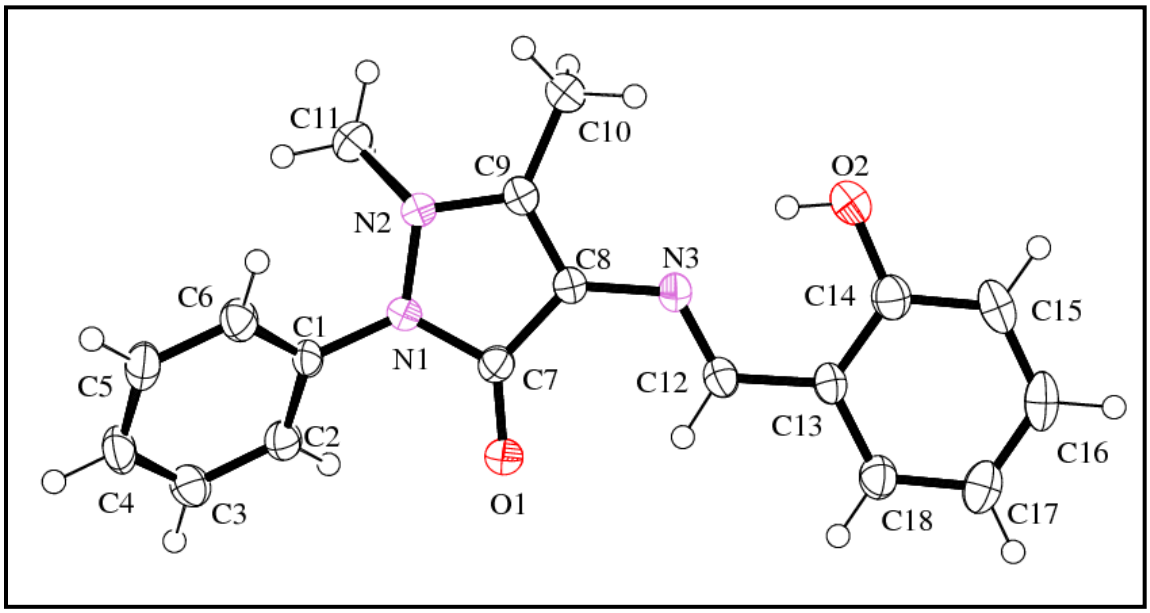

Figure 3.10: An ORTEP view of ligand Hoap showing 50% probability displacement ellipsoids and the atom labeling.

The N(3)-C(12) bond length of 1.286(2) Å is indicative of an imine double bond with the N(3)-C(12)-C(13) = 121.2(1)˚ and C(8)-N(3)-C(12) = 122.1(1)˚ bond angles close to the expected 120˚ angle for sp^2 hybridized atoms. The C-O bond distances of C(7)-O(1) [1.235(2) Å] and C(14)-O(2) [1.359(2) Å] are typical of C=O and C-OH bonds respectively, and correspond to similar compounds in the literature [15,16]. The delocalization of π electrons in the aromatic rings is evident in the bond lengths of the C(1)-C(6) [average = 1.385(2) Å] phenyl and the C(13)-C(18) [average = 1.389(2) Å] phenol rings. The C(8)-C(9) [1.358(2) Å] bond length in the 5-membered pyrazole ring is considerably shorter than the C(7)-C(8) [1.445(2) Å] bond, and can be regarded as a double bond while the latter is considered to be single. Intramolecular hydrogen-bonding is found within the molecule between the phenol hydrogen [O(2)-H(2)] and the imine nitrogen atom [N(3)] (Figure 3.11). Adjacent molecules are connected through intermolecular bonds involving the ketonic oxygen atom (Table 3.1).

Table 3.1: Hydrogen-bond distances (Å) and angles (˚) in Hoap**.**

D-H•••A	D-H	H•••A	D•••A	D-H•••A
O(2)-H(2)•••N(3)	0.84	1.87	2.612(2)	146
C(10)-H(10B)•••O(1)	0.98	2.46	3.193(2)	131
C(11)-H(11A)•••O(1)	0.98	2.46	3.433(2)	175
C(12)-H(12)•••O(1)	0.95	2.40	3.079(2)	128

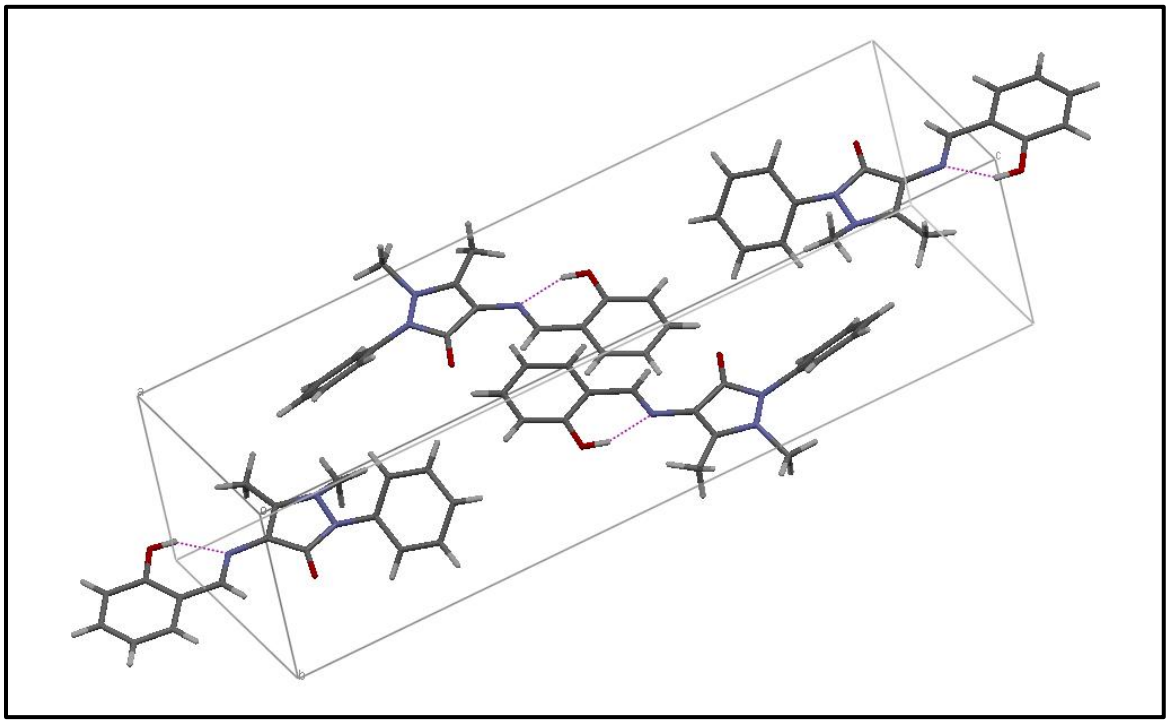

Figure 3.11: Packing diagram in the unit cell of Hoap showing the intramolecular hydrogen-bonds.

3.3.2 Synthesis and characterization of bap

The potentially tridentate Schiff base ligand bap was isolated by the condensation reaction of 2,6-pyridinedicarbaldehyde with two mole equivalents of 4-aminoantipyrine. Yellow crystals were obtained by recrystallization from a CH_2Cl_2:MeOH (1:1) solution. The ligand is soluble in acetonitrile and dichloromethane, but is insoluble in alcohols.

The infrared spectrum for the bap ligand shows the C=N stretching frequency as a medium intensity peak at 1581 cm^{-1}. The strong peak at 1639 cm^{-1} is ascribed to *v*(C=O). The ^{1}H NMR spectrum of bap (Figure 3.12) emphasizes the symmetry within the molecule. The nine protons of one half of the molecule are magnetically equivalent to the corresponding nine protons of the other half of the molecule. The imine protons appear clearly as a two-proton singlet at 9.57 ppm. The three protons on the pyridine ring can be seen as a two-proton doublet (8.09 ppm) and a one-proton triplet (7.94 ppm). The phenyl protons appear as a four-proton triplet (7.52 ppm) and a six-proton multiplet (7.35-7.43 ppm). The four methyl groups are displayed as two separate six-proton singlets.

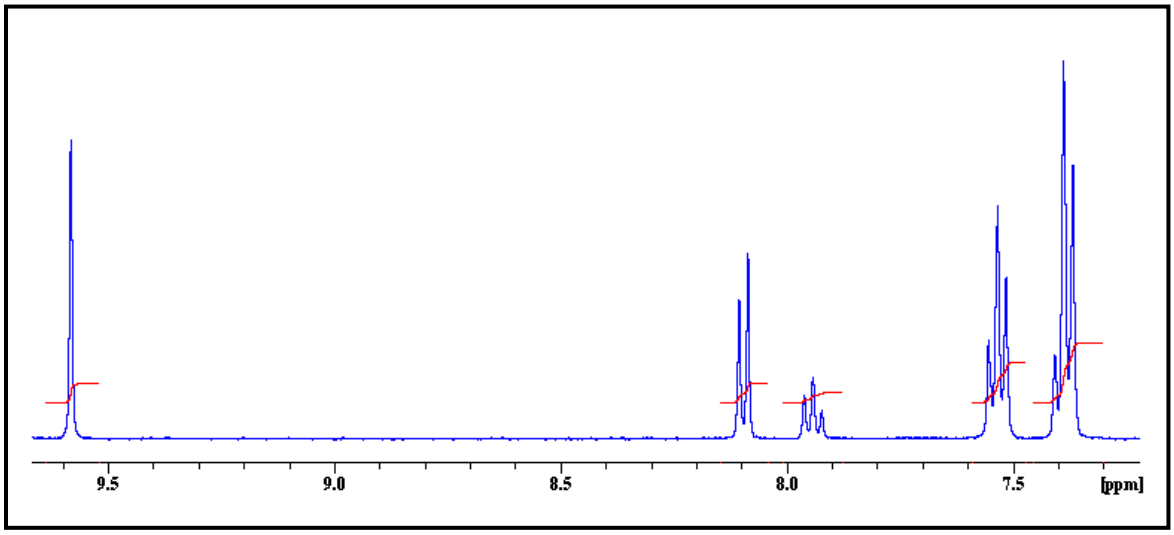

Figure 3.12: ^{1}H NMR spectrum of bap in the 7.20-9.70 ppm range.

Ligand bap is a symmetric diimine containing a central pyridine ring joined, at the *ortho* positions, to two antipyrine moieties through imine bonds (Figure 3.13). A dichloromethane solvent of crystallization is present in the structure. The two halves of the molecule are identical and this discussion will therefore focus on one half of the bap molecule. The molecule adopts an (*E*)-configuration about the N(3)-C(12) bonds. The five membered pyrazole rings lie practically in the same plane as the central pyridine ring with dihedral angles of 12.04˚. The nitrogen-bonded phenyl moieties are however staggered relative to the pyrazole rings with planes forming dihedral angles of 44.92˚.

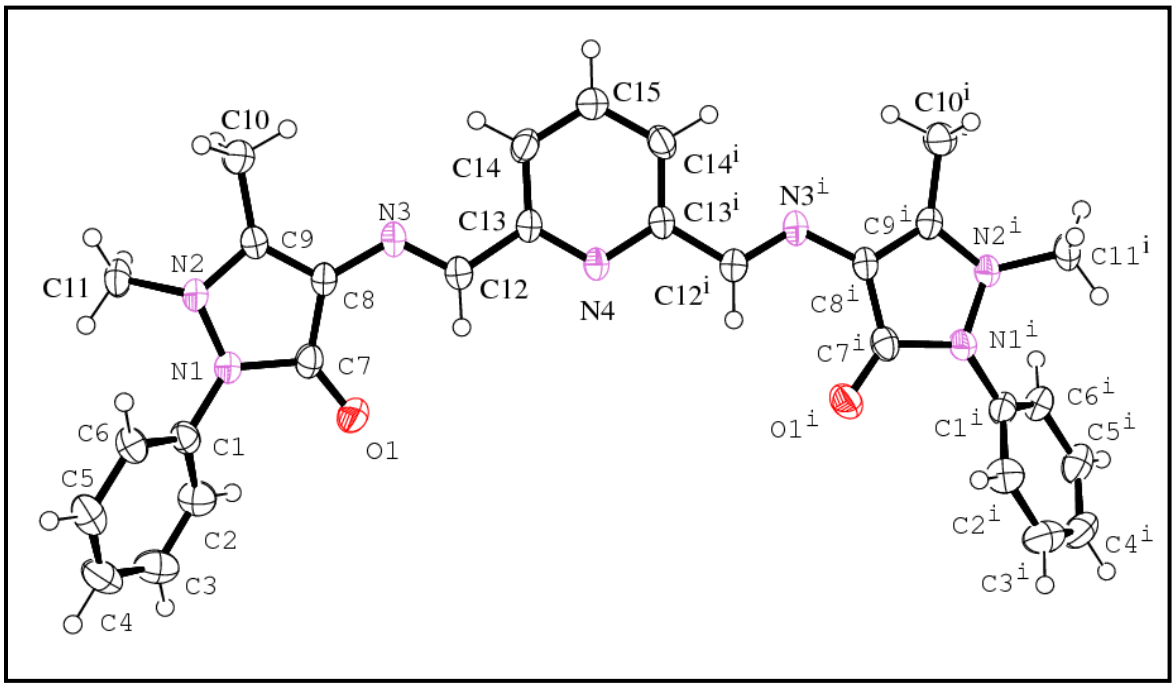

Figure 3.13: An ORTEP view of bap showing 50% probability displacement ellipsoids and the atom labeling.

The C(12)-N(3) bond distance of 1.281(2) Å is typical for imine double bonds [15-17]. Further evidence of the double C=N bond can be seen in the bond angle around N(3) [C(8)-N(3)-C(12) = 122.8(2)˚] which is characteristic of sp^2 hybridized atoms. The C(7)-O(1) bond length of 1.230(2) Å shows that it is a double bond. The C-C bond lengths in the phenyl ring C(1)-C(6) [average = 1.383 Å] indicates that the π electron density is delocalized in this aromatic system. Intermolecular hydrogen-bonding is present between a pyridyl nitrogen and a phenyl hydrogen of neighbouring molecules. The ketonic oxygen is extensively involved in intermolecular hydrogen bonds with a methyl group [C(11)-H(11B)•••O(1)] and the imine hydrogen [C(12)-H(12)•••O(1)] of adjacent molecules, as well as the two protons of the dichloromethane solvent of crystallization [C(16)-H(16A)•••O(1), C(16)-H(16B) •••O(1)] (Table 3.2).

Table 3.2: Hydrogen-bond distances (Å) and angles (˚) in bap**.**

D-H•••A	D-H	H•••A	D•••A	D-H•••A
C(6)-H(6)•••N(4)	0.95	2.55	3.496(3)	177
C(11)-H(11B)•••O(1)	0.98	2. 50	3.369(2)	147
C(12)-H(12)•••O(1)	0.95	2.44	3.090(2)	126
C(16)-H(16A)•••O(1)	0.99	2.44	3.084(3)	122
C(16)-H(16B)•••O(1)	0.99	2.44	3.084(3)	122

3.3.3 Synthesis and characterization of $[ReX_2(pap)(H_2pap)(PPh_3)](ReO_4)$ (X = Cl (1), Br (2))

Exactly the same experimental conditions were used for the synthesis of the two complexes $[ReX_2(pap)(H_2pap)(PPh_3)](ReO_4)$ (X = Cl (**1**), Br (**2**)) from the reactions of *trans*-$[ReOX_3(PPh_3)_2]$ with H_2pap in a 1:2 molar ratio in ethanol. The reactions are described by the equation:

$$[ReOX_3(PPh_3)_2] + 2H_2pap \longrightarrow [ReX_2(pap)(H_2pap)(PPh_3)]^+ + PPh_3 + X^- + H_2O$$

Heating was necessary to form and isolate the products, and no products with sensible analysis could be isolated for heating periods of less than an hour. For **1**, a precipitate formed on cooling the reaction solution down to room temperature, but for **2** no solid residue was precipitated, and crystals were only obtained by slow evaporation of the mother liquor.

The elemental analyses of the complex salts are in good agreement with their formulations. There is no solvent of crystallization. The infrared spectra (Figure 3.14) display the Re=N stretching frequencies as medium intensity peaks around 1070 cm^{-1}, similar to those observed in other rhenium(V)-imido complexes [18-19]. Each complex displays two peaks that can be ascribed to *v*(C=O): one close to the value of *v*(C=O) in the free ligand H_2pap (at 1676 cm^{-1}), and another around 1610 cm^{-1}. The former value is

assigned to the uncoordinated CO entity of pap, with the latter value ascribed to the coordinated group of H_2pap. Only one weak absorption was observed for $\nu(NH_2)$ (at 3060 cm^{-1} (**1**) and 3054 cm^{-1} (**2**)), and the presence of the perrhenate is supported by a strong peak around 910 cm^{-1} [$\nu(Re^{VII}=O)$]. The conductivity values indicate that the complexes are 1:1 electrolytes in DMF.

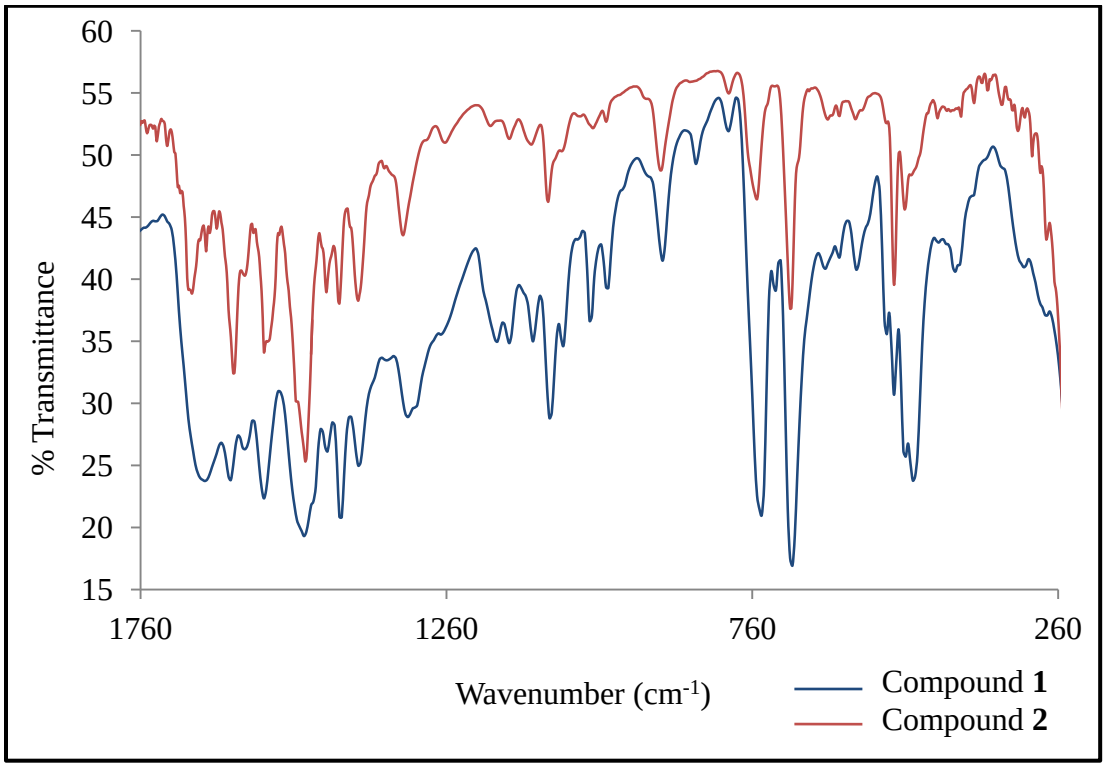

Figure 3.14: IR spectra of **1** and **2** in the 260-1760 cm^{-1} region.

The diamagnetism of **1** and **2** is indicated by the sharp well-resolved peaks in their proton NMR spectra, which occur at their expected positions. There are no paramagnetic shifts. The products are stable in air, and for days in solution. They dissolve in polar solvents (DMF, DMSO, acetonitrile, dichloromethane, and chloroform) to give green solutions.

As can be expected, the ^{1}H NMR spectra of **1** and **2** are similar (Figure 3.15). The protons of the PPh_3 give rise to a multiplet of signals in the range 7.60-7.90 ppm, which integrate for 15 protons. The signals of the ten protons on the two phenyl rings of pap and H_2pap occur as a two-proton doublet (around 7.59 ppm), a four-proton triplet around 7.56 ppm (assigned to the four *meta* protons), a two-proton doublet at 7.50 ppm, and a two-proton

doublet of doublets at 7.46 ppm (assigned to the *para* protons). The four methyl groups in each complex are clearly distinguishable as three proton signals. The UV-Vis spectra of both complexes **1** and **2** show an intense band 374 nm (with different extinction coefficients). This band is ascribed to a combination of the ligand-to-metal charge transfer transitions [$p_\pi(N^{2-}) \rightarrow d^*_\pi(Re)$] and the [$p_\pi(X^-) \rightarrow d^*_\pi(Re)$] (Figure 3.16).

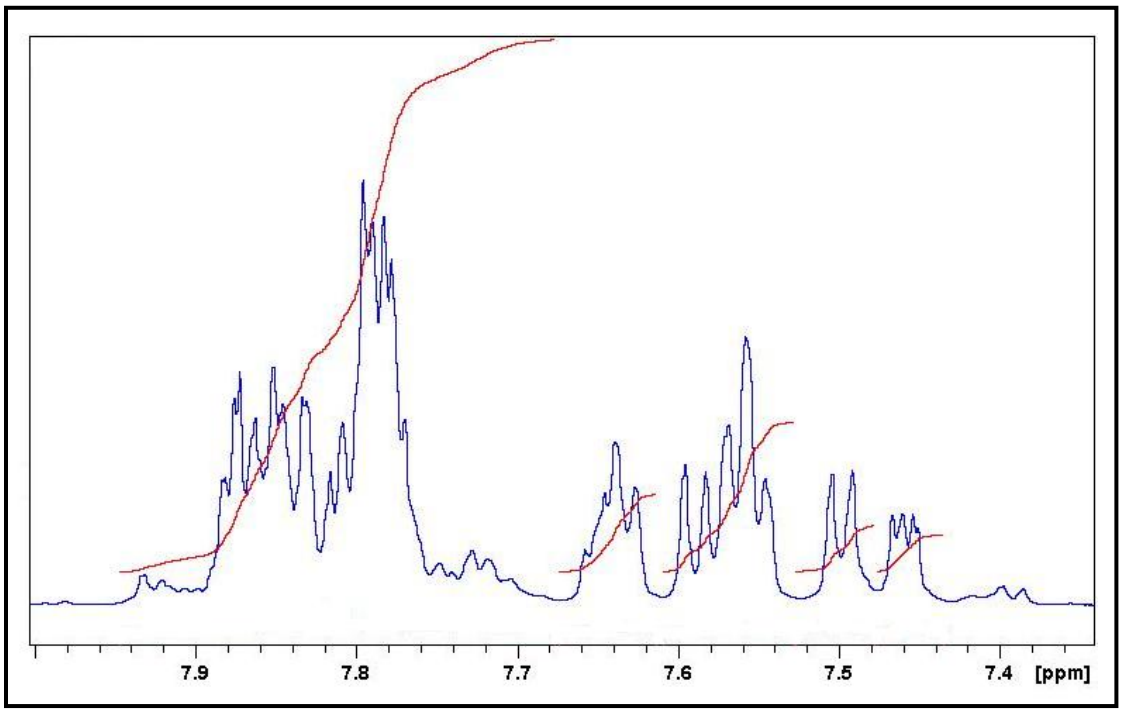

Figure 3.15: ^{1}H NMR spectrum for the aromatic region of **2**.

Crystals for X-ray crystallographic studies were obtained from an ethanol/dichloromethane mixture (for **1**), and from the mother liquor (for **2**). Perspective views of the complexes **1** and **2** are given in Figures 3.17 and 3.18 respectively. Both complexes display a distorted octahedral geometry around the central rhenium atom, and are mirror images of each other. Figure 3.19 shows a superimposition of **1** and **2** with the angle between the C(17)C(18)C(19)C(20)C(22) planes of the phenyl rings attached to N(5) being 6.26˚. The bond parameters of the two complexes (see Table 3.12) are for all purposes the same (except for the halide) if the standard deviations are taken into account. This discussion will therefore focus on both **1** and **2** collectively, and will use the average bond angles and lengths of the two compounds.

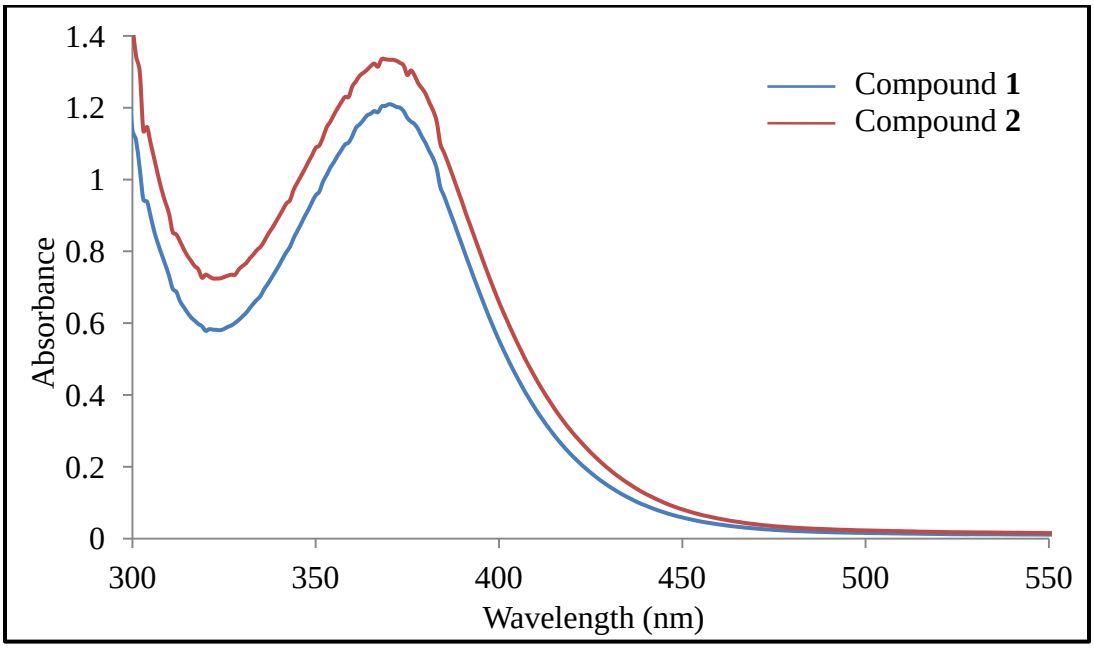

Figure 3.16: UV-Vis spectra of **1** and **2**.

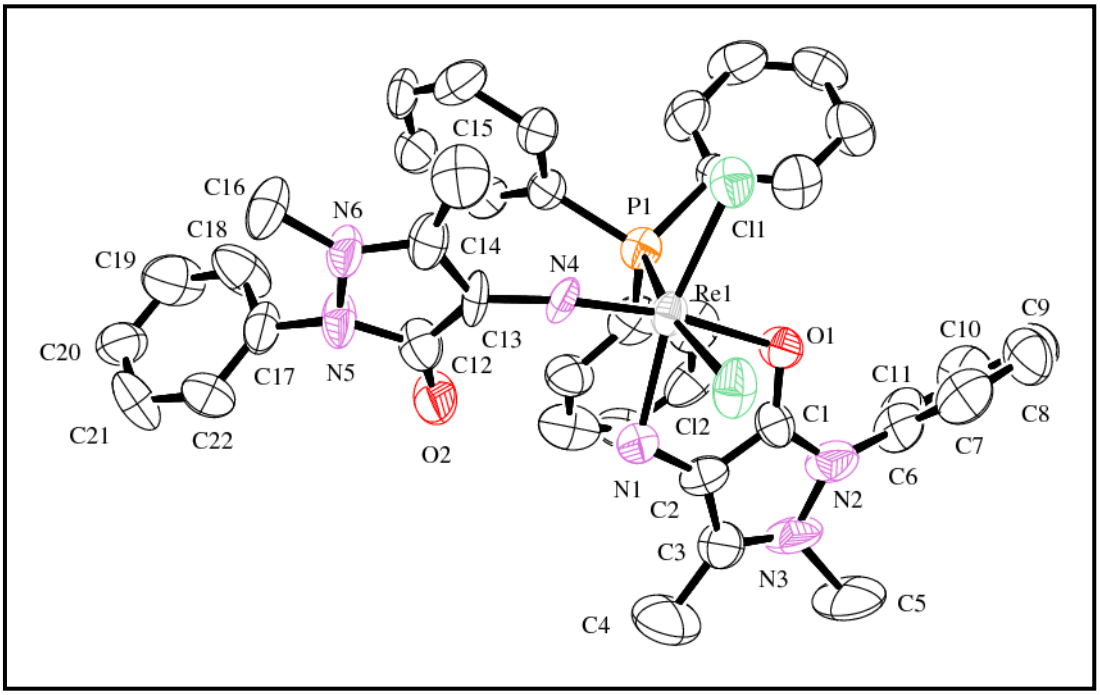

Figure 3.17: An ORTEP view of **1** showing 50% probability displacement ellipsoids and the atom labeling. Hydrogen atoms and the perrhenate counter-ion were omitted for clarity.

The distortion from ideal octahedral geometry is mainly the result of the *cis* angles N(4)-Re-X(1) = 100.7 (4)˚, N(4)-Re-X(2) = 103.2(3)˚, N(4)-Re-N(1) = 89.0(5)˚ and N(4)-Re-P(1) = 90.5(3)˚. The effect is that the rhenium atom is lifted out of the mean equatorial plane $PX_2N(1)$ by 0.15 Å. The bite angle N(1)-Re-O(1) = 79.5(4)˚, and the X(1)-Re-X(2) angles are close to orthogonality [88.2(2)˚].

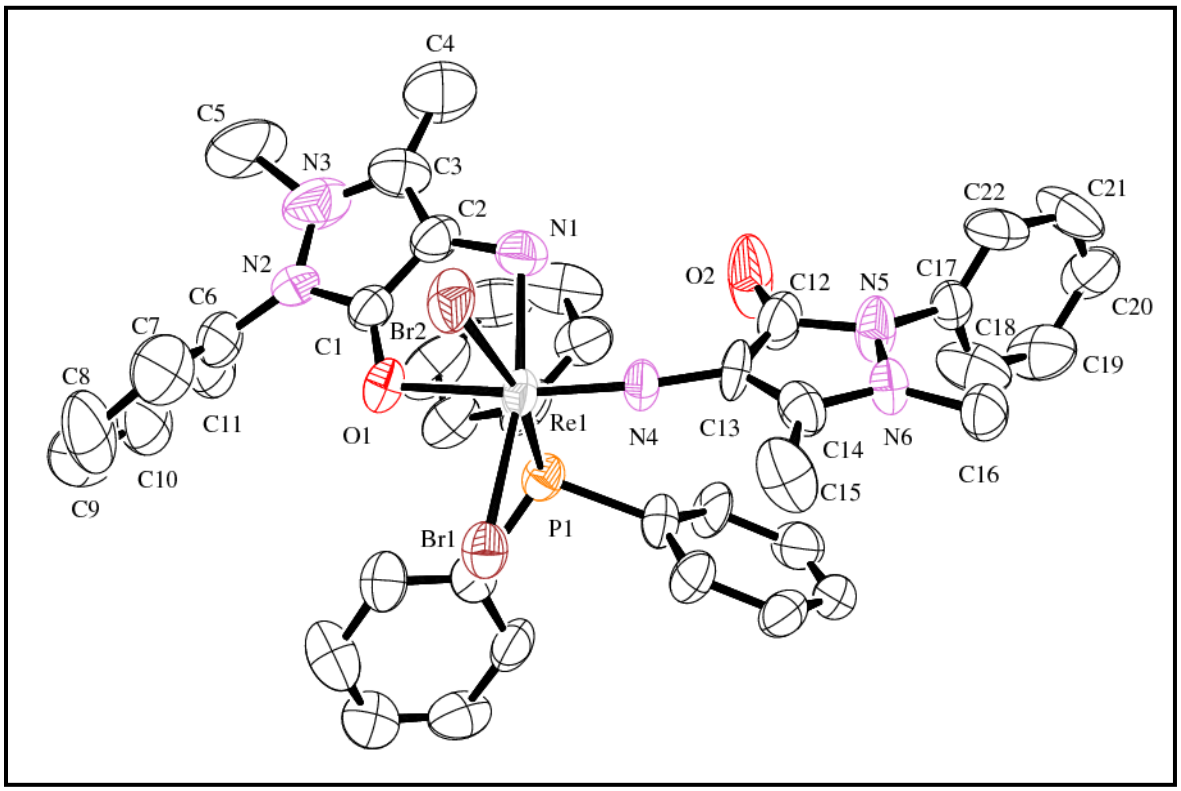

Figure 3.18: An ORTEP view of **2** showing 50% probability displacement ellipsoids and the atom labeling. Hydrogen atoms and the perrhenate counter-ion were omitted for clarity.

Pap acts as a dianionic monodentate chelate, with coordination through the doubly deprotonated imido nitrogen N(4) only. The ketonic oxygen O(2) is not coordinated. The average Re-N(4)-C(13) bond angle of 168.9(9)˚ illustrates an unusual significant deviation from linearity of the coordination mode of the triply bonded imido unit, and the Re-N(4) distance of 1.73(1) Å falls well within the range [1.72(1)-1.75(1) Å] normally found in octahedral rhenium(V)-phenylimido complexes [20-21]. The intraligand pap bond distances show that O(2)-C(12) [1.21(2) Å] and N(6)-C(14) [1.34(2) Å] are double

bonds, with all the others in the pyrazole ring single. The non-planarity of the pyrazole ring is reflected in the torsion angles N(6)-N(5)-C(12)-C(13) = -7(2)˚ and N(5)-N(6)-C(14)-C(13) = -5(2)˚.

The H_2pap ligand acts as a neutral bidentate chelate, with coordination through the neutral amino nitrogen N(1)H_2 and the ketonic oxygen O(1). The N(4)-Re-O(1) bond angle [164.5(4)˚] deviates considerably from linearity due to the restrictions imposed by the bite angle of the five-membered metalloring. The Re-N(1) bond length of 2.19(1) Å is typical of rhenium(V)-amino bond distances, which normally occur in the range 2.15(1)-2.23(1) Å [21-24]. The Re-O(1) bond length of 2.11(9) Å is considerably longer than those found for Re-O (phenolate, alcoholate) distances, which typically occur in the 1.96(2)-2.01(2) Å range [18-20, 25, 26].

The O(1)-C(1) bond length of 1.31(2) Å shows that it is still a double bond, and also shows the lengthening of this double bond brought about by coordination to the metal when compared with the uncoordinated O(2)-C(12) length [1.21(2) Å]. Again the N(3)-C(3) bond is double [1.33(2) Å]. The Re-X(2) bond lengths are longer than the Re-X(1) ones, due to the larger *trans* effect of the phosphorus atom when compared to the amino nitrogen N(1). In **1,** hydrogen-bonds exist between N(1)H(1A) and O(2) and between N(1)H(1B) and O(6), and in **2** there is only one hydrogen-bond [N(1)H(1A)•••O(6); Table 3.1].

Table 3.3: Hydrogen-bond distances (Å) and angles (˚) in **1** and **2.**

	D-H•••A	D-H	H•••A	D•••A	D-H•••A
1	N(1)H(1A)•••O(2)	0.92	2.57	3.35(2)	143
	N(1)H(1B)•••O(6)	0.92	2.14	2.89(2)	138
2	N(1)H(1A)•••O(6)	0.92	2.13	2.92(2)	143

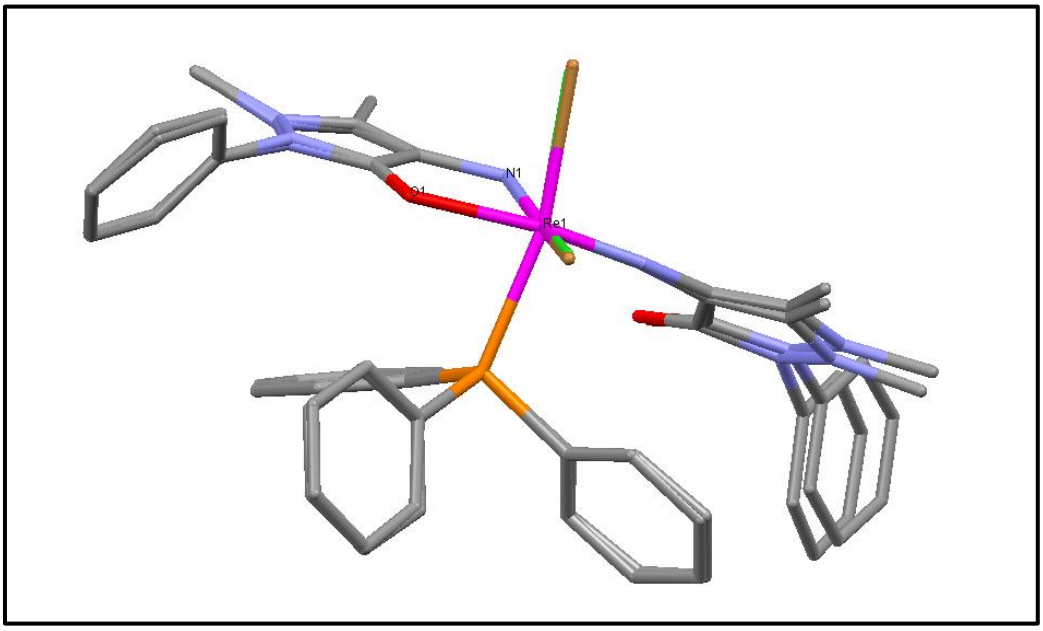

Figure 3.19: Superimposition of the structures of **1** and **2.**

3.3.4 Synthesis and characterization of *cis*-[Re(nap)Br_2(PPh_3)]Br (3)

The reaction of a twofold molar excess of H_2nap with *trans*-[$ReOBr_3(PPh_3)_2$] in ethanol led to the formation of the six-coordinate rhenium(V) complex salt **3**, according to the equation:

$$[ReOBr_3(PPh_3)_2] + H_2nap \longrightarrow [Re(nap)Br_2(PPh_3)]Br + H_2O + PPh_3$$

The product is stable in air and in solution, and is soluble in a wide variety of polar solvents. It is a 1:1 electrolyte in DMF.

In the infrared spectrum of **3** (Figure 3.20) a peak of medium intensity at 1095 cm^{-1} is assigned to the Re=N stretching frequency, with ν(C=O) and ν(C=N) of the coordinated nap at 1593 and 1575 cm^{-1}, respectively. There is no band in the 890-1020 cm^{-1} region that can be ascribed to ν(Re=O). The ^{1}H NMR spectrum of **3** shows a one-proton signal at 9.64 ppm due to the methine proton (H(7)). The aromatic region is characterized by a multiplet which integrates for the 24 protons of the three triphenylphosphine rings and the phenyl rings of the nap moiety. The methyl signals appear as two singlets at 3.18 and

2.32 ppm, each integrating for three protons. The electronic spectrum of **3** shows an absorption band at 313 nm due to the intraligand charge transfer bands of the coordinated nap^{2-} moiety. A transition is found at 370 nm due to the $[p_\pi(N^{2-}) \rightarrow d^*_\pi(Re)]$ and the $[p_\pi(Br^-) \rightarrow d^*_\pi(Re)]$ ligand-to-metal charge transfer transitions.

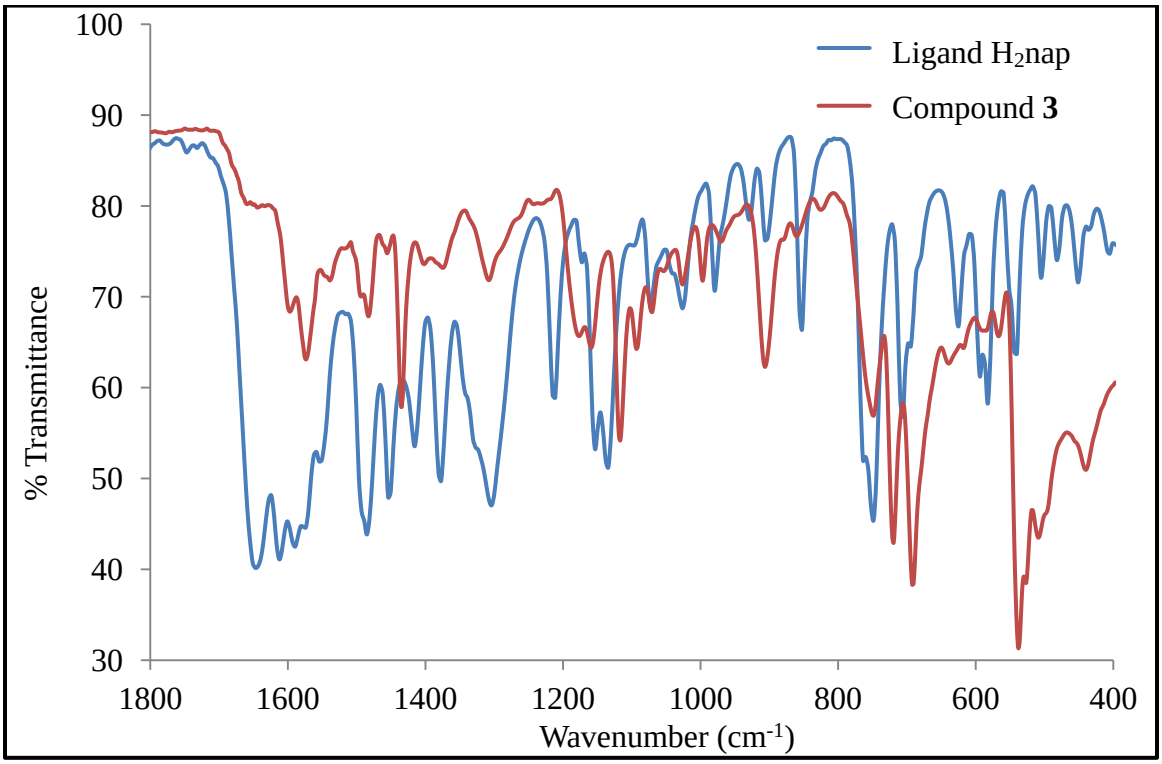

Figure 3.20: IR spectra of H_2nap and **3** in the 400-1800 cm^{-1} region.

An ORTEP perspective view of the complex cation is shown in Figure 3.21. Due to the disorder of the bromide counter-ion, the structure could not be properly refined. The connectivity and other general features of the structure, however, were confidently determined, and the molecular positional parameters of the atoms in the 'inner core' are well defined. The rhenium atom is at the centre of a distorted octahedron. The nap ligand acts as a dianionic tridentate ligand with coordination through the doubly deprotonated imido nitrogen N(1), the imino nitrogen N(2), and the ketonic oxygen O(1). The basal plane can be defined by the three donor atoms of the nap chelate [N(1), N(2) and O(1)] and Br(1), with P(1) and Br(2) in *trans* axial positions. The distortion is mainly the result of a non-linear N(1)=Re-O(1) axis of 160.3(4)°, accomplished by Br(1)-Re-N(2) and Br(2)-Re-P(1) angles of 170.3(3)° and 171.53(9)°, respectively.

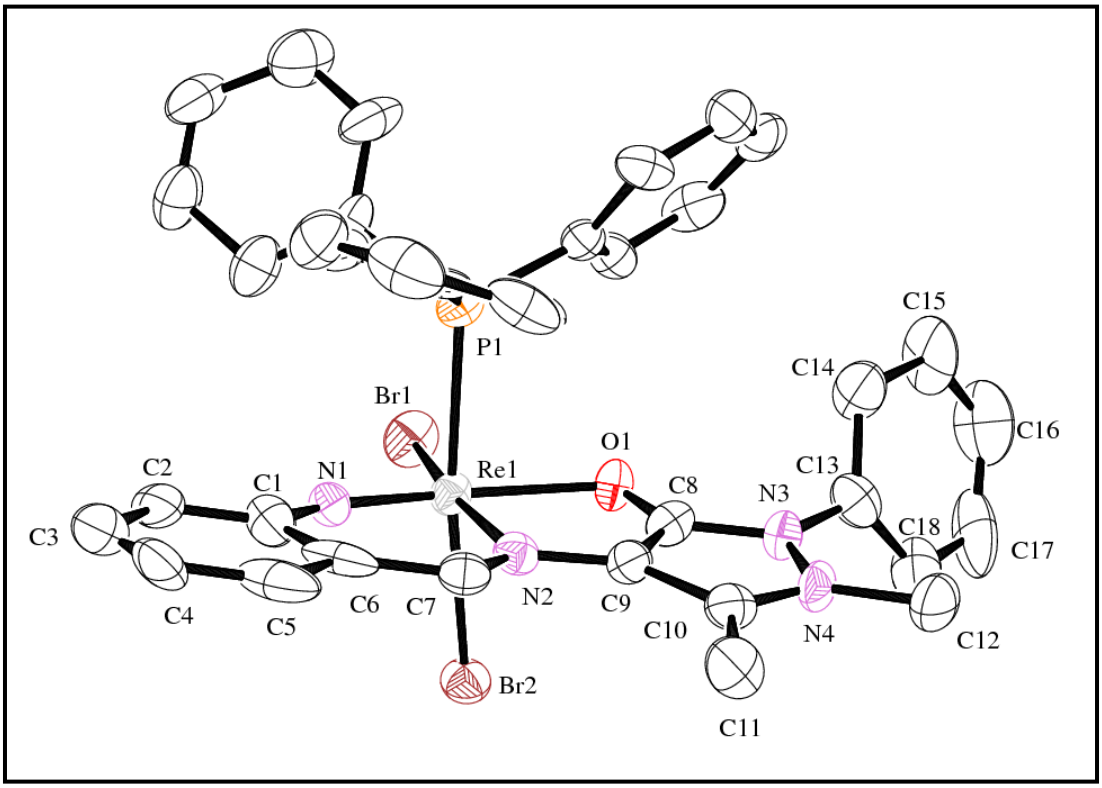

Figure 3.21: An ORTEP view of complex **3** showing 50% probability displacement ellipsoids and the atom labeling. Hydrogen atoms and the bromide counter-ion were omitted for clarity.

The bite angles of nap are N(1)-Re-N(2) = 81.4(4)° and N(2)-Re-O(1) = 79.7(4)°. The nap ligand acts as a tridentate dianionic moiety, with N(1) coordinated as a negatively charged imido nitrogen. The Re-N(1) bond length of 1.72(1) Å is considerably shorter than the values found for Re(V)-NH and Re(V)-NH_2 bonds [1.91(1)-2.01(1) Å and 2.15(1)-2.23(1) Å, respectively] [24, 27, 28]. The Re-N(1)-C(1) bond angle of 148(1)° indicates a significant deviation from linearity of the coordination mode of the phenylimido unit with a reduction in bond order of the Re=N(1) bond. The Re-N(2) length [2.15(1) Å] is typical of Re(V)-N(imine) bonds [27]. The O(1)-C(8) bond length of 1.27(2) Å indicates a double bond, with the Re-O(1) length of 2.098(8) Å. The C(7)-N(2)-C(9) bond angle of 124(1)° is close to the ideal of 120° for a sp^2 hybridized nitrogen atom, with the N(2)-C(7) bond double at 1.27(2) Å. The crystal lattice of **3** is stabilized by π-π stacking (Figure 3.22). The centroid to centroid distance between the C(1)-C(6) aromatic rings of adjacent molecules of **3** is 3.640 Å.

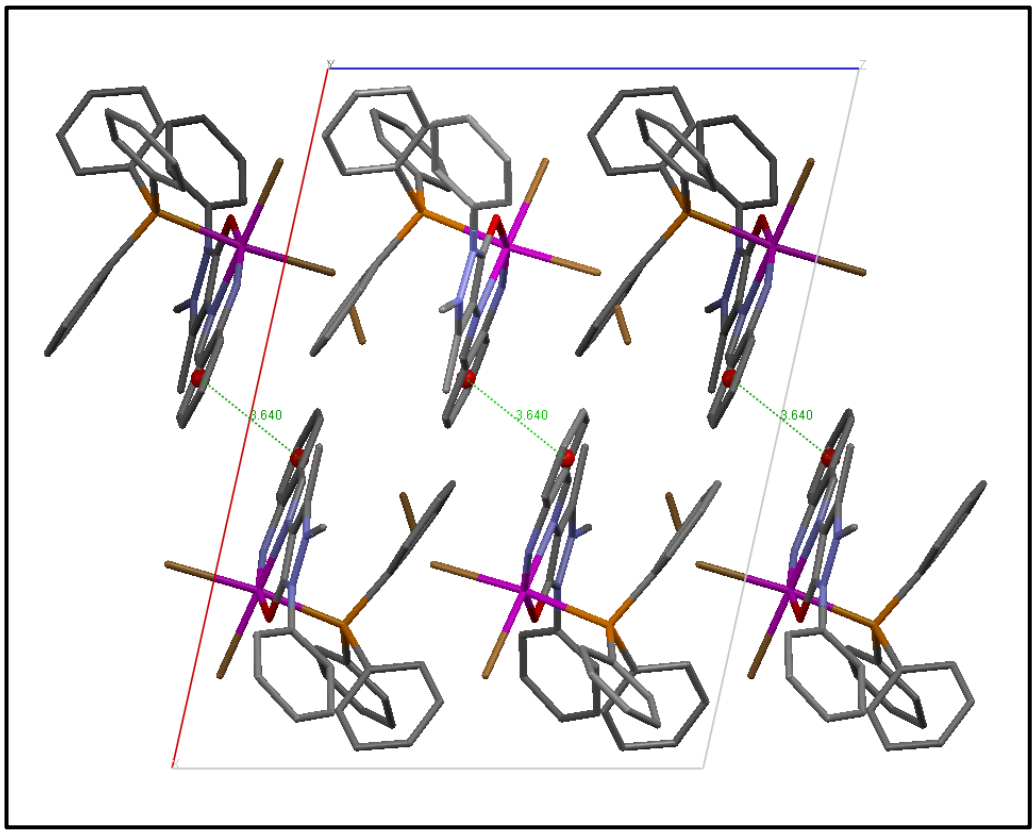

Figure 3.22: A perspective view of **3**, showing the π-π interactions.

3.3.5 Synthesis and characterization of [ReO(OEt)(Hnap)(PPh_3)]I (4) and [ReO(OMe)(oap)(PPh_3)]I (5)

These complex salts were prepared by the reaction of *cis*-[$ReO_2I(PPh_3)_2$] with a twofold molar excess of H_2nap and Hoap, according to the equation

$$[ReO_2I(PPh_3)_2] + H_2nap/Hoap + EtOH/MeOH \longrightarrow \mathbf{4/5} + H_2O + PPh_3$$

Complexes **4** and **5** are air stable and 1:1 electrolytes in methanol. Both complexes are soluble in a wide range of polar solvents, including alcohols, acetonitrile and dichloromethane. A single peak at 940 cm^{-1} in both the infrared spectra of **4** and **5** (Figure 3.23) is assigned to the Re=O stretching vibrations, with *ν*(C=O) and *ν*(C=N) at 1600/1599 cm^{-1} and 1578/1569 cm^{-1}, respectively. The presence of the ethoxide is shown by an intense peak at 907 cm^{-1}, which corresponds to the ethoxy bending mode.

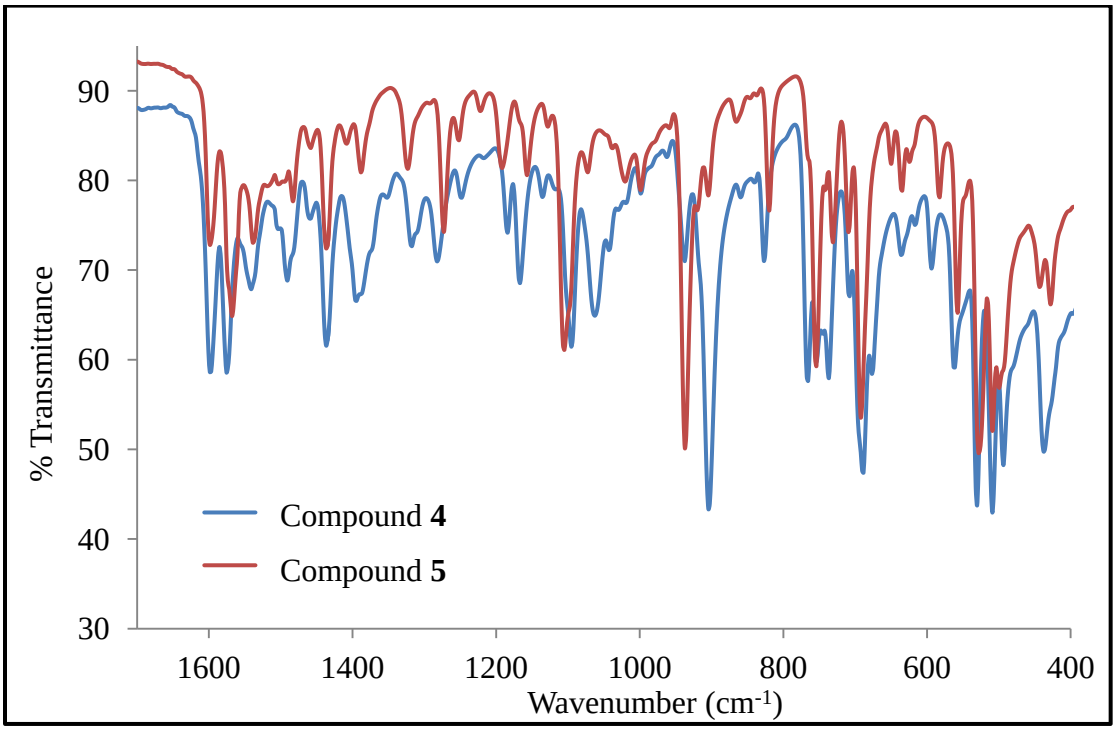

Figure 3.23: Overlay IR spectra of **4** and **5**.

In the ^{1}H NMR spectra of **4** and **5** (Figures 3.24 and 3.25), the protons of the methane groups appear as singlets at 9.62 and 9.10 ppm respectively. The aromatic region of **4** consists of three separate multiplets integrating for the protons of the aromatic rings of the ligand and the protons of the triphenylphosphine rings. For **5**, the triphenylphosphine protons appear in the aromatic region as a multiplet in the 7.42-7.66 ppm range. The remainder of the aromatic region is characterized by a doublet (7.92 ppm), multiplet (7.74-7.88 ppm), doublet (7.69 ppm), triplet (7.04 ppm) and a doublet (6.75 ppm) ascribed to the aromatic protons of the coordinated Hnap moiety. The methyl protons' signals of **4** are found at 2.35 and 3.18 ppm as two singlets while the signals of the coordinated ethoxide appear as a two-proton triplet (2.68 ppm) and a three-proton doublet (2.34 ppm) for the ethyl and methyl protons respectively. For **5**, three separate three-proton singlets are found at 3.63 ppm, 2.94 ppm and 2.85 ppm due to the methyl groups of the pyrazole ring and the coordinated methoxide.

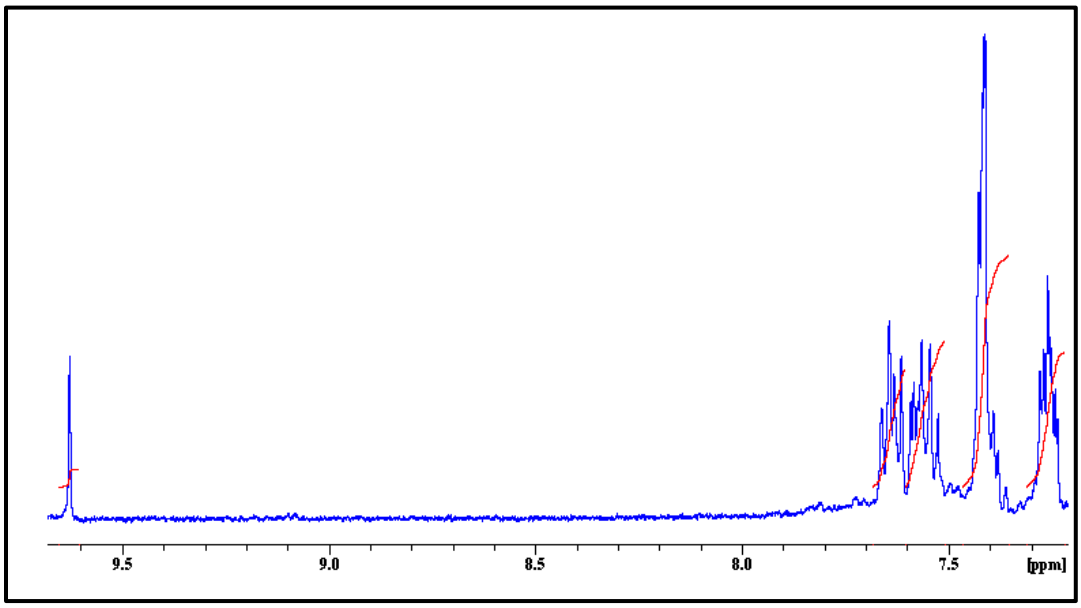

Figure 3.24: ^{1}H NMR spectrum of **4** in the 7.20-9.70 ppm region.

The electronic spectra of **4** and **5** (Figure 3.26) in methanol show two intense absorptions at about 315 and 370 nm, with a weaker one at around 485 nm. With reference to previous studies [29] the band at highest energy is ascribed to a ligand-to-metal charge transfer transition [$p_{\pi}(O^{2-}) \rightarrow d_{\pi}^{*}(Re)$], and the one at 370 nm to the $p_{\pi}(O(1)) \rightarrow d_{\pi}^{*}(Re)$ [$d_{\pi}^{*} = d_{xz},d_{yz}$]. The weak absorption at lowest energy is probably due to a $(d_{xy})^{2} \rightarrow (d_{xy})^{1}(d_{\pi}^{*})^{1}$ transition.

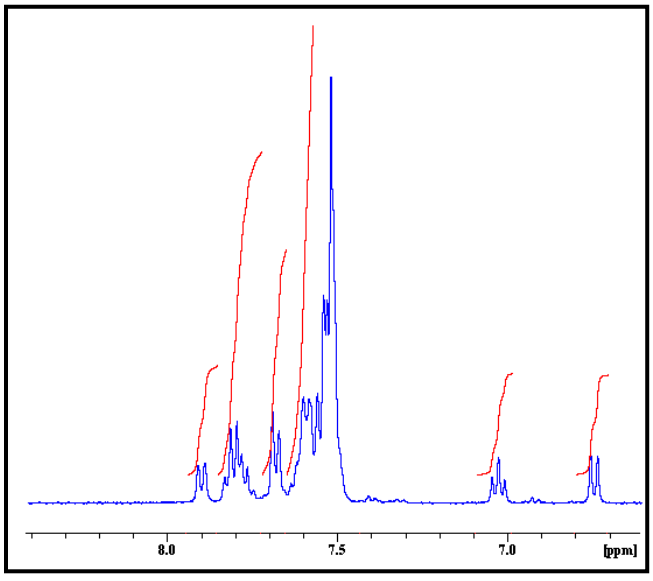

Figure 3.25: ^{1}H NMR spectrum for the aromatic region of **5**.

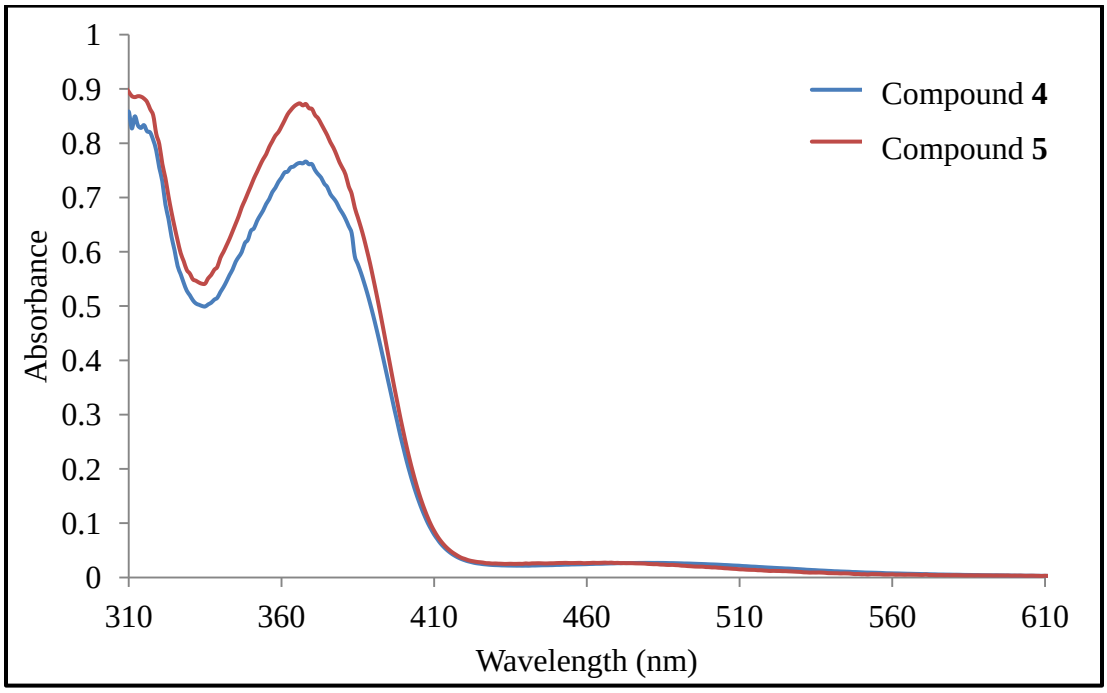

Figure 3.26: Overlay UV-Vis spectra of **4** and **5**.

The asymmetric unit of **4** contains half molecules of ethanol and water of crystallization. The coordinated Hnap ligand acts as a monoanionic tridentate chelate with coordination through the singly deprotonated amino nitrogen N(4), imino nitrogen N(3) and ketonic oxygen O(1). The molecular structure (Figure 3.27) shows a distorted octahedral geometry around the Re(V) atom, with the equatorial plane formed by the P(1)O(1)N(3)N(4) donor set, and the oxo O(2) and O(3) in *trans* axial positions. The *trans* angles O(2)-Re-O(3) [165.0(2)°] and O(1)-Re-N(4) [169.4(2)] contribute significantly to the distortion, with P(1)-Re-N(3) equal to 174.9(2)°.

The N(3)-Re-N(4) bite angle [90.2(2)°], being part of a six-membered metallocycle, is considerably larger than the O(1)-Re-N(3) one [80.4(2)°]. The Re=O(2) distance of 1.646(5) Å is shorter than for similar *trans* oxo-ethoxorhenium(V) complexes [average = 1.691(2) Å] [30]. The Re-O(3) ethoxo bond [1.877(4) Å] is similar to related bonds [31], but is substantially less than 2.04 Å, which is considered to be representative of a Re(V)-O single bond [26]. Partial multiple bonding in Re-O(3) is consistent with the large Re-O(3)-C(37) angle of 145.0(5)°. The O(3)-C(37) length of 1.41(1) Å is normal for a single

bond. The Re-N(4) [1.979(6) Å] and Re-N(3) [2.155(5) Å] bond lengths are typical for the coordination of amido and imino nitrogen atoms, respectively [26, 27]. The Re-O(1) [2.209(4) Å] and O(1)-C(7) [1.278(8) Å] lengths illustrate the rare coordination of a ketonic oxygen to rhenium(V).

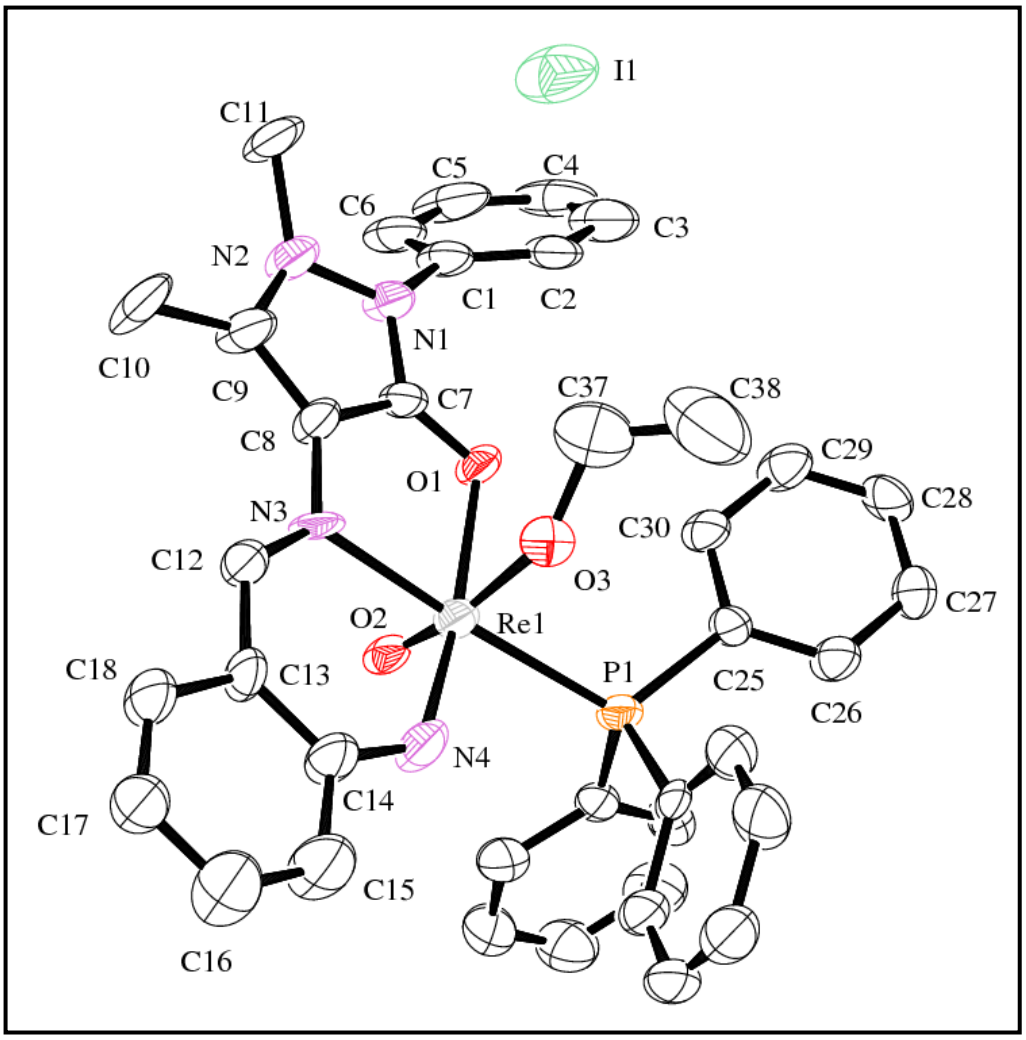

Figure 3.27: An ORTEP view of **4** showing 50% probability displacement ellipsoids and the atom labeling. Hydrogen atoms were omitted for clarity.

The structure of **5** (Figure 3.28) is very similar to that of **4**. The rhenium atom is displaced from the least-squares P(1)O(1)N(1)O(2) plane towards the oxo oxygen atom O(3) by 0.133˚. This displacement is the result of the non-orthogonal angles O(3)-Re-P(1) = 91.7(2)°, O(3)-Re-O(1) = 98.8(2)°, O(3)-Re-N(1) = 96.3(2)° and O(3)-Re-O(2) =

87.5(3)°. This distortion results in a non-linear O(3)-Re-O(4) axis of 168.5(2)°, with the Re=O(3) distance [1.702(6) Å] significantly longer than in **4**. The Re-O(4) length and Re-O(4)-C(37) angle are 1.886(5) Å and 147.1(5)°, respectively, which are very similar to those values in **4**. In the tridentate oap chelate, O(1) is monoanionic [Re-O(1) = 1.985(5) Å], N(1) is an imino nitrogen [Re-N(1) = 2.130(5) Å, C(7)-N(1)-C(9) = 126.5(6)°], and O(2) is a neutral ketonic oxygen [C(8)-O(2) = 1.27(1) Å, Re-O(2) = 2.171(7) Å]. The O(1)-Re-N(1) bite angle [92.3(2)°] is larger than the corresponding angle in complex **4** [90.2(2)°], with the N(1)-Re-O(2) angle [80.5(2)°] identical to that found in **4**.

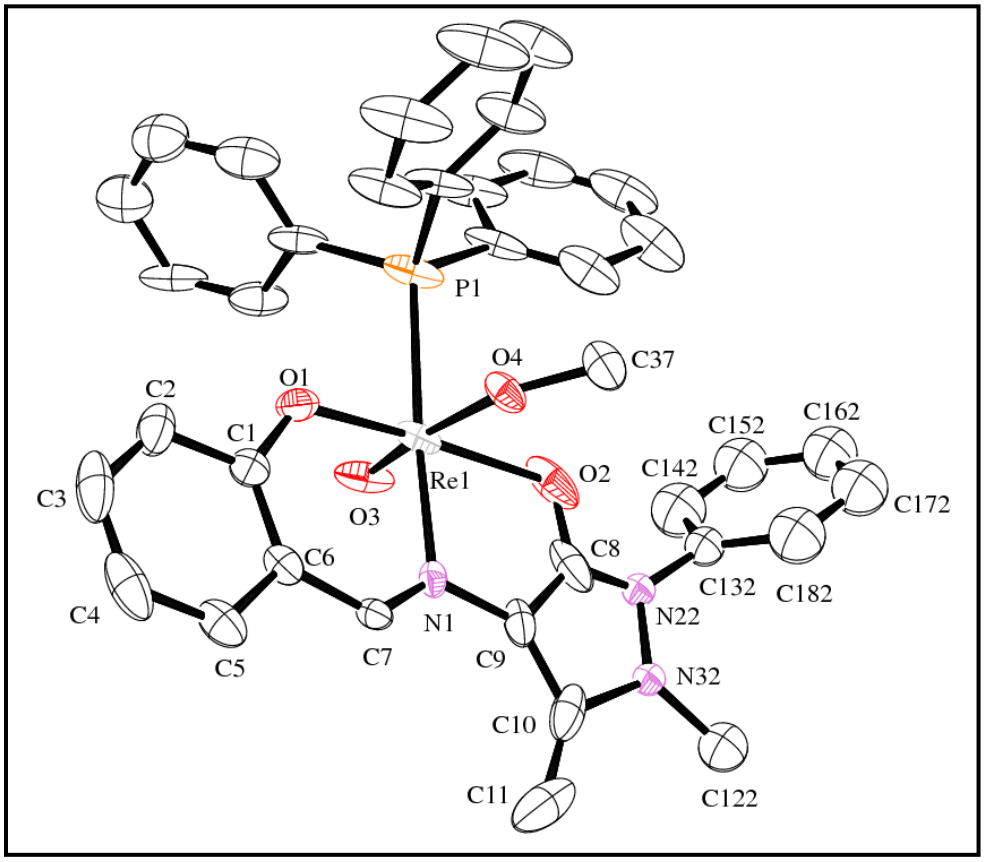

Figure 3.28: An ORTEP view of **5** showing 50% probability displacement ellipsoids and the atom labeling. Hydrogen atoms and the iodide counter-ion were omitted for clarity.

In complexes **1**, **2**, **3**, **4** and **5**, the rhenium(V) is coordinated to a neutral ketonic oxygen. This coordination is unusual and no bonding distance values could be found in literature for comparison. Complexes of rhenium(V) with N,O-donor ligands are common in the literature. These ligands are mostly of the Schiff base type and these complexes contain mainly the $[ReO]^{3+}$ core. Bidentate N,O-donor Schiff bases (HNO), containing an imine nitrogen and a phenolic oxygen, always produce complexes of the $[ReOX_2(NO)PPh_3]$ or $[ReOX(NO)_2]$ types, with a phenolate oxygen atom *trans* to the oxo group in distorted octahedral geometries [32-33].

3.3.7 Synthesis and characterization of *fac*-[Re(CO)$_3$(dae)Cl] (6)

The compound *fac*-$[Re(CO)_3(dae)Cl]$ (**6**) was formed by the reaction of $[Re(CO)_5Cl]$ with a 1.5 molar excess of dae in refluxing toluene under nitrogen.

$$[Re(CO)_5Cl] + dae \longrightarrow \textit{fac}\text{-}[Re(CO)_3(dae)Cl] + 2CO$$

Complex **6** is stable in air, diamagnetic and a non-electrolyte (Λ_M = 21 $ohm^{-1}cm^2mol^{-1}$) in acetonitrile. It is soluble in alcohols, dichloromethane, acetonitrile and dimethylsulfoxide. Diimine *fac*-$[Re(CO)_3]^+$ complexes has been widely studied [34] due to their superior photophysical properties. It is thought that the bidentate diimine coordination of the dae ligand could possibly exhibit photochemical behaviour, while the pyrazole moiety of dae provides potential biological acitivity.

The infrared spectrum of **6** (Figure 3.29) contains a sharp intense band at 2017 cm^{-1}, and a broad strong band at 1905 cm^{-1}, typical of ν(C≡O) of the *fac*-$[Re(CO)_3]^+$ unit. The medium intensity band at 467 cm^{-1} is assigned to ν(Re-N(1)) and ν(Re-N(2)). The peaks at 1654 and 1562 cm^{-1} are due to ν(C=O) and ν(C=N) of the coordinated Schiff base ligand. The ^{1}H NMR spectrum of **6** (Figure 3.30) displays the magnetic equivalence of the protons which emphasizes the symmetry of the complex. The two methine protons of the symmetrically coordinated dae ligand appear as a singlet at 8.88 ppm. The aromatic

region contains a multiplet in the 7.32-7.64 ppm region integrating for the ten aromatic protons of dae. Two six-proton singlets are found at 2.32 and 3.28 ppm for the four methyl groups of the pyrazole unit.

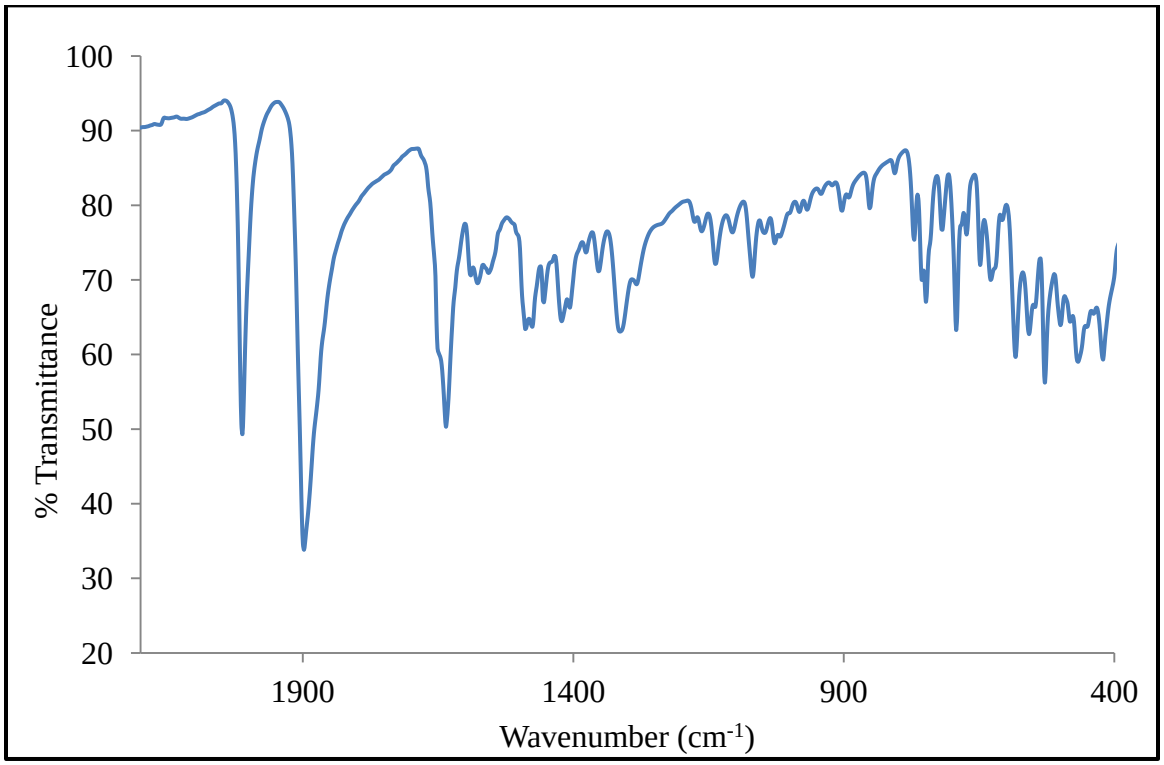

Figure 3.29: IR spectrum of **6**.

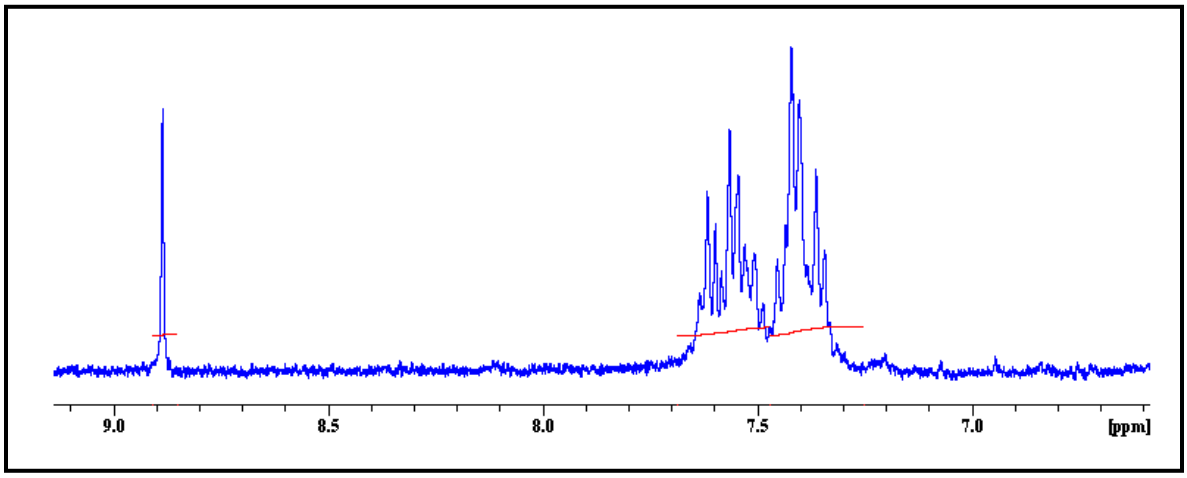

Figure 3.30: ^{1}H NMR spectrum for the aromatic region of **6**.

The electronic spectrum of **6** (Figure 3.31) in acetonitrile shows two intra-ligand charge transfer processes ($\pi \rightarrow \pi^*$) as a sharp band at 385 nm and a shoulder at 402 nm. These bands are similar to those found in the spectrum of the free dae ligand (378 and 400 nm) (Figure 3.31). The metal-to-ligand charge transfer band $d_\pi(Re) \rightarrow \pi^*(N\text{-}N)$ is found at 510 nm and is typical of rhenium complexes containing NN donor ligands [35].

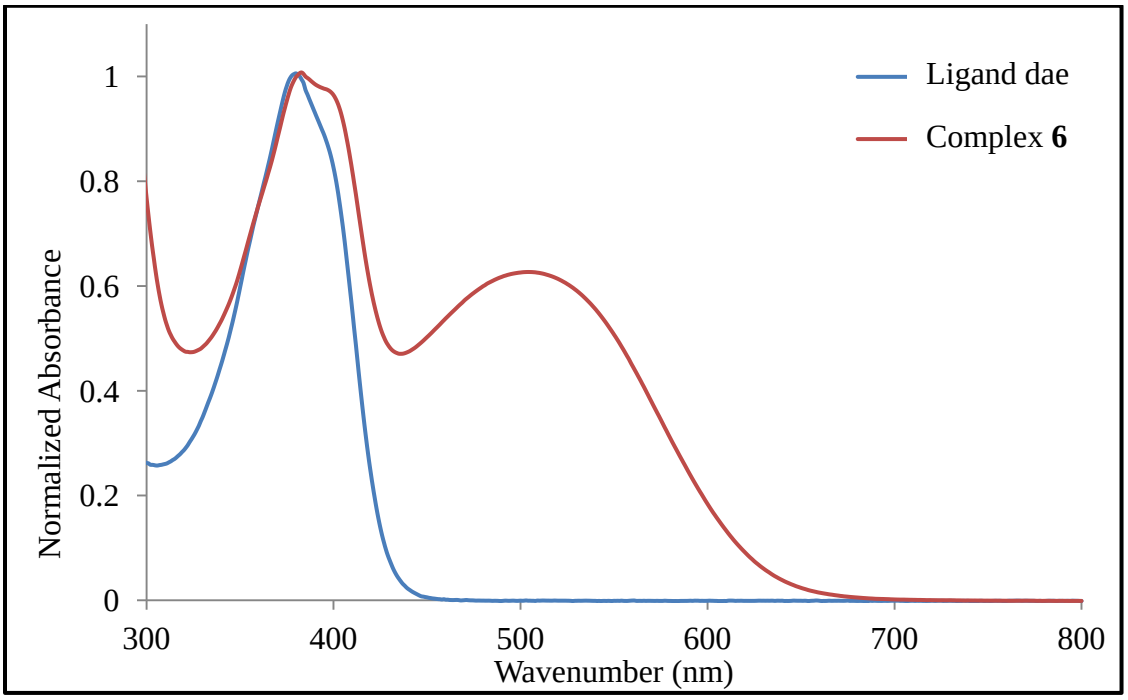

Figure 3.31: Overlay UV-Vis spectra of dae and **6**.

The X-ray structure analysis of **6** reveals that the rhenium atom adopts a distorted octahedral geometry and is coordinated to three carbonyl donors in a *facial* orientation, the two imino nitrogen atoms N(1) and N(2), and a chloride (Figure 3.32). The two Re-N bond lengths are similar [average of 2.178(2) Å] and are typical of $Re(I)\text{-}N_{imine}$ bonds [36]. The distortion from octahedral ideality is mainly the result of the *trans* angles N(2)-Re-C(90) =169.4(1)˚, N(1)-Re-C(92) =174.7(1)˚ and Cl-Re-C(91) = 178.2(1)˚. These distortions are the result of constraints caused by the bidentate coordination of the dae ligand with a bite angle of N(1)-Re-N(2) = 74.08(8)˚.

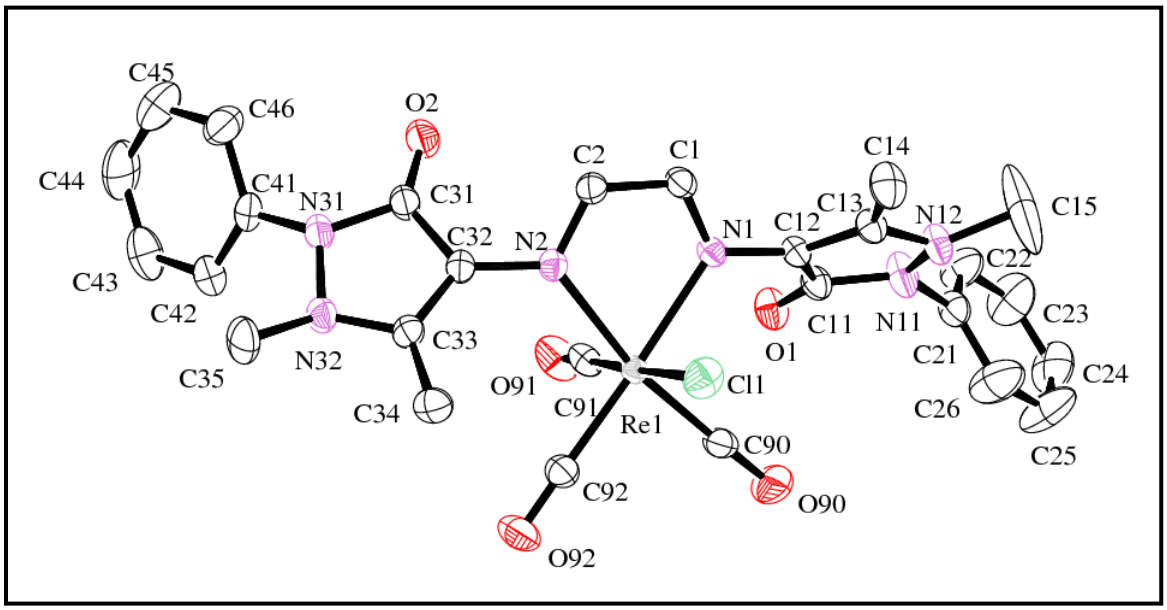

Figure 3.32: An ORTEP view of complex **6** showing 50% probability displacement ellipsoids and the atom labeling. Hydrogen atoms were omitted for clarity.

The N(1)-C(1) [1.292(4) Å] bond is double and the N(1)C(1)C(2)N(2) torsion angle is 5.0(4)˚. The two five-membered heterocyclic rings form a dihedral angle of 81.02˚ with one another. The nitrogen bonded phenyl rings adopt staggered conformations relative to their respective parent heterocycles, with the least-square planes intersecting at angles of 52.22 and 74.02˚.

3.3.6 Synthesis and characterization of *fac*-[Re(CO)$_3$(bap)Br] (7)

The reaction of [Re(CO)$_5$Br] with a two molar excess of the potentially tridentate bap ligand led to the formation of *fac*-[Re(CO)$_3$(bap)Br] in which the bap coordinated bidentately through a pyridyl and imino nitrogen.

$$[Re(CO)_5Br] + bap \longrightarrow \textit{fac}\text{-}[Re(CO)_3(bap)Br] + 2CO$$

Complex **7** is stable for days in solution and for months in air as a solid. The small molar conductivity value (Λ_M = 21 ohm^{-1}cm^{2}mol^{-1}) indicates that it is a non-electrolyte in

acetonitrile and is therefore neutral. The elemental analysis confirms the predicted formulation of **7**. The complex is partially soluble in alcohols but soluble in other polar solvents such as acetonitrile, dimethylformamide, dichloromethane and dimethylsulfoxide.

The infrared spectrum of **7** (Figure 3.33) is dominated by three intense bands at 1902, 1920 and 2020 cm^{-1}, which is characteristic of the ν(C≡O) of the *fac*-$[Re(CO)_3]^+$ core. The imine stretching frequency ν(C=N) appears as a medium intensity peak at 1586 cm^{-1} while a sharp peak at 1658 cm^{-1} is attributed to ν(C=O) of the pyrazole unit. The two stretching frequencies at 456 and 475 cm^{-1} are assigned to the ν(Re-N(1)) and ν(Re-N(2)).

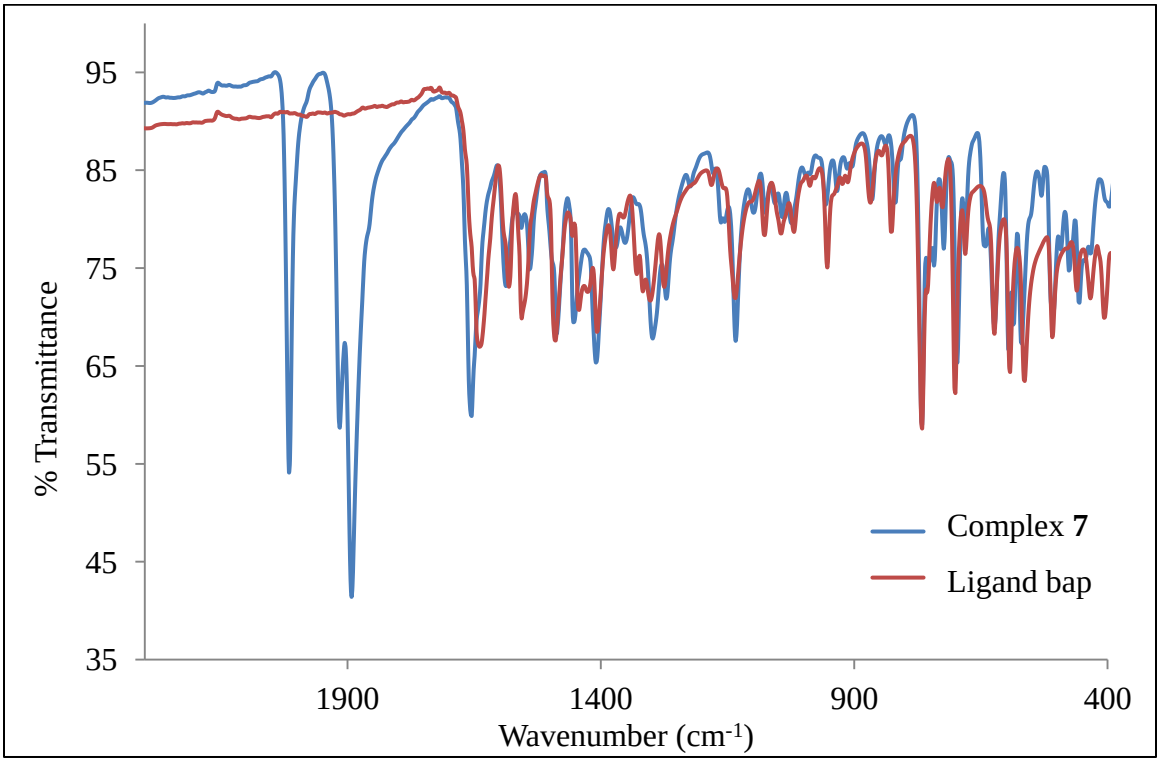

Figure 3.33: Overlay IR spectra of bap and **7** in the 400-2300 cm^{-1} range.

In contrast to the free ligand bap, the proton spectrum of **7** does not display magnetic equivalence, indicating that **7** is unsymmetrical as a result of the bidentate coordination of bap in **7**. The ^{1}H NMR spectrum of **7** (Figure 3.34) shows two singlets at 10.14 and 9.33 ppm due to the methine protons. The aromatic region integrates for the 13 protons of the

pyridine and phenyl rings. Four singlets integrating for three protons each are found in the 2.50-3.50 ppm region and are assigned to the four methyl groups of the pyrazole rings.

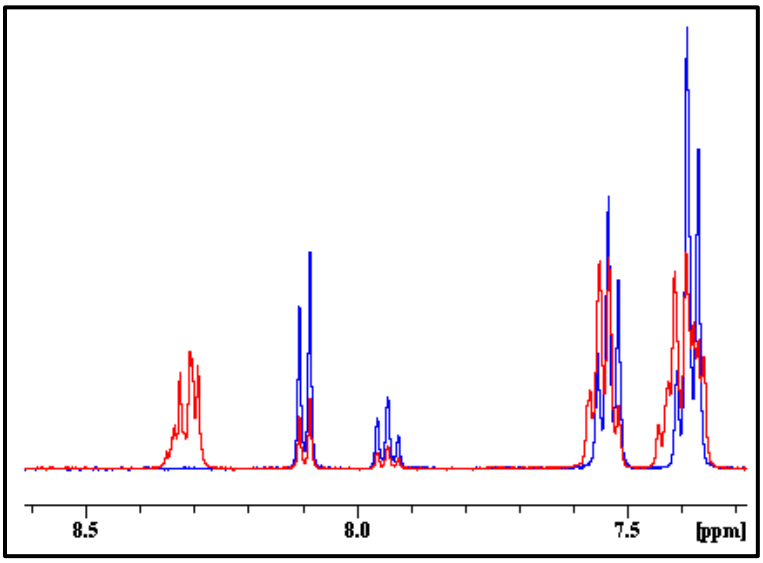

Figure 3.34: Overlay ^{1}H NMR spectra of bap (blue) and **7** (red) in the 7.28-8.62 ppm region.

The UV-Vis spectrum of **7** (Figure 3.35) shows an intraligand ($\pi \rightarrow \pi^*$) transition at 371 nm which is at a lower energy relative to the free bap ligand (355 nm). The absorption at 446 nm is due to the metal-to-ligand charge transfer, $d_\pi(Re) \rightarrow \pi^*(N\text{-}N)$, and is more intense than that of complex **6**. This is expected since **7** has a more conjugated system. The photoexcitation of **6** and **7** at room temperature in acetonitrile does not show any detectable emissions.

The X-ray crystallographic data of **7** confirms that the complex contains the robust *fac*-$[Re(CO)_3]^+$ core in a distorted octahedral environment around the rhenium(I) centre (Figure 3.36). The bap ligand is coordinated bidentatly through the pyridyl nitrogen N(1) and the imine nitrogen N(2) with N(3) uncoordinated. The Re-C bond distances [average = 2.028(8) Å] fall in the range observed [1.900(2)-1.928(2) Å] for similar complexes [37-41]. The Re-N(2) [2.206(5) Å] is shorter than the Re-N(1) [2.227(5) Å] and are typical of Re-$N_{pyridine}$ and Re-N_{imine} bonds [39-41].

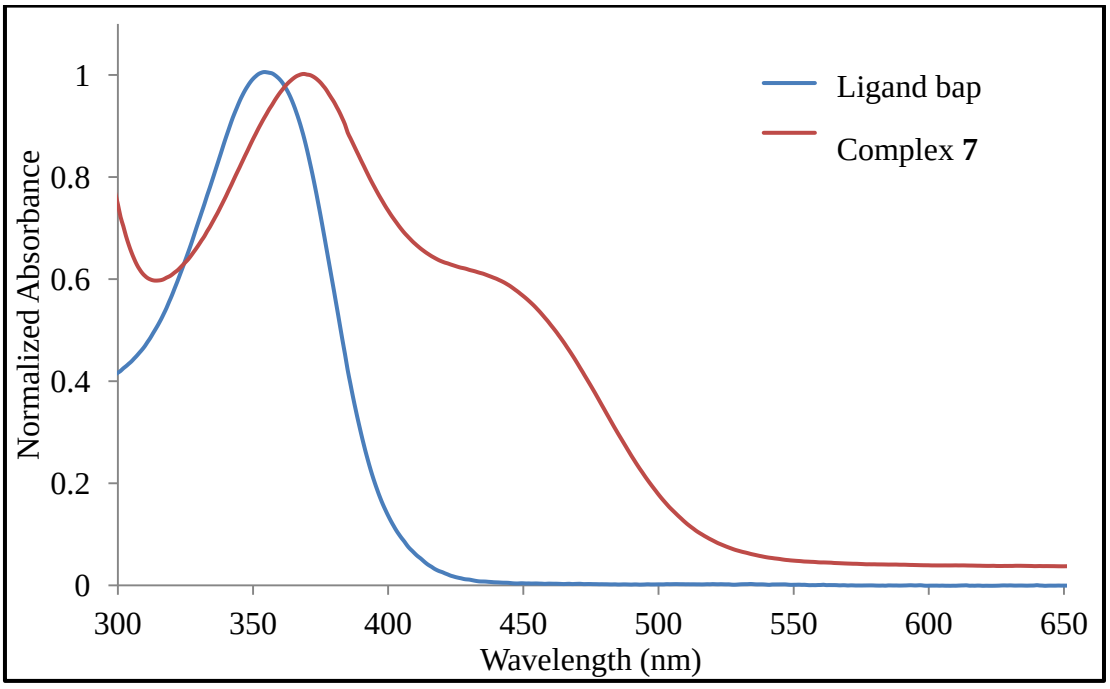

Figure 3.35: Overlay UV-Vis spectra for the aromatic region of bap and **7**.

The small bite angle of bap [N(1)-Re-N(2) = 75.1(2)˚] contributes considerably to the distortion from octahedral geometry, with the average *trans* angle being 171.4(3)˚. The N(1)C(1)C(6)N(2) torsion angle is small [-1.4(9)˚]. The differences in the two C=N bond lengths emphasizes the effect of the coordination of the imine group with the N(2)-C(6) bond [1.288(8) Å] noticeably shorter than the N(3)-C(7) bond [1.305(8) Å]. As with the free ligand bap, complex **7** contains intramolecular hydrogen-bonding between the ketonic oxygens [O(1) and O(2)] and the imine hydrogens [C(6)-H(6) and C(7)-H(7)] (Figure 3.37). Intermolecular hydrogen-bonding exists between ketonic oxygens and the hydrogens of the methyl groups (Table 3.4).

Table 3.4: Hydrogen-bond distances (Å) and angles (˚) in **7.**

D-H•••A	D-H	H•••A	D•••A	D-H•••A
C(6)-H(6)•••O(1)	0.95	2.39	2.914(10)	115
C(7)-H(7)•••O(2)	0.95	2.34	2.998(8)	138
C(14)-H(14A)•••O(1)	0.98	2.38	3.337(9)	143
C(15)-H(15C)•••O(1)	0.98	2.45	3.417(9)	143

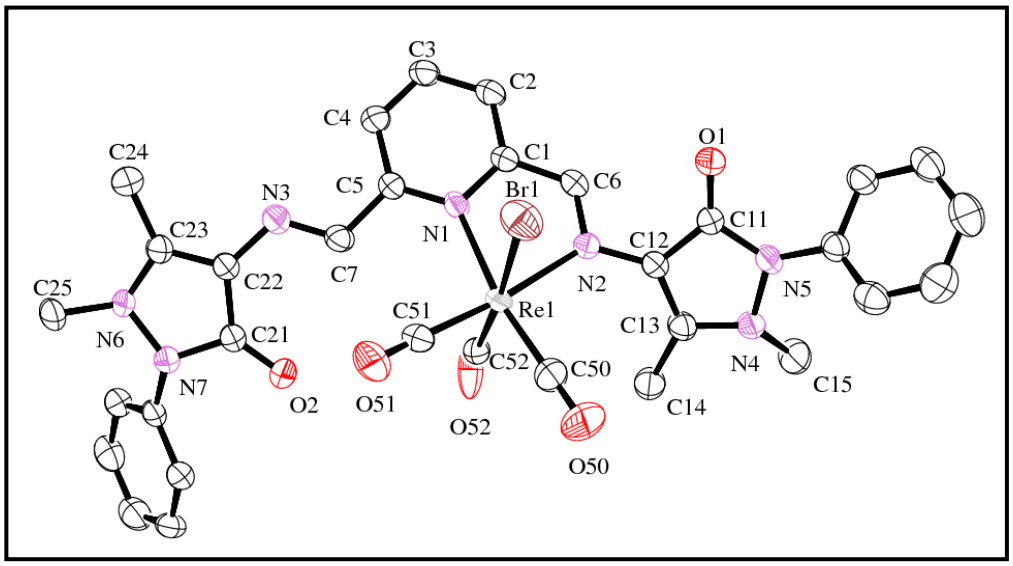

Figure 3.36: An ORTEP view of complex **7** showing 50% probability displacement ellipsoids and the atom labeling. Hydrogen atoms were omitted for clarity.

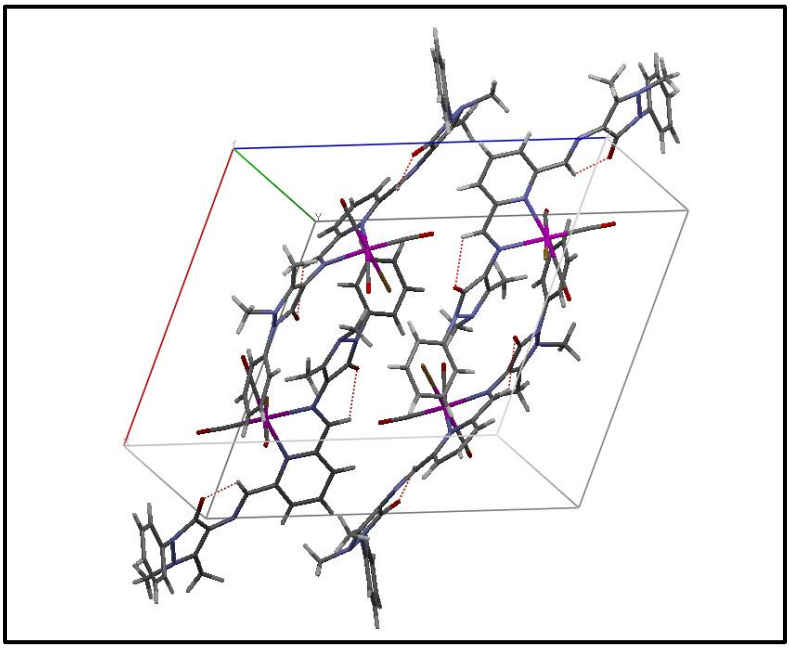

Figure 3.37: Packing diagram in the unit cell of **7** showing the intramolecular hydrogen-bonds.

The cyclic voltammetric properties of **6** and **7** were examined in CH_2Cl_2. For complex **6** an oxidation peak is observed at 0.997 V, ascribed to the Re(I)/Re(II) redox couple. There is no cathode counter peak associated with this oxidative wave indicating that the

process is irreversible. Complex **7** shows similar redox behaviour with an irreversible oxidation peak observed at 1.07 V. The oxidation potentials of the two complexes are similar and occur well within the range observed [0.80-1.30 V] for Re(I) based oxidation processes (Re(I)/Re(II)) under similar conditions [42-46]. Complex **6** has a slightly less positive potential for its oxidation than complex **7**, indicating that **6** undergoes oxidation more readily. This is expected taking the π donating abilities of ligands dae and bap into account. Ligand dae is more electron donating, resulting in an electron-rich rhenium(I) centre for **6**, and therefore the oxidation capability increases.

3.4 References

[1] S.M. Sondi, V.K. Sharma, R.P. Verma, N. Singhal, R. Shukla, R. Raghubir, M.P. Dubey, *Synthesis*, 1999, 878.

[2] A.P. Mishra, *J. Indian. Chem. Soc*., 1999, **76**, 35.

[3] V.C. Filho, R. Correa, Z. Vaz, J.B. Calixto, R.J. Nunes, T.R. Pinheiro, A.D. Andricopulo, R.A. Yunes, *Farmaco*, 1998, **53**, 55.

[4] R. Rose, D.S.R. Murty, G. Chakrapani, *J. Radioanal. Nucl. Chem*., 2005, **265**, 115.

[5] T. Ito, C. Goto, K. Noguchi, *Anal. Chim. Acta*, 2001, **443**, 41.

[6] S.M. Sondhi, N. Singhal, R.P. Verma, S.K. Arora, S.G. Dastidar, *Indian J. Chem.*, 2001, **B40**, 113.

[7] F. Bao, X. Lu, B. Kang, Q. Wu, *Eur. Polym. J.*, 2006, **42**, 928.

[8] S. Cunha, S.M. Oliveira, M.T. Rodrigues, R.M. Bastos, J. Ferrari, C.M.A. de Oliveira, L. Kato, H.B. Napolitano, I. Vencato, C. Lariucci, *J. Mol. Struct.*, 2005, **752**, 32.

[9] M.E. Wolff, *Burger's Medicinal Chemistry*, 3rd Ed.; Wiley: New York, USA, 1970, **Vol. 1.**

[10] R.A. Bailey, T.R. Peterson, *Can. J. Chem*., 1969, **47**, 1681.

[11] A. Altomare, M.C. Burla, M. Camalli, G.L. Gascarano, C. Giacavazco, A. Guagliardi, A.G. Moliterni, G. Polidori, R. Spagna, *J. Appl. Crystallogr*., 1999, **32**, 115.

[12] G.M. Sheldrick, SHELXL-97, Programs for Structure Solution and Refinement, University of Göttingen, Germany, 1997.

[13] Xred, rev. **1.09**, STOE: Darmstadt, Germany.

[14] XShape, rev. **1.02**, STOE: Darmstadt, Germany.

[15] T. Hokelek, Z. Kilic, M. Isikilan, M. Hayvali, *Anal. Sci*., 2002, **18**, 215.

[16] T. Rosu, E. Pahontu, C. Maxim, R. Georgescu, N. Stanica, A. Gulea, *Polyhedron*, 2011, **30**, 154.

[17] T. Hokelek, Z. Kilic, M. Isikilan, H. Dal, H. Nazir, *Anal. Sci*., 2002, **18**, 1281.

[18] T.I.A. Gerber, D. Luzipo, P. Mayer, *J. Coord. Chem*., 2003, **56**, 1564.

[19] O.D. Sloan, P. Thornton, *Polyhedron*, 1988**, 7,** 329 and references therein.

[20] T.I.A. Gerber, Z.R. Tshentu, P. Mayer, *J. Coord. Chem*., 2003, **16**, 1357.

[21] T.I.A. Gerber, D. Luzipo, P. Mayer, *Inorg. Chim. Acta*, 2004, **357**, 429 and references therein.

[22] T.I.A. Gerber, D. Luzipo, P. Mayer, *J. Coord. Chem*., 2006, **59**, 1515.

[23] T.I.A. Gerber, D. Luzipo, P. Mayer, *J. Coord. Chem*., 2004, **57**, 1345.

[24] T.I.A. Gerber, D. Luzipo, P. Mayer, *J. Coord. Chem*., 2004, **57**, 1419.

[25] F.A. Cotton, S. Lippard, *Inorg. Chem*., 1965, **4,** 1621.

[26] P. Mayer, E. Hosten, T.I.A. Gerber, A. Abrahams, *Bull. Korean Chem.Soc*., 2009, **30**, 1204.

[27] T.I.A. Gerber, D. Luzipo, P. Mayer, *J. Coord. Chem.*, 2005, **58**, 637 and references therein.

[28] I. Booysen, T.I.A. Gerber; P. Mayer, H.J. Schalekamp, *J. Coord. Chem*., 2007, **60**, 1755.

[29] V.W.W. Yam, K.K. Tam, M.C. Cheng, S.M. Peng, Y. Wang, *J. Chem. Soc. Dalton Trans.*, 1992, 1717; J.R. Winkler, H.B. Gray, *Inorg. Chem.,* 1985, **24**, 346; V.W.W. Yam, Y.L. Pui, K.M.C.Wong, K.K. Cheung, *Inorg. Chim. Acta*, 2000, **300**, 721.

[30] J.M. Mayer, *Inorg. Chem.*, 1988, **27**, 3899.

[31] T.I.A. Gerber, A. Abrahams, C. Imrie, P. Mayer, *J. Coord. Chem.*, 2004, **57**, 1339.

[32] U. Mazzi, E. Roncari, R. Rossi, V. Bertolasi, O. Traverso, L. Magon, *Transition Met. Chem*., 1980, **5**, 289.

[33] G. Bandoli, U. Mazzi, D.A. Clemente, E. Roncari, *J. Chem. Soc. Dalton Trans*., 1982, 2455.

[34] D.J. Stufkens, *Comments Inorg. Chem*., 1992, **13**, 359.

[35] J. Qin, L. Hu, G.N. Li, X.S. Wang, Y. Xu, J.L. Zuo, X.Z. You, *Organometallics*, 2011, **30**, 2173.

[36] M. Chatterjee, G. Achari, S. Das, R. Banerjee, C. Chakrabarti, J.K. Dattagupta, S. Banerjee, *Inorg. Chem*., 1998, **37**, 5424.

[37] J. Agarwal, R.P. Johnson, G. Li, *J. Phys. Chem. A*, 2011, **115**, 2877.

[38] C.O. Ng, S.W. Lai, H. Feng, S.M. Yiu, C.C. Ko, *Dalton Trans*., 2011, **40**, 10020.

[39] N.S. Fleur, J.C. Hili, A. Mayr, *Inorg. Chim. Acta*, 2009, **362,** 1571.

[40] L. Wei, J.W. Babich, W. Ouellette, J. Zubieta, *Inorg. Chem*., 2006, **45,** 3057.

[41] L. Maria, C. Moura, A. Paolo, I.C. Santos, *J. Organomet. Chem.*, 2006, **691**, 4773; L. Wei, S.R. Banerjee, M.K. Levadala, J. Babich, J. Zubieta, *Inorg. Chim. Acta*, 2004, **357,** 1499.

[42] Y. Chen, W. Liu, J.S. Jin, B. Liu, Z.G. Zou, J.L. Zuo, X.Z. You, *J. Organomet. Chem.*, 2009, **694**, 763.

[43] Z. Si, J. Li, B. Li, F. Zhao, S. Liu, W. Li, *Inorg. Chem*., 2007, **46**, 6155.

[44] K. Wang, L. Huang, L. Gao, L. Jin, C. Huang, *Inorg. Chem.*, 2002, **41**, 3353.

[45] H. Tsubaki, A. Sekine, Y. Ohashi, K. Koike, H. Takeda, O. Ishitani, *J. Am. Chem. Soc*., 2005, **127**, 15544.

[46] V.W.-W. Yam, S.H.-F. Chong, C.-C. Ko, K.-K. Cheung, *Organometallics*, 2000**,** **19**, 5092.

Table 3.5: Crystal and structure refinement data for Hoap and bap

	Hoap	**bap**
Chemical formula	$C_{18}H_{17}N_3O_2$	$C_{29}H_{27}N_7O_2.CH_2Cl_2$
Formula weight	307.35	590.50
Crystal system	Monoclinic	Monoclinic
Space group	$P2_1/n$	$P2/c$
a (Å)	7.4868(5)	9.2167(4)
b (Å)	7.4777(4)	10.6724(5)
c (Å)	27.283(2)	14.7564(8)
β (˚)	95.516(6)	91.642(5)
Volume (Å^3)	1520.3(2)	1450.9(1)
Z	4	2
Density (Calcd.) (gcm^{-3})	1.343	1.352
Absorption coefficient (mm^{-1})	0.090	0.265
F (000)	648	616
Crystal size (mm)	0.05 x 0.13 x 0.43	0.10 x 0.20 x 0.48
θ range	4.2-26.3	4.4-26.4
Index ranges *h*	-9/9	-11/9
k	-5/ 9	-8/13
l	-32/34	-11/18
Reflections measured	6896	5981
Independent/observed reflections	3082/1682	2946/1801
Data/parameters	3082/211	2946/189
Goodness-of-fit on F^2	0.80	1.00
Final *R* indices [$I > 2\ \sigma(I)$]	0.0384	0.0455
	(*wR2* = 0.0800)	(*wR2* = 0.1220)
Largest diff. peak/hole (eÅ^{-3})	0.19/-0.19	0.44/-0.48

Table 3.6: Crystal and structure refinement data for **1** and **2.**

	1	**2**
Chemical formula	$C_{40}H_{39}N_6O_6PCl_2Re_2$	$C_{40}H_{39}N_6O_6PBr_2Re_2$
Formula weight	1174.07	1262.97
Crystal system	Monoclinic	Monoclinic
Space group	$P2_1$	$P2_1$
a (Å)	11.2622(6)	11.5145(6)
b (Å)	11.3572(8)	11.5330(5)
c (Å)	17.8115(9)	17.5492(9)
β (˚)	105.220(3)	105.322(2)
Volume (Å^3)	2198.3(2)	2247.6(2)
Z	2	2
Density (Calcd.) (gcm^{-3})	1.774	1.866
Absorption coefficient (mm^{-1})	5.710	7.244
F (000)	1136	1208
Crystal size (mm)	0.01 x 0.10 x 0.12	0.02 x 0.07 x 0.15
θ range	3.2-25.4	3.2-25.4
Index ranges *h*	-13/13	-13/13
k	-13/13	-13/13
l	-21/21	-21/20
Reflections measured	30594	26769
Independent/observed reflections	8049/5546	8072/6487
Data/parameters	8049/498	8072/514
Goodness-of-fit on F^2	1.04	1.04
Final *R* indices [$I > 2\sigma(I)$]	0.0489	0.0545
	(*wR2* = 0.1186)	(*wR2* = 0.1314)
Largest diff. peak/hole (eÅ^{-3})	-1.48/1.31	-2.47/1.27

Table 3.7: Crystal and structure refinement data for **3**.

	3
Chemical formula	$C_{36}H_{31}N_4Br_3OPRe$
Formula weight	992.60
Crystal system	Monoclinic
Space group	$P2_1/c$
a (Å)	18.4849(5)
b (Å)	15.7325(5)
c (Å)	13.6918(4)
β (˚)	102.563(2)
Volume (Å^3)	3886.4(2)
Z	4
Density (Calcd.) (gcm^{-3})	1.562
Absorption coefficient (mm^{-1})	5.255
F (000)	1778
θ range	3.2–25.4
Index ranges *h*	–22/22
k	–18/17
l	–16/16
Reflections measured	23596
Independent/observed reflections	7096/5723
Data/parameters	7096/415
Goodness-of-fit on F^2	1.954
Final *R* indices [$I > 2\sigma(I)$]	0.2476
	(*wR2* = 0.0802)

Table 3.8: Crystal and structure refinement data for **4** and **5**.

	4	**5**
Chemical formula	$C_{38}H_{37}IN_4O_3PRe.½EtOH.½H_2O$	$C_{38}H_{36}C_{l2}IN_3O_4PRe$
Formula weight	973.85	1013.70
Crystal system	Monoclinic	Triclinic
Space group	$P2_1/n$	P-1
a (Å)	18.1552(7)	8.9777(2)
b (Å)	10.5717(5)	14.8943(5)
c (Å)	20.1771(6)	16.3963(5)
α (˚)		65.274(3)
β (˚)	96.620(5)	87.686(2)
γ (˚)		74.037(2)
Volume ($Å^3$)	3846.8(3)	1907.7(1)
Z	4	2
Density (Calcd.) (gcm^{-3})	1.682	1.765
Absorption coefficient (mm^{-1})	4.047	4.219
F (000)	1908	988
Crystal size (mm)	0.12 × 0.11 × 0.03	0.04 x 0.11 x 0.22
θ range	4.2-26.3	4.2-26.4
Index ranges h	-16/22	-11/11
k	-13/11	-18/18
l	-22/25	-20/20
Reflections measured	18454	27595
Independent/observed reflections	7764/3976	7727/6249
Data/parameters	7764/453	7727/419
Goodness-of-fit on F^2	0.80	1.09
Final R indices [$I > 2\ \sigma(I)$]	0.0420	0.0496
	($wR2$ = 0.0833)	($wR2$ = 0.1049)
Largest diff. peak/hole ($eÅ^{-3}$)	1.50/-0.99	2.13/-1.80

Table 3.9: Crystal and structure refinement data for **6** and **7**.

	6	**7**
Chemical formula	$C_{27}H_{24}ClN_6O_5Re.H_2O$	$C_{32}H_{27}Br\ N_7O_5Re$
Formula weight	752.20	855.72
Crystal system	Monoclinic	Monoclinic
Space group	$P2_1/c$	$P2_1/c$
a (Å)	15.3940(3)	14.284(2)
b (Å)	10.5480(2)	14.580(2)
c (Å)	20.9820(4)	17.233(3)
β (˚)	122.544(1)	109.020(6)
Volume ($Å^3$)	2872.00(10)	3393.0(9)
Z	4	4
Density (Calcd.) (gcm^{-3})	1.740	1.675
Absorption coefficient (mm^{-1})	4.376	4.808
F (000)	1480	1672
θ range	2.3-28.3	2.5-28.2
Index ranges *h*	-20/20	-18/13
k	-11/14	-18/19
l	-27/27	-22/22
Reflections measured	26124	31694
Independent/observed reflections	7050/6474	8311/6494
Data/parameters	7050/381	8311/415
Goodness-of-fit on F^2	1.26	1.04
Final *R* indices [$I > 2\ \sigma(I)$]	0.0199	0.0439
	(*wR2* = 0.0475)	(*wR2* = 0.1307)
Largest diff. peak/hole ($eÅ^{-3}$)	1.35/-1.02	2.70/-2.53

Table 3.10: Selected bond lengths (Å) and angles (˚) for Hoap.

Bond lengths			
O(1)-C(7)	1.235(2)	C(15)-C(16)	1.379(3)
O(2)-C(14)	1.359(2)	C(13)-C(14)	1.402(2)
N(1)-N(2)	1.411(2)	C(17)-C(18)	1.381(2)
N(1)-C(7)	1.398(2)	N(1)-C(1)	1.426(2)
N(2)-C(9)	1.368(2)	N(2)-C(11)	1.471(2)
N(3)-C(12)	1.286(2)	C(1)-C(2)	1.383(2)
N(3)-C(8)	1.397(2)	C(1)-C(6)	1.387(2
C(7)-C(8)	1.445(2)	C(2)-C(3)	1.387(2)
C(8)-C(9)	1.358(2)	C(3)-C(4)	1.382(2)
C(12)-C(13)	1.453(2)	C(4)-C(5)	1.382(2)
C(16)-C(17)	1.380(3)	C(5)-C(6)	1.387(2)
C(14)-C(15)	1.393(2)	C(9)-C(10)	1.485(2)
Bond angles			
N(2)-N(1)-C(7)	109.9(1)	N(1)-C(7)-C(8)	104.5(1)
N(1)-N(2)-C(9)	106.1(1)	C(7)-C(8)-C(9)	108.2(1)
C(8)-N(3)-C(12)	122.1(1)	C(8)-C(9)-C(10)	127.7(2)
O(1)-C(7)-C(8)	132.0(2)	N(3)-C(12)-C(13)	121.2(1)

Table 3.11: Selected bond lengths (Å) and angles (˚) for bap.

Bond lengths			
O(1)-C(7)	1.230(2)	C(9)-N(2)	1.359(2)
C(12)-C(13)	1.471(3)	C(8)-N(3)	1.389(2)
N(1)-N(2)	1.406(2)	C(13)-C(14)	1.390(3)
N(1)-C(7)	1.404(2)	C(14)-C(15)	1.378(2)
N(3)-C(12)	1.281(2)	N(4)-C(13)	1.350(2)
N(3)-C(8)	1.389(2)	C(1)-C(2)	1.383(3)
C(7)-C(8)	1.445(3)	C(2)-C(3)	1.383(3)
C(8)-C(9)	1.368(3)	C(3)-C(4)	1.380(4)
N(1)-C(1)	1.430(2)	C(4)-C(5)	1.383(3)
N(2)-C(11)	1.457(3)	C(5)-C(6)	1.379(3)
C(9)-C(10)	1.488(3)	C(6)-C(1)	1.387(3)
Bond angles			
N(2)-N(1)-C(7)	109.7(1)	N(3)-C(8)-C(7)	130.0(2)
C(8)-N(3)-C(12)	122.8(2)	C(8)-C(9)-C(10)	128.5(1)
O(1)-C(7)-N(1)	124.3(2)	N(3)-C(12)-C(13)	118.6(2)
O(1)-C(7)-C(8)	131.5(2)	N(3)-C(8)-C(9)	121.8(2)

Table 3.12: Selected bond lengths (Å) and angles (˚) for **1** and **2**.

Bond lengths					
	1	**2**		**1**	**2**
Re-X(1)	2.381(3)	2.522(1)	N(4)-C(13)	1.36(2)	1.35(2)
Re-X(2)	2.410(3)	2.555(1)	C(1)-O(1)	1.32(2)	1.29(2)
Re-N(1)	2.189(9)	2.19(1)	N(1)-C(2)	1.40(2)	1.42(2)
Re-O(1)	2.121(9)	2.102(9)	N(2)-N(3)	1.43(2)	1.39(2)
Re-N(4)	1.73(1)	1.736(1)	N(5)-N(6)	1.41(2)	1.39(2)
Re-P(1)	2.408(3)	2.410(4)	C(1)-C(2)	1.41(2)	1.38(2)
O(2)-C(12)	1.21(2)	1.20(2)	N(3)-C(3)	1.32(2)	1.35(2)
Bond angles					
	1	**2**		**1**	**2**
O(1)-Re-N(4)	164.5(4)	165.1(4)	N(4)-Re-P(1)	90.5(3)	90.5(3)
N(1)-Re-X(1)	168.0(3)	168.2(3)	Re-N(4)-C(13)	167.8(9)	170.3(9)
P(1)-Re-X(2)	166.0(1)	166.72(9)	X(1)-Re-X(2)	88.3(2)	88.04(5)
P(2)-Re-X(1)	89.7(2)	89.9(8)	N(1)-Re-O(1)	79.7(4)	79.2(4)
N(4)-Re-X(1)	101.1(4)	100.3(3)	C(1)-N(2)-C(6)	130(1)	129(1)
N(4)-Re-X(2)	103.5(3)	102.8(3)	Re-N(1)-C(2)	109.8(7)	108.8(8)
N(4)-Re-N(1)	88.5(5)	89.4(5)	Re-O(1)-C(1)	110.5(8)	111.7(8)

Table 3.13: Selected bond lengths (Å) and angles (˚) for **3.**

Bond lengths			
Re-N(1)	1.72(1)	Re-N(2)	2.15(1)
Re-Br(1)	2.505(2)	Re-P(1)	2.422(3)
Re-O(1)	2.098(8)	C(7)-N(2)	1.27(2)
Re-Br(2)	2.560(1)	C(8)-O(1)	1.27(2)
Bond angles			
N(1)-Re-O(1)	160.3(4)	P(1)-Re-Br(2)	171.53(9)
C(7)-N(2)-C(9)	124(1)	N(1)-Re-Br(1)	107.9(3)
N(1)-Re-N(2)	81.4(4)	N(2)-Re-Br(1)	170.3(3)
N(2)-Re-O(1)	79.7(4)	Re-N(1)-C(1)	148(1)

Table 3.14: Selected bond lengths (Å) and angles (˚) for **4.**

Bond lengths			
Re-O(1)	2.209(4)	N(3)-C(8)	1.397(8)
Re-O(2)	1.646(5)	C(8)-C(9)	1.38(1)
Re-O(3)	1.877(4)	C(7)-C(8)	1.422(9)
Re-N(3)	2.155(5)	C(7)-N(1)	1.333(8)
Re-N(4)	1.979(5)	N(1)-N(2)	1.384(8)
Re-P(1)	2.454(6)	N(2)-C(9)	1.364(9)
O(1)-C(7)	1.276(8)	N(4)-C(14)	1.363(9)
C(12)-N(3)	1.296(7)	O(3)-C(37)	1.41(1)
Bond angles			
O(2)-Re-O(3)	165.0(2)	O(2)-Re-O(1)	84.9(2)
O(1)-Re-N(4)	169.4(2)	O(2)-Re-N(3)	91.8(2)
O(1)-Re-N(3)	80.4(2)	O(2)-Re-P(1)	93.2(1)
N(3)-Re-N(4)	90.2(2)	O(2)-Re-N(4)	100.3(2)
P(1)-Re-N(3)	174.9(2)	O(1)-Re-P(1)	99.1(1)
C(8)-N(3)-C(12)	126.6(6)	O(3)-Re-N(3)	87.2(2)

Table 3.15: Selected bond lengths (Å) and angles (˚) for **5.**

Bond lengths			
Re-O(3)	1.702(6)	C(8)-N(22)	1.21(2)
Re-O(4)	1.886(5)	N(22)-N(32)	1.41(3)
Re-O(1)	1.985(5)	N(32)-C(10)	1.59(3)
Re-O(2)	2.171(7)	C(10)-C(9)	1.39(1)
Re-P(1)	2.454(2)	N(1)-C(9)	1.40(1)
Re-N(1)	2.130(5)	C(1)-O(1)	1.35(9)
N(1)-C(7)	1.296(8)	C(6)-C(7)	1.44(1)
C(8)-O(2)	1.27(1)	O(4)-C(37)	1.39(1)
Bond angles			
O(3)-Re-O(4)	168.5(2)	O(3)-Re-O(2)	87.5(3)
O(1)-Re-O(2)	170.9(2)	O(3)-Re-P(1)	91.7(2)
C(7)-N(1)-C(9)	126.5(6)	O(3)-Re-N(1)	96.3(2)
Re-O(4)-C(37)	147.1(5)	O(1)-ReO(4)	92.5(2)
O(1)-Re-N(1)	92.3(2)	O(3)-Re-O(1)	98.8(2)
N(1)-Re-O(2)	80.5(2)	O(4)-Re-N(1)	85.1(2)
O(3)-Re-O(1)	98.8(2)	O(2)-Re-O(4)	81.5(2)

Table 3.16: Selected bond lengths (Å) and angles (˚) for **6.**

Bond lengths			
Re(1)-Cl(1)	2.4741(8)	N(2)-C(32)	1.407(3)
Re(1)-N(1)	2.173(2)	N(1)-C(12)	1.401(3)
Re(1)-N(2)	2.182(2)	C(31)-C(32)	1.437(5)
Re(1)-C(90)	1.918(3)	C(32)-C(33)	1.373(4)
Re(1)-C(91)	1.906(3)	C(12)-C(13)	1.369(3)
Re(1)-C(92)	1.922(3)	C(12)-C(11)	1.442(3)
N(1)-C(1)	1.292(4)	C(91)-O(91)	1.145(4)
N(2)-C(2)	1.303(3)	C(92)-O(92)	1.148(4)
C(2)-N(1)	1.443(4)	C(90)-O(90)	1.147(4)
Bond angles			
Cl(1)-Re(1)-N(1)	81.98(6)	C(32)-N(2)-C(2)	116.7(2)
Cl(1)-Re(1)-C(91)	178.2(1)	C(1)-N(1)-C(12)	120.0(2)
N(1)-Re(1)-C(92)	174.7(1)	N(2)-C(2)-C(1)	117.4(2)
N(2)-Re(1)-C(90)	169.4(1)	C(91)-Re(1)-N(2)	94.0(1)
N(1)-Re(1)-N(2)	74.08(8)	C(91)-Re(1)-N(1)	96.6(1)
Cl(1)-Re(1)-N(2)	84.63(7)	N(2)-Re(1)-C(92)	101.8(1)
N(1)-C(1)-C(2)	116.7(2)	N(1)-Re(1)-C(91)	96.6(1)

Table 3.17: Selected bond lengths (Å) and angles (˚) for **7.**

Bond lengths			
Re(1)-Br(1)	2.612(1)	N(2)-C(12)	1.404(9)
Re(1)-N(1)	2.227(5)	C(12)-C(11)	1.44(1)
Re(1)-N(2)	2.206(5)	C(11)-O(1)	1.234(7)
Re(1)-C(50)	1.911(8)	C(11)-N(5)	1.393(9)
Re(1)-C(51)	1.936(7)	N(5)-N(4)	1.404(7)
Re(1)-C(52)	2.24(1)	N(4)-C(13)	1.38(1)
N(2)-C(6)	1.288(8)	C(13)-C(12)	1.383(8)
N(3)-C(7)	1.305(8)	C(21)-O(2)	1.236(8)
Bond angles			
N(1)-Re(1)-N(2)	75.1(2)	Br(1)-Re(1)-N(1)	83.6(1)
Br(1)-Re(1)-C(52)	172.1(2)	Br(1)-Re(1)-N(2)	84.3(1)
N(1)-Re(1)-C(50)	170.2(3)	C(50)-Re(1)-C(51)	87.0(3)
N(2)-Re(1)-C(51)	171.9(2)	N(2)-Re(1)-C(50)	96.2(3)
Br(1)-Re(1)-C(50)	91.2(2)	N(1)-Re(1)-C(51)	101.0(2)
Br(1)-Re(1)-C(51)	88.3(2)	C(51)-Re(1)-C(52)	94.1(4)
N(2)-C(6)-C(1)	119.7(6)	C(50)-Re(1)-C(52)	96.5(3)

Chapter 4

Coordination of Bidentate Aniline Derivatives to the *fac*-$[Re(CO)_3]^+$ core

4.1 Introduction

The nuclear properties of the ^{99m}Tc and $^{186/188}Re$ isotopes have made them ideal for application as diagnostic and therapeutic radiopharmaceuticals respectively [1]. Initially most research efforts were focussed on the $[M^{V}O]^{3+}$ core (M = Tc, Re), since it could easily be obtained from the permetalate, but since the discovery of the cardiac imaging agent $[^{99m}Tc(MIBI)_6]^+$ (MIBI = 2-methoxy-2-methylpropylisocyanide) [2] and the easy preparation of the synthons $[M(CO)_3(H_2O)_3]^+$ and $[M(CO)_3X_3]^{2-}$ (X = Cl, Br), the research efforts have shifted to the +I oxidation state [3]. Studies on these synthons have illustrated a high substitution lability of the three halides and water molecules, with a concomitant stability of the three carbonyl ligands [4]. It was therefore not surprising that tridentate chelates with a combination of oxygen, sulfur, nitrogen and phosphorus donor atoms were initially investigated as possible ligands for the $[M(CO)_3]^+$ core [5].

Derivatives of aniline have received considerable interest in coordination chemistry due to their chelating abilities [6-8]. Aniline derivatives are also employed in the formation of Schiff bases through condensation reactions with aldehydes or ketones. These ligand systems are suitable for the study of the coordination chemistry of rhenium since they are able to provide a variety of donor atoms, stability and multidenticity towards the metal centre [9]. Furthermore, it has been shown that Schiff bases of aniline and their corresponding metal complexes possess potent biological activity. For example, the Schiff base H_2L (H_2L = (2E)-2-(2-((E)-(2-hydroxyphenylimino)methyl)

benzylideneamino)phenol and its metal complexes exhibited promising antifungal activity and proved to be promising antimicrobial agents for application in the medicinal and pharmaceutical field [10].

This chapter focuses on the synthesis and structural characterization of the rhenium(I) complexes formed by the reaction of $[Re(CO)_5Br]$ and the potentially bi- and tridentate ligands containing an aromatic backbone (Scheme 4.1).

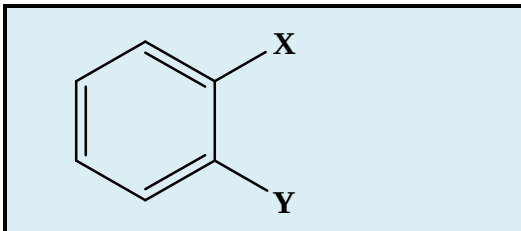

X	Y	Abbv
NH_2	NH_2	Hpda
NH_2	OH	Hno
SH	OH	Hsop

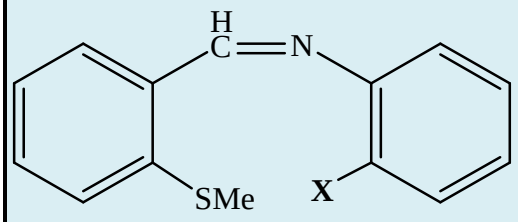

NH_2	Htpn
OH	Hons

Scheme 4.1: Structures of ligands used.

4.2 Experimental

4.2.1 Synthesis of 2-[(2-methylthio)benzylideneimino]phenol (Hons)

2-(Methylthio)benzaldehyde (0.31 g, 0.95 mmol) in 20 cm^3 of methanol was added to 2-aminophenol (0.10 g, 0.92 mmol) in 30 cm^3 of methanol. The yellow solution was heated at reflux temperature under nitrogen for 4 hours. The solvent was removed under vacuum to produce a yellow precipitate, which was dried under vacuum. Yield = 60 %, m.p. = 63-65 ˚C. Anal. Calcd. (%) for $C_{14}H_{13}NOS$: C, 69.1; H, 5.4; N, 5.8; S, 13.2. Found: C, 69.1;

H, 5.3; N, 5.8; S, 13.2. IR (ν_{max}/cm^{-1}): ν(O-H) 3373; ν(C=N) 1628. ^{1}H NMR (295K, ppm): 9.35 (d, 1H, *H*(9)); 9.28 (s, 1H, *H*(5)); 7.81 (t, 1H, *H*(7)); 7.74 (d, 1H, *H*(1)); 7.62 (t, 1H, *H*(3)); 7.49 (d, 1H, *H*(6)); 7.42 (t, 1H, *H*(8)); 7.26 (d, 1H, *H*(4)); 7.18 (t, 1H, *H*(2)); 2.77 (s, 3H, C*H*$_3$).

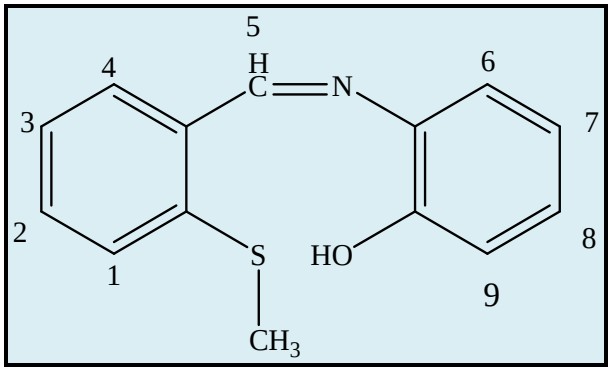

Figure 4.1: Structure of Hons.

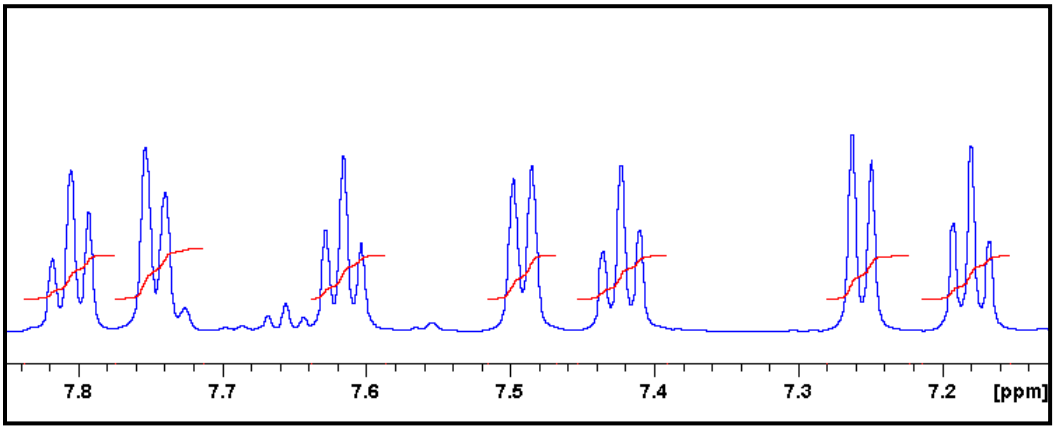

Figure 4.2: ^{1}H NMR spectrum illustrating the aromatic region of Hons.

4.2.2 Synthesis of *N*-(2-(methylthio)benzylidene)benzene-1,2-diamine (Htpn)

1,2-Diaminobenzene (1.00 g, 9.24 mmol) and 2-(methylthio)benzaldehyde (1.40 g, 9.24 mmol) were dissolved in 50 cm^3 of methanol and refluxed for 5 hours under nitrogen. After cooling the resultant orange solution to room temperature, the solvent was removed under vacuum to form an orange precipitate which was dried under vacuum. Yield = 77 %, m.p. = 67 ˚C. Anal. Calcd. (%) for $C_{14}H_{13}N_2S$: C, 69.4; H, 5.8; N, 11.6; S, 13.2.

Found: C, 68.2; H, 5.7; N, 11.2; S, 14.1. IR (ν_{max}/cm^{-1}): ν(NH$_2$) 3051; ν(C=N) 1627. ^{1}H NMR (295K, ppm): 8.87 (s, 1H, *H*(5)); 7.11 (d, 1H, *H*(9)); 7.07 (t, 1H, *H*(7)); 6.88 (d, 1H, *H*(1)); 6.83 (t, 1H, *H*(3)); 6.64 (d, 1H, *H*(6)); 6.59 (d, 1H, *H*(4)); 6.54 (t, 1H, *H*(8)); 6.42 (t, 1H, *H*(2)). UV-Vis (MeOH, λ_{max} (ε, M^{-1}cm^{-1})): 360 (8580).

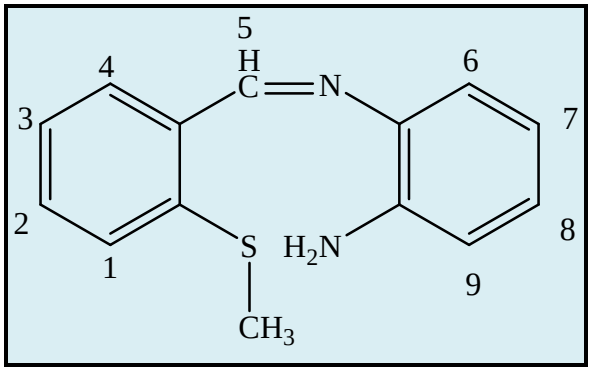

Figure 4.3: Structure of Htpn.

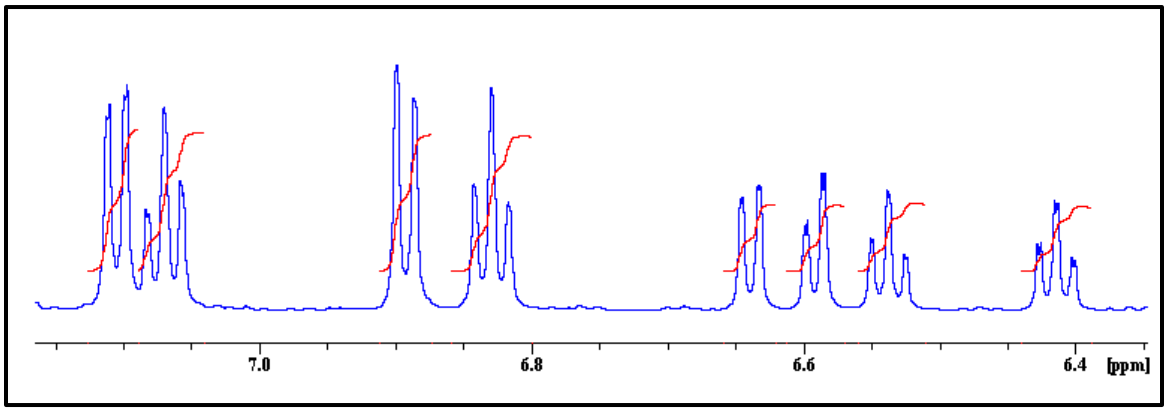

Figure 4.4: ^{1}H NMR spectrum of the aromatic region of Htpn.

4.2.3 Synthesis of *fac*-[Re(CO)$_3$(κ^1-Hpda)(κ^2-Hpda)]Br (1)

A mass of 60 mg (556 µmol) of 1,2-diaminobenzene (Hpda) was added to 100 mg (246 µmol) of [Re(CO)$_5$Br] in 20 cm^3 of toluene. The mixture was heated under reflux in a nitrogen atmosphere for two hours. The solution was left to cool to room temperature, after which the resultant white precipitate was collected by filtration. The filtrate was left to evaporate slowly at room temperature producing lavender crystals. Yield = 57 %, m.p. = 252 ˚C. Anal. Calcd. (%) for $C_{15}H_{16}N_4O_3BrRe$: C, 31.8; H, 2.8; N, 9.9. Found: C, 31.8;

H, 3.0; N, 9.7. IR (ν_{max}/cm^{-1}): ν(NH$_2$) 3104(m), 3169(m), 3194(m), 3245(m); ν(C≡O) 2031(s), 1925(s), 1880(s); ν(Re-N) 528(m), 513(m), 484(m). ^{1}H NMR (295K, ppm): 7.14-7.34 (m, 4H, *H*(3), *H*(4), *H*(5), *H*(6)); 6.48 (d, 1H, *H*(12)); 6.17 (m, 3H, *H*(9), *H*(10), *H*(11)). UV-Vis (MeOH, λ_{max} (ε, M^{-1}cm^{-1})): 538 (2567), 631 (760). Conductivity (10^{-3} M, MeOH): 126 ohm^{-1}cm^{2}mol^{-1}.

4.2.4 Synthesis of [Re$_2$(CO)$_7$(spo)$_2$] (2)

2-Mercaptophenol (Hspo) (70 mg, 559 μmol) was dissolved in 10 cm^3 of toluene, and added to *fac*-[Re(CO)$_5$Br] (100 mg, 246 μmol) in 10 cm^3 of toluene. The mixture was heated under reflux for 90 min. The resultant light brown solution was left to cool to room temperature. Beige crystals were obtained from the slow evaporation of the mother liquor. Yield = 62 %, m.p. = 155 ˚C. Anal. Calcd. (%) for $C_{19}H_{10}O_9S_2Re_2$: C, 27.9; H, 1.2; S, 7.8. Found: C, 27.8; H, 1.5; S, 8.2. IR (ν_{max}/cm^{-1}): ν(C≡O) 2016(s), 1932(s), 1914(s), 1887(s); ν(Re-O) 472; ν(Re-S) 357. ^{1}H NMR (295K, ppm): 7.76 (d, 2H, *H*(16), *H*(26)); 7.33 (d, 2H, *H*(13), *H*(23)); 7.15 (t, 2H, *H*(15), *H*(25)); 6.96 (t, 2H, *H*(14), *H*(24)). Conductivity (10^{-3} M, CH_3OH) = 33 ohm^{-1}cm^2 mol^{-1}.

4.2.5 Synthesis of *fac*-[Re(CO)$_3$(ons)(Hno)] (3)

A mixture of Hons (194 mg, 329 μmol) and *fac*-[Re(CO)$_5$Br] (103 mg, 255 μmol) was heated under reflux in 20 cm^3 of toluene for 90 min. The resultant green solution was cooled to room temperature and the precipitate which formed was filtered, washed with diethyl ether and dried under vacuum. Orange crystals were obtained by the slow evaporation of the mother liquor. Yield = 37 %, m.p. = 172-175 ˚C. Anal. Calcd. (%) for $ReC_{23}H_{19}N_2O_5S.C_7H_8$: C, 50.5; H, 3.8; N, 3.9; S, 4.5. Found: C, 50.4; H, 3.8; N, 4.0; S, 4.5. IR (ν_{max}/cm^{-1}): ν(N-H) 3414, 3471; ν(C≡O)$_{fac}$ 2021(s), 1905(s); ν(C=N) 1601; ν(Re-N) 490, 474; ν(Re-O) 394. ^{1}H NMR (295K, ppm): 10.02 (s, 1H, *H*(11)); 9.65 (s, br, 1H, O*H*); 9.41 (d, 1H, *H*(9)); 7.74 (t, 1H, *H*(8)); 7.46-7.60 (m, 2H, *H*(7), *H*(6)); 7.38 (d, 1H, *H*(17)); 7.05-7.30 (m, 3H, *H*(14), *H*(15), *H*(16)); 6.46-6.88 (m, 4H, *H*(20), *H*(21), *H*(22),

H(23)); 3.50 (s, br, 1H, N*H*); 2.23 (s, 3H, CH_3). UV-Vis (MeOH, λ_{max} (ε, $M^{-1}cm^{-1}$)): 426 (3190). Conductivity (MeOH, 10^{-3} M): 41 $ohm^{-1}cm^2mol^{-1}$.

4.2.6 Synthesis of *fac*-[Re(CO)$_3$(Htpn)Br] (4)

A mass of 122 mg (503 μmol) of Htpn dissolved in 10 cm^3 of toluene was added to 101 mg (249 μmol) of *fac*-[Re(CO)$_5$Br] in 10 cm^3 of toluene. The solution was heated under nitrogen for 3 hours with stirring. The resultant orange solution was left at room temperature overnight after which yellow crystals formed. The product was filtered and dried under vacuum. Yield = 66 %, m.p. = 195-197 ˚C. Anal. Calcd. (%) for $C_{17}H_{14}N_2O_3SBrRe$: C, 34.5; H, 2.4; N, 4.7; S, 5.4. Found: C, 34.6; H, 2.6; N, 4.9; S, 5.8. IR (ν_{max}/cm^{-1}): *ν*(NH_2) 3064(m); *ν*(C≡O) 2033(s), 1923(s), 1896(s); *ν*(C=N) 1583; *ν*(Re-S) 354(m). ^{1}H NMR (295K, ppm): 9.36 (s, 1H, *H*(11)); 7.89–7.33 (m, 5H, *H*(7), *H*(10), *H*(14), *H*(16), *H*(17)); 7.11 (t, 1H, *H*(8)); 6.72 (t, 1H, *H*(15)); 6.55 (t, 1H, *H*(9)); 3.08 (s, 3H, SCH_3). UV-Vis (MeOH, λ_{max} (ε, $M^{-1}cm^{-1}$)): 313 (8190), 433 (3680). Conductivity (MeOH, 10^{-3} M): 75 $ohm^{-1}cm^2mol^{-1}$.

4.2.7 X-ray Crystallography

X-ray diffraction studies of **1**, **3**.C_7H_8 and **4** were performed at 200(2) K using a Nonius Kappa CCD diffractometer with graphite monochromated Mo Kα radiation (λ = 0.71072 Å). Crystals of **2** were studied with a Bruker Kappa Apex II diffractometer. The structures were solved by direct methods applying SIR97 [11] and refined by least-squares procedures using SHELXL-97 [12]. All non-hydrogen atoms were refined anisotropically, and the hydrogen atoms were calculated in idealized geometrical positions. In complex **1**, the monodentate Hpda ligand is disordered, and a split model was applied with a *sof* ratio of 0.7:0.3. The non-hydrogen atoms of the main part were refined anisotropically, and those of the minor part isotropically. The data were corrected by a numerical absorption correction [13] after optimizing the crystal shape with XShape [14]. Crystal and structure refinement data are given in Tables 4.5, 4.6, 4.7 and 4.8 for **1**,

2, **3** and **4** respectively, with selected bond distances and angles in Tables 4.9, 4.10, 4.11 and 4.12.

4.3 Results and Discussion

4.3.1 Synthesis and characterization of *fac*-[Re(CO)$_3$(κ^1-Hpda)(κ^2-Hpda)]Br (1)

The reaction of *fac*-[Re(CO)$_5$Br] with two equivalents of Hpda in refluxing toluene resulted in the formation of [Re(CO)$_3$(κ^1-Hpda)(κ^2-Hpda)]Br (**1**). Two carbonyls and the bromide of [Re(CO)$_5$Br] were substituted by two Hpda units, with one Hpda chelating bidentately and the second acting as a neutral monodentate ligand.

$$[Re(CO)_5Br] + 2Hpda \longrightarrow [Re(CO)_3(\kappa^1\text{-Hpda})(\kappa^2\text{-Hpda})]Br + 2CO$$

Compound **1** is a 1:1 electrolyte in methanol (Λ_M = 126 ohm^{-1}cm^{2}mol^{-1}). The light lavender solid is soluble in alcohols and when left to stand for a few days in solution, a deep purple solution forms. The complex is stable for months in the solid state and only for days in solution.

Characteristic of the *fac*-[Re(CO)$_3$]$^+$ core, the IR spectrum exhibits three strong ν(C≡O) stretches at 1880, 1925 and 2031 cm^{-1}. The N-H stretches appear as four medium intensity peaks in the 3100-3250 cm^{-1} range. The absorptions at 484, 513 and 528 cm^{-1} are assigned to the Re-N stretching mode. The aromatic region of the ^{1}H NMR spectrum of **1** displays the signals due to the eight protons of the two coordinated 1,2-diaminobenzene (Hpda) moieties. These signals appear as two multiplets and a doublet, and it is clear from the spectrum that the two Hpda units are not magnetically equivalent. This is to be expected since the two ligands coordinate differently, resulting in the protons being present in different magnetic environments.

The electronic absorption and emission spectra of **1** is shown in Figure 4.5. Two bands are visible on the UV-Vis spectrum: an intense absorption at 538 nm and a less intense absorption at 631 nm, which appears as a shoulder. These are due to the metal-to-ligand charge transfer (MLCT) $d\pi(Re) \rightarrow \pi^*(L)$ transition. Upon excitation (λ_{ex} = 450 nm) of a methanolic solution of **1**, a broad emission band was observed at 526 nm. It is thought that this emission results from ligand-centred $\pi^* \rightarrow \pi$ relaxations.

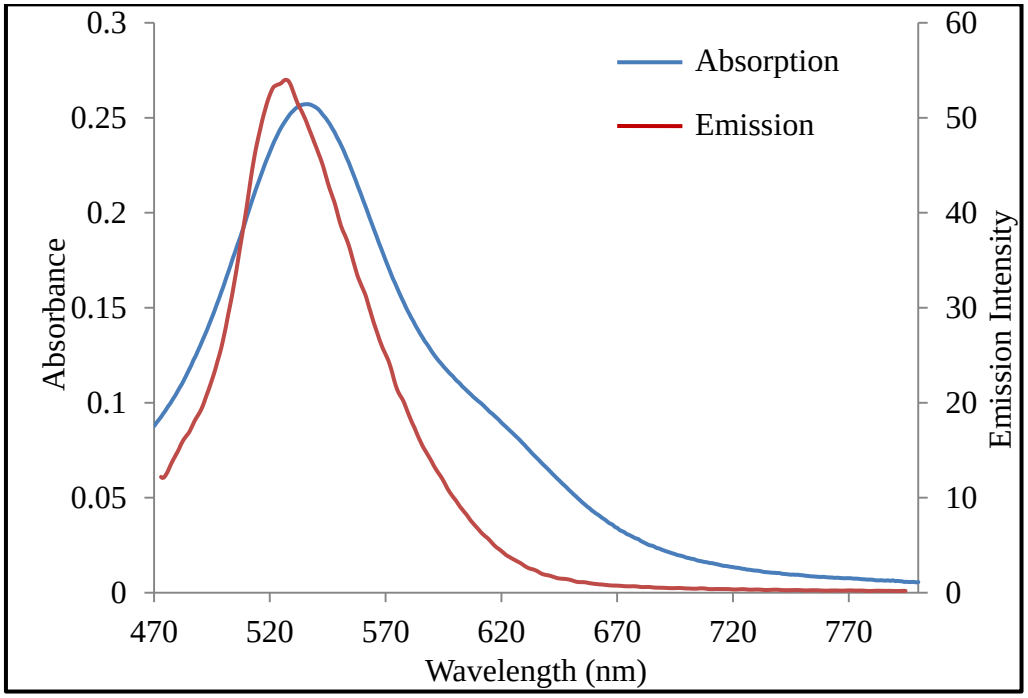

Figure 4.5: Absorption (blue) and emission (red) spectra of **1**.

A perspective view of the asymmetric unit of **1** is shown in Figure 4.6. The X-ray results show that the rhenium(I) complex cation contains the chemically robust *fac*-$[Re(CO)_3]^+$ core in a distorted octahedral geometry. The rhenium(I) is coordinated to three carbonyl donors in a *facial* orientation, to the two amino nitrogen atoms N(1) and N(2) of one Hpda ligand, and to one nitrogen atom N(3) of a second Hpda. The amino group $N(4)H_2$ is uncoordinated. The Re-C bond distances [average of 1.905(4) Å] fall in the range observed [1.900(2)-1.928(2) Å] for similar complexes [15, 16]. The two Re-N bond lengths of the bidentate ligand is similar [average of 2.218(3) Å], and noticeably shorter

than the Re-N(3) length [2.256(3) Å]. However, all three lengths are typical for Re-N(amino) bonds [16, 17].

The distortion from octahedral ideality is mainly the result of the *trans* angles, with N(1)-Re-C(13) = 176.3(1)°, N(2)-Re-C(14) = 171.6(1)° and N(3)-Re-C(15) = 178.1(2)°. These distortions are the result of the constraints imposed by the bidentate ligand, which forms a five-membered [N(1)-Re-N(2) = 76.8(1)°] metalloring. This argument is manifested in the larger (closer to linearity) bond angle between the *trans* monodentate ligand/donor C(15)O and N(3)H2. The average C-Re-C bond angle is 88.6(2)°.

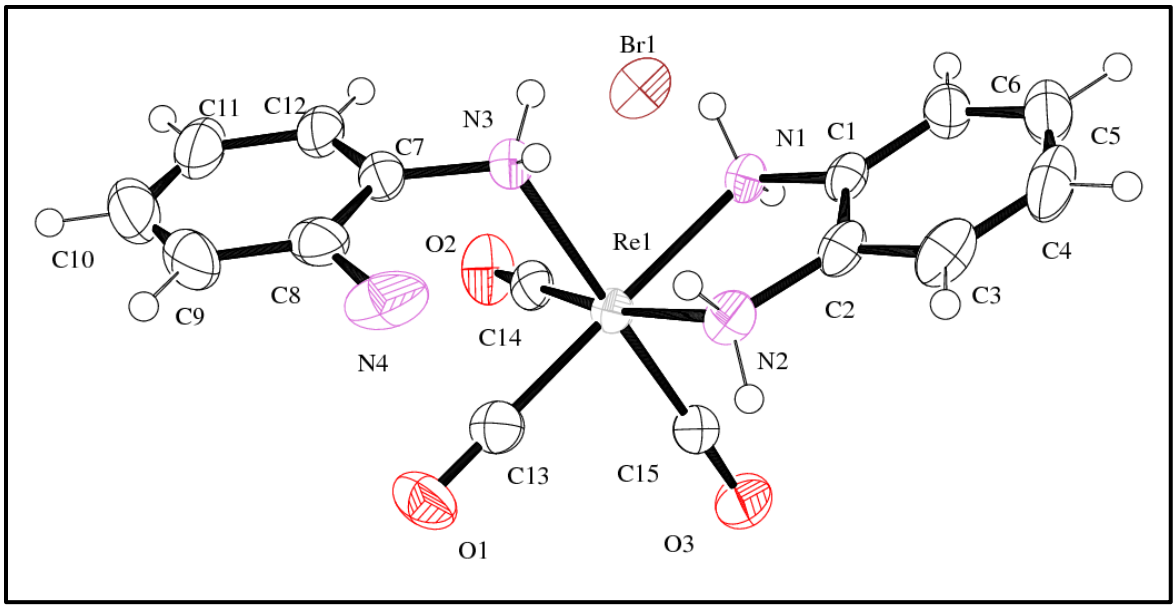

Figure 4.6: ORTEP view of **1** showing 50% probability displacement ellipsoids and the atom labeling.

A comparison of the N(4)-C(8) bond length [1.41(2) Å] with the longer N(3)-C(7) one [1.501(9) Å] clearly shows the effect of coordination on this type of bond. The bromide counter-ion is involved in a series of hydrogen-bonds in the lattice (see Table 4.1). The formation of $[Re(CO)_3(\kappa^1\text{-Hpda})(\kappa^2\text{-Hpda})]Br$ (**1**) is surprising since neutral bidentate nitrogen-donor ligands usually form neutral complexes of the type $[Re(CO)_3(NN)Br]$ [17-20]. The preparation of cationic Re(I) complexes (containing the $[Re(CO)_3]^+$ core) under mild conditions by the simple ligand substitution of $[Re(CO)_5X]$ (X = Cl, Br) is unusual.

For example, the reaction of 2,2':6',2''-terpyridine (terpy) with $[Re(CO)_5Cl]$ led to the formation of $[Re(CO)_3(\sigma^2\text{-terpy})Cl]$. Only by drastic action (by refluxing with silver perchlorate in acetonitrile overnight) could the cationic complex $[Re(CO)_3(\sigma^2\text{-terpy})(CH_3CN)]^+$ be formed [20]. $[Re(CO)_3(\kappa^1\text{-Hpda})(\kappa^2\text{-Hpda})]Br$ (**1**) is an unusual example of a '2+1' compound with the $[Re(CO)_3]^+$ core prepared in an one-pot procedure. A similar example is the complex $[Re(CO)_3(phen)(pyridine)]^+$, which was synthesized under harsh conditions in a two-step process [21].

Table 4.1: Hydrogen-bond distances (Å) and angles (˚) in **1**.

D-H•••A	D-H	H•••A	D•••A	D-H•••A
N(1)H(1A)•••Br(1)	0.92	2.64	3.529(3)	163
N(1)H(1B)•••Br(1)	0.92	2.53	3.422(3)	164
N(2)H(2A)•••Br(1)	0.92	2.66	3.495(3)	151
N(2)H(2A)•••O(1)	0.92	2.58	2.893(4)	100
N(2)H(2B)•••O(1)	0.92	2.39	2.893(4)	115
N(3)H(3A)•••Br(1)	0.92	2.60	3.506(3)	167
N(3)H(3A)•••N(4)	0.92	2.48	2.827(6)	103
N(3)H(3B)•••Br(1)	0.92	2.52	3.428(3)	168

4.3.2 Synthesis and characterization of $[Re_2(CO)_7(spo)_2]$ (2)

The neutral dimeric complex $[Re_2(CO)_7(spo)_2]$ (**2**) was formed by the reaction of 2-mercaptophenol (Hspo) with $[Re(CO)_5Br]$. The sulfur atom of each spo ligand deprotonated, forming a double bridge between the metal centres.

$$2[Re(CO)_5Br] + 2Hspo \longrightarrow [Re_2(CO)_7(spo)_2] + 3CO + 2HBr$$

The reaction solution produced no precipitate and brown crystals of **2** were obtained by the slow evaporation of the mother liquor. Complex **2** is only partially soluble in dichloromethane and acetonitrile, but completely soluble in alcohols. It is stable for months in the solid state and for weeks in solution.

Complex **2** is dimeric with one rhenium coordinated to three carbonyls and the other to four carbonyls. As a result, the three strong stretching frequencies, typical of the *fac*-$[Re(CO)_3]^+$ core, are not detected in the IR spectrum of **2** (Figure 4.7). Instead four strong carbonyl stretching frequencies [ν(C≡O)] in the 1880-2020 cm^{-1} region are observed. The peaks at 472 and 357 cm^{-1} are assigned to ν(Re-O) and ν(Re-S) respectively.

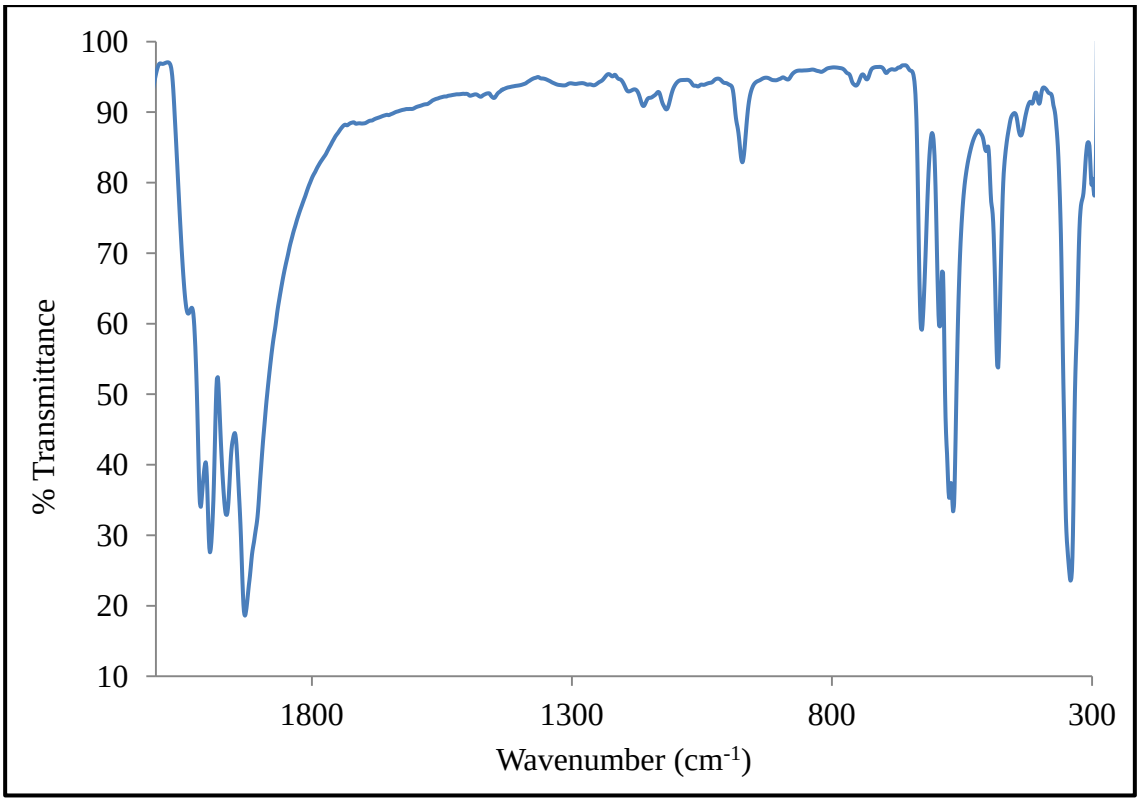

Figure 4.7: IR spectrum of **2**.

The aromatic region of the ^1H NMR spectrum of **2** (Figure 4.8) consists of four two-proton signals (two doublets and two triplets). These signals are ascribed to the eight protons on the phenyl rings of the spo ligands, and show that the corresponding protons

on the two aromatic rings are magnetically equivalent. This is surprising considering that the two spo ligands are not coordinated in the same manner, and indicates that the magnetic nature of the phenyl rings are not affected by the unsymmetrical nature of the dimeric complex. The UV-Vis spectrum of complex **2** revealed no observable transitions, and the excitation of dilute ethanol solutions of **2** at various excitation wavelengths produced no emission transitions.

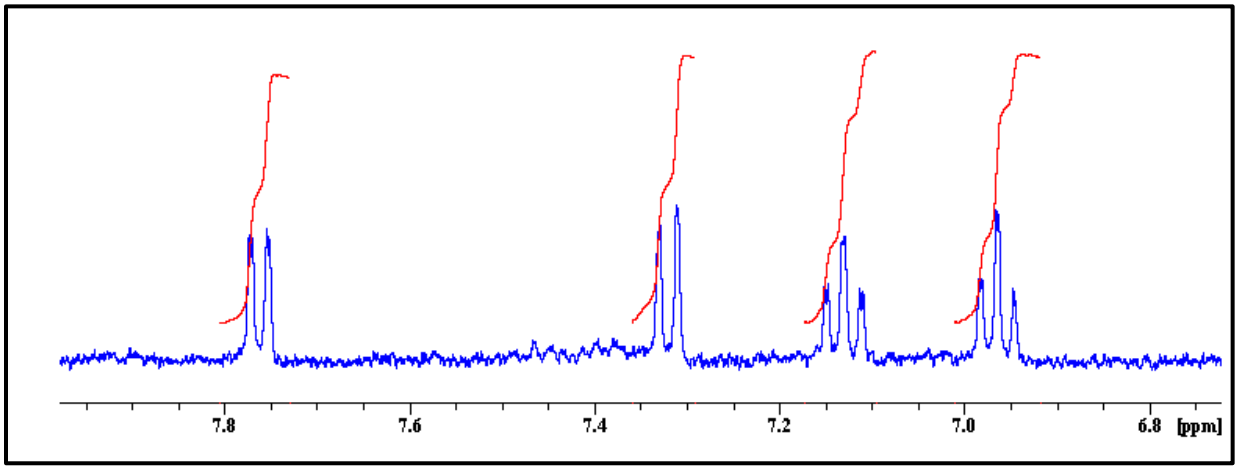

Figure 4.8: ^{1}H NMR spectrum of the aromatic region for **2**.

The structure of **2** is shown in Figure 4.9. The dimeric molecule has a rhombic $(\mu\text{-S})_2Re_2$ unit at the centre. Each sulfido-bridge is symmetrical, with unequal Re-S distances of 2.488(1) [Re(1)-S(11)], 2.522(1) [Re(1)-S(21)], 2.527(1) [Re(2)-S(11)] and 2.516(1) Å [Re(2)-S(21)]. The Re-Re distance across the rhombus is 3.8038(3) Å, implying no Re-Re bonding. The dimer consists of two different halves. Each rhenium is in a distorted octahedral environment. Re(1) is coordinated to the carbon atoms of three carbonyls, the two charged sulfur atoms S(11) and S(21), and the phenolic oxygen O(12). The Re(1)-O(12) bond length of 2.220(5) Å intimates that this oxygen is neutral, and thus protonated. The length of a rhenium(I)-phenoxy bond falls in the expected range of 2.120(8)–2.152(9) Å [22]. The bite angle of the bidentate ligand is 77.0(1)° [S(11)-Re(1)-O(12)], leading to *trans* angles in the range 168.9(2)–174.4(2)°.

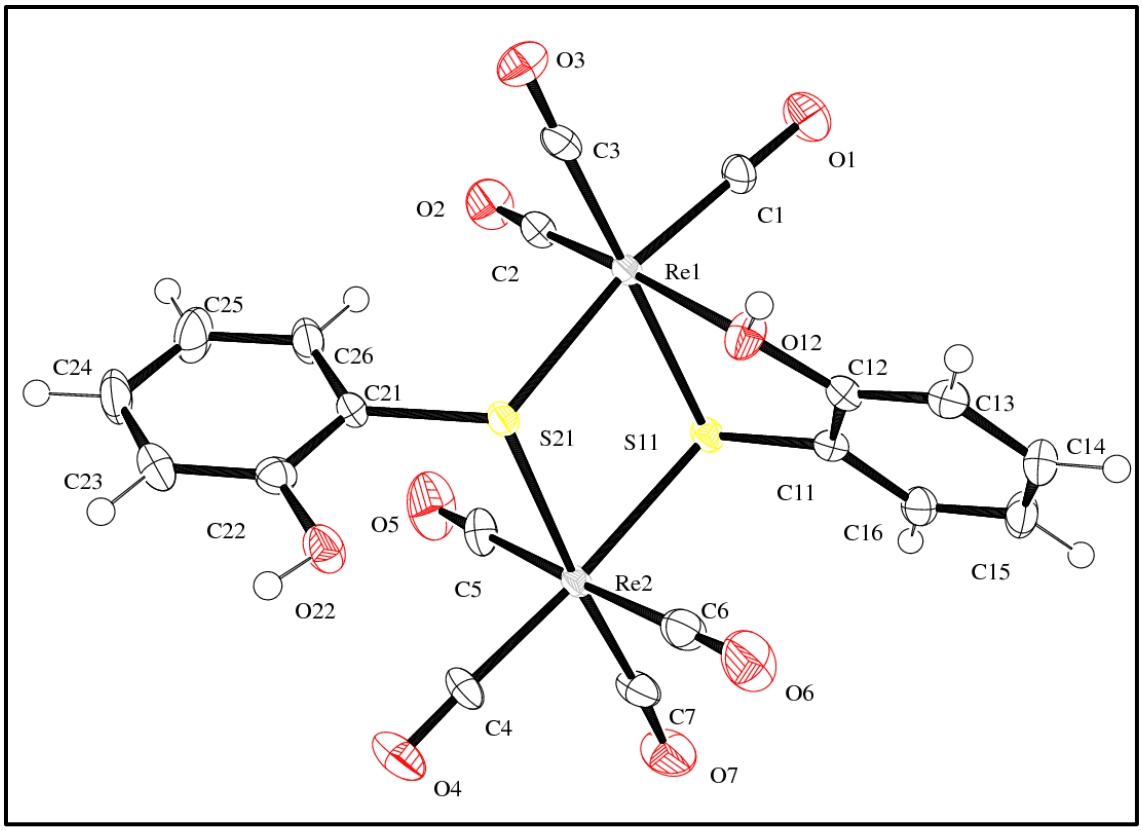

Figure 4.9: ORTEP view of **2** showing 50% probability displacement ellipsoids and the atom labeling.

In the second half of the molecule, Re(2) is bonded to four carbonylic carbons and the two sulfido bridging atoms. The O(22)H group is not coordinated. The Re(2)-C(4) and Re(2)-C(7) bond lengths are practically identical, as are Re(2)-C(5) and Re(2)-C(6). The difference between the C(22)-O(22) [1.377(8) Å] and C(12)-O(12) [1.397(8) Å] lengths are small. The C(4)-Re(2)-C(6) [90.4(3)°], C(4)-Re(2)-C(5) [91.5(3)°] and C(4)-Re(2)-C(7) [90.5(3)°] are close to orthogonality. The hydroxyl hydrogen O(12)H(12) is involved in intermolecular hydrogen-bonding between the sulfur atom S(21) and the oxygen atom O(22) of an adjacent molecule (Table 4.2). A third hydrogen-bond exists in the asymmetric unit between O(22)H(22)•••O(1) (Figure 4.10).

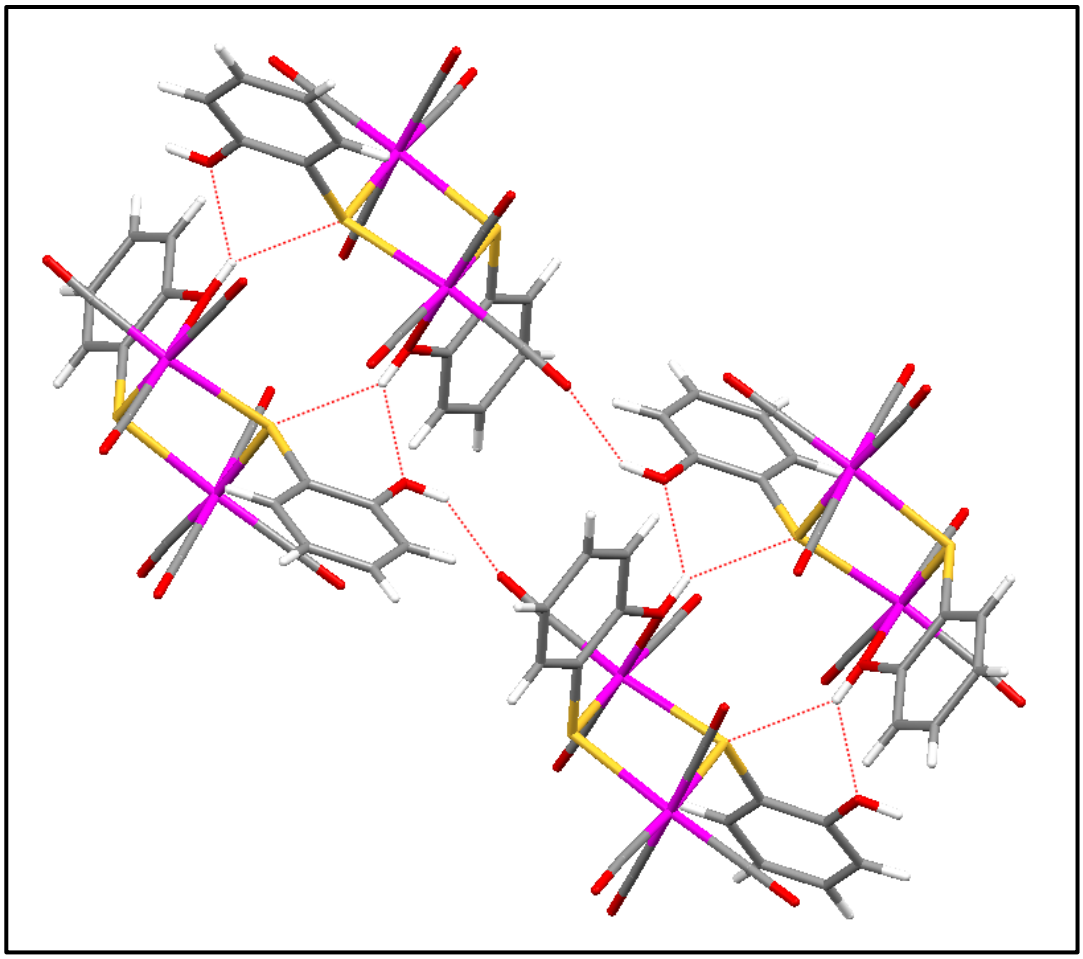

Figure 4.10: Packing diagram in the unit cell of **2** showing the hydrogen-bonds.

Table 4.2: Hydrogen-bond distances (Å) and angles (˚) in **2**.

D-H•••A	D-H	H•••A	D•••A	D-H•••A
O(12)H(12)•••S(21)	0.84	2.56	3.273(4)	144
O(12)H(12)•••O(22)	0.84	2.15	2.767(7)	130
O(22)H(22)•••O(1)	0.84	2.32	2.976(8)	135

The potentially bidentate ligand Hspo provides somewhat of a dilemma for the $[Re(CO)_3]^+$ core, since both the OH and SH groups can be deprotonated. However, in the complex $[Re_2(CO)_7(spo)_2]$ only the mercapto sulfur atoms are deprotonated. The different coordination behaviour of the two spo ligands is surprising, since bidentate coordination of both would have led to the symmetrical complex $[Re(CO)_3(spo)]_2$, with sulfide

bridges. A second possibility would be to form the symmetrical dimer $[Re(CO)_4(spo)]_2$, with sulfide bridges and free OH groups. This anomalous behaviour cannot be explained. Interestingly, with tropolone (Htrp) the anionic monomer $[Re(CO)_3(trp)Br]^-$ was isolated [23].

4.3.3 Synthesis and characterization of *fac*-[Re(CO)$_3$(ons)(Hno)] (3)

The compound *fac*-$[Re(CO)_3(ons)(Hno)]$ (**3**) was prepared by the reaction of $[Re(CO)_5Br]$ with two-fold molar excess of Hons in refluxing toluene under nitrogen.

$$[Re(CO)_5Br] + 2Hons + H_2O \longrightarrow [Re(CO)_3(ons)(Hno)] + 2CO + HBr + mbt$$

The decomposition of a molecule of Hons to form a coordinated 2-aminophenol (Hno) and free 2-(methylthio)benzaldehyde (mtb) was surprising since all precautions were taken to exclude water from the reaction mixture. Also, the preferred affinity of the *fac*-$[Re(CO)_3]^+$ core for an amino nitrogen, rather than the chelated methylthiolic sulfur atom, is surprising. All our efforts to synthesize *fac*-$[Re(CO)_3(ons)]$, with ons coordinated as a tridentate ONS-donor chelate, were unsuccessful. The synthesis of **3** was also attempted by the reaction of $[Re(CO)_5Br]$ with equimolar quantities of Hons and Hno in toluene. However, only the complex *fac*-$[Re^I(CO)_3(no)(Hno)]$ was isolated from the reaction mixture. Complex **3** is stable in air and is a non-electrolyte in methanol. It is soluble in a wide variety of solvents like methanol, DMF, DMSO, acetonitrile and acetone.

The infrared spectrum of **3** (Figure 4.11) is characterized by intense bands at 1905 and 2021 cm^{-1}, typical of ν(C=O) of the *fac*-$[Re(CO)_3]^+$ unit. The two medium intensity bands at 474 and 490 cm^{-1} are assigned to ν(Re-N(2)) and ν(Re-N(1)) respectively, and the medium intensity band at 394 cm^{-1} is attributed to ν(Re-O(4)). The ν(C=N) of the Schiff base is found at 1601 cm^{-1} and is at a lower frequency relative to that of the free Hons ligand, which occurs at 1628 cm^{-1}. The two peaks at 3414 and 3471 cm^{-1} are due to ν(N-H) of the amino nitrogen N(2).

The imine proton of the ons ligand appears at 10.02 ppm in the ^{1}H NMR spectrum of **3**. The other protons of the ons chelate appear in the 7.00-7.80 ppm range as a triplet, multiplet, doublet and multiplet integrating for one, two, one and three protons respectively (Figure 4.12). The multiplet in the 6.46-6.88 ppm region are assigned to the four protons of the Hno ligand. The broad singlets at 9.65 and 3.50 ppm are due to the phenolate and amino protons respectively. The protons of the methylthiol group appears as a singlet at 2.23 ppm and integrates for three protons.

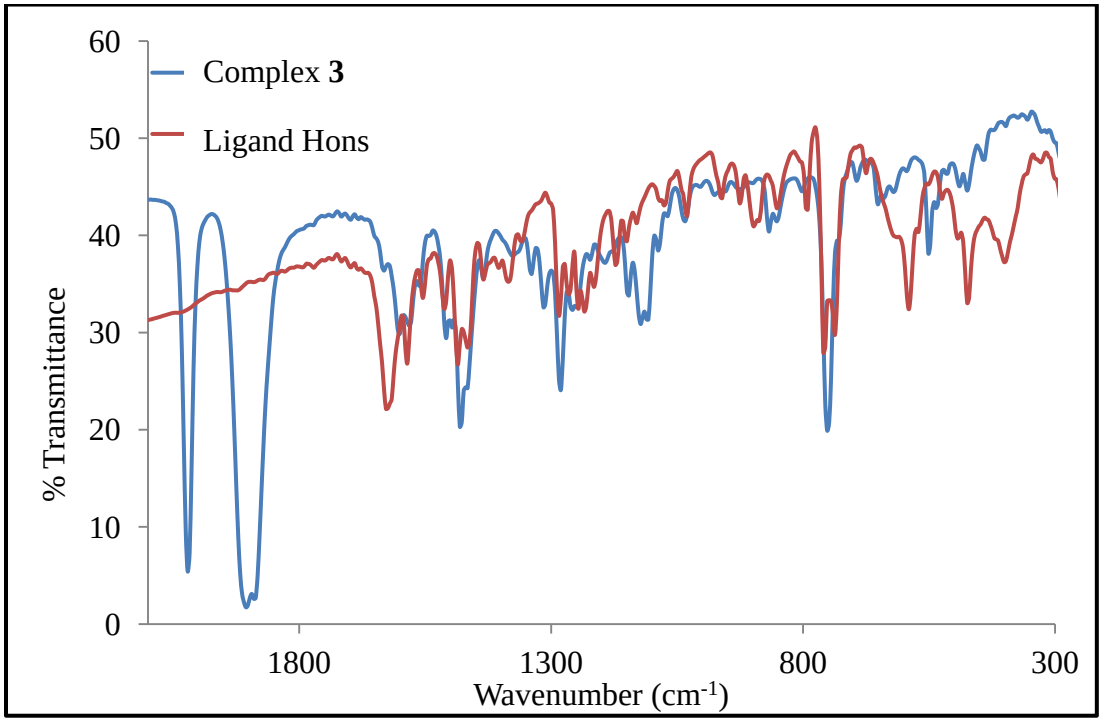

Figure 4.11: IR spectra of Hons and **3**.

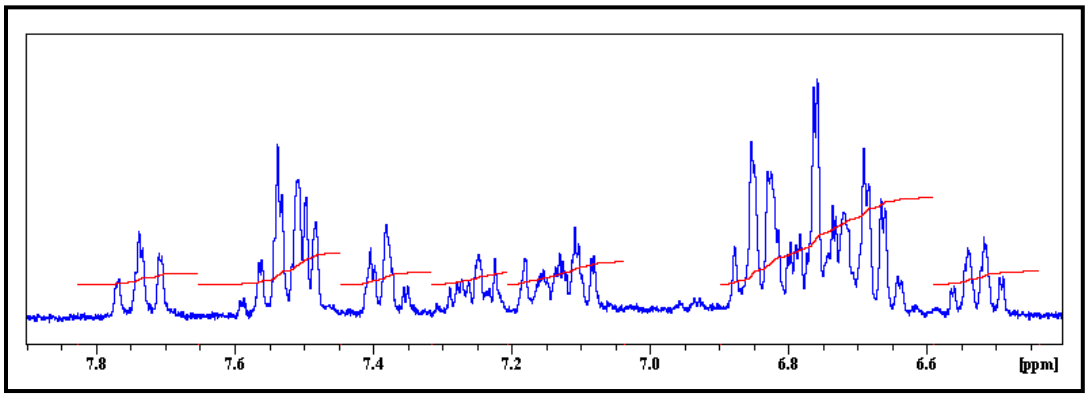

Figure 4.12: ^{1}H NMR spectrum of the aromatic region of **3**.

The UV-Vis spectrum of **3** (Figure 4.13) in methanol shows a metal-to-ligand charge transfer band at 426 nm with an extinction coefficient of 3190 $M^{-1}cm^{-1}$. The emission spectrum (λ_{ex} = 435 nm) of a methanol solution of **3** revealed an intense metal-centred transition at 537 nm (Figure 4.13) at room temperature, characteristic of MLCT emissions of *fac*-$[Re(CO)_3]^+$ complexes [24].

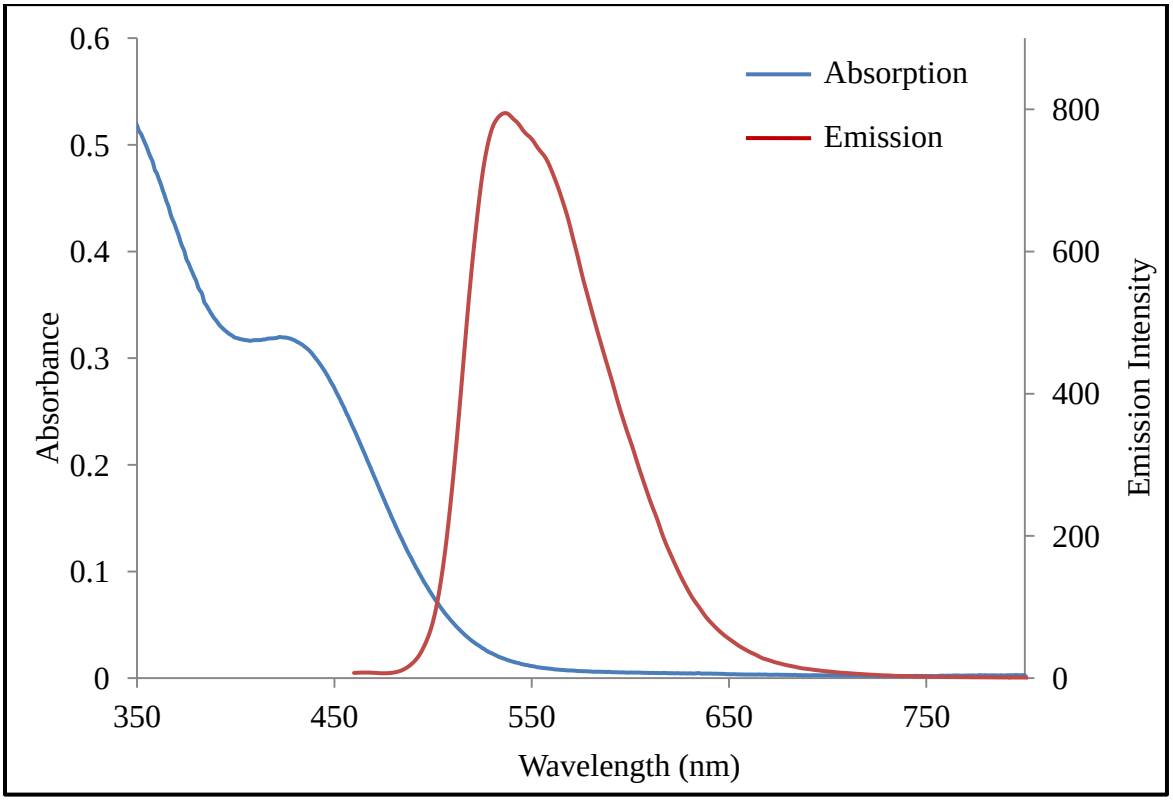

Figure 4.13: Absorption (blue) and emission (red) spectra of **3**.

A perspective view of the asymmetric unit is shown in Figure 4.14. It contains a molecule of $[Re(CO)_3(ons)(Hno)]$, and a toluene molecule of crystallization. The X-ray results show that the rhenium(I) complex contains the chemically robust *fac*-$[Re(CO)_3]^+$ core and a distorted octahedral geometry. The rhenium(I) is coordinated to three carbonyl donors in a *facial* orientation, to the imino nitrogen N(1), the amino nitrogen N(2) and the phenolate oxygen O(4). The phenolic oxygen O(5)H and thioether sulfur S(1) are uncoordinated. The Re-CO bond distances [average of 1.907(6) Å, Table 4.11] fall in the range observed [1.900(2)-1.928(2) Å] for similar complexes [15, 25]. The Re-N(2) bond

length of 2.248(4) Å is typical for Re-N(amino) bonds [16, 17]. The Re-N(1) bond distance of 2.204(4) Å, the bond length of N(1)-C(11) of 1.299(6) Å (a double bond), and the C(11)-N(1)-C(12) bond angle of 119.3(4)° leave no doubt that N(1) is an sp^2-hybridized imino-coordinated nitrogen.

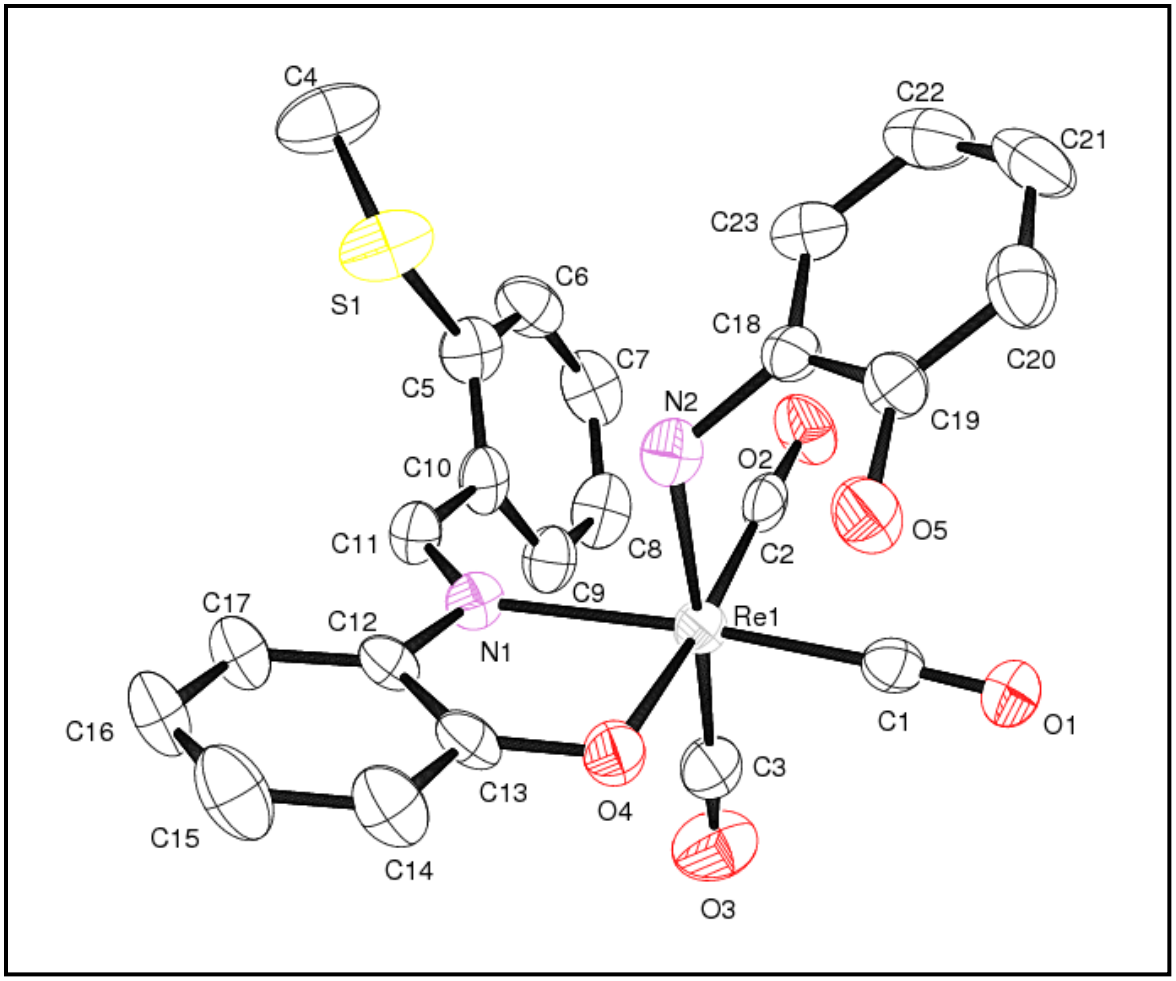

Figure 4.14: ORTEP view of complex **3** showing 50% probability displacement ellipsoids and the atom labeling. Hydrogen atoms and the solvent of crystallization were omitted for clarity.

The *trans* angles [C(1)-Re-N(1) = 170.0(2)˚, C(2)-Re-O(4) = 172.2(2)˚, and C(3)-Re-N(2) = 176.3(2)˚] results in the distortion from octahedral ideality of the complex. These distortions are due to the small bite angle [N(1)-Re-O(4) = 76.5(1)˚] formed by the five-membered chelate ring of the bidentate ligand, ons. The average C-Re-C bond angle of

88.6(2)˚ is close to orthogonality. The sp^3-hybridization of the uncoordinated thioether sulfur atom S(1) is reflected in the C(4)-S(1)-C(5) bond angle of 103.4(3)˚. A comparison of the O(5)-C(19) bond length [1.346(6) Å] with the shorter O(4)-C(13) distance [1.337(6) Å] clearly shows the effect of coordination on this type of bond. The dihedral angle between the two phenyl rings of ons is 60.5˚. The average C-C distance in the three phenyl rings C(5)-C(10), C(12)-C(17) and C(18)-C(23) is 1.380(9), 1.383(9) and 1.385(9) Å respectively. There are two hydrogen-bonds in the unit cell: N(2)H•••O(5) (intramolecular) and O(5)H•••O(4) (intermolecular) [Table 4.3; Figure 4.15].

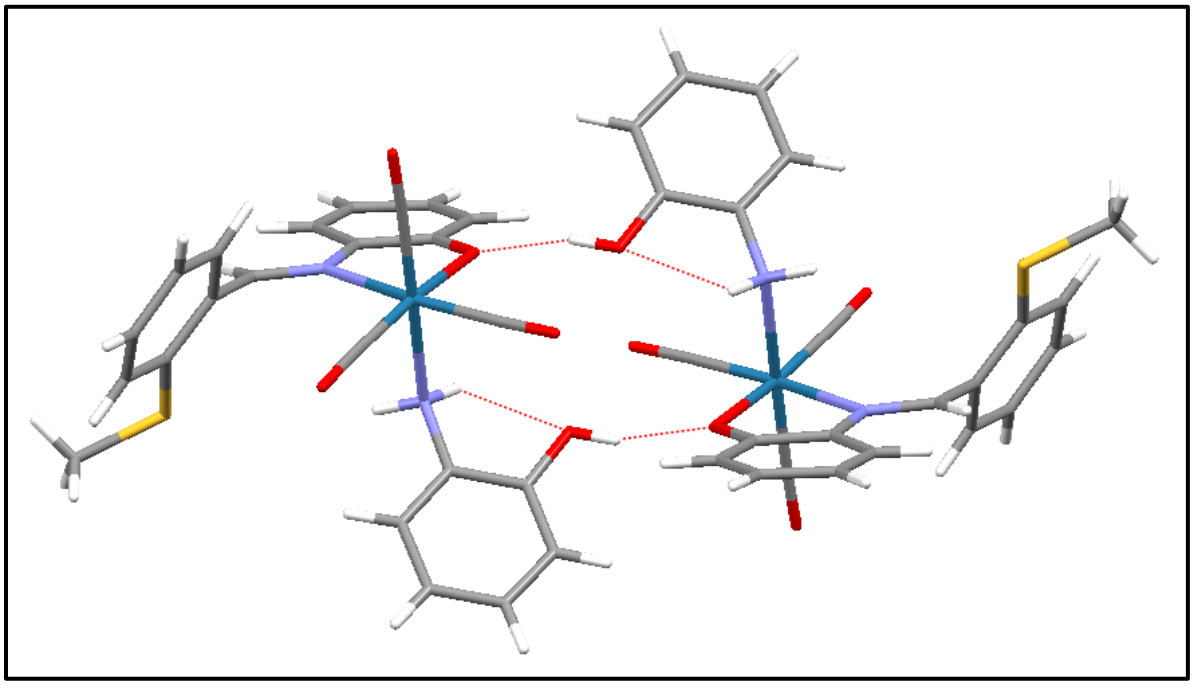

Figure 4.15: A perspective view of **3** showing the hydrogen-bonding.

Table 4.3: Hydrogen-bond distances (Å) and angles (˚) in **3**.

D-H•••A	D-H	H•••A	D•••A	D-H•••A
N(2)-H(2B)•••O(5)	0.92	2.24	2.639(5)	105
O(5)-H(5)•••O(4)	0.84	1.79	2.598(5)	161

4.3.4 Synthesis and characterization of *fac*-[Re(CO)$_3$(Htpn)Br] (4)

The reaction of the potentially tridentate ligand Htpn with [Re(CO)$_5$Br] in refluxing toluene gave the complex [Re(CO)$_3$(Htpn)Br] (**4**), with Htpn coordinating as a neutral bidentate chelate.

$$[Re(CO)_5Br] + Htpn \longrightarrow [Re(CO)_3(Htpn)Br] + 2CO$$

Complex **4** is air stable and a non-electrolyte in methanol. The complex is soluble in a variety of solvents, including alcohols, dichloromethane and acetonitrile.

The IR spectrum of **4** (Figure 4.17) contains sharp intense peaks at 1896, 1923 and 2023 cm^{-1}, typical of ν(C≡O) of the *fac*-[Re(CO)$_3$]$^+$ unit [26]. The peak at 1583 cm^{-1} is due to the ν(C=N) of the Schiff base and is at a lower frequency relative to that of the free ligand which is found at 1627 cm^{-1}. The medium intensity peak at 354 cm^{-1} is due to the Re-S stretch. The diamagnetism of **4** is evident from its ^{1}H NMR spectrum. The methine proton C(11)H occurs at 9.36 ppm and is shifted downfield relative to the imine proton of the free ligand (at 8.87 ppm). The aromatic protons' signals appear as a multiplet and three triplets in the 6.50-7.90 ppm region. A three-proton singlet at 3.08 ppm is ascribed to the methylthiol protons.

An intense band is found at 313 nm in the electronic spectrum of **4 (**Figure 4.18). This band is due to the intraligand transition of the coordinated Htpn ligand, and is at a lower wavelength relative to the free ligand which appears as an intense band at 360 nm. A metal-to-ligand charge transfer band (MLCT) is observed at 433 nm for **4**. Excitation of **4** in methanol at room temperature with a λ_{ex} = 450 nm, resulted in a broad MLCT emission centred at 544 nm (Figure 4.22). The rhenium centre of complexes **3** and **4** are coordinated to different ligands (a NO-donor ligand in **3** and a NS-donor ligand in **4**), and therefore different metal-ligand interactions are found in the two complexes which account for complex **4** having a higher MLCT emission energy compared to **3**.

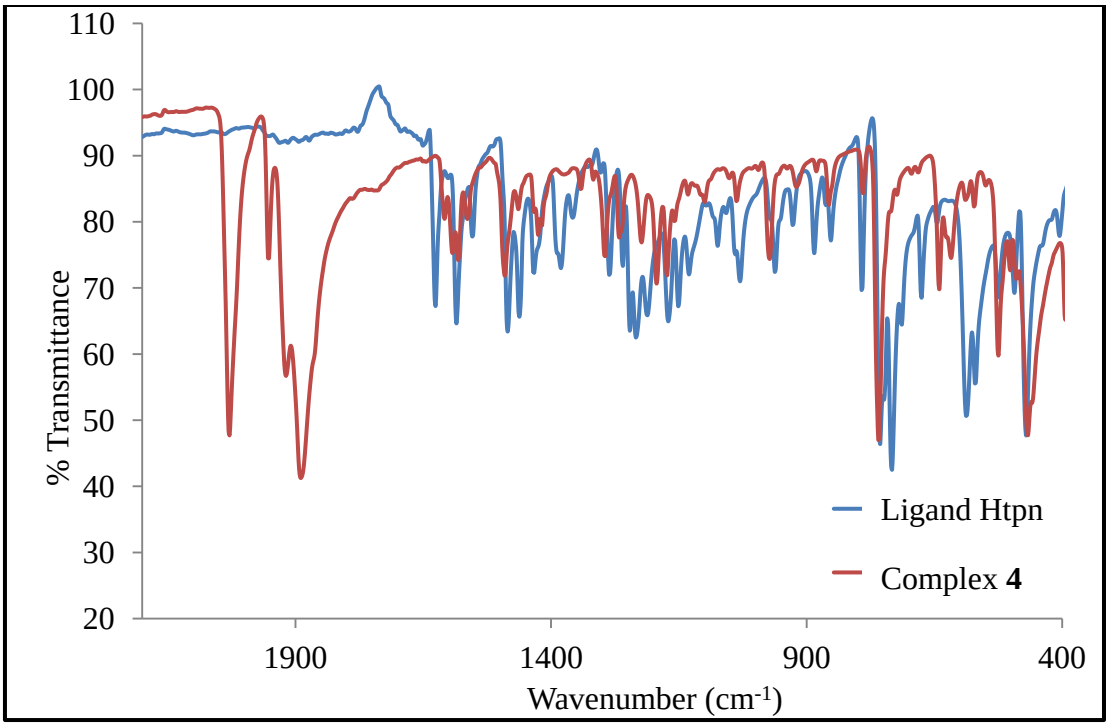

Figure 4.17: IR spectra of ligand Htpn and complex **4**.

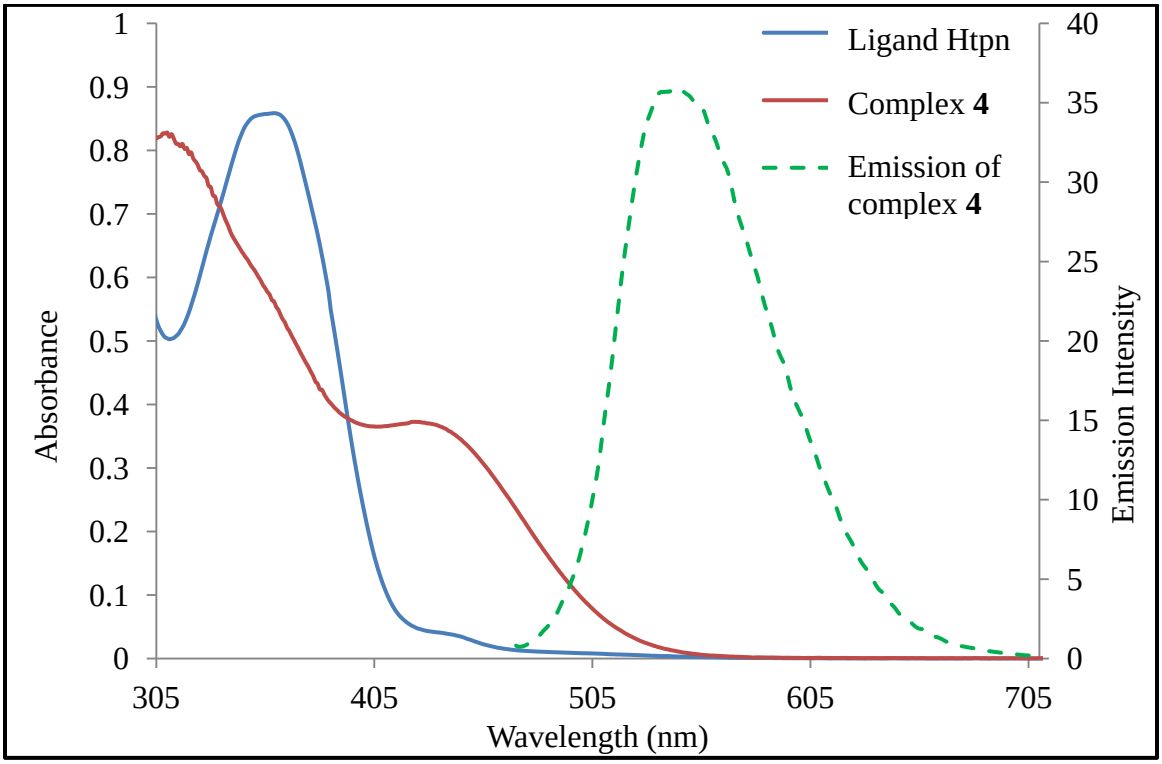

Figure 4.18: Overlay UV-Vis spectra of ligand Htpn (blue) and complex **4** (red) and emission spectrum of complex **4** (green dotted line).

The X-ray results shows that the bidentate ligand Htpn is coordinated *via* the imino nitrogen, N(1) and the thioethereal sulfur S(1) to the metal, which resides in a distorted octahedral environment (Figure 4.19). The Re-N(1) bond length of 2.202(2) Å is typical of rhenium(I)-imine bonds [18], and the Re-S(1) length of 2.4684(8) Å is in the range observed for similar bonds [27]. The N(1)-C(11) distance exhibits double bond character, with a length of 1.287(4) Å, and the angle C(11)-N(1)-C(12) [114.3(2)°] is slightly smaller than would be expected around a sp^2-hybridized nitrogen atom. The smaller bite angle of Htpn [N(1)-Re-S(1) = 86.78(7)°] results in larger *trans* angles [175.2(1)–177.0(1)°], when compared to the previous complexes in the study.

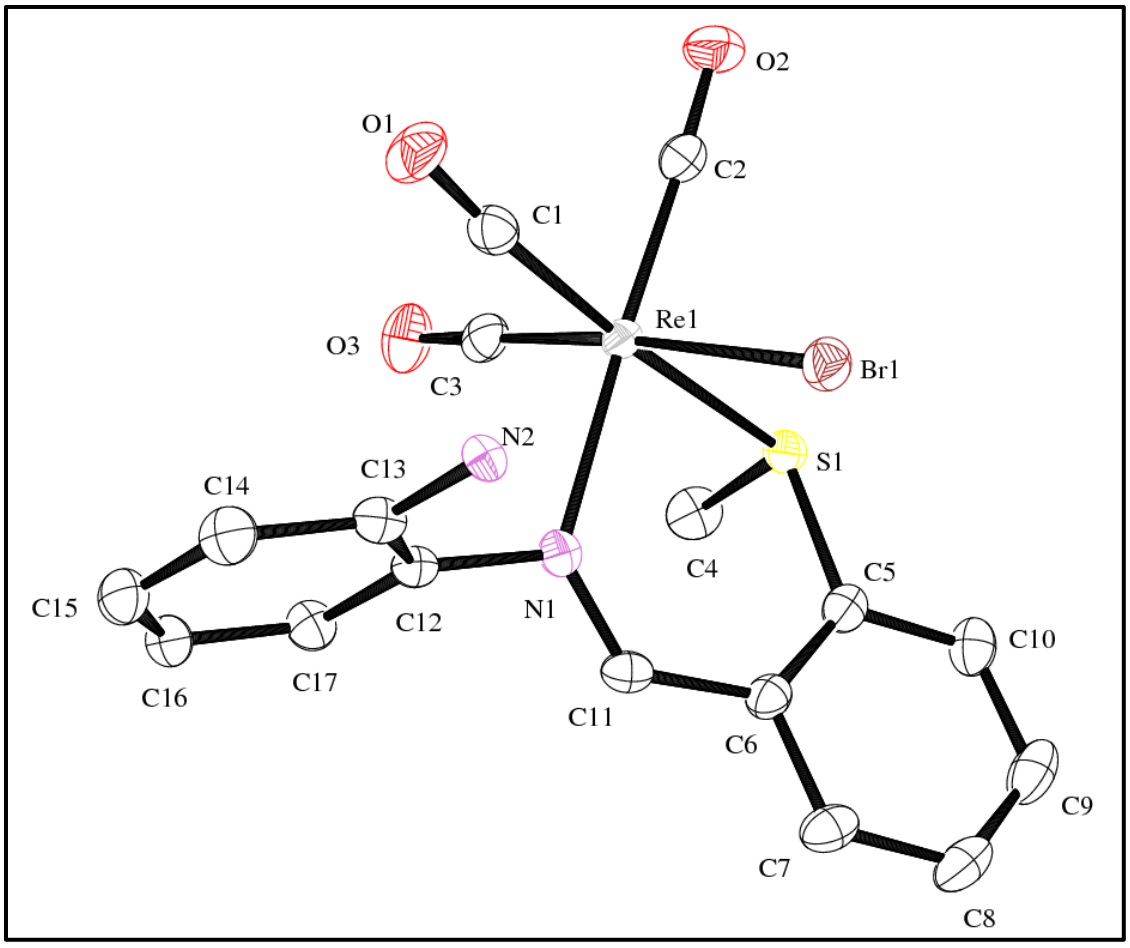

Figure 4.19: ORTEP view of **4** showing 50% probability displacement ellipsoids and the atom labeling. Hydrogen atoms were omitted for clarity.

One of the hydrogen atoms of the free amino group [N(2)H(2B)] is involved in two hydrogen-bonds to Br(1) and N(1) (Table 4.4, Figure 4.20). These interactions may be responsible for the remarkable value of -0.2(4)° for the N(1)-C(12)-C(13)-N(2) torsion angle. Whereas in complex **4** the potentially tridentate N_2S-donor ligand Htpn coordinates as a bidentate NS-donor (with a free amino group), the very similar NSO-donor ligand Hons coordinates as a NO-donor (*via* the imino nitrogen and deprotonated oxygen with a free methylthio group) in the complex $[Re(CO)_3(ons)(Hno)]$ (**3**). Complexes with the *fac*-$[Re(CO)_3]^+$ core have been well studied with potentially tridentate ligands, which commonly contain N, O and S donor atoms from amine [28], pyridyl [29], carboxyl [30] or thioether [31] groups in octahedral complexes of the type $[Re(CO)_3L]X$ (X = Cl, Br, PF_6). Conclusions have been made that nitrogen donor ligands are preferred by the $[Re(CO)_3]^+$ core above sulfur donor ligands, which is in contradiction with the results found in complex **4** [29, 31].

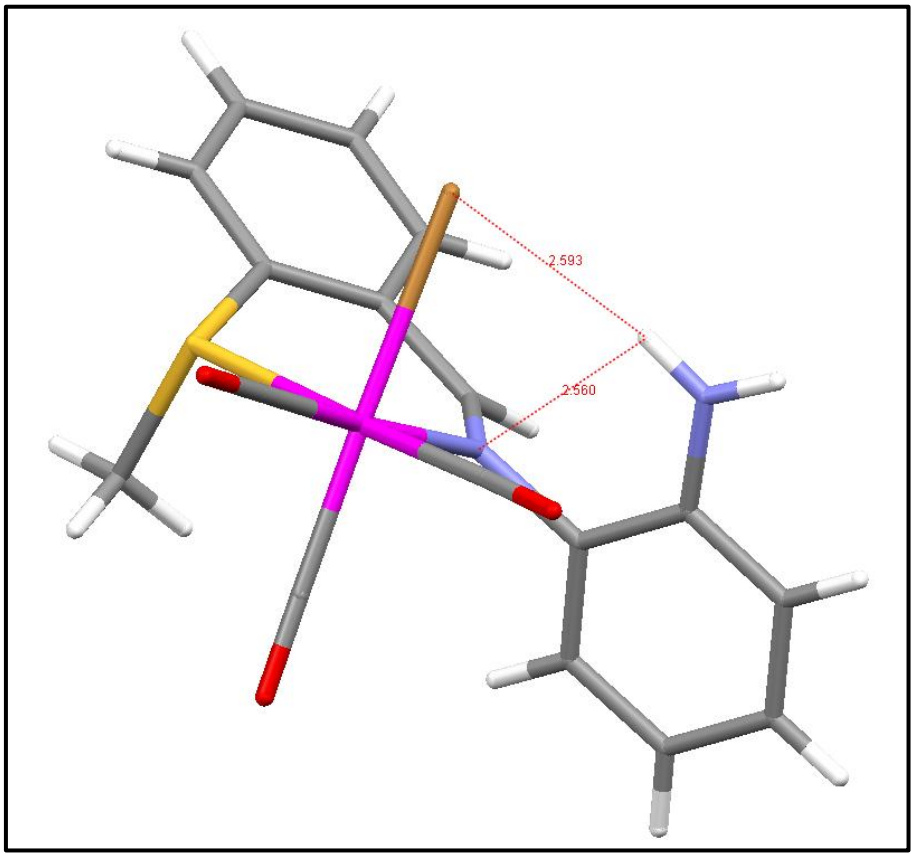

Figure 4.20: Intramolecular hydrogen-bonding in **4**.

Table 4.4: Hydrogen-bond distances (Å) and angles (˚) in **4**.

D-H•••A	D-H	H•••A	D•••A	D-H•••A
N(2)H(2B)•••Br(1)	0.88	2.59	3.457(2)	167
N(2)H(2B)•••N(1)	0.88	2.56	2.868(3)	101

The electrochemical processes of the complexes were studied *via* cyclic voltammetry and the results are summarized in Table 4.5. Compound **1** revealed an irreversible oxidation peak at 1.09 V. This process is ascribed to the Re(I)/Re(II) redox couple. The cyclic voltammograms of **2** and **3** displayed no redox processes in the region scanned (-1.50 to 1.50 V). An irreversible oxidation process was observed at 1.17 V for complex **4** corresponding to the Re(I)/Re(II) redox process. This oxidation peak is more positive than that of complex **1**, signifying that **1** undergoes oxidation more readily. As mentioned in Chapter 3, this effect is due to the π donating properties of the coordinated ligand. The nitrogen donor ligands (Hpda) of **1** is more electron donating than the Htpn ligand of **4**, resulting in **1** having an electron rich metal centre, which causes **1** to undergo oxidation more readily.

Table 4.5: Cyclic voltammetry redox potentials.

Compound	**Solvent**	**Oxidation**
		E_{pa} (V)
1	CH_2Cl_2	1.09
2	CH_3CN	-
3	CH_2Cl_2	-
4	CH_2Cl_2	1.17

4.4 References

[1] E.D. Yorke, P. Beaumier, B. Wessels, A. Fritzberg, A. Morgan, *Nucl. Med. Biol*., 1991, **18**, 827; S.S. Jurisson, J.D. Lydon, *Chem. Rev*., 1999, **99**, 2205; W.A. Volkert, T.J. Hoffman, *Chem. Rev*., 1999, **99**, 2269.

[2] B.L. Holman, A.G. Jones, J. Lister-James, A. Davison, M.J. Abrams, J.M. Kirschenbaum, S.S. Tubeh, R.J. English, *J. Nucl. Med*., 1984, **25**, 1350.

[3] R. Alberto, R. Schibli, R. Waihel, P.A. Schubiger, *Coord. Chem. Rev*., 1999, **190–192**, 901.

[4] J.K. Pak, P. Benny, B. Springler, K. Ortner, R. Alberto, *Chem. Eur. J*., 2003, **9**, 2053; R. Garcia, A. Paulo, A. Domingos, I. Santos, K. Ortner, R. Alberto, *J. Am. Chem. Soc*., 2000, **122**, 11240.

[5] T. Kniess, J.D.G. Correia, A. Domingos, E. Palma, I. Santos, *Inorg. Chem*., 2003, **42**, 6130; R. Schibli, K.V. Katti, W.A. Volkert, C.L. Barnes, *Inorg. Chem*., 2001, **40**, 2358.

[6] J.L. Pratihar, S. Bhaduri, P. Pattanayak, D. Patra, S. Chattopadhyay, *J. Organomet. Chem*., 2009, **694**, 3401.

[7] J. Schroer, U. Abram, *Polyhedron*, 2011, **30**, 2157.

[8] J.L. Pratihar, P. Pattanayak, D. Patra, R. Rathore, S. Chattopadhyay, *Inorg. Chim. Acta*, 2011, **367**, 182.

[9] G. Bandoli, M. Nicolini, U. Mazzi, F. Refosco, *J. Chem. Soc., Dalton Trans.*, 1984, 2505.

[10] S.M. Abdallah, G.G. Mohamed, M.A. Zayed, M.S.A. El-Ela, *Spectrochim. Acta, Part A*, 2009, **73**, 833; S.M. Abdallah, M.A. Zayed, G.G. Mohamed, *Arabian J. Chem*., 2010, **3**, 103.

[11] A. Altamore, M.C. Burla, M. Camalli, G.L. Gascarano, C. Giacavazco, A. Guagliardi, A.G. Moliterni, G. Polidori, R. Spagna, *J. Appl. Crystallogr*., 1999, **32**, 115.

[12] G.M. Sheldrick, SHELXL-97, Programs for Structure Solution and Refinement, University of Göttingen, Germany, 1997.

[13] Xred, rev. **1.09**, STOE: Darmstadt, Germany.

[14] XShape, rev. **1.02**, STOE: Darmstadt, Germany.

[15] L. Maria, C. Moura, A. Paulo, I.C. Santos, *J. Organomet. Chem*., 2006, **691**, 4773.

[16] C. Melian, C. Kremer, K. Suescun, A. Mombru, R. Mariezcurrena, E. Kremer, *Inorg. Chim. Acta*, 2000, **306**, 70.

[17] G. Bandoli, A. Dolmella, T.I.A. Gerber, D. Mpinda, J. Perils, J.G.H. du Preez, *J. Coord. Chem.*, 2002, **55**, 823, and references therein.

[18] M. Chatterjee, G. Achari, S. Das, R. Banerjee, C. Chakrabarti, J.K. Dattagupta, S. Banerjee, *Inorg. Chem.,* 1998, **37**, 5424.

[19] N. St. Fleur, J.C. Hili, A. Mayr, *Inorg. Chim. Acta*, 2009, **362**, 1571; B.R. Yeo, A.J. Hallett, B.M. Kariuki, S.J.A. Pope, *Polyhedron*, 2010, **29**, 1088.

[20] A.J. Amoroso, A. Banu, M.P. Coogan, P.G. Edwards, G. Hossain, K.M.A. Malik, *Dalton Trans*., 2010, **39,** 6993.

[21] L. Wallace, D.P. Rillema, *Inorg. Chem*., 1993, **32**, 3836.

[22] L. Wei, S.R. Banerjee, M.K. Levadala, J. Babich, J. Zubieta, *Inorg. Chem. Commun*., 2003, **6**, 1099; C. Moura, C. Fernandes, L. Gano, A. Paulo, I.C. Santos, I. Santos, M.J. Calhorda, *J. Organomet. Chem*., 2009, **694,** 950; P. Barbazan, R. Carballo, U. Abram, G. Pereiras-Gabian, E.M. Vazquez-Lopez, *Polyhedron*, 2006, **25**, 3343; P. Kyprianidou, C. Tsoukalas, G. Patsis, D. Papagiannopoulou,

N. Nikolic, D. Jankovic, D. Djokic, C.P. Raptopoulou, M. Pelecanou, M. Papadopoulos, I. Pirmettis, *Polyhedron*, 2009, **28**, 3171.

[23] M. Schutte, H.G. Visser, A. Roodt, *Acta Crystallogr*., 2010, **E66**, m859.

[24] H. Kunkely, A. Vogler, *Inorg. Chim. Acta*, 2003, **343**, 357; K. Wang, L. Huang, L. Gao, L. Jin, C. Huang, *Inorg. Chem.*, 2002, **41** 3353; Z. Si, J. Li, B. Li, F. Zhao, S. Liu, W. Li, *Inorg. Chem.*, 2007, **46**, 6155.

[25] L. Wei, S.R. Banerjee, M.K. Levadala, J. Babich, J. Zubieta, *Inorg. Chim. Acta*, 2004, **357**, 1499.

[26] J. Granifo, *Polyhedron*, 1999, **18**, 1061; D.R. Gamelin, M.W. George, P. Glyn, F.W. Grevek, K. Schafner, J.J. Turner, *Inorg. Chem*., 1995, **33**, 3246.

[27] S. Mundwiler, L. Candreia, P. Hafliger, K. Ortner, R. Alberto, *Bioconjug. Chem*., 2004, **15**, 195.

[28] N. Lazarova, J.W. Babich, J. Valliant, P. Schaffer, S. James, J. Zubieta, *Inorg. Chem.*, 2005, **44**, 6763.

[29] M. Lipowska, R. Cini, G. Tamasi, X.L. Xu, A.T. Taylor, L.G. Marzilli, *Inorg. Chem*., 2004, **43**, 7774.

[30] H. He, M. Lipowska, X. Xu, A.T. Taylor, M. Carlone, L.G. Marzilli, *Inorg. Chem.*, 2005, **44**, 5437.

[31] S.R. Banerjee, M.K. Levadala, N. Lazarova, L. Wei, J.F. Valliant, K.A. Stephenson, J.W. Babich, K.P. Maresca, J. Zubieta, *Inorg. Chem*., 2002, **41**, 6417.

Table 4.5: Crystal and structure refinement data for **1**.

Chemical formula	$C_{15}H_{16}N_4O_3BrRe$
Formula weight	566.42
Crystal system	Triclinic
Space group	*P*-1
a (Å)	8.3815(2)
b (Å)	10.5477(2)
c (Å)	10.8571(3)
α (˚)	108.126(2)
β (˚)	92.235(2)
γ (˚)	105.478(2)
Volume (Å^3)	871.28(4)
Z	2
Density (Calcd.) (gcm^{-3})	2.151
Absorption coefficient (mm^{-1})	9.287
F (000)	532
Crystal size (mm)	0.03 x 0.04 x 0.24
θ range	3.2-27.5
Index ranges *h*	-10/10
k	-13/13
l	-14/14
Reflections measured	18983
Independent/observed reflections	3971/3587
Data/parameters	3971/222
Goodness-of-fit on F^2	1.06
Final *R* indices [$I > 2\sigma(I)$]	0.0213
	(*wR2* = 0.0452)
Largest diff. peak/hole (eÅ^{-3})	0.92/-0.71

Table 4.6: Crystal and structure refinement data for **2**.

Chemical formula	$C_{19}H_{10}O_9S_2Re_2$
Formula weight	818.83
Crystal system	Monoclinic
Space group	*P*2/n
a (Å)	12.5117(5)
b (Å)	9.1612(3)
c (Å)	18.9629(8)
β (˚)	94.910(1)
Volume ($Å^3$)	2165.6(1)
Z	4
Density (Calcd.) (gcm^{-3})	2.511
Absorption coefficient (mm^{-1})	11.411
F (000)	1512
θ range	2.9-28.3
Index ranges *h*	-16/16
k	-7/12
l	-25/25
Reflections measured	20003
Independent/observed reflections	5316 5012
Data/parameters	5316/289
Goodness-of-fit on F^2	1.13
Final *R* indices [$I > 2\ \sigma(I)$]	0.0432
	(*wR2* = 0.1112)
Largest diff. peak/hole ($eÅ^{-3}$)	3.20/-4.19

Table 4.7: Crystal and structure refinement data for **3**.

Chemical formula	$C_{30}H_{27}N_2O_5SRe$
Formula weight	713.82
Crystal system	Monoclinic
Space group	$P2_1/c$
a (Å)	10.1391(4)
b (Å)	13.0964(5)
c (Å)	21.6913(8)
α (˚)	90
β (˚)	98.970(4)
γ (˚)	90
Volume (Å^3)	2845.1(2)
Z	4
Density (Calcd.) (g.cm^{-1})	1.666
Absorption coefficient (mm^{-1})	4.386
F(000)	1408
Crystal size (mm)	0.08 x 0.10 x 0.16
θ range	4.2-26.3
Index ranges *h*	-12/7
k	-16/8
l	-26/25
Reflections measured	12385
Independent/observed reflection	5763/3887
Data/parameters	5763/320
Goodness-of-fit on F^2	0.89
Final *R* indices ($I > 2\ \sigma(I)$]	0.0318
	(*wR2*=0.0685)
Largest diff. peak/hole (eÅ^{-3})	0.94/-0.72

Table 4.8: Crystal and structure refinement data for **4**.

Chemical formula	$C_{17}H_{14}N_2O_3SBrRe$
Formula weight	592.48
Crystal system	Monoclinic
Space group	$P2_1/c$
a (Å)	7.0339(1)
b (Å)	19.7023(3)
c (Å)	12.8887(2)
β (˚)	94.3615(8)
Volume (Å^3)	1781.00(5)
Z	4
Density (Calcd.) (gcm^{-3})	2.210
Absorption coefficient (mm^{-1})	9.202
F (000)	1120
Crystal size (mm)	0.05 x 0.07 x 0.31
θ range	3.2-27.5
Index ranges *h*	-9/9
k	-25/25
l	-16/16
Reflections measured	46334
Independent/observed reflections	4076
Data/parameters	4076/227
Goodness-of-fit on F^2	1.06
Final *R* indices [$I > 2\sigma(I)$]	0.0193
	(*wR2* = 0.0458)
Largest diff. peak/hole (eÅ^{-3})	0.87/-1.04

Table 4.9: Selected bond lengths (Å) and angles (˚) for **1**.

Bond lengths			
Re–C(13)	1.906(4)	N(2)-C(2)	1.450(5)
Re–N(1)	2.211(3)	N(1)–C(1)	1.456(5)
Re–C(14)	1.906(4)	N(3)–C(7)	1.501(9)
Re–N(2)	2.224(3)	N(4)–C(8)	1.41(2)
Re–C(15)	1.904(4)	O(1)–C(13)	1.162(5)
Re–N(3)	2.256(3)	O(3)-C(15)	1.156(5)
Bond angles			
N(1)–Re–N(2)	76.8(1)	N(1)–Re–C(15)	93.4(1)
N(1)–Re–C(13)	176.3(1)	N(2)–Re–C(13)	99.7(1)
Re–N(3)–C(7)	115.8(2)	N(3)–Re–C(13)	92.1(1)
N(2)–Re–C(14)	171.6(1)	C(13)–Re–C(14)	88.5(2)
C(13)–Re–C(15)	87.9(2)	C(14)–Re–C(15)	89.4(2)
N(3)–Re–C(15)	178.1(2)	N(1)–Re–N(3)	86.6(1)
N(1)–Re–C(14)	95.0(1)	N(2)–Re–N(3)	85.1(1)

Table 4.10: Selected bond lengths (Å) and angles (˚) for **2**.

Bond lengths			
Re(1)–S(11)	2.488(1)	O(12)–C(12)	1.397(8)
Re(1)–S(21)	2.522(1)	O(22)–C(22)	1.377(8)
Re(2)–S(11)	2.527(1)	Re(1)–C(1)	1.912(6)
Re(2)–S(21)	2.516(1)	Re(2)–C(4)	1.931(6)
Re(1)–O(12)	2.220(5)	Re(2)–C(5)	2.003(7)
Re(1)–C(2)	1.895(6)	Re(2)–C(6)	2.007(7)
R(1)-C(3)	1.948(6)	Re(2)-C(7)	1.932(7)
Bond angles			
Re(1)–S(11)–Re(2)	98.65(5)	S(21)–Re(1)–C(1)	168.9(2)
S(11)–Re(1)–S(21)	81.63(4)	C(5)–Re(2)–C(6)	178.0(3)
Re(1)–S(21)–Re(2)	98.06(5)	S(11)–Re(1)– C(3)	172.7(2)
S(11)–Re(2)–S(21)	80.98(4)	S(11)–Re(2)–C(4)	175.4(2)
S(11)-Re(1)-O(12)	77.0(1)	C(4)-Re(2)-C(5)	91.5(3)
C(2)-Re(1)-O(12)	174.4(2)	C(4)-Re(2)-C(7)	90.5(3)
C(4)-Re(2)-C(6)	90.4(3)	S(11)-Re(2)-C(6)	90.6(2)

Table 4.11: Selected bond lengths (Å) and angles (˚) for **3**.

Bond lengths			
Re-C(1)	1.910(5)	Re-N(1)	2.204(4)
Re-C(2)	1.908(5)	Re-N(2)	2.248(4)
Re-C(3)	1.899(6)	Re-O(4)	2.107(4)
S(1)-C(5)	1.773(6)	N(1)-C(11)	1.299(6)
O(4)-C(13)	1.337(6)	O(5)-C(19)	1.346(6)
N(2)-C(18)	1.426(7)	S(1)-C(4)	1.790(5)
Bond angles			
C(1)-Re-N(1)	170.0(2)	C(1)-Re-C(2)	88.2(2)
C(2)-Re-O(4)	172.2(2)	C(1)-Re-C(3)	88.8(2)
C(3)-Re-N(2)	176.3(2)	C(2)-Re-C(3)	89.9(2)
N(1)-Re-O(4)	76.5(1)	C(11)-N(1)-C(12)	119.3(4)
C(4)-S(1)-C(5)	103.4(3)	N(2)-Re-N(1)	82.5(1)
N(2)-Re-O(4)	79.5(1)	C(11)-N(1)-Re	128.4(4)
N(2)-Re-C(2)	101.3(2)	N(2)-Re-C(1)	93.9(2)
O(4)-Re-C(3)	97.7(2)	N(1)-Re-C(3)	94.4(2)

Table 4.12: Selected bond lengths (Å) and angles (˚) for **4**.

Bond lengths			
Re–Br(1)	2.626(3)	Re–C(3)	1.911(3)
Re–C(1)	1.934(3)	N(1)–C(11)	1.287(4)
Re–N(1)	2.202(2)	S(1)-C(4)	1.810(4)
Re–C(2)	1.924(3)	S(1)-C(5)	1.782(3)
Re–S(1)	2.468(8)	N(2)-C(13)	1.361(4)
Bond angles			
N(1)–Re–C(2)	177.0(1)	Br(1)–Re–C(1)	93.0(1)
Br(1)–Re–S(1)	85.31(2)	C(11)–N(1)–C(12)	114.3(2)
S(1)–Re–C(1)	175.7(1)	Br(1)–Re–C(2)	93.8(1)
Br(1)–Re–N(1)	83.35(6)	C(4)–S(1)–C(5)	99.7(2)
Br(1)–Re–C(3)	175.2(1)	C(2)–Re–C(3)	90.9(1)
N(1)-Re-S(1)	86.78(7)	N(1)-Re-S(1)	86.78(7)

Chapter 5

Isolation of *tris*(bidentate) Complexes of Rhenium(III) from the *cis*-$[ReO_2]^+$ Core and Benzenethiol Derivatives

5.1 Introduction

It has been well established that the potentially bidentate ligands in Scheme 5.1 are redox non-innocent when coordinated to transition metals [1]. For example, 2-aminothiophenol (Scheme 5.2) can coordinate as a NS-donor chelate as the 2-aminothiophenolate (1-) anion ($Hatp^-$), as the 2-amidothiophenolate (2-) anion (atp^{2-}), or as the 2-iminothiobenzosemiquinonato (1-) ion ($ibsq^-$) [1]. Surprisingly, the benzosemiquinonato π-radical form of these ligands has been found to be quite common as a ligand. It was shown that high quality X-ray crystallographic data can allow the assignment of the three different forms of 2-aminothiophenol ($Hatp^-$, atp^{2-} and $ibsq^-$) in metal complexes [2].

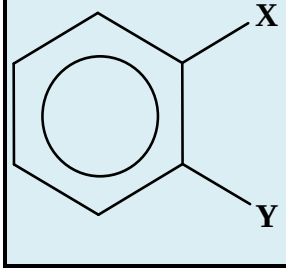

X	Y	
NH_2	SH	H_2atp
OH	SH	H_2otp
SH	SH	H_2tdt
OH	OH	H_2cat
NH_2	OH	H_2nap

Scheme 5.1: Non-innocent bidentate ligands.

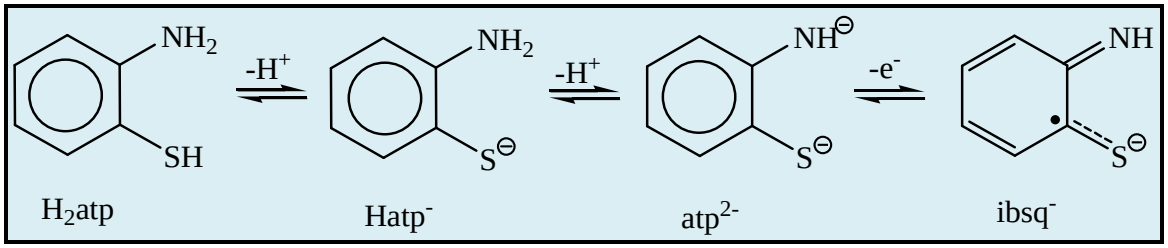

Scheme 5.2: Redox and protonation levels of 2-aminothiophenol.

Due to the favourable nuclear properties of the ^{99m}Tc and $^{186/188}$Re radionuclides for application in nuclear medicine, many studies of these metals with the bidentate ligands in Scheme 5.1 were initiated [3]. Several of the complexes isolated were of the *tris*(bidentate) type, in which the bidentate ligands have not been identified as the benzosemiquinonate radical anions. For example, with catechol (H_2cat) the complex [$Re^{VI}(cat)_3$] was isolated, in which the bidentate chelates cat^{2-} are in the catecholato, rather than the semiquinone, form [4]. This was also the case with the dithiolate (tdt^{2-}) complexes [$Re^{VI}(tdt)_3$] and [$Re^{V}(tdt)_3]^-$, and in the amidothiophenolate (atp^{2-}) complex [$Re^{VI}(atp)_3$] [5]. In most of these *tris*(bidentate) complexes, the rhenium lies in a distorted trigonal prism environment. Preference of this geometry above the octahedral geometry is not common in six-coordinate complexes. The trigonal prismatic coordination geometry is, however, generally encountered in metal ions with few electrons in the d-orbitals, with non-bulky ligands coordinated to the metal [6]. The trigonal twist angle θ (Figure 5.1) is used to structurally describe the coordination geometry of a structure (θ = 0˚ for a perfect trigonal prism and θ = 60˚ for an ideal octahedron) [7].

The reactions of the rhenium(V) complex *cis*-[$ReO_2I(PPh_3)_2$] with 2-aminothiophenol (H_2atp), benzene-1,2-dithiol (H_2tdt) and 2-hydroxybenzenethiol (H_2otp) led to the formation of the rhenium(III) compounds [Re(Hatp)$(ibsq)_2$].$OPPh_3$ (**1**), [Re$(sbsq)_3$].$OPPh_3$ (**2**) and [Re$(obsq)_3$].$OPPh_3$ (**3**) (ibsq = 2-iminothiobenzosemi-quinonate, sbsq = 1,2-dithiobenzosemiquinonate, obsq = 2-hydroxothiobenzosemi-quinonate) respectively. The reactions were conducted in boiling methanol in the presence of air. In all three cases the metal has been reduced from oxidation state +V to +III by the reduction of the oxo species by oxidative dissociation of triphenylphosphine to form triphenylphosphine oxide.

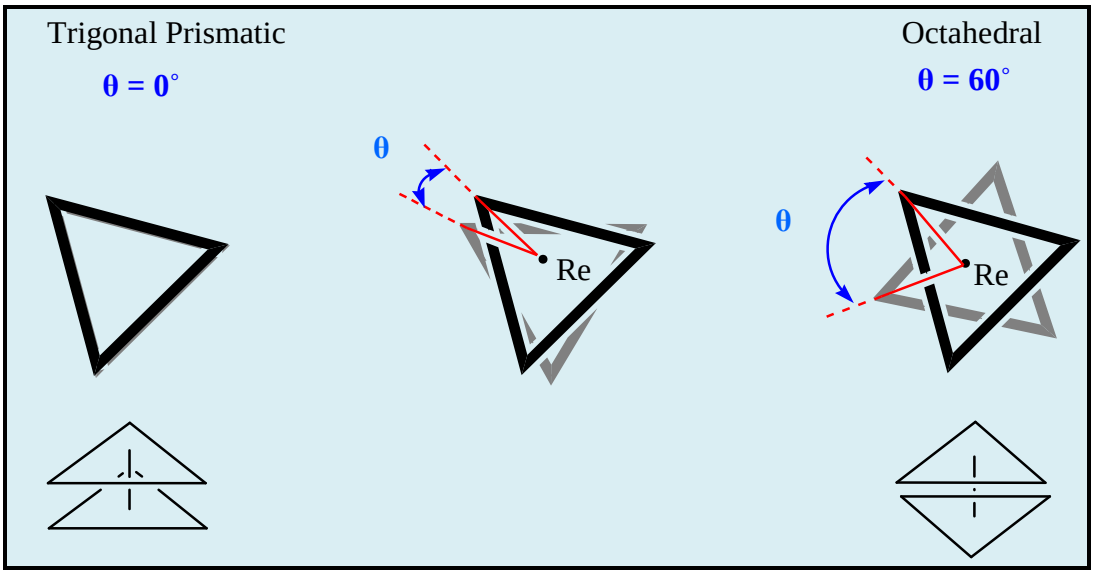

Figure 5.1: Twist angle for trigonal prismatic and octahedral geometries.

5.2 Experimental

5.2.1 Syntheses of [Re(Hatp)(ibsq)$_2$].OPPh$_3$ (1), [Re(sbsq)$_3$].OPPh$_3$ (2) and [Re(obsq)$_3$].OPPh$_3$ (3)

The relevant benzenethiol derivative {H_2atp (**1**), H_2tdt (**2**) or H_2otp (**3**) (345 μmol)} was dissolved in 10 cm^3 of methanol and added to *cis*-[$ReO_2I(PPh_3)_2$] (100 mg, 115 μmol) in 10 cm^3 of methanol. The mixture was heated at reflux for three hours in air. The resultant green solution was allowed to cool to room temperature and filtered. Green crystals were obtained from the slow evaporation of the filtrate.

Analysis of ***1***: Yield = 66 %, m.p. = 245 °C. Anal. Calcd. (%) for $C_{18}H_{16}N_3ReS_3.C_{18}H_{15}OP$: C, 51.8; H, 3.7; N, 5.0; S, 11.5. Found: C, 51.3; H, 3.6; N, 4.8; S, 11.7. μ_{eff} = 1.69 BM. IR (ν_{max}/cm^{-1}): ν(N-H) 3208w, 3183w; ν(C=C) 1537m; ν(P=O) 1118s; ν(C-S) 1088s; ν(P-C) 720s; ν(Re-N) 572m, 537m; ν(Re-S) 319m. ^{1}H NMR (295K, ppm): 7.62 (m, 15H, OPP*h*$_3$); 7.37 (t, 1H, *H*(25)); 7.13 (t, 2H, *H*(14), *H*(34)); 7.06 (d, 2H, *H*(13), *H*(33)); 6.98 (d, 1H, *H*(23)); 6.90 (t, 1H, *H*(24)); 6.79 (d, 2H, *H*(16), *H*(36)); 6.77 (d, 1H, *H*(26)); 6.52 (t, 2H, *H*(15), *H*(35)); 3.57 (s, br, 2H, N(2)*H*$_2$). Conductivity (10^{-3} M,

MeOH): 20 $ohm^{-1}cm^2mol^{-1}$. UV-Vis (MeOH, λ_{max} (ε, $M^{-1}cm^{-1}$)): 311 (6950), 364 (10500), 458sh (2300), 594 (7750), 681 (6950).

*Analysis of **2***: Yield = 78 %, m.p. = 86 °C. Anal. Calcd. (%) for $C_{18}H_{12}ReS_6.C_{18}H_{15}OP$: C, 48.9; H, 3.1; S, 21.7. Found: C, 49.0; H, 3.3; S, 20.9. μ_{eff} = 1.78 BM. IR (ν_{max}/cm^{-1}): ν(C=C) 1436; ν(P=O) 1113s; ν(C-S) 1096; ν(P-C) 685s; ν(Re-S) 348m. ^{1}H NMR (295K, ppm): 7.85-7.94 (m, 6H, *H*(14), *H*(15), *H*(24), *H*(25), *H*(34), *H*(35)); 7.71-7.82 (m, 15H, OPPh_3); 6.96-7.04 (m, 6H, *H*(13), *H*(16), *H*(23), *H*(26), *H*(33), *H*(36)). Conductivity (10^{-3} M, DMF): 12 $ohm^{-1}cm^2mol^{-1}$. UV-Vis (CH_2Cl_2, λ_{max} (ε, $M^{-1}cm^{-1}$)): 309 (17370), 440 (2850), 429 (3090), 723 (1590).

*Analysis of **3***: Yield = 63 %, m.p. = 209 °C. Anal. Calcd. (%) for $C_{18}H_{12}O_3ReS_3.C_{18}H_{15}OP$: C, 51.7; H, 3.3; S, 11.5. Found: C, 51.5; H, 3.3; S, 11.9. μ_{eff} = 1.70 BM. IR (ν_{max}/cm^{-1}): ν(C=C) 1436s; ν(P=O) 1114s; ν(C-S) 1066; ν(P-C) 741s; ν(Re-O) 458m; ν(Re-S) 307m. ^{1}H NMR (295K, ppm): 7.86-7.95 (m, 3H, OPPh_3); 7.72-7.82 (m, 12H, OPPh_3); 7.55 (d, 3H, *H*(13), *H*(23), *H*(33)), 7.30 (d, 3H, *H*(16), *H*(26), *H*(36)); 6.87 (t, 3H, *H*(14), *H*(24), *H*(34)); 6.75 (t, 3H, *H*(15), *H*(25), *H*(35)). Conductivity (10^{-3} M, MeOH): 16 $ohm^{-1}cm^2mol^{-1}$. UV-Vis (MeOH, λ_{max} (ε, $M^{-1}cm^{-1}$)): 316 (3150), 386 (2500), 614 (1550), 748 (960).

5.2.2 X-ray Crystallography

X-ray diffraction studies of **1.**CH_3OH, **2** and **3.**CH_3OH were performed at 200 K using a Bruker Kappa Apex II diffractometer with graphite monochromated Mo Kα radiation (λ = 0.71073 Å). APEX-II was used for data collection and SAINT for cell refinement and data reduction [8]. The structures were solved by direct methods using SHELXS-97 [9] or SIR97 [10], and refined by least-squares procedures using SHELXL-97 [9] with SHELXLE [11] as a graphical interface. All non-hydrogen atoms were refined anisotropically, and the hydrogen atoms were calculated in idealised geometrical positions. Data were corrected for absorption effects by the numerical method using SADABS [8].

5.3 Results and Discussion

5.3.1 Synthesis and characterization of $[Re(Hatp)(ibsq)_2].OPPh_3$ (1)

The reaction of *cis*-$[ReO_2I(PPh_3)_2]$ with 2-aminothiophenol (H_2atp) in methanol in the presence of air led to the formation of $[Re(Hatp)(ibsq)_2].OPPh_3$. The elemental analysis and X-ray crystallography indicated that $OPPh_3$ co-crystalizes with the complex. The formation of $OPPh_3$ intimates that the metal was reduced by PPh_3 to the +III oxidation state. This would necessitate the ligands to either be in the 2-aminothiophenolato form $Hatp^-$, or the 2-iminothiobenzosemiquinonato form $ibsq^-$. However, from the spectroscopic and crystallographic data the product was formulated as the rhenium(III) compound $[Re(Hatp)(ibsq)_2].OPPh_3$ (**1**). The reaction is described by the equation:

$$[ReO_2I(PPh_3)_2] + 3H_2atp + \tfrac{1}{2}O_2 \longrightarrow [Re(Hatp)(ibsq)_2].OPPh_3 + PPh_3 + HI + 2H_2O$$

Complex **1** is soluble in a number of different solvents such as acetonitrile, acetone, alcohols, DMSO, chloroform and DMF. The complex is a non-electrolyte in methanol and therefore neutral. It is stable for months in both the solid state and solution. The complex is paramagnetic at ambient temperature, with a magnetic moment of 1.69 BM. This value is low for two unpaired electrons (due to spin-orbit coupling), but it agrees well with those of mononuclear octahedral rhenium(III) complexes [μ_{eff} = 1.5-2.1 BM] [12, 13].

Although complex **1** is paramagnetic, the ^1H NMR spectrum displays sharp signals (Figure 5.2). A broad singlet at 3.57 ppm is assigned to the two amino protons on N(2). The presence of $OPPh_3$ is established by a 15 proton multiplet centered at 7.62 ppm. In the region 6.43-7.40 ppm a total of eight signals are observed. Two two-proton doublets [at 7.06 and 6.79 ppm] and two two-proton triplets [at 7.13 and 6.52 ppm] are the result of the four phenyl protons on the two coordinated ibsq chelates, with the four aromatic protons on the Hatp moiety giving rise to two one-proton triplets [at 7.37 and 6.90 ppm] and two one-proton doublets [at 6.98 and 6.77 ppm]. The NH resonances are not

observed, possibly due to the broadening of the nitrogen quadrupole exacerbated by the unpaired electron spin.

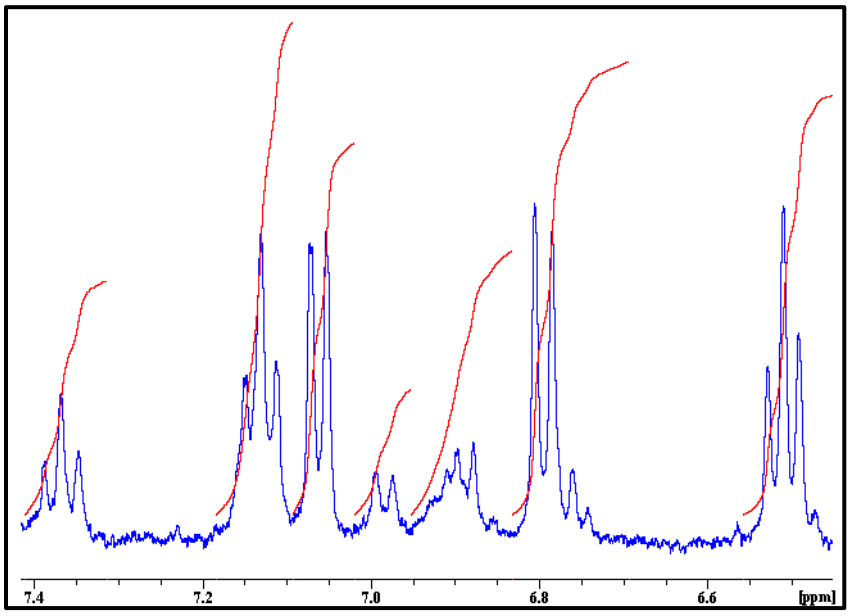

Figure 5.2: ^{1}H NMR spectrum of **1**.

The IR spectrum of **1** (Figure 5.3) shows no intense peaks in the 890-1020 cm^{-1} region, suggesting the absence of the Re=O entity. The medium intensity peaks at 537 and 572 cm^{-1} are due to *ν*(Re-N), with the Re-S stretch at 319 cm^{-1}. The peaks at 1118 cm^{-1} [*ν*(P=O)] and 720 cm^{-1} [*ν*(P-C)] are further evidence of the presence of the uncoordinated triphenylphosphine oxide in the crystal lattice. The electronic absorption data for **1** is complex with a large number of transitions, and the interpretation is not straightforward (Figure 5.4). The main feature of the spectrum is two intense bands at 594 nm (ε7750 $M.cm^{-1}$) and 681 nm (ε6950 $M.cm^{-1}$). Bands in this region are characteristic of the presence of benzosemiquinonate (1-) π-radical ligands coordinated to a rhenium ion [3, 5]. The band of highest energy (311 nm) is due to the intra-ligand transitions ($\pi \rightarrow \pi^*$) of the coordinated Hatp and ibsq ligands and is at a lower wavelength relative to the free 2-aminothiophenol (344 nm). Ligand-to-metal charge transitions [$p_\pi(S^-) \rightarrow d^*_\pi(Re)$] occur at 364 and 458 nm.

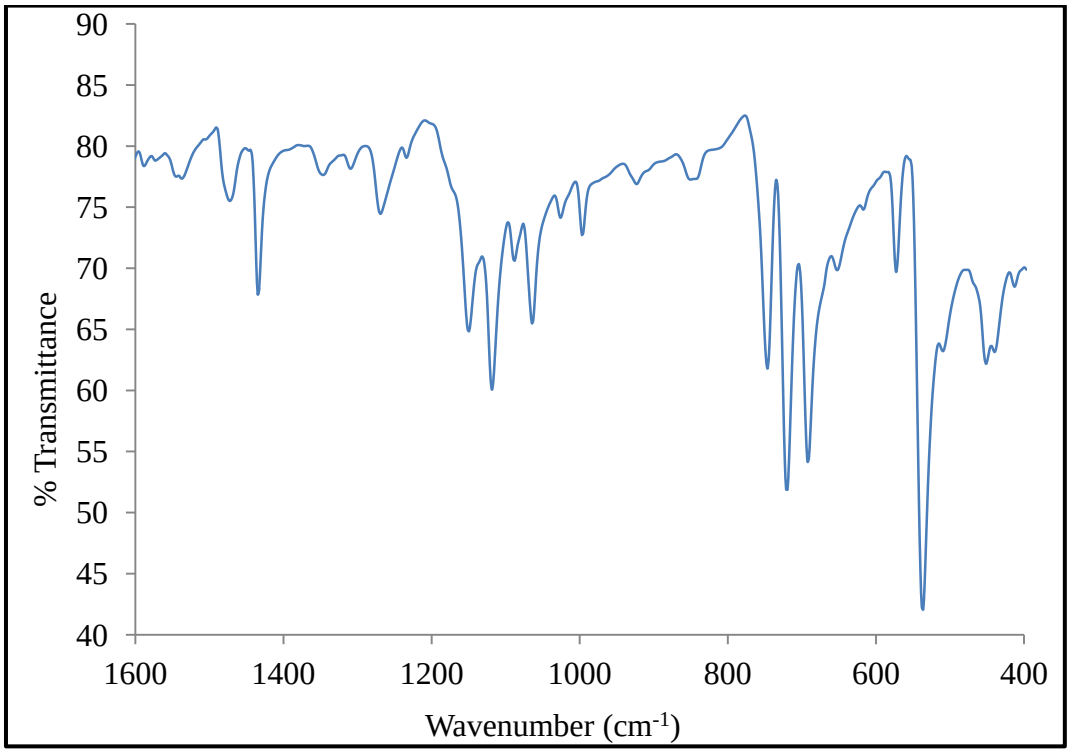

Figure 5.3: IR spectrum of complex **1**.

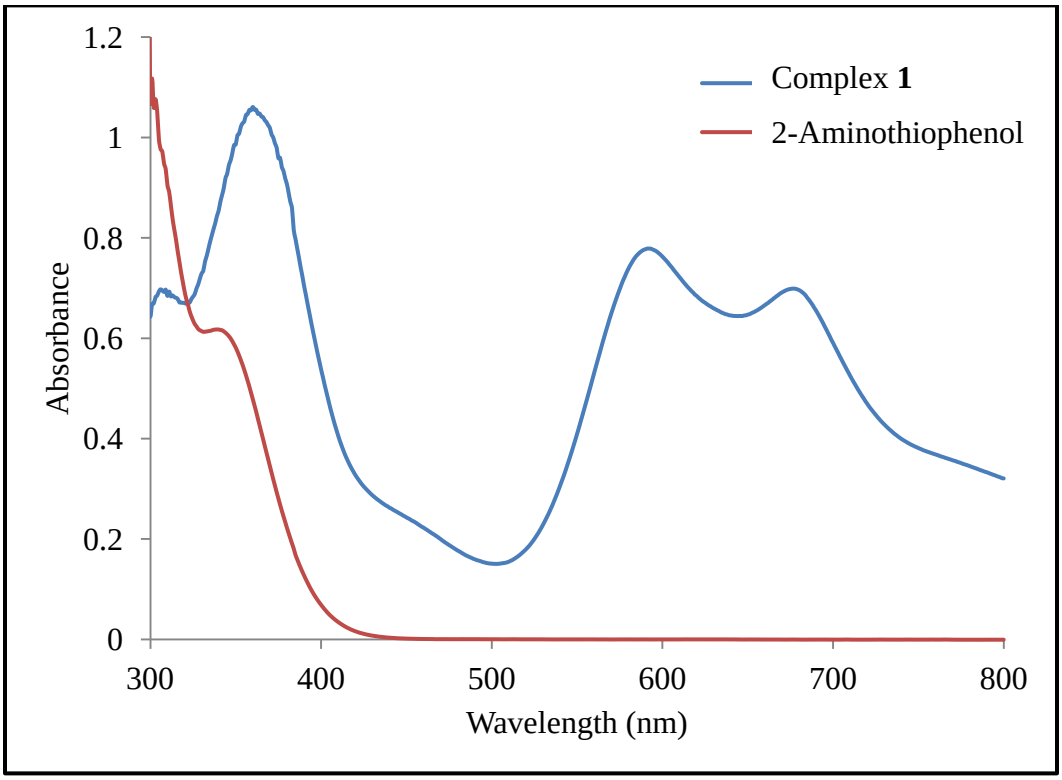

Figure 5.4: UV-Vis spectra of complex **1** and 2-aminothiophenol (H_2atp).

The molecular structure of **1** was obtained to a high precision by X-ray crystallography (Figure 5.5). The neutral molecule of **1** adopts a trigonal prismatic geometry around the rhenium center. The average twist angle between the upper and lower triangular faces (θ = 3.26˚) is small and indicates that the geometry is close to that of a perfect trigonal prism. It is interesting to note that the three chelate ring fold angles of **1** are different (Figure 5.6). Two are small in value (α' = 9.88˚ and α'' = 1.14˚), with the third being markedly larger (α''' = 35.54˚). This distortion is brought about by the geometrical differences which exist between the ibsq and Hatp chelates.

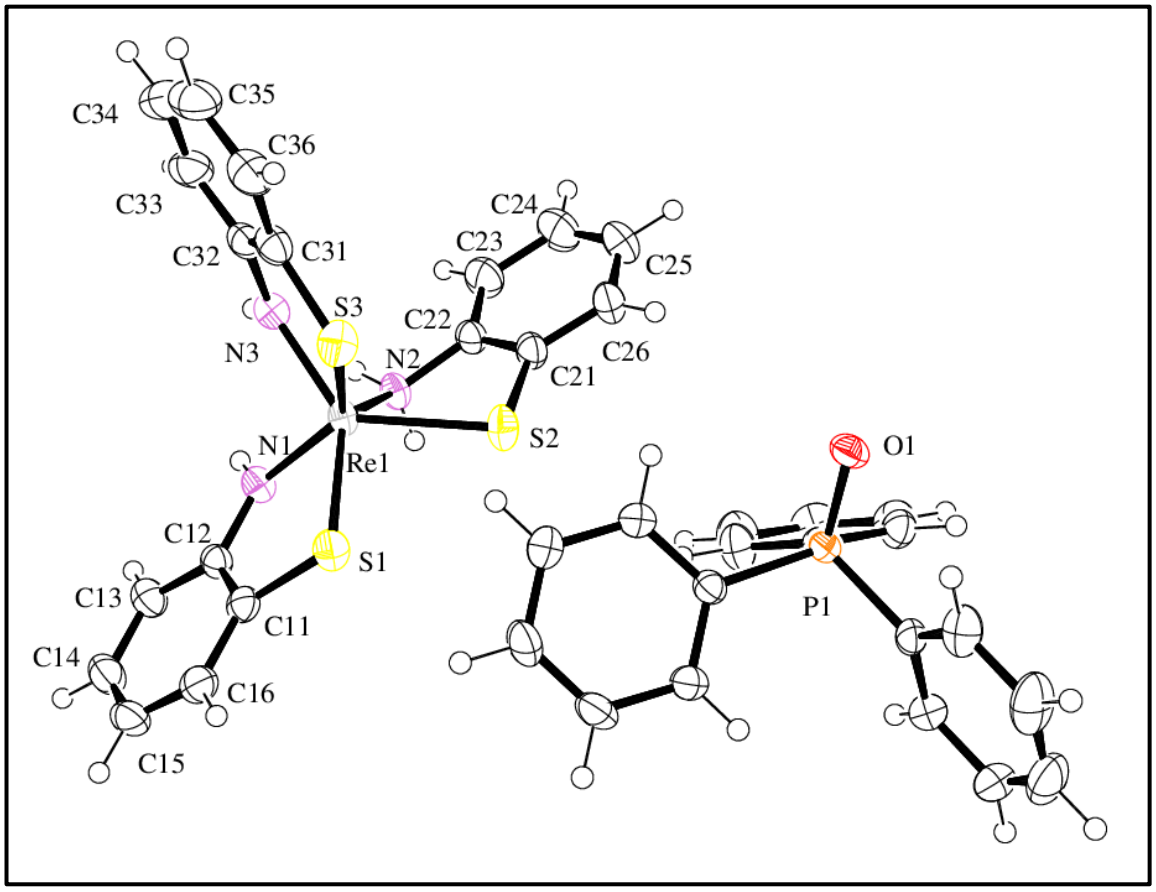

Figure 5.5: An ORTEP view of **1** showing 50% probability displacement ellipsoids and the atom labeling. The methanol solvent of crystallization was omitted for clarity.

The geometrical details of the three NS-coordinated ligands show that two of them are equivalent, and different from the third one. Two of the chelates have similar bite angles [S(1)-Re-N(1) = 79.57(8)˚ and S(3)-Re-N(3) = 78.66(7)˚], and are markedly different

from the angle S(2)-Re-N(2) [76.80(7)˚]. The two Re-S(1) [2.315(1) Å] and Re-S(3) [2.313(1) Å] bond lengths are practically identical, with the Re-S(2) length [2.406(1) Å] significantly different. These bond distances fall in the range [2.29(1)-2.54(1) Å] typically observed for thiolate sulfur bonds to rhenium [14]. The two bond lengths Re-N(1) [1.975(2) Å] and Re-N(3) [1.973(3) Å] are significantly different from the Re-N(2) bond [2.158(3) Å], with the latter typical of rhenium-amino nitrogen distances [15]. However, it is the intraligand bonding parameters which show that the oxidation levels of the ibsq ligands are above that of the 2-aminothiophenolate ligand (Hatp). The C-S [average 1.734(3) Å] and C-N [average 1.371(4) Å] bond lengths in the ibsq ligands display double bond character and are considerably shorter than the corresponding distances in Hatp [S(2)-C(21) = 1.762(4) Å, N(2)-C(22) = 1.447(4) Å]. Also, the phenyl rings in the ibsq ligands display distortions which are typical of quinoid type structures, *i.e.* two shorter and four longer C=C bond lengths.

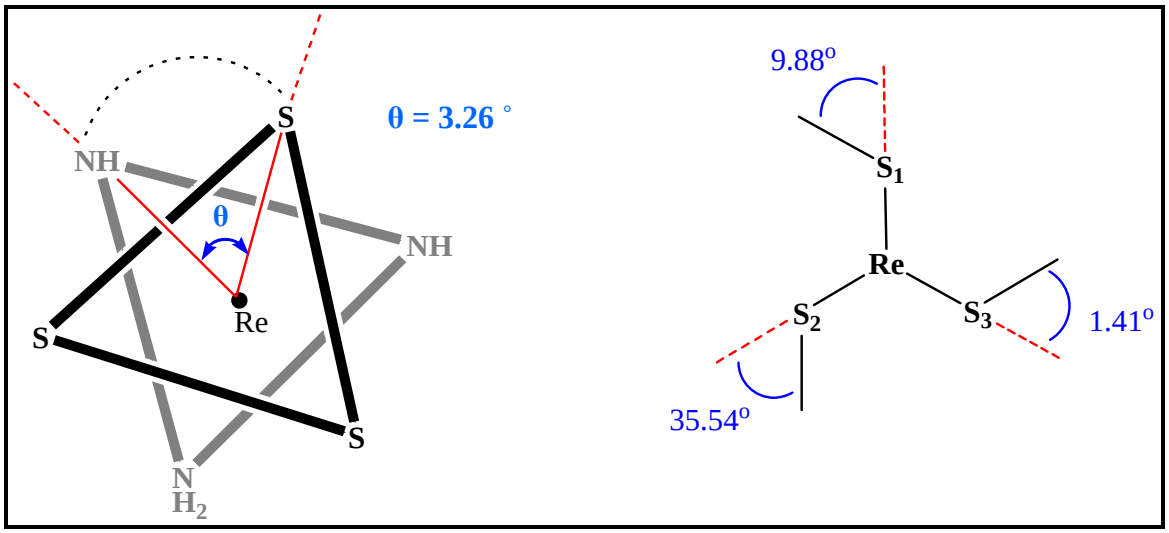

Figure 5.6: Twist angle (θ) and chelate ring fold angles (α) of **1**.

In previous studies, it was also experimentally possible to distinguish between the electronic structures of Hatp$^-$ and ibsq$^-$ [1, 2, 16]. In general, Hatp$^-$ has a C-N bond length of ~1.46 Å and a C-S distance of ~1.76 Å. In contrast, in the semiquinone form ibsq$^-$, respective C-N and C-S lengths of ~1.36 and ~1.72 Å are typically observed. In addition, it has been shown in earlier studies that the reaction of 2-aminothiophenol with *trans*-[$ReOCl_3(PPh_3)_2$] in benzene led to the isolation of the oxo-free rhenium(V)

complex [ReCl(PPh_3)$(atp)_2$] [17]. In this complex the average bite angle of the chelates is 78.8(1)˚, the Re-S bonds are identical [2.297(1) Å] and the average Re-NH bond length is 1.977(4) Å.

The oxygen atom O(1) of the $OPPh_3$ molecule is involved in hydrogen-bonding contacts N-H···O(1) to the amine/imine protons of the three chelates (Figure 5.7, Table 5.1), with the result that the P(1)=O(1) bond distance of 1.503(2) Å is slightly longer than in free $OPPh_3$ [18]. The methanol solvent of crystallization is involved in three intermolecular hydrogen-bonds. The hydroxyl hydrogen O(90)H(90) of the methanol forms intermolecular bonds with the sulfur atoms S(2) and S(3), while the hydroxyl oxygen O(90) interacts with the protons of the amino nitrogen N(2)H(721).

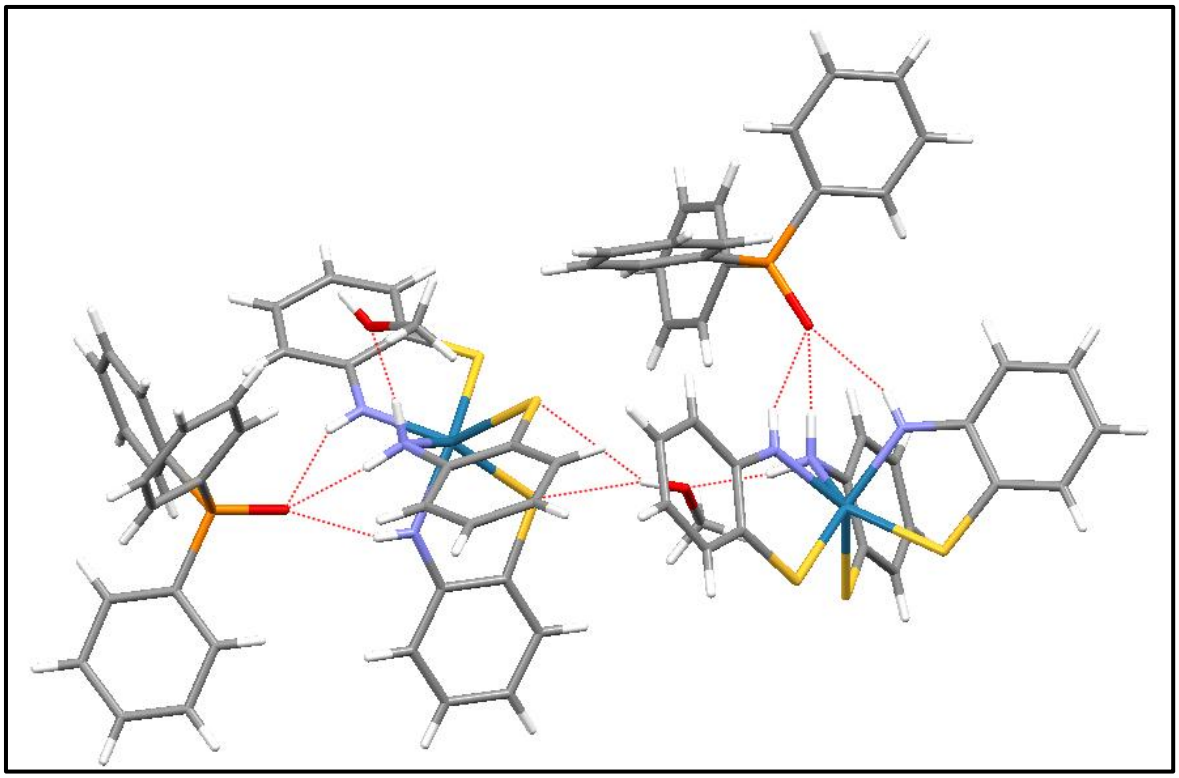

Figure 5.7: Perspective view of **1** showing the hydrogen-bonds.

Table 5.1: Hydrogen-bond distances (Å) and angles (˚) in **1.**

D-H•••A	D-H	H•••A	D•••A	D-H•••A
N(1)H(71)•••O(1)	0.81	2.40	3.124(4)	150
N(2)H(722)•••O(1)	0.88	1.98	2.831(3)	163
N(3)H(73)•••O(1)	0.78	2.26	2.982(3)	155
N(2)H(721)•••O(90)	0.88	2.07	2.887(5)	155
O(90)H(90)•••S(2)	0.84	2.84	3.595(5)	150
O(90)H(90)•••S(3)	0.84	2.79	3.442(5)	135

The cyclic and square-wave voltammograms of **1** are shown in Figure 5.8. Two redox couples (**B** and **C**) are present together with an irreversible cathodic peak (**A**). The square-wave voltammogram confirms that only these three processes occur in the potential region scanned (-1.500 to 0.400 V). The electrochemical data for the three processes are summarized in Table 5.2.

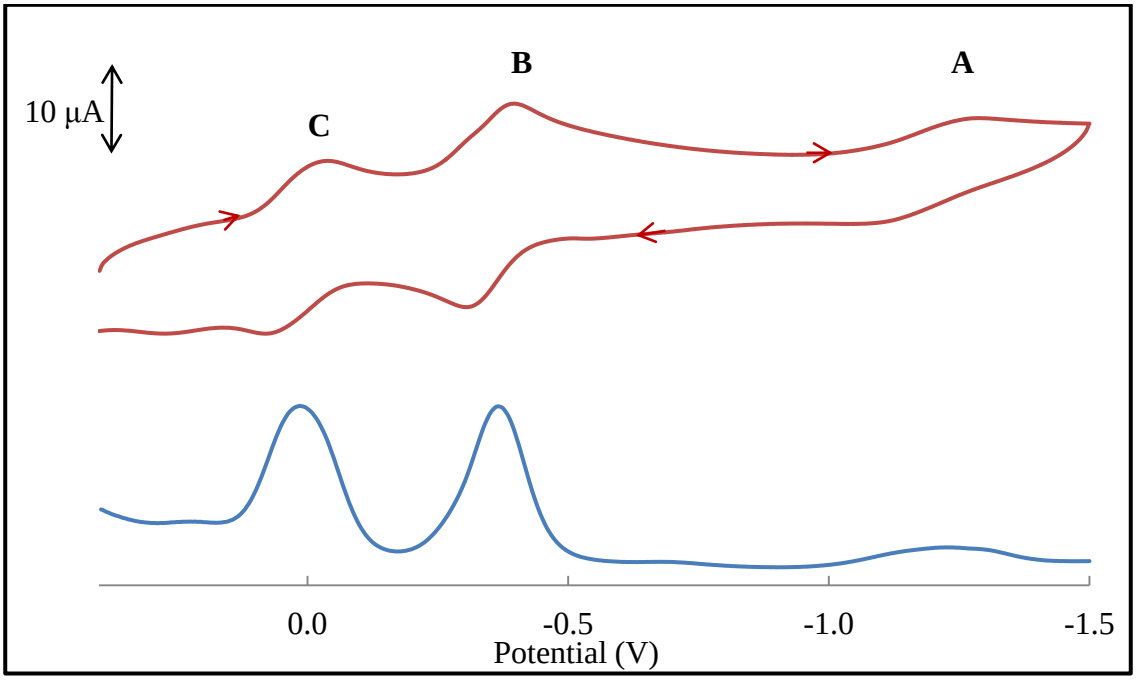

Figure 5.8: Cyclic voltammogram (red line) of **1** in CH_2Cl_2 (at a scan rate of 100 mV/s) and square-wave voltammogram (blue line).

Table 5.2: Electrochemical data (potential in V, current in μA) of **1**, scan rate 100 mV/s.

Process	E_{pc}	i_c	E_{pa}	i_a	$E_{1/2}$	i_a/i_c	ΔE_p	Assignment
A	-1.290	4.23	-	-	-	-	-	$ibsq^-/atp^{2-}$
B	-0.306	4.91	-0.397	8.14	-0.352	1.66	0.091	$ibsq^-/atp^{2-}$
C	-0.038	5.09	0.080	5.79	0.022	1.14	0.118	Re(III)/Re(IV)

The peak-to-peak separations for processes **B** and **C** were found to be 0.091 and 0.118 V respectively, suggesting that they are quasi-reversible. The quasi-reversibility of the two redox processes is further established by the ratios between the anodic and cathodic currents which are greater than one for processes **B** and **C**. The peak-to-peak separations are comparable to that of the ferrocene redox couple (ΔE = 0.105 V) indicating that **B** and **C** take place *via* a one electron charge transfer. The reduction wave at E_{pc} = -1.290 V (**A**) is assigned to the redox processes occurring within one coordinated ligand $ibsq^-/atp^{2-}$ ($L^{\bullet}/L$), with the quasi-reversible wave at $E_{1/2}$ = -0.352 V (**B**) due to an identical process for a second $ibsq^-$ ligand. The quasi-reversible wave at $E_{1/2}$ = 0.022 V (**C**) is ascribed to the Re(III)/Re(IV) redox couple and is at a similar value to those observed for rhenium(III) complexes in the literature [13]. These processes are described by the following equation:

$$[Re^{IV}(Hatp)(ibsq)_2]^+ \underset{-e^-}{\overset{+e^-}{\rightleftharpoons}} [Re^{III}(Hatp)(ibsq)_2]^0 \underset{-e^-}{\overset{+e^-}{\rightleftharpoons}} [Re^{III}(Hatp)(atp)(ibsq)]^-$$

$$-e^- \Big\| +e^-$$

$$[Re^{III}(Hatp)(atp)_2]^{2-}$$

The cyclic voltamograms of **1** were obtained at different scan rates ranging from 50-500 mV/s. The $E_{1/2}$ values remain constant with increasing scan rates. The Randles-Sevcik equation [19] can be used to determine whether the main mass transport of a compound to the electrode surface is controlled by a diffusion step and is given by the following expression:

$$i = (2.69\text{x}10^5)n^{3/2}AD^{1/2}Cv^{1/2}$$

were *i* is the peak current (in amperes), *A* is the electrode area (in cm^3), *D* is the diffusion coefficient (in cm^2/s), *C* is the concentration(in mol/cm^3) and *v* is the sweep rate (in V/s). A plot of peak current (*i*) against the square-root of the scan rate ($v^{1/2}$) for each of the processes produced linear curves (Figure 5.9). This dependence of the peak currents on the square-root of the scan rate suggests that all the processes are diffusion controlled.

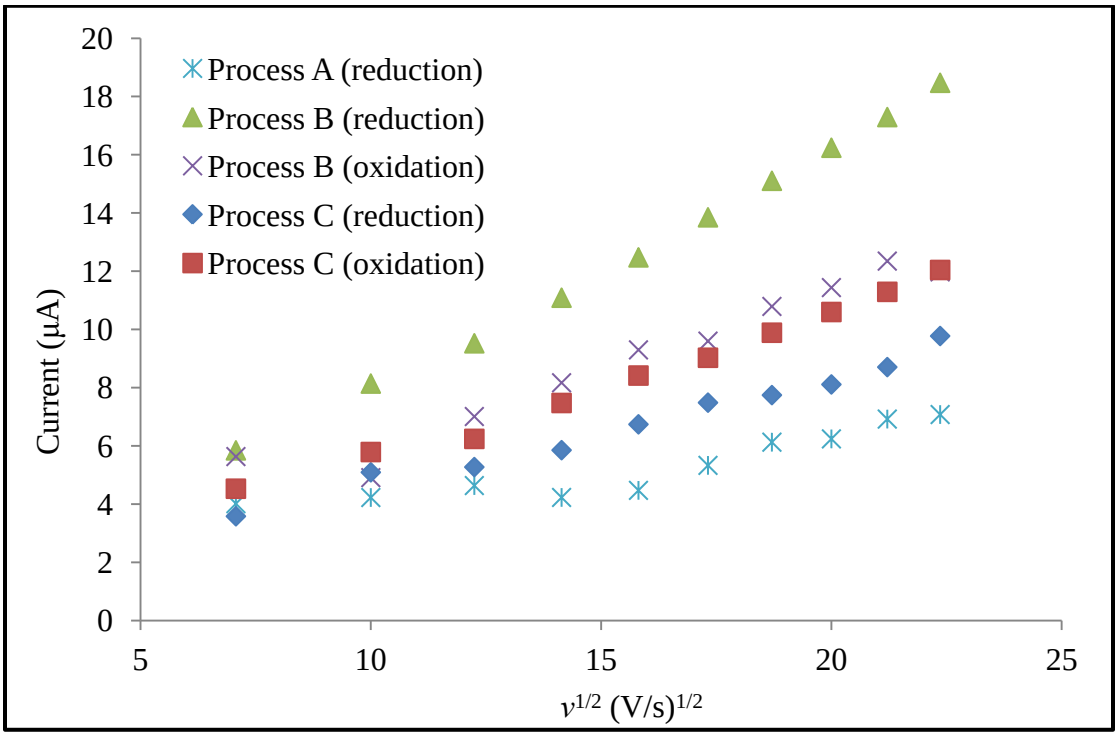

Figure 5.9: Plots of peak current (*i*) *vs.* the square root of the scan rate ($v^{1/2}$) for the different processes.

5.3.2 Synthesis and characterization of $[Re(sbsq)_3].OPPh_3$ (2)

The reaction of *cis*-$[ReO_2I(PPh_3)_2]$ with three equivalents of benzene-1,2-dithiol (H_2tdt) in air resulted in the formation of $[Re(sbsq)_3].OPPh_3$ (**2**) in which the metal has been reduced to the +III oxidation state. The oxidation state is confirmed by the magnetic moment of 1.78 BM. The three chelates are equivalent as indicated by spectroscopic and X-ray crystallographic data, which implies that the ligand is coordinated as a monoanionic bidentate chelate. The ligands are therefore present in the complex in the dithiobenzosemiquinonato (1-) π-radical form ($sbsq^-$).

$$2[ReO_2I(PPh_3)_2] + 6H_2tdt + {}^3/_2O_2 \longrightarrow 2[Re(sbsq)_3].OPPh_3 + 2PPh_3 + 5H_2O + 2HI$$

Complex **2** is soluble only in methanol, dichloromethane and DMF. It is stable in solution for days and for months in the solid state. The microanalytical data are in good agreement with the calculated values.

The aromatic region of the ^{1}H NMR spectrum of **2** (Figure 5.10) is characterized by three multiplets. The multiplet which appears in the 7.71-7.82 ppm region is assigned to the fifteen protons of the triphenylphosphine oxide. The remaining two multiplets correspond to the protons of the three aromatic sbsq moieties. The IR spectrum of **2** (Figure 5.11) confirms the presence of the triphenylphosphine oxide compound in the formulation of **2**, with the peaks at 1113 and 685 cm^{-1} assigned to the P=O and P-C stretching frequencies respectively. The Re-S stretch is found at 348 cm^{-1}.

The electronic spectrum of **2** displays a high intensity band at 309 nm. This band is due to a ligand-to-ligand charge transfer transition occurring in the coordinated sbsq moieties. The band at 440 nm is assigned as ligand-to-metal charge transitions with a d-d transition occurring at 723 nm.

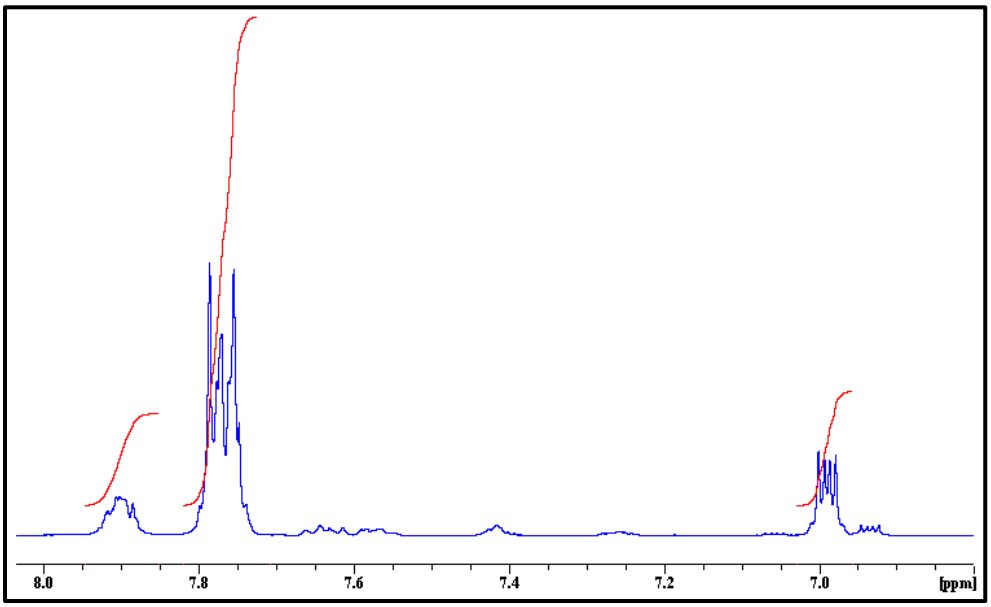

Figure 5.10: ^{1}H NMR spectrum of **2**.

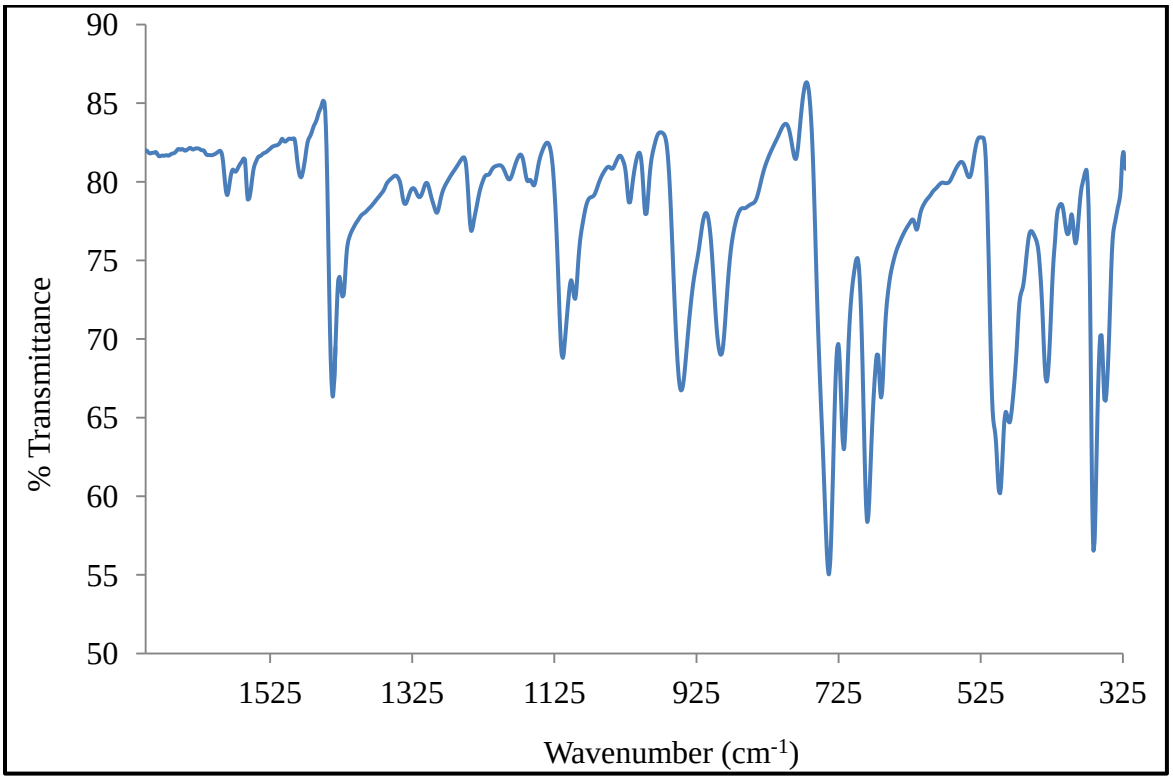

Figure 5.11: IR spectrum of complex **2**.

Complex **2** has a distorted trigonal prismatic ReS_6 polyhedron with a central Re(III) ion (Figure 5.12). The distortion from ideal trigonal prismatic geometry can be seen in the twist angle of θ = 25.60˚ (Figure 5.13), which indicates that the geometry is an intermediate between trigonal prismatic (θ = 0˚) and octahedral (θ = 60˚). The geometric parameters of the three bidentate chelates show that they are equivalent. The six Re-S bond lengths are similar, with an average length of 2.342(2) Å. In contrast to complex **1**, all three fold angles (Figure 5.13) are small with an average value of 7.67˚.

The three bidentate chelates form similar bite angles of 83.41(5)˚ [S(1)-Re-S(2)], 82.43(5)˚ [S(5)-Re-S(6)] and 82.87(5)˚ [S(3)-Re-S(4)]. In each ligand, one C-S [S(2)-C(12) = 1.742(6) Å, S(4)-C(22) = 1.736(6) Å, S(6)-C(32) = 1.732(5) Å] bond length displays double bond character and is shorter than the second C-S [S(1)-C(11) = 1.745(6) Å, S(3)-C(21) = 1.750(6) Å and S(5)-C(31) = 1.743(5) Å] bond distance. These C-S bond lengths indicates that each ligand is coordinated as a dithiobenzosemiquinonate (1-) radical bidentate chelate. The C-S bond lengths are, however, slightly longer than the

literature values [short C-S ~1.72 Å and long C-S ~1.74 Å] for benzene-1,2-dithiol coordinated in the dithiobenzosemiquinonato (1-) radical form [2].

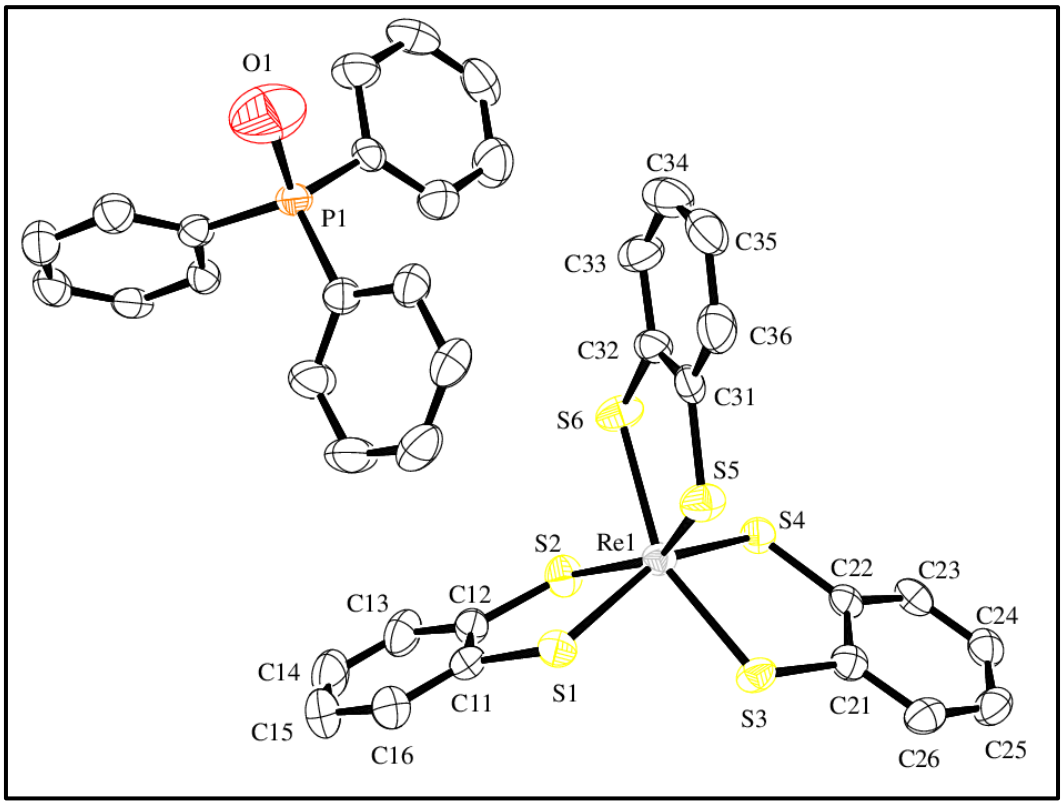

Figure 5.12: An ORTEP view of **2** showing 50% probability displacement ellipsoids and the atom labeling. Hydrogen atoms were omitted for clarity.

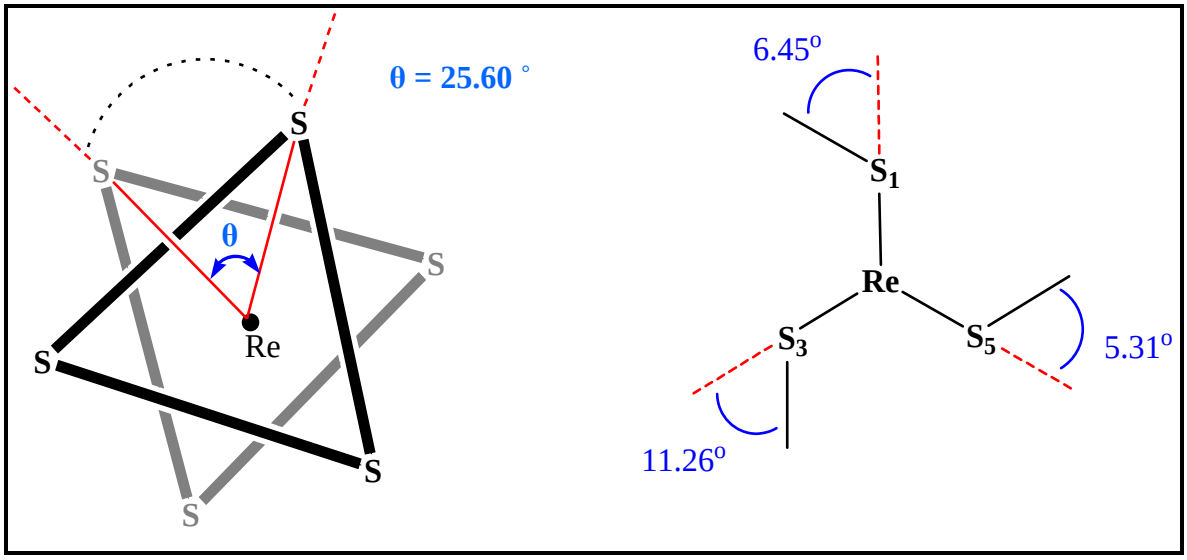

Figure 5.13: Twist angle (θ) and chelate ring fold angles (α) of **2**.

The cyclic and square wave voltammograms of **2** (Figure 5.14) displays two redox processes, **A** and **B** as well as a slight shoulder at -0.900 V. The electrochemical data for the two processes are summarized in Table 5.3.

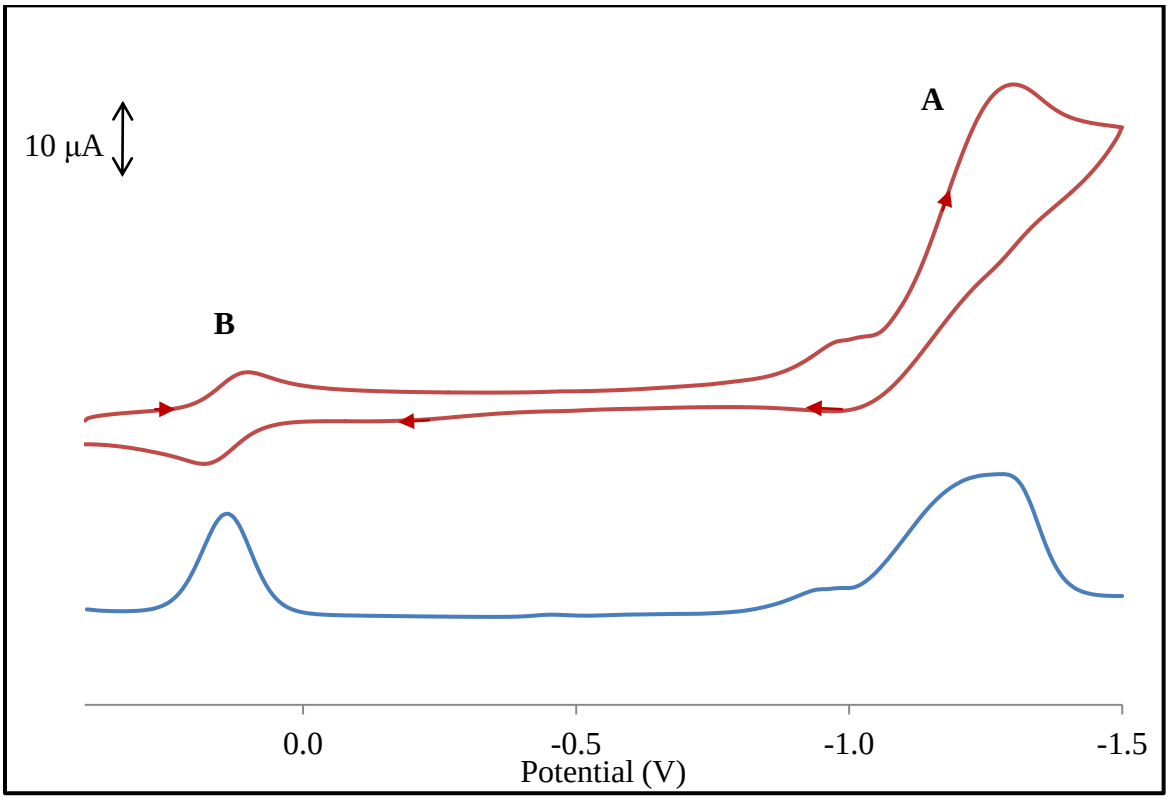

Figure 5.14: Cyclic voltammogram (red line) of **2** in CH_2Cl_2 at a scan rate of 100 mV/s and square-wave voltammogram (blue line).

Table 5.3: Electrochemical data (potential in V, current in µA) of **2**, scan rate 100 mV/s.

Process	E_{pc}	i_c	E_{pa}	i_a	$E_{1/2}$	i_a/i_c	ΔE_p	Assignment
A	-1.300	40.54	-	-	-	-	-	$sbsq^-/tdt^{2-}$
B	0.103	3.88	0.181	5.30	0.142	1.37	0.078	Re(III)/Re(IV)

The peak-to-peak separations for process **B** was found to be 0.078 V with the ratio between the anodic and cathodic peak currents less than one, indicating that the process is quasi-reversible. A reductive wave (**A**), due to an intraligand redox process ($sbsq^-/tdt^{2-}$)

occurs at -1.300 V. The quasi-reversible redox wave at 0.142 V (**B**) is assigned to the Re(III)/Re(IV) redox couple. These processes occur as follows:

$$[Re^{IV}(sbsq)_3]^+ \underset{-e^-}{\overset{+e^-}{\rightleftharpoons}} [Re^{III}(sbsq)_3]^0 \underset{-e^-}{\overset{+e^-}{\rightleftharpoons}} [Re^{III}(sbsq)_2(tdt)]^-$$

Cyclic voltammograms of **2** were generated at different scan rates ranging from 50-500 mV/s. The $E_{1/2}$ values remain constant with increasing scan rate. A plot of peak current (*i*) against the square-root of the scan rate ($v^{1/2}$) for each of the processes produced linear curves (Figure 5.15). This dependence of the peak currents on the square-root of the scan rate suggests that processes **A** and **B** are diffusion controlled.

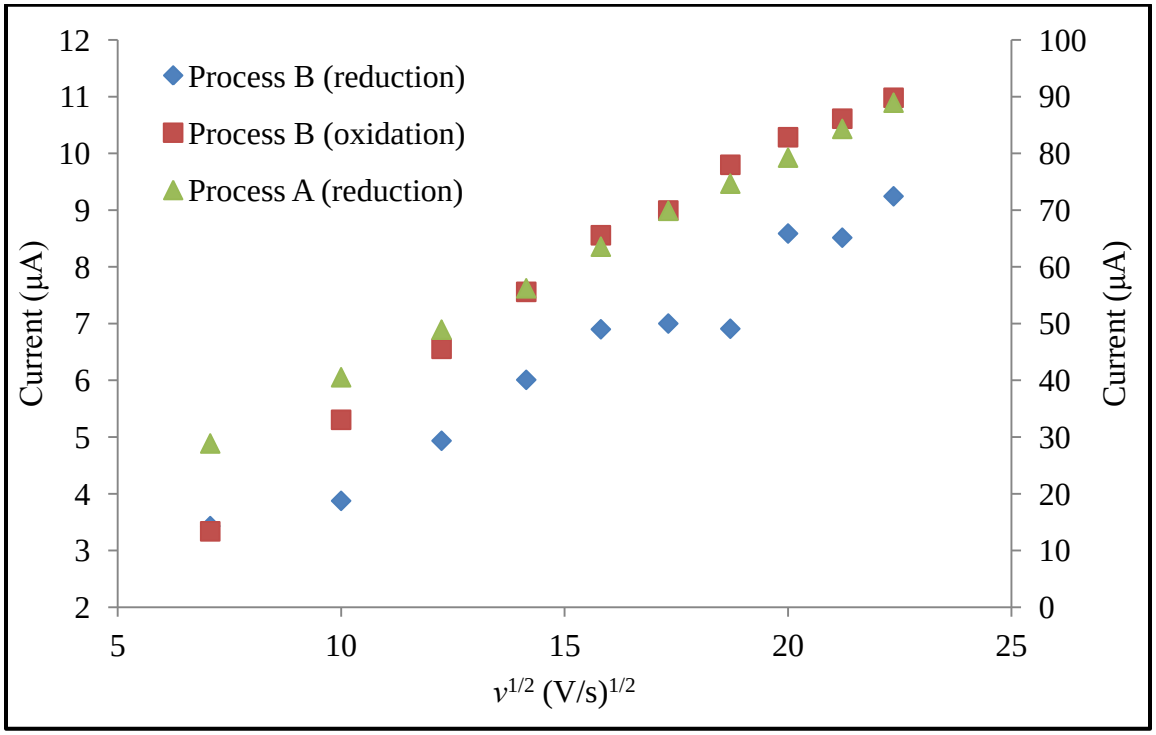

Figure 5.15: Plots of current (*i*) *vs.* the square root of the scan rate ($v^{1/2}$) for the different processes.

5.3.3 Synthesis and characterization of $[Re(obsq)_3].OPPh_3$ (3)

The compound $[Re(obsq)_3].OPPh_3$ (**3**) was formed by the reaction of *cis*-$[ReO_2I(PPh_3)_2]$ with 2-hydroxybenzenethiol (H_2otp) in air. Similar to complexes **1** and **2**, the metal in **3** has been reduced to the +III state by PPh_3. The oxidation state is verified by the magnetic moment of 1.70 BM. The spectroscopic and X-ray crystallographic data indicates that the three chelates are equivalent, implying that the charge on the ligands must be monoanionic. This conclusion would therefore mean that the ligands can only be present in the complex in the benzosemiquinonato (1-) π-radical form $obsq^-$.

$$2ReO_2I(PPh_3)_2 + 6H_2otp + {}^3/_2O_2 \longrightarrow 2[Re(obsq)_3].OPPh_3 + 2PPh_3 + 5H_2O + 2HI$$

Complex **3** is soluble in methanol and dichloromethane, producing intense green solutions. The complex is stable for weeks in solution and for months in the solid state. The low conductivity value (Λ_M = 16 $ohm^{-1}cm^2mol^{-1}$) indicates that it is a non-electrolyte in methanol.

The ^1H NMR spectrum of **3** is shown in Figure 5.16. The signals of the 15 protons of the triphenylphosphine oxide appear as two multiplets in the 7.72-7.95 ppm region. In addition, there are four other three-proton signals in the aromatic region: two doublets at 7.30 and 7.55 ppm and two triplets at 6.75 and 6.87 ppm. These signals are ascribed to the 12 aromatic protons of the phenyl rings of the three coordinated ligands, implying that the corresponding protons on the three aromatic rings are magnetically equivalent.

The infra-red spectrum of **3** (Figure 5.17) contains medium intensity peaks at 307 and 458 cm^{-1} due to the *ν*(Re-S) and *ν*(Re-O) respectively. The P=O and P-C stretches occur at 1114 and 741 cm^{-1} respectively. An intra-ligand transition ($\pi \rightarrow \pi^*$) of the coordinated ligand is observed at 316 nm on the UV-Vis spectrum of **3** (Figure 5.18), and is at a lower energy compared to the free 2-hydroxybenzenethiol ligand (295 nm). The band at 386 nm is assigned to a ligand-to-metal charge transition and d-d transitions occur at 614 and 748 nm.

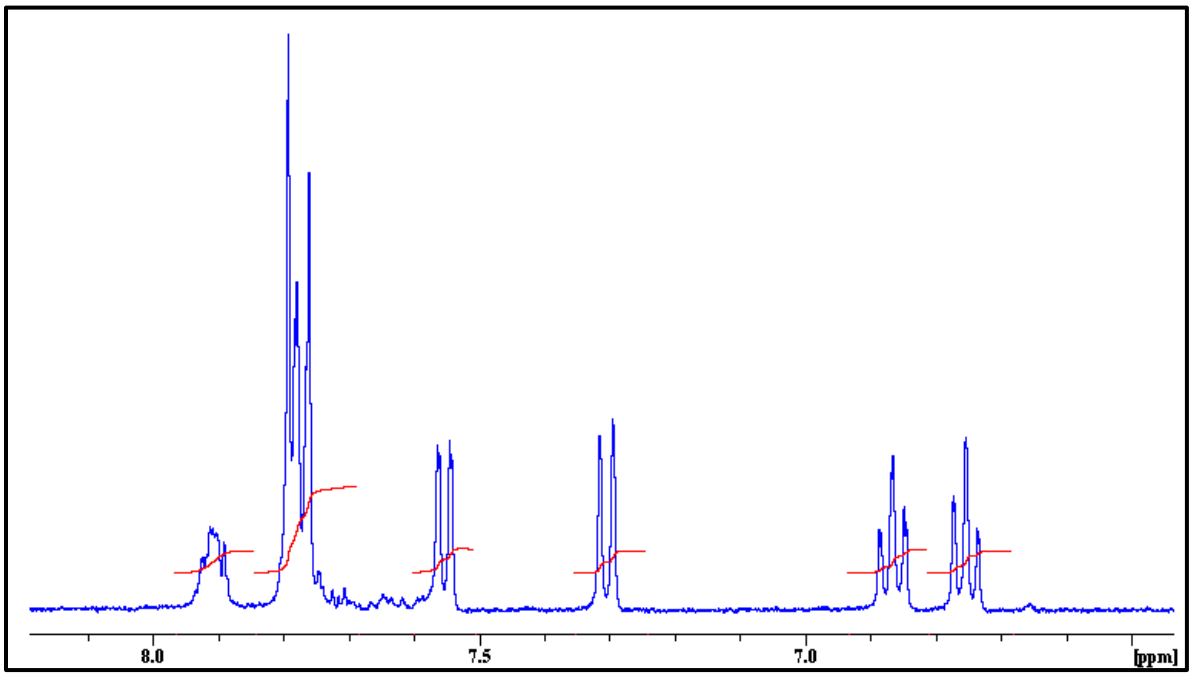

Figure 5.16: ^{1}H NMR spectrum of the aromatic region for **3**.

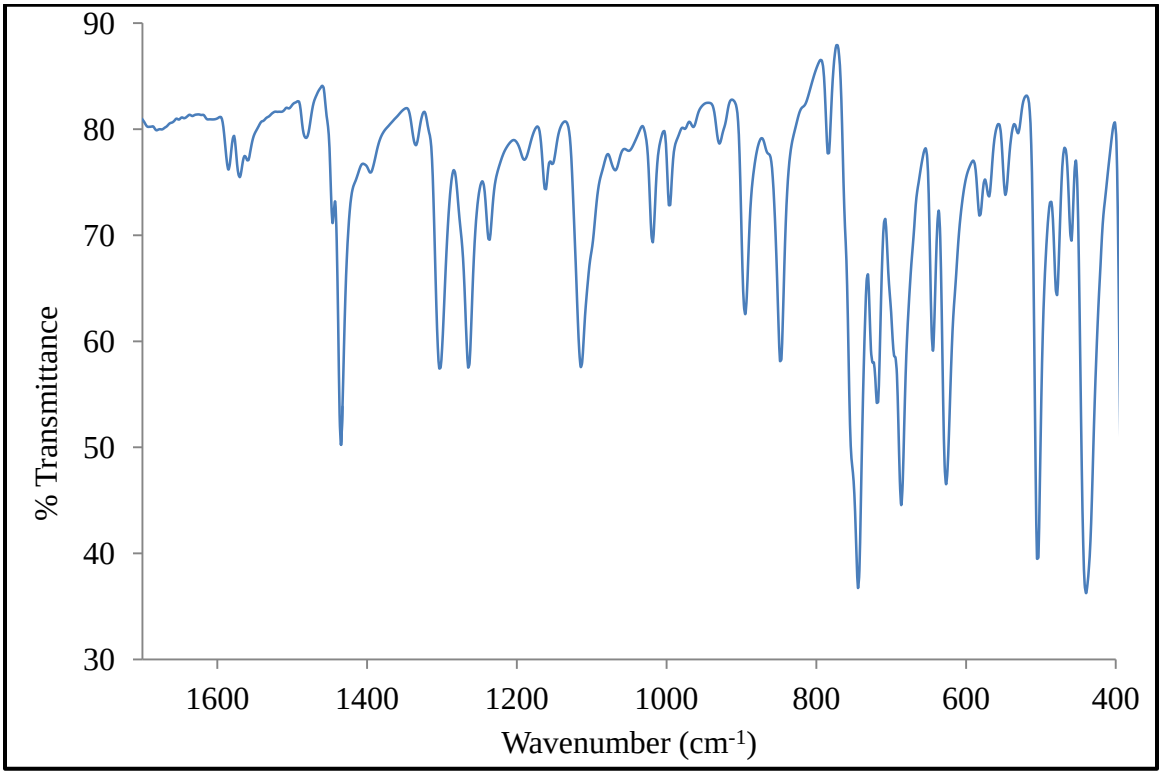

Figure 5.17: IR spectrum of complex **3**.

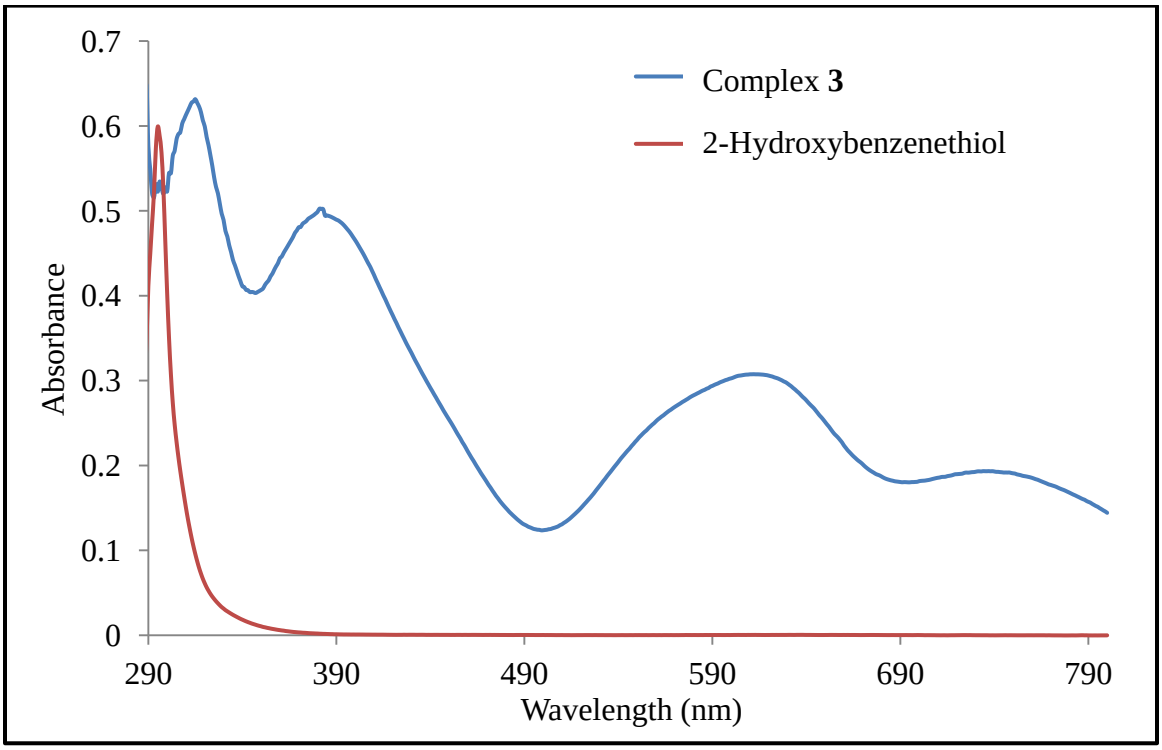

Figure 5.18: UV-Vis spectra of complex **3** and 2-hydroxybenzenethiol.

The crystal structure of $[Re(obsq)_3].OPPh_3$ (**3**) was determined by X-ray crystallography. The rhenium resides in the center of a distorted trigonal prism (Figure 5.19). The twist angle (θ = 24.24˚) is similar to that of complex **2** and indicates that the geometry is between trigonal prismatic and octahedral (Figure 5.20). The fold angles are small with an average value of 2.44˚.

The geometric parameters of the three chelates show that they are equivalent. The bite angles of the ligands are nearly identical [S(11)-Re-O(12) = 80.52(6)˚, S(21)-Re-O(22) = 80.96(7)˚, S(31)-Re-O(32) = 80.37(7)˚]. The corresponding Re-S and corresponding Re-O bond lengths are similar, with average lengths of 2.3076(9) Å and 1.996(2) Å respectively. The C-S and C-O bond lengths [average of 1.751(4) Å and 1.339(4) Å respectively] are longer than previously found for H_2otp in the benzosemiquinonato radical form $obsq^-$, with average C-S and C-O distances of ~1.72 Å and ~1.30 Å respectively [2]. These results therefore intimate that the C-X bond lengths cannot solely be used as an indicator of the oxidation level of these ligands.

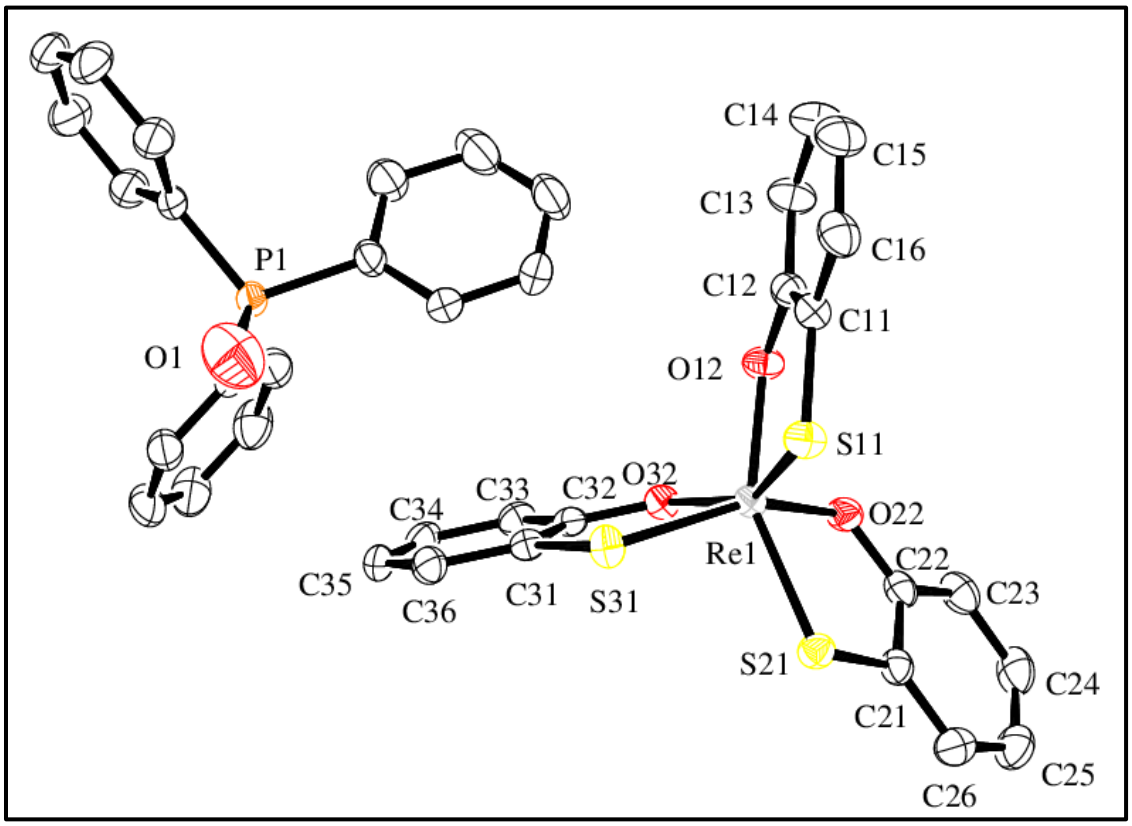

Figure 5.19: An ORTEP view of **3** showing 50% probability displacement ellipsoids and the atom labeling. Hydrogen atoms and the methanol solvent of crystallization are omitted for clarity.

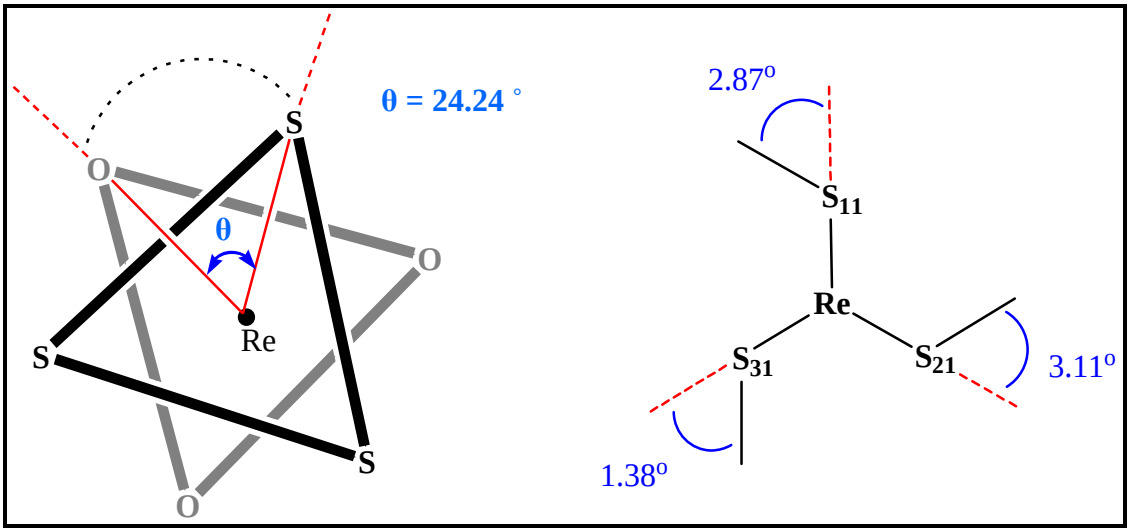

Figure 5.20: Twist angle (θ) and chelate ring fold angles (α) of **3**.

The cyclic voltammogram (CV) and the square-wave (SW) voltammogram of complex **3** are shown in Figure 5.21. The CV displays two redox couples **A** and **B** and the electrochemical data for the two processes are summarized in Table 5.4. The SW voltammogram confirms that only these two processes occurs in the potential region scanned (-1.500 to 0.400 V).

For processes **A** and **B**, the peak-to-peak separation was found to be 0.101 and 0.100 V respectively, suggesting that they are one electron quasi-reversible processes. The peak current ratios for the two processes **A** and **B** are 0.67 and 1.31 respectively, further indicating quasi-reversibility. The quasi-reversible wave (**A**) at the more negative potential value of -1.280 V corresponds to the redox processes occurring within one of the ligands, $obsq^{-}/otp^{2-}$ ($L^{\bullet}/L$). The quasi-reversible redox wave (**B**) occurring at 0.126 V is assigned to the Re(III)/Re(IV) couple. The two redox process observed for complex **3** are described by the following equation:

$$[Re^{IV}(obsq)_3]^{+} \underset{-e^{-}}{\overset{+e^{-}}{\rightleftharpoons}} [Re^{III}(obsq)_3]^{0} \underset{-e^{-}}{\overset{+e^{-}}{\rightleftharpoons}} [Re^{III}(obsq)_2(otp)]^{-}$$

The CV behaviour of **3** was determined at various scan rates (Figure 5.22). The $E_{1/2}$ values remains constant with increasing scan rate. The dependence of the currents on the square-root of the scan rate (50-500 mV/s) for the redox processes (shown in Figure 5.23) suggests that all the processes are diffusion controlled.

Table 5.4: Electrochemical data (potential in V, current in μA) of **3**, scan rate 150 mV/s.

Process	E_{pc}	i_c	E_{pa}	i_a	$E_{1/2}$	i_a/i_c	ΔE_p	Assignment
A	-1.330	24.80	-1.229	16.61	-1.280	0.67	0.101	$obsq^{-}/otp^{2-}$
B	0.076	20.72	0.176	27.04	0.126	1.31	0.100	Re(III)/Re(IV)

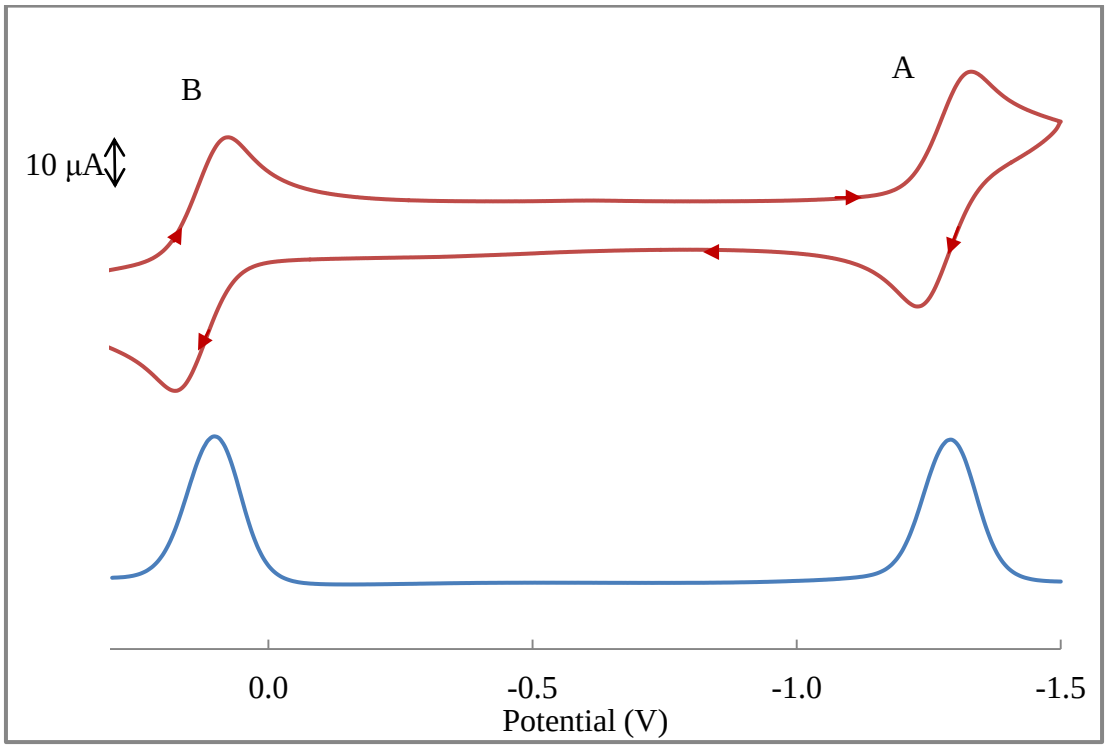

Figure 5.21: Cyclic voltammogram (red line) of **3** in CH_2Cl_2 at a scan rate of 150 mV/s and square-wave voltammogram (blue line).

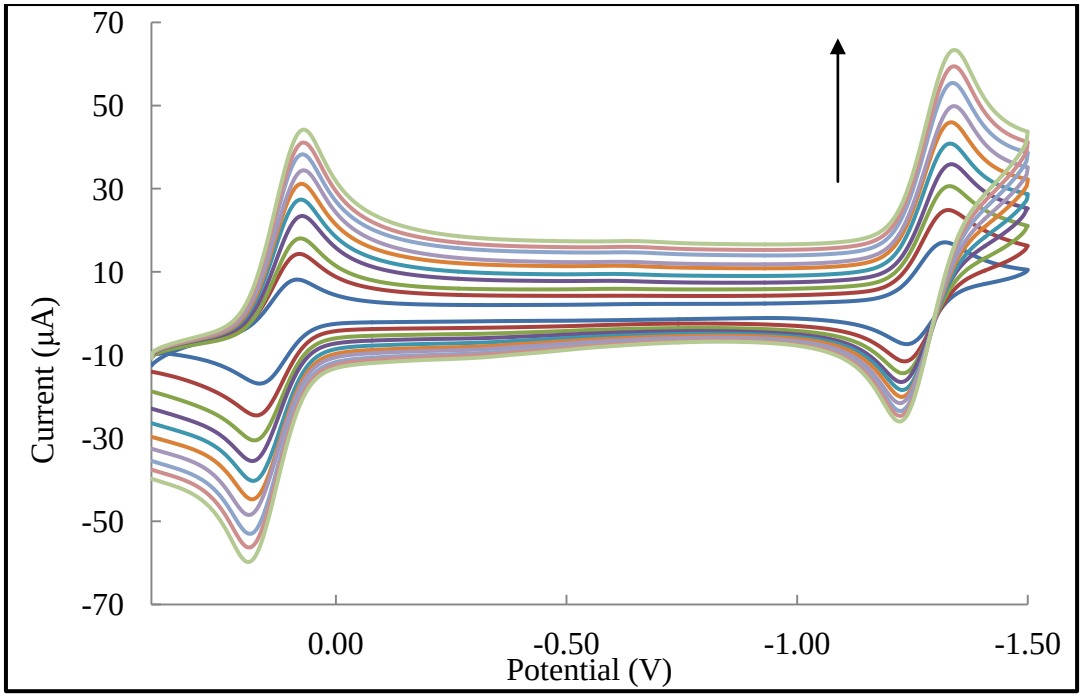

Figure 5.22: Cyclic voltammograms of **3** at varying scan rates (50-500 mV). The arrow indicates increasing scan rate.

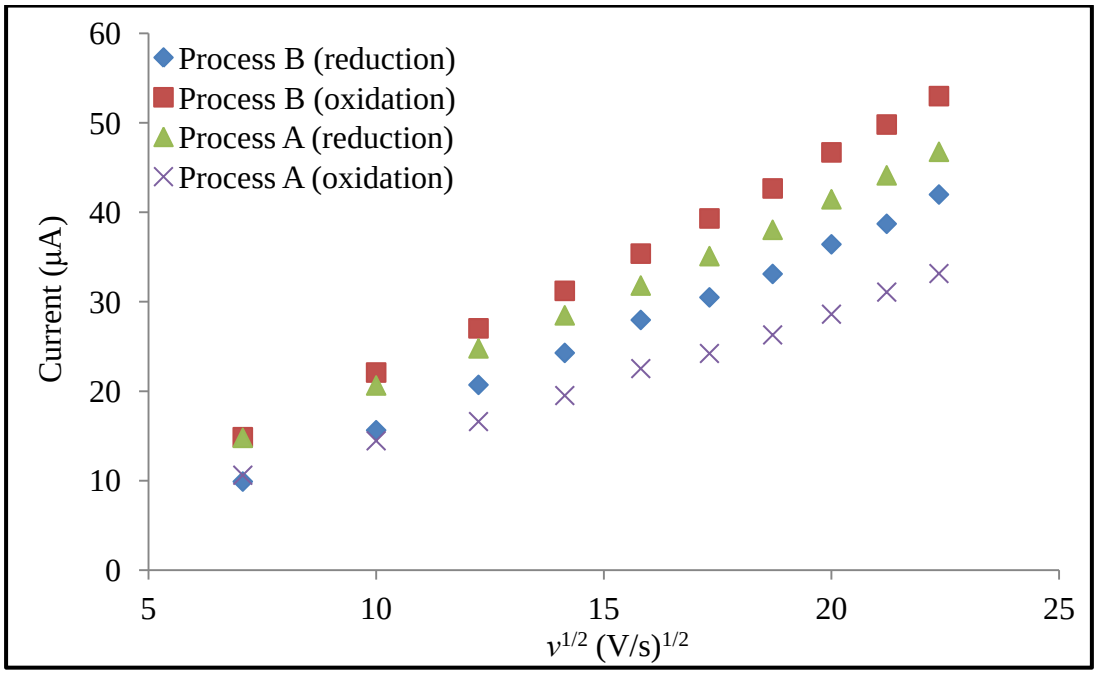

Figure 5.23: Plots of current (*i*) *vs.* the square root of the scan rate ($v^{1/2}$) for the different processes.

The $E_{1/2}$ values for the Re(III)/Re(IV) redox couple of the three complexes are summarized in Table 5.5. It can be seen that the $E_{1/2}$ value for the Re(III)/Re(IV) redox couple of complex **1** is smaller positive compared to complexes **2** and **3**. This indicates that **1** undergoes oxidation more readily, which is expected since the nitrogen atoms on the ibsq$^-$ ligands has a more electron donating effect in comparison to that of the sulfur and oxygen atoms of the sbsq$^-$ and obsq$^-$ ligands of complexes **2** and **3** respectively.

Table 5.5: Comparison of the Re(III)/Re(IV) redox couple of **1**, **2** and **3**.

Complex	Donor Atoms	$E_{1/2}$ (V)
1	S,N	0.022
2	S,S	0.142
3	S,O	0.126

5.4 References

[1] K. Ray, T. Petrenko, K. Wieghardt, F. Neese, *Dalton Trans*., 2007, 1552.

[2] S. Bhattacharya, P. Gupta, F. Basuli, C.G. Pierpont, *Inorg. Chem*., 2002, **41**, 5810; K. Ray, T. Weyhermüller, A. Goossens, M.W. Crojé, K. Wieghardt, *Inorg. Chem*., 2003, **42**, 4082.

[3] E.I. Stiefel, H.B. Gray, *J. Am. Chem. Soc*., 1965, **87**, 4012; J.K. Gardner, N. Pariyadath, J.L. Corbin, E.I. Stiefel, *Inorg. Chem*., 1978, **17**, 897; A.A. Danopoulos, A.C.C. Wong, G. Wilkinson, M.B. Hursthouse, B. Hussain, *J. Chem. Soc. Dalton Trans*., 1990, 315.

[4] J.R. Dilworth, S.K. Ibrahim, S.R. Kahn, M.B. Hursthouse, A.A. Karaulov, *Polyhedron*, 1990, **9**, 1323.

[5] M. Kawashima, M. Koyama, T. Fujinaga, *J. Inorg. Nucl. Chem*., 1976, **38**, 801.

[6] I. Chakraborty, S. Bhattacharya, A. Chakravorty, *Polyhedron*, 2002, **21**, 1597.

[7] J.L. Martin, J. Takats, *Can. J. Chem*., 1989, **67**, 1914.

[8] APEX2, SADABS and SAINT, Bruker AXS Inc., Madison, Wisconsin, USA, 2010.

[9] G.M. Sheldrick, *Acta Cryst*., 2008, **A64**, 112.

[10] A. Altomare, M.C. Burla, G. Cascarano, C. Giacovazzo, A. Guagliardi, A.G.G. Moliterni, G. Polidori, *J. Appl. Cryst*., 1995, **28**, 842.

[11] C.B. Hübschle, G.M. Sheldrick and B. Dittrich. *J. Appl. Cryst*., 2011, **44**, 1281.

[12] G. Rouschias, *Chem. Rev*., 1974, **74**, 531.

[13] G. Battistuzzi, M. Cannio, R. Battistuzzi, *Polyhedron*, 2000, **19**, 2163.

[14] S.R. Fletcher, J.F. Rowbottom, A.C. Skapski, G. Wilkinson, *Chem. Commun*., 1970, 1572; R. Rossi, A. Marchi, A. Duatti, L. Magon, U. Casellato, R. Graziani, *J. Chem. Soc. Dalton Trans*., 1988, 899; V.G. Albano, P.L. Bellon, G. Ciani, *J. Organomet. Chem*., 1971, **31**, 75.

[15] M.J. Al-Jeboori, J.R. Dilworth, W. Hiller, *Inorg. Chim. Acta*, 1999, **285**, 76; D. Morales-Morales, Y. Zheng, J.R. Dilworth, R. Redón, H. Torrens, *Inorg. Chim. Acta*, 2001, **314**, 37; C. Bolzati, F. Fisato, F. Refosco, G. Bandoli, A. Dolmella, *Inorg. Chem*., 1996, **35**, 6221.

[16] D. Herebian, E. Bothe, E. Bill, T. Weyhermüller, K. Wieghardt, *J. Am. Chem. Soc*., 2001, **123**, 10012.

[17] T.I.A. Gerber, D. Luzipo, P. Mayer, *J. Coord. Chem*., 2004, **57**, 1393.

[18] K.A. Al-Farhan, *J. Cryst. Spectrosc. Res.*, 1992, **22**, 687.

[19] S. Petrovic, *Chem. Educ*., 2000, **5**, 231.

Table 5.6: Crystal and structure refinement data for **1**.

Chemical formula	$C_{18}H_{16}N_3S_3Re.C_{18}H_{15}OP.CH_3OH$
Formula weight	867.07
Crystal system	Monoclinic
Space group	*C*2/c
a (Å)	22.181(5)
b (Å)	14.617(5)
c (Å)	24.452(5)
β (˚)	115.620(5)
Volume ($Å^3$)	7148(3)
Z	8
Density (Calcd.) (gcm^{-3})	1.611
Absorption coefficient (mm^{-1})	3.657
F (000)	3456
θ range	1.9-28.3
Index ranges *h*	-29/27
k	-19/19
l	-32/32
Reflections measured	33827
Independent/observed reflections	8902/7717
Data/parameters	8902/442
Goodness-of-fit on F^2	1.01
Final *R* indices [$I > 2\sigma(I)$]	0.0234
	(*wR2* = 0.0540)
Largest diff. peak/hole ($eÅ^{-3}$)	1.90/-1.22

Table 5.7: Crystal and structure refinement data for **2**.

Chemical formula	$C_{18}H_{12}ReS_6.C_{18}H_{15}OP$
Formula weight	885.18
Crystal system	Monoclinic
Space group	$P2_1/c$
a (Å)	13.6500(3)
b (Å)	12.0640(3)
c (Å)	24.6300(5)
β (˚)	122.050(1)
Volume (Å^3)	3437.7(1)
Z	4
Density (Calcd.) (gcm^{-3})	1.710
Absorption coefficient (mm^{-1})	3.975
F (000)	1748
θ range	1.8-28.0
Index ranges *h*	-17/17
k	-15/12
l	-32/32
Reflections measured	32604
Independent/observed reflections	8223/6006
Data/parameters	8223/406
Goodness-of-fit on F^2	1.01
Final *R* indices [$I > 2\sigma(I)$]	0.0399
	(*wR2* = 0.0842)
Largest diff. peak/hole (eÅ^{-3})	2.72/1.29

Table 5.8: Crystal and structure refinement data for **3**.

Chemical formula	$C_{18}H_{12}O_3S_3Re.C_{18}H_{15}OP.CH_3OH$
Formula weight	869.01
Crystal system	Monoclinic
Space group	$P2_1/c$
a (Å)	9.9165(2)
b (Å)	12.8811(2)
c (Å)	27.3005(5)
β (˚)	98.6913(6)
Volume ($Å^3$)	3447.2(1)
Z	4
Density (Calcd.) (gcm^{-3})	1.674
Absorption coefficient (mm^{-1})	3.796
F (000)	1724
θ range	2.6-28.3
Index ranges *h*	-11/13
k	-17/15
l	-36/34
Reflections measured	33936
Independent/observed reflections	8554/6750
Data/parameters	8554/414
Goodness-of-fit on F^2	0.96
Final *R* indices [$I > 2\sigma(I)$]	0.0295
	(*wR2* = 0.0692)
Largest diff. peak/hole ($eÅ^{-3}$)	1.18/-0.93

Table 5.9: Selected bond lengths (Å) and angles (˚) for **1.**

Bond lengths			
Re(1)-S(1)	2.315(1)	N(1)-C(12)	1.369(4)
Re(1)-S(2)	2.406(1)	N(2)-C(22)	1.447(4)
Re(1)-S(3)	2.313(1)	N(3)-C(32)	1.372(4)
Re(1)-N(1)	1.975(2)	S(1)-C(11)	1.738(3)
Re(1)-N(2)	2.158(3)	S(2)-C(21)	1.762(4)
Re(1)-N(3)	1.973(3)	S(3)-C(31)	1.732(3)
Bond angles			
S(1)-Re(1)-N(1)	79.57(8)	S(1)-Re(1)-S(3)	84.14(3)
S(2)-Re(1)-N(2)	76.80(7)	N(1)-Re(1)-N(2)	80.6(1)
S(3) -Re(1)-N(3)	78.66(7)	N(1) -Re(1)-N(3)	87.0(1)
S(1)-Re(1)-S(2)	86.79(3)	S(2)-Re(1)-N(1)	133.64(7)

Table 5.10: Selected bond lengths (Å) and angles (˚) for **2.**

Bond lengths			
Re(1)-S(1)	2.334(2)	S(1)-C(11)	1.745(6)
Re(1)-S(2)	2.340(2)	S(2)-C(12)	1.742(6)
Re(1)-S(3)	2.343(2)	S(3)-C(21)	1.750(6)
Re(1)-S(4)	2.337(2)	S(4)-C(22)	1.736(6)
Re(1)-S(5)	2.339(1)	S(5)-C(31)	1.743(5)
Re(1)-S(6)	2.357(2)	S(6)-C(32)	1.732(5)
Bond angles			
S(1)-Re(1)-S(2)	83.41(5)	S(2)-Re(1)-S(3)	119.63(5)
S(5)-Re(1)-S(6)	82.43(5)	S(2)-Re(1)-S(6)	80.27(5)
S(3)-Re(1)-S(4)	82.87(5)	S(3)-Re(1)-S(6)	155.18(6)
S(1)-Re(1)-S(4)	152.53(5)	S(4)-Re(1)-S(5)	114.45(5)
S(1)-Re(1)-S(5)	86.35(5)	S(2)-Re(1)-S(4)	84.30(5)

Table 5.11: Selected bond lengths (Å) and angles (˚) for **3.**

Bond lengths			
Re(1)-S(11)	2.3018(8)	S(11)-C11)	1.758(3)
Re(1)-S(21)	2.3048(9)	S(21)-C21)	1.747(4)
Re(1)-S(31)	2.3162(8)	S(31)-C31)	1.748(3)
Re(1)-O(12)	1.989(2)	O(12)-C12)	1.343(4)
Re(1)-O(22)	2.001(2)	O(22)-C22)	1.337(4)
Re(1)-O(32)	1.999(2)	O(32)-C32)	1.338(4)
Bond angles			
S(11)-Re(1)-O(12)	80.52(6)	S(11)-Re(1)-S(31)	86.90(3)
S(11)-Re(1)-O(22)	118.43(6)	O(12)-Re(1)-O(22)	81.52(9)
S(11)-Re(1)-O(32)	152.02(7)	O(12)-Re(1)-O(32)	83.02(9)
S(11)-Re(1)-S(21)	88.66(3)	O(22)-Re(1)-O(32)	80.97(9)
S(21)-Re(1)-O(22)	80.96(7)	S(31)-Re(1)-O(32)	80.37(7)

Chapter 6

Coordination of Bidentate Heterocyclic Derivatives to the $[ReO]^{3+}$ core

6.1 Introduction

The chemistry of rhenium is of great interest due to its diverse applications as radiopharmaceuticals [1-4] and as oxidation catalysts [5-8]. Of significant research interest is the +V oxidation state, which is readily accessible from the reduction of $[ReO_4]^-$. Rhenium(V) complexes are however unstable and readily undergo reduction or are easily converted back to perrhenate by *in vivo* oxidation. Therefore, of particular research interest is the coordination of aromatic ligands to rhenium which can provide stability, a variety of donor atoms and multidenticity to the metal centre [9].

Oxazoline and benzoxazole derivatives have proven to be versatile ligands in the coordination chemistry of transition metals [10]. Most of the studies based on this class of heterocyclic compounds incorporated a combination of soft and hard donor groups and were able to coordinate as bidentate chelates to the metal centre. Oxorhenium(V) complexes containing bidentate heterocyclic ligands have been well researched. For example, the reaction of the bidentate heterocyclic ligands 2-(2'-hydroxyphenyl)-2-oxazoline (Hoz) and 2-(2'-hydroxyphenyl)-2-benzoxazole (Hhbo) with (*n*-$Bu_4N)[ReOBr_4]$ afforded $[ReOBr(oz)_2].H_2O$ and $[ReOBr(hbo)_2]$ respectively [11]. In both complexes the two bidentate ligands form six-membered chelate rings, with one ligand coordinated in the equatorial plane relative to the axial Re=O group (Figure 6.1). The second ligand has a phenolate oxygen atom coordinated *trans* to the Re=O bond with the oxazole nitrogen coordinated equatorially relative to the Re=O moiety. It has also been shown that the benzoxazole derivative 2-(2-pyridyl)benzoxazole (pbb) reacts with *trans*-$[ReOCl_3(PPh_3)_2]$ in benzene to produce $[ReOCl_3(pbb)]$ [12]. This ligand

coordinates as a neutral bidentate chelator, with the pyridine nitrogen atom coordinated *trans* to the Re=O moiety (Figure 6.1). These bidentate benzoxazole ligands incorporated suitable donor atoms for coordination to rhenium, thereby stabilizing the oxorhenium(V) core.

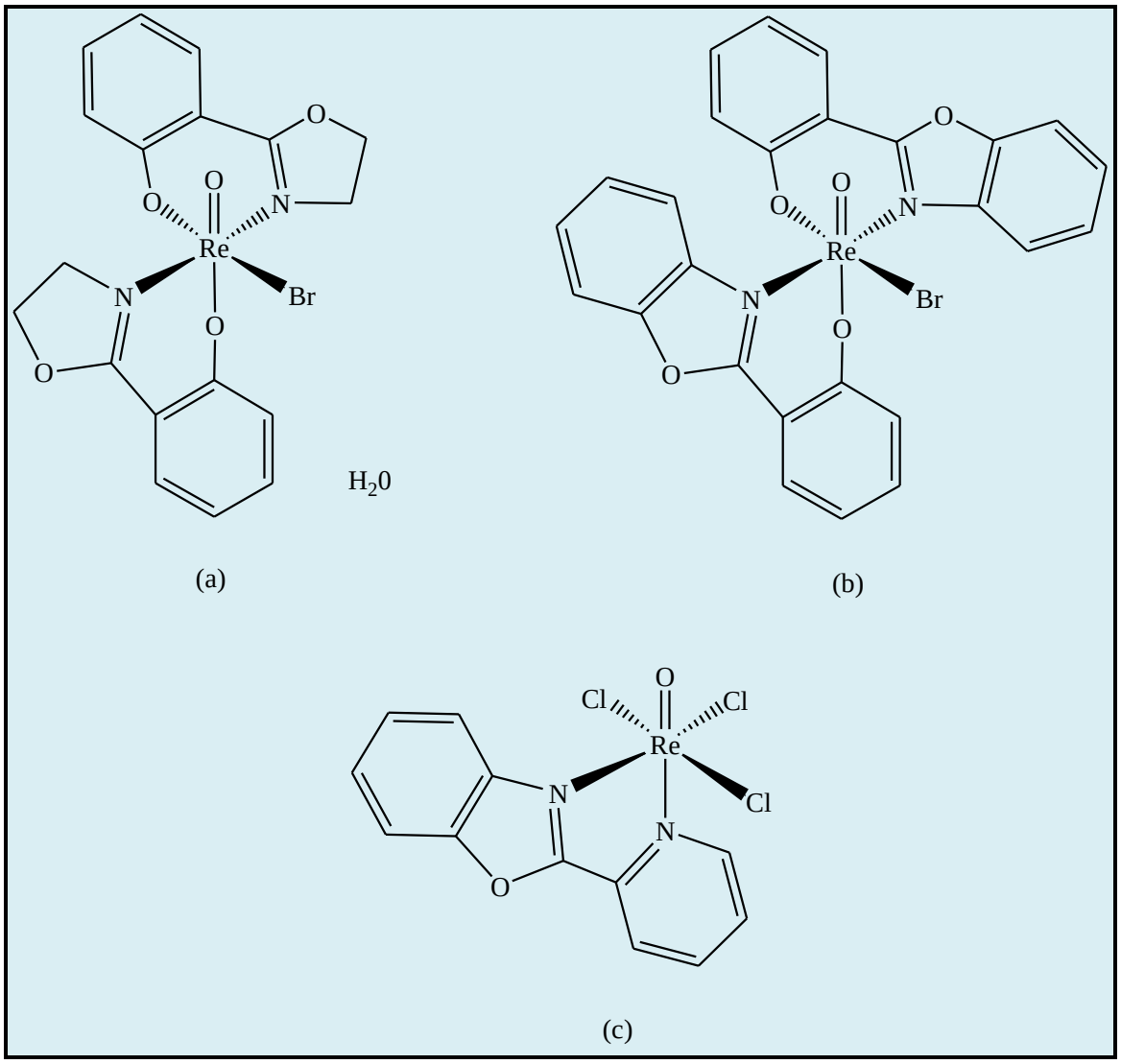

Figure 6.1: Coordination modes of (a) $[ReOBr(oz)_2].H_2O$, (b) $[ReOBr(hbo)_2]$ and (c) $[ReOCl_3(ppb)]$.

This chapter highlights the use of bidentate benzoxazole ligands as chelating agents to the rhenium(V) core (Scheme 6.1). The reaction of the mixed crystal [3-(benzoxazol-2-yl)pyridin-2-ol:2-hydroxy-*N*-(2-hydroxyphenyl)pyridine-3-carboxamide] (Hbop.Hppc)

with *trans*-[$ReOCl_3(PPh_3)_2$] in methanol led to the rhenium(III) complex, [$ReCl_2$(bop)($PPh_3)_2$] (**1**). When 5-amino-2-(benzoxazol-2-yl)phenol (Habo) was reacted with *cis*-[$ReO_2I(PPh_3)_2$] the complex salt [ReO(abo)I($PPh_3)_2$]ReO_4 (**2**) formed. In **1** and **2** the ligands coordinated as monoanionic N,O chelates through an oxazole nitrogen atom and a phenolate oxygen atom.

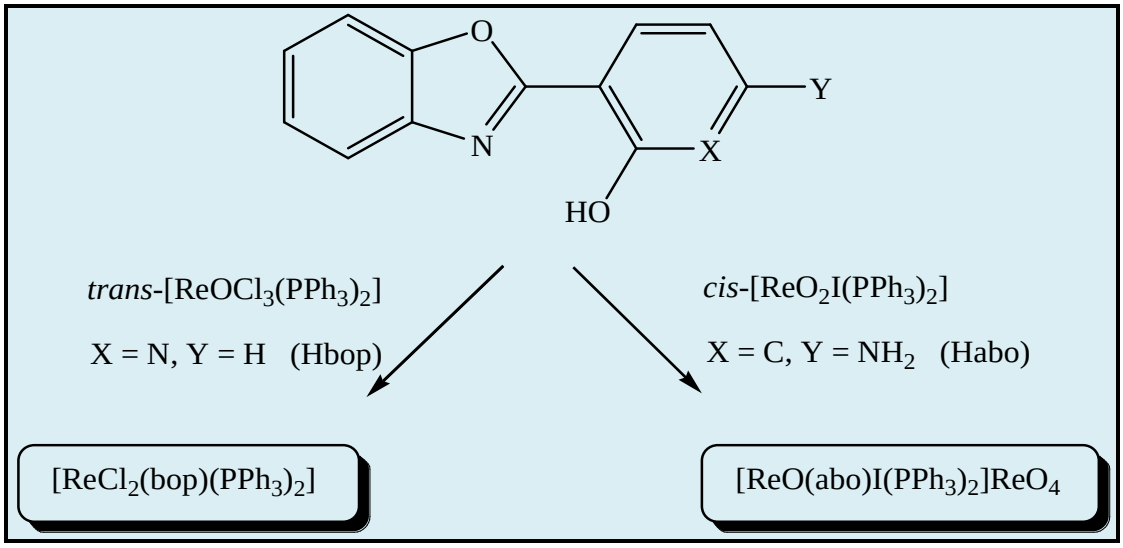

Scheme 6.1: Reaction pathway for the synthesis of [$ReCl_2$(bop)($PPh_3)_2$] (**1**) and [ReO(abo)I($PPh_3)_2$]ReO_4 (**2**).

6.2 Experimental

6.2.1 Synthesis of [3-(benzoxazol-2-yl)pyridin-2-ol:2-hydroxy-*N*-(2-hydroxyphenyl)pyridine-3-carboxamide] (Hbop.Hppc)

A mixture of 2.00 g of 2-hydroxy-nicotinic acid (14.4 mmol) and 1.57 g of 2-aminophenol (14.4 mmol) was added to hot polyphosphoric acid (50 cm^3). The stirred solution was heated to 220 ˚C for four hours. The reaction solution was cooled to room temperature and poured into a 10% aqueous potassium carbonate solution. The precipitate which formed was filtered and dried under vacuum. The recrystallization from a 1:1 (v/v) ethanol/water mixture produced beige crystals. Yield = 96 %, m.p. = 232 ˚C.

Anal. Calcd. (%) for $C_{12}H_{10}N_2O_3.C_{12}H_8N_2O_2$: C, 65.2; H, 4.1; N, 12.7. Found: C, 66.4; H, 3.7; N, 12.9. IR (ν_{max}/cm^{-1}): *v*(O-H) 3097, 3044; *v*(N-H) 2993; *v*(C=N) 1673; *v*(C=O) 1655. ^{1}H NMR (295K, ppm): 12.26 (s, br, 2H, 2 x O*H*); 8.36 (d, 2H, *H*(1), *H*(4)); 7.68-7.84 (m, 6H, *H*(5), *H*(6), *H*(7), *H*(12), *H*(13), *H*(14)); 7.35-7.47 (m, 4H, *H*(8), *H*(9), *H*(10), *H*(11)); 6.44 (t, 2H, *H*(2), *H*(3)); 3.35 (s, br, 1H, O*H*). UV-Vis (DMF, λ_{max} (ε, M^{-1}cm^{-1})): 359 (16127).

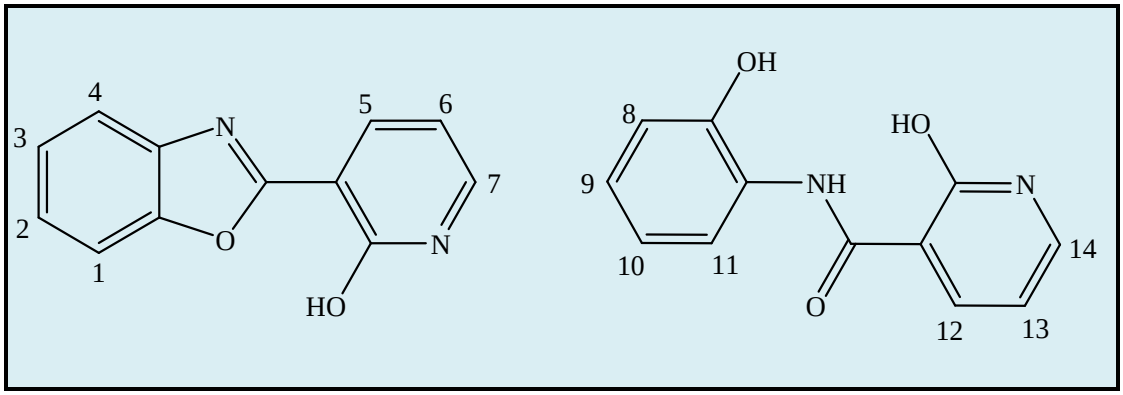

Figure 6.2: Structure and numbering scheme of [Hbop.Hppc].

6.2.2 Synthesis of 5-amino-2-(benzoxazol-2-yl)phenol (Habo)

A mixture of 2.00 g (13.0 mmol) of 4-amino-2-hydroxybenzoic acid and 1.43 g (13.1 mmol) of 2-aminophenol was added to 50 cm^3 of polyphosphoric acid. The solution was stirred at 200˚C for five hours, after which it was allowed to cool to room temperature. A brown precipitate formed when the solution was added to a 10 % potassium carbonate solution. The precipitate was filtered, washed with water and dried under vacuum. Yield = 78 %, m.p. = 182 ˚C. Anal. Calcd. (%) for $C_{13}H_{10}N_2O_2$: C, 69.0; H, 4.5; N, 12.4. Found: C, 70.2; H, 4.1; N, 12.8. IR (ν_{max}/cm^{-1}): *v*(N-H) 3448; *v*(O-H) 3358; *v*(C=N) 1603. ^{1}H NMR (295K, ppm): 7.73 (d, 1H, *H*(4)); 7.67 (d, 1H, *H*(1)); 7.51 (s, br, 1H, O*H*); 7.26-7.42 (m, 3H, *H*(2), *H*(3), *H*(5)); 6.31 (d, 1H, *H*(6)); 6.21 (s, 1H, *H*(7)); 3.95 (s, br, 2H, NH_2). UV-Vis (CH_3OH, λ_{max} (ε, M^{-1}cm^{-1})): 335 (20880).

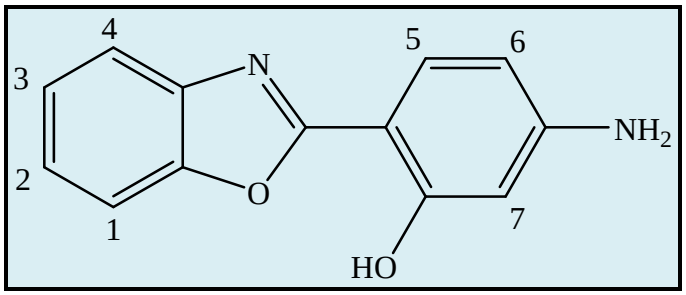

Figure 6.3: Structure and numbering scheme of Habo.

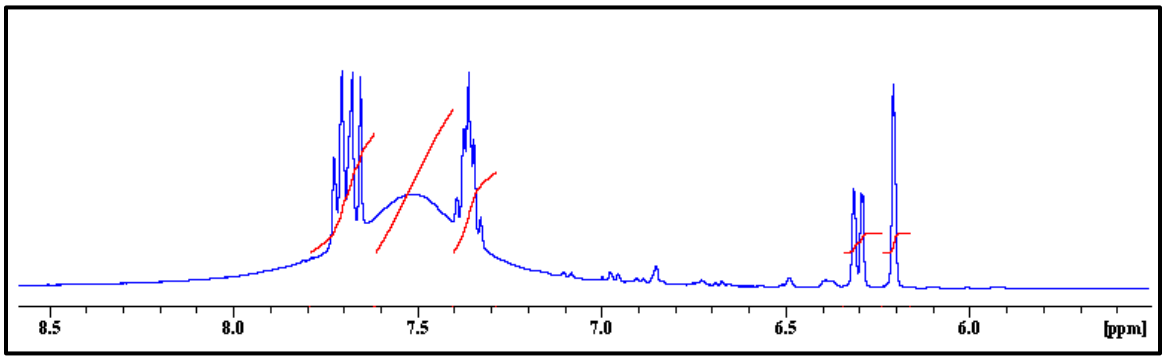

Figure 6.4: ^{1}H NMR spectrum of the aromatic region of Habo.

6.2.3 Synthesis of [$ReCl_2$(bop)(PPh_3)$_2$] (1)

Trans-[$ReOCl_3(PPh_3)_2$] (105 mg, 120 μmol) and [Hbop.Hppc] (100 mg, 226 μmol) were added to methanol (20 cm^3), and the mixture was heated under reflux overnight. The resultant brown solution was allowed to cool to room temperature, and filtered. Brown crystals were grown by the slow evaporation of the mother liquor at room temperature. Yield = 56 %, m.p. = 163 ˚C. Anal. Calcd. (%) for $C_{48}H_{37}Cl_2N_2O_2P_2Re.3H_2O$: C, 55.1; H, 4.1; N, 2.7. Found: C, 55.8; H, 4.3; N, 3.0. IR (ν_{max}/cm^{-1}): *ν*(C=N) 1600; *ν*(Re-N) 500; *ν*(Re-O) 424; *ν*(Re-Cl) 324. ^{1}H NMR (295K, ppm): 8.34 (t, 1H, C(24)*H*); 8.17 (t, 2H, C(14)*H*, C(15)*H*); 7.54-7.66 (m, 30H, 2 x P*Ph*$_3$); 7.37-7.46 (m, 4H, C(13)*H*, C(16)*H*, C(23)*H*, C(25)*H*). Conductivity (10^{-3} M, DMF): 37 $ohm^{-1}cm^2mol^{-1}$. UV-Vis (DMF, λ_{max} (ε, $M^{-1}cm^{-1}$)): 343 (22500), 454 (5300), 569 (1500).

6.2.4 Synthesis of $[ReO(abo)I(PPh_3)_2]ReO_4$ (2)

A mass of 56 mg (248 μmol) of Habo was added to 104 mg (120 μmol) of *cis*-$[ReO_2I(PPh_3)_2]$ in 20 cm^3 of methanol. The mixture was heated under reflux for three hours. The resultant solution was left to cool to room temperature and filtered. The mother liquor was left to evaporate slowly at room temperature producing brown crystals suitable for XRD analysis. Yield = 54 %, m.p. = 69 ˚C. Anal. Calcd. (%) for $C_{49}H_{39}IN_2O_3P_2Re.CH_3OH.ReO_4$: C, 49.8; H, 3.6; N, 2.3. Found: C, 48.8; H, 3.8; N, 1.8. IR (ν_{max}/cm^{-1}): *v*(C=N) 1603; *v*(Re=O) 959; *v*(Re-N) 507; *v*(Re-O) 486; *v*(Re-I) 288. ^1H NMR (295K, ppm): 7.53-7.68 (m, 30H, 2 x PP*h*$_3$); 7.42-7.52 (m, 2H, C(13)*H*, C(23)*H*); 7.35-7.41 (m, 5H, C(14)*H*, C(15)*H*, C(16)*H*, C(25)*H*, C(26)*H*); 3.82 (s, br, 2H, NH_2). Conductivity (10^{-3} M, CH_3OH): 93 $ohm^{-1}cm^2mol^{-1}$. UV-Vis (CH_3OH, λ_{max} (ε, $M^{-1}cm^{-1}$)): 336 (38970).

6.2.5 X-ray Crystallography

X-ray diffraction studies of [Hbop.Hppc], **1**.3H_2O and **2.**$CH_3OH.2H_2O$ were performed at 200 K using a Bruker Kappa Apex II diffractometer with graphite monochromated Mo Kα radiation (λ = 0.71073 Å). APEX-II was used for data collection and SAINT for cell refinement and data reduction [13]. The structures were solved by direct methods using SHELXS-97 [14] or SIR97 [15], and refined by least-squares procedures using SHELXL-97 [14] with SHELXLE [16] as a graphical interface. All non-hydrogen atoms were refined anisotropically, and the hydrogen atoms were calculated in idealised geometrical positions. Data were corrected for absorption effects by the numerical method using SADABS [13]. Crystal and structure refinement data are given in Tables 6.4, 6.5 and 6.6 for [Hbop.Hppc], **1**.3H_2O and **2.**$CH_3OH.2H_2O$ respectively, with selected bond distances and angles in Tables 6.7, 6.8 and 6.9.

6.3 Results and Discussion

6.3.1 Synthesis and characterization of [3-(benzoxazol-2-yl)pyridin-2-ol:2-hydroxy-*N*-(2-hydroxyphenyl)pyridine-3-carboxamide] (Hbop.Hppc)

In an attempt to isolate 3-(benzoxazole-2-yl)pyridin-2-ol (Hbop), equimolar amounts of 2-hydroxy-nicotinic acid and 2-aminophenol was reacted in hot polyphosphoric acid (PPA). The X-ray crystallographic data indicated that a mixed crystal formed (Scheme 6.2) which contains the benzoxazole molecule, 3-(benzoxazol-2-yl)pyridin-2-ol (Hbop) and the amide molecule, 2-hydroxy-*N*-(2-hydroxyphenyl)pyridine-3-carboxamide (Hppc). The compound is insoluble in most organic solvents, except DMF and dimethylsulfoxide.

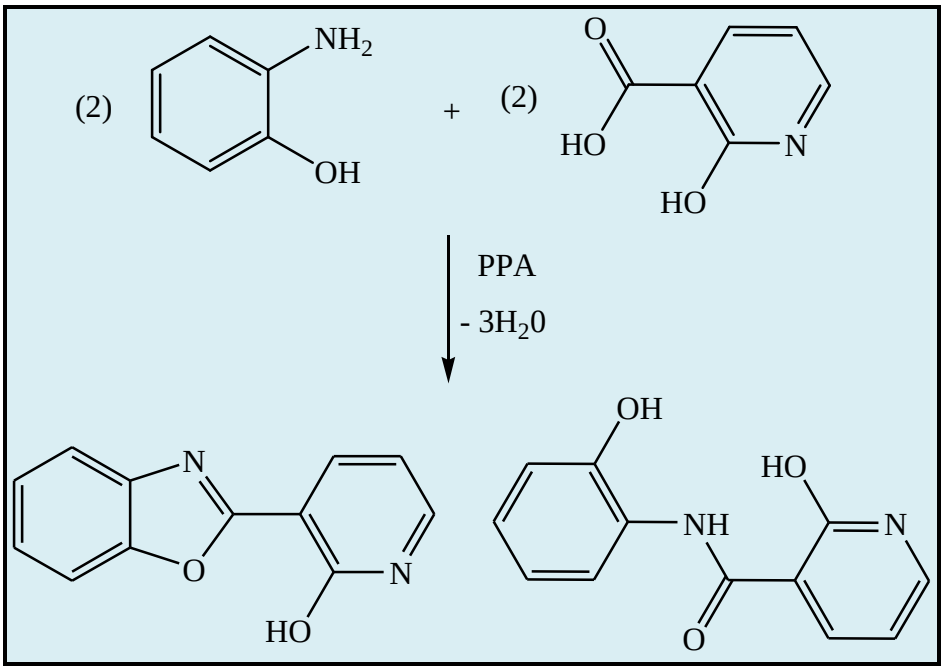

Scheme 6.2: Reaction pathway for the formation of [Hbop.Hppc].

The ^{1}H NMR spectrum (Figure 6.5) displays the signals of the phenol protons as two broad singlets at 12.26 and 3.35 ppm. Four signals appear in the aromatic region in the form of a doublet (at 8.36 ppm), multiplet (between 7.68-7.84 ppm), multiplet (between 7.35-7.47 ppm) and triplet (at 6.44 ppm) integrating for two, six, four and two protons

respectively. The IR spectrum (Figure 6.6) of [Hbop.Hppc] displays two peaks at 1673 and 1655 cm^{-1} assigned to the imine [ν(C=N)] and ketone [ν(C=O)] stretching frequencies respectively. The peaks at 3044 and 3097 cm^{-1} is ascribed to the phenol [ν(O-H)] stretching vibrations, with ν(N-H) at 2993 cm^{-1}.

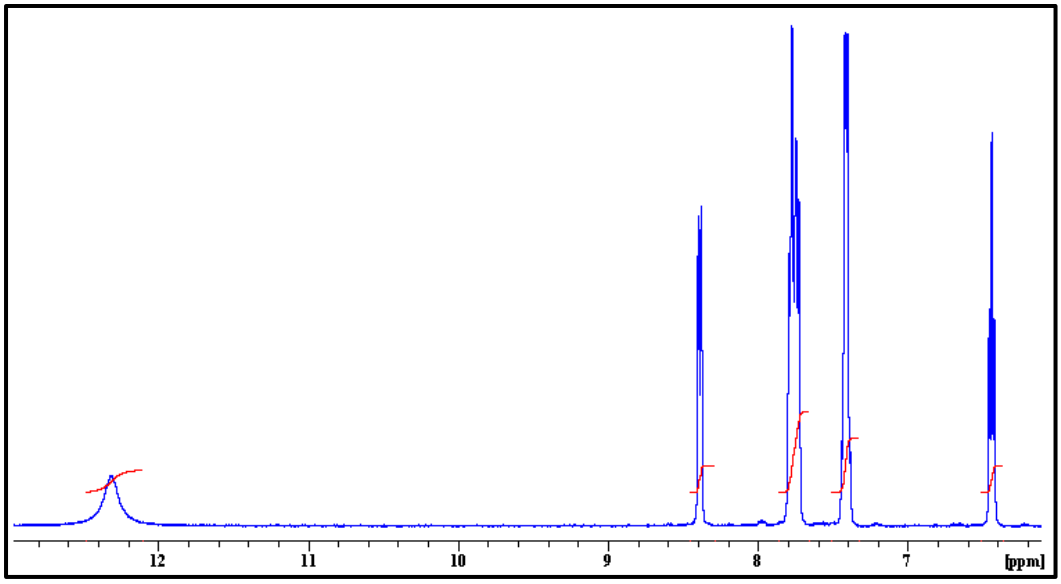

Figure 6.5: ^{1}H NMR spectrum of the aromatic region for [Hbop.Hppc].

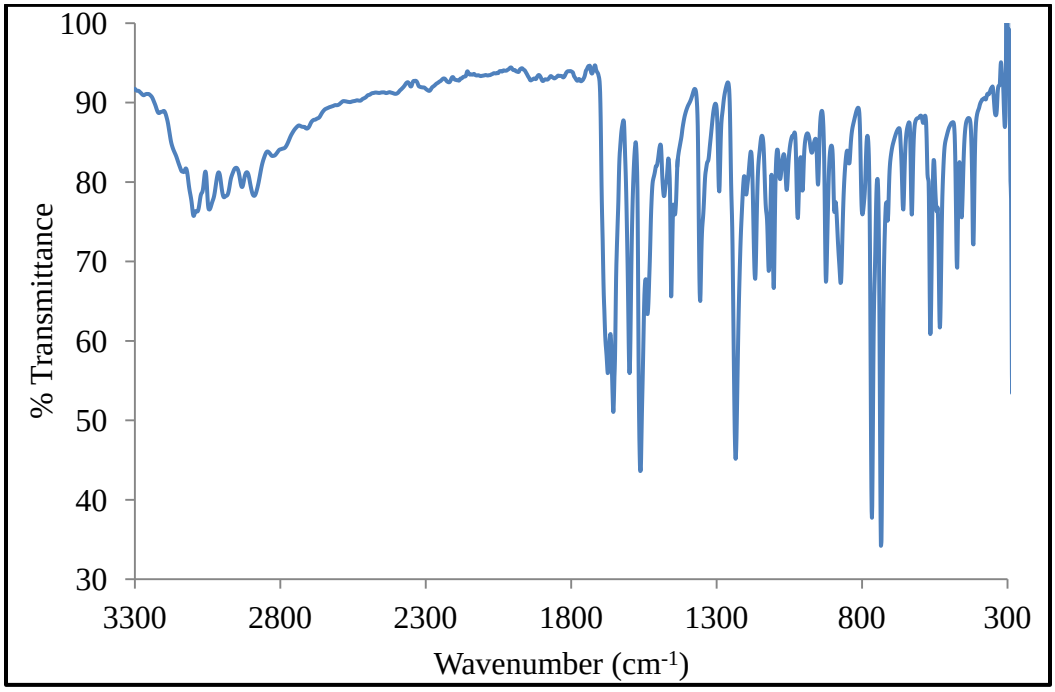

Figure 6.6: IR spectrum of [Hbop.Hppc].

The X-ray structure determination revealed that the asymmetric unit of the mixed crystal contains the 3-(benzoxazol-2-yl)pyridin-2-ol molecule (Hbop) and the 2-hydroxy-*N*-(2-hydroxyphenyl)pyridine-3-carboxamide molecule (Hppc) (Figure 6.7). The pyridinol and oxazole rings of Hbop are practically co-planar, making a dihedral angle of 10.12˚ with each other. The C(1)-N(1) bond distance [1.2875(1) Å] is close to that of imine double bonds found in benzoxazoles [17, 18]. The C-C bond lengths in the phenyl ring C(11)-C(16) [average = 1.3849(1) Å] shows that the π electron density is delocalized in the aromatic system.

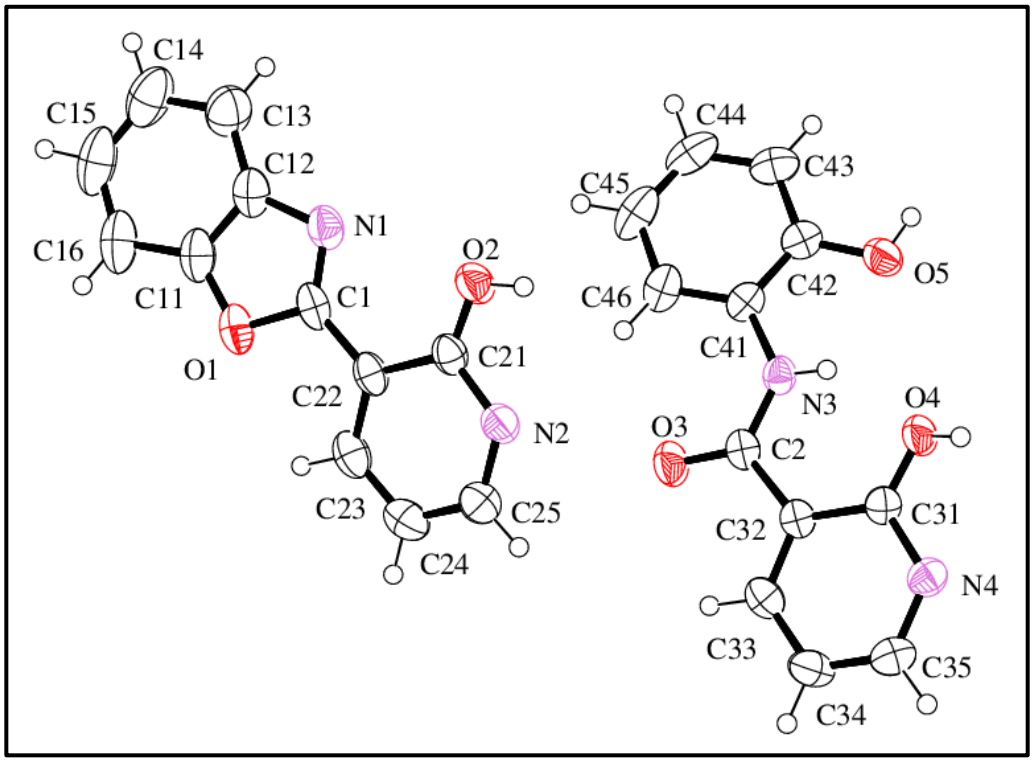

Figure 6.7: ORTEP view of [Hbop.Hppc] showing 50% probability displacement ellipsoids and the atom labeling.

The Hppc molecule is essentially planar, with the least-squares planes defined by the ring atoms of the pyridinol moiety and the ring atoms of the phenol group enclosing an angle of 17.04˚. The N(3)-C(2) bond distance [1.3387(1) Å] is indicative of a C-N single bond [19], revealing that the nitrogen atom N(3) is in its protonated form. The O(4)-C(31) and O(5)-C(42) bond distances of 1.2473(1) Å and 1.3578(1) Å respectively are typical of C-

OH bonds [18, 20]. However, the C(2)-O(3) bond is shorter [1.2321(1) Å] and indicative of a double bond.

The hydrogen of the amide nitrogen atom [N(3)H(3)] of Hppc is involved in two intramolecular hydrogen-bonds with the pyridinol oxygen [O(4)] and phenol oxygen [O(5)] (Figure 6.8). The Hppc molecule is connected through intermolecular hydrogen-bonds to the Hbop molecule involving the phenol and pyridinol hydrogens [O(2)H(2), O(4)H(4) and O(5)H(5)] (Table 6.1).

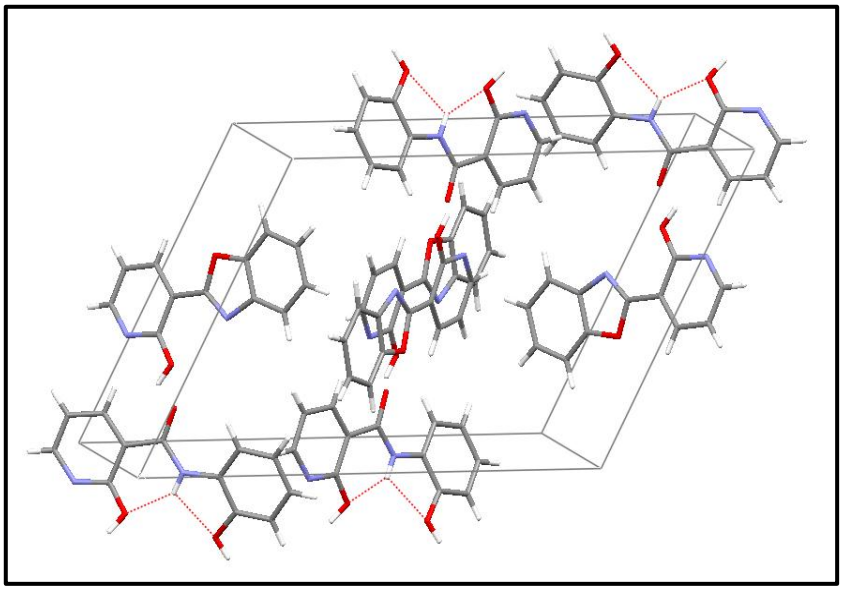

Figure 6.8: Packing diagram of [Hbop.Hppc], showing the intramolecular hydrogen-bonds.

Table 6.1: Hydrogen-bond distances (Å) and angles (˚) in [Hbop.Hppc].

D-H•••A	D-H	H•••A	D•••A	D-H•••A
O(2)H(2)•••N(4)	0.8400	2.0500	2.8353(1)	156.00
N(3)H(3)•••O(4)	0.7956	2.0091	2.6638(1)	139.38
N(3)H(3)•••O(5)	0.7956	2.2069	2.6191(1)	112.72
O(4)H(4)•••N(2)	0.8400	2.0300	2.8262(1)	157.00
O(5)H(5)•••N(1)	0.8400	1.9300	2.7418(1)	163.00

6.3.2 Synthesis and characterization of $[ReCl_2(bop)(PPh_3)_2]$ (1)

The mixed crystal [3-(benzoxazol-2-yl)pyridin-2-ol:2-hydroxy-*N*-(2-hydroxyphenyl) pyridine-3-carboxamide] (Hbop.Hppc) was reacted with *trans*-$[ReOCl_3(PPh_3)_2]$ in methanol. The X-ray crystallographic data indicates that the rhenium selectively coordinated to Hbop forming the rhenium(III) complex $[ReCl_2(bop)(PPh_3)_2]$ (**1**). The reduction of oxo-phosphine-rhenium(V) complexes to rhenium(III) is well known in the literature [21-24]. This is usually the result of a disproportionation reaction of the oxorhenium(V) complex to the rhenium(III) species and perrhenate [22, 23]. Alternatively, the change in oxidation state can come about by the reduction of the oxo species by dissociated triphenylphosphine to form $OPPh_3$ [21]. In the formation of **1**, no dissociation of PPh_3 has occurred to produce free PPh_3. The yield of complex **1** is also higher than 50%, indicating that it is not a product of a disproportionation reaction. The change in oxidation state is therefore the result of a complicated redox process which has occurred during the reaction.

Prolonged heating was necessary for the product to form. Brown needles were obtained by the slow evaporation of the mother liquor. Complex **1** is soluble in various organic solvents like dichloromethane, DMF and acetone. The complex is a non-electrolyte in DMF (Λ_M = 37 $ohm^{-1}cm^2mol^{-1}$) and therefore neutral. It is stable for months in the solid state and for days in solution.

A section of the aromatic region of the ^1H NMR spectrum of **1** is shown in Figure 6.9. The signals of the protons of the bop moiety appear as a one-proton triplet (at 8.34 ppm), a two-proton triplet (at 8.17 ppm) and a four-proton multiplet (between 7.37-7.46 ppm). The multiplet in the 7.54-7.66 ppm region integrates for the thirty protons of the triphenylphosphine groups. The IR spectrum of **1** (Figure 6.10) shows the *v*(C=N) of the benzoxazole group at 1600 cm^{-1} and is at a lower frequency compared to the free ligand (1673 cm^{-1}). The medium intensity peaks at 424 and 500 cm^{-1} is ascribed to *v*(Re-O) and *v*(Re-N) respectively, and the medium intensity band at 324 cm^{-1} is attributed to *v*(Re-Cl).

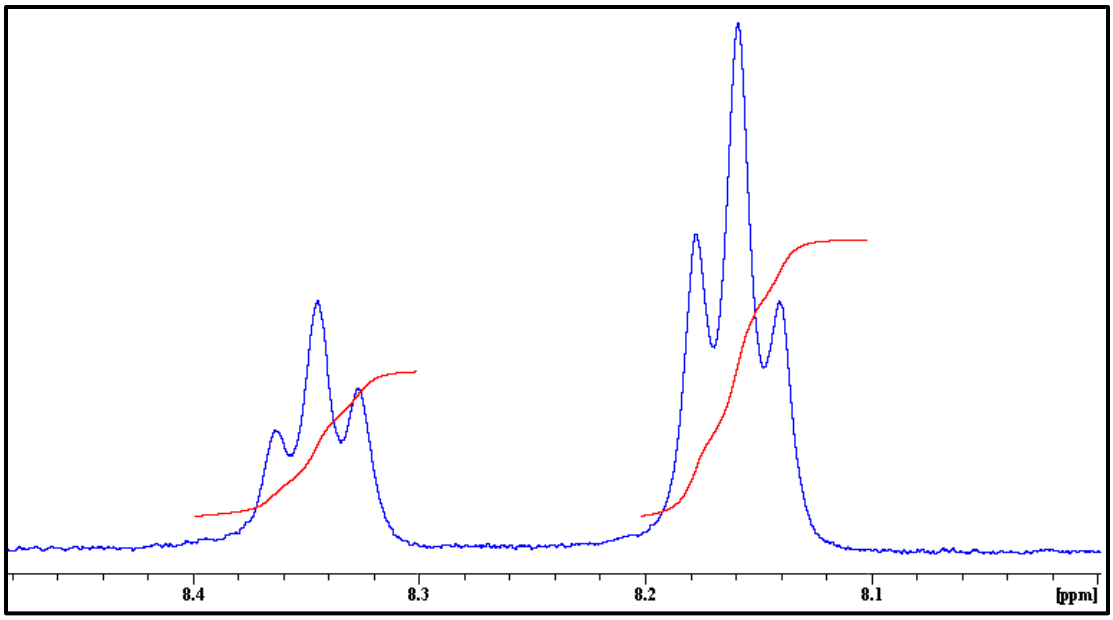

Figure 6.9: ^{1}H NMR spectrum of **1** in the 8.0-8.5 ppm region.

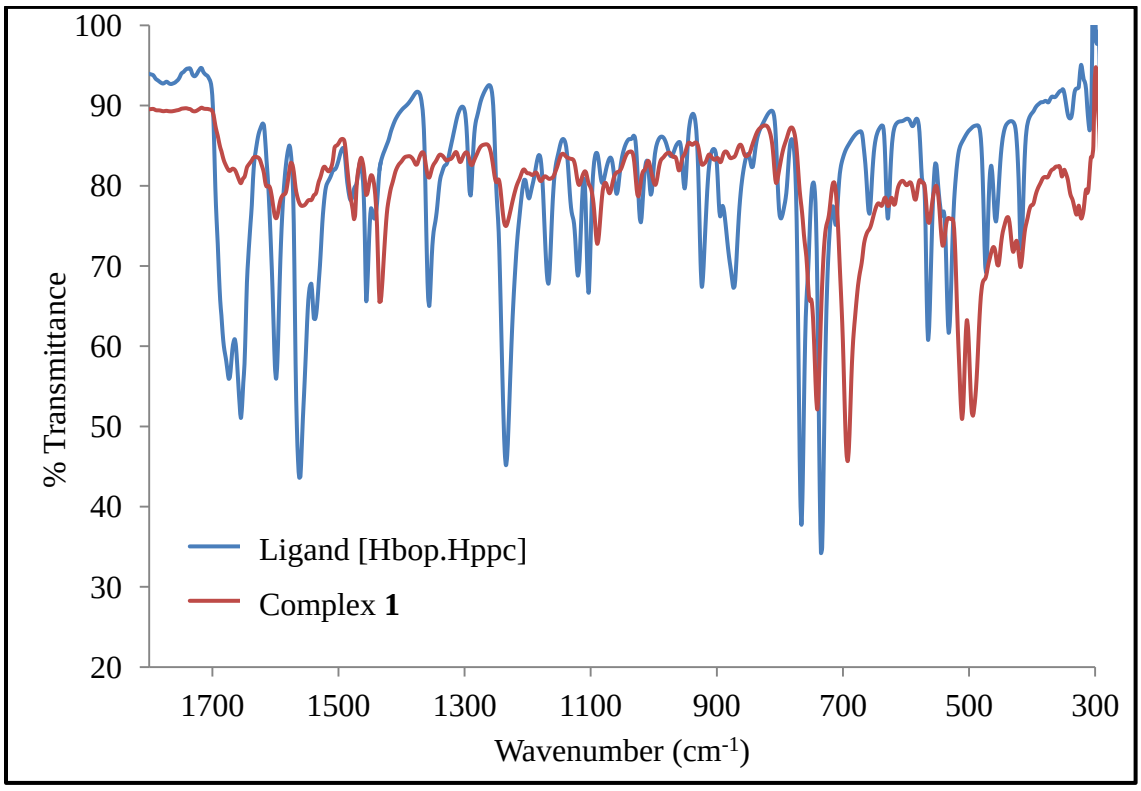

Figure 6.10: Overlay IR spectra of ligand [Hbop.Hppc] and **1**.

The electronic spectrum of **1** (Figure 6.11) in DMF consists of an intense absorption at 343 nm and two less intense bands at 454 and 569 nm. The intense band at 343 nm is ascribed to an intraligand transition of the coordinated ligand and is found at a higher energy relative to the free ligand (359 nm). The two low energy bands are ascribed to a ligand-to-metal charge transition (454 nm) and a d-d transition (569 nm).

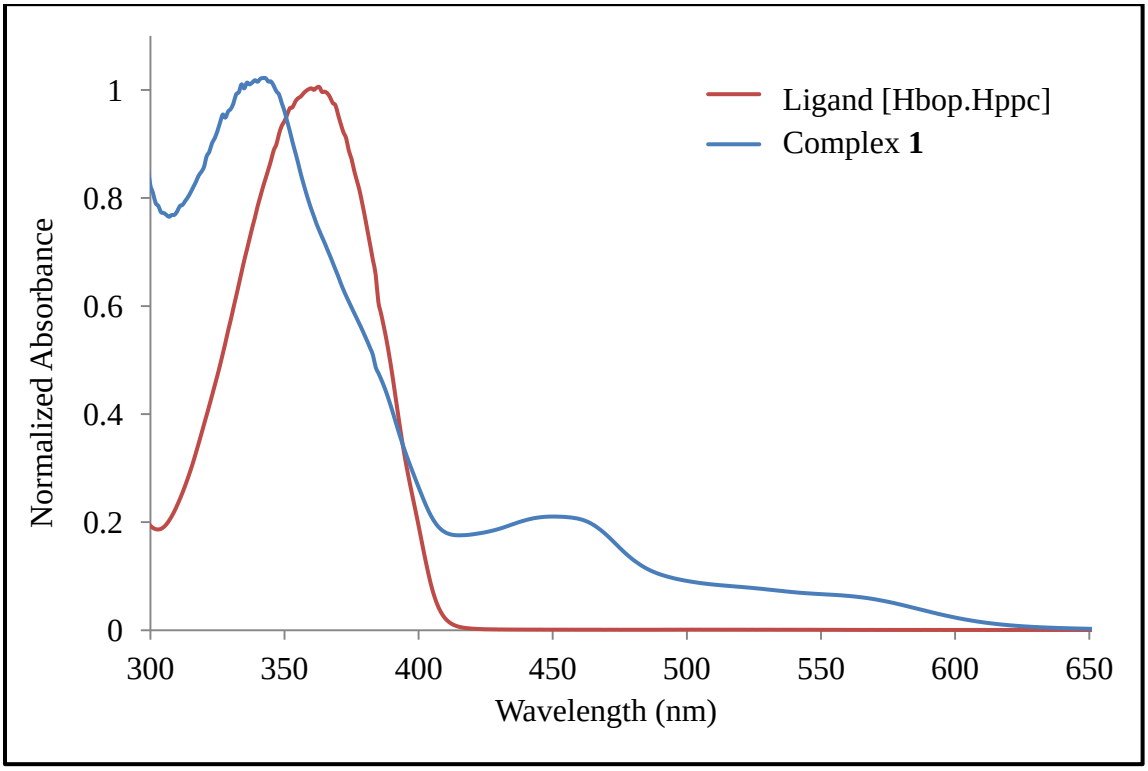

Figure 6.11: Overlay absorption spectra of ligand [Hbop.Hppc] and complex **1**.

The structure of **1** is shown in Figure 6.12. The rhenium(III) is six-coordinated and lies in a distorted octahedral geometry. The two phosphorus atoms are in *trans* axial positions with the basal plane defined by the two chloride atoms Cl(1) and Cl(2), the phenolate oxygen atom O(2) and the oxazole nitrogen N(1). Distortion from octahedral geometry is evident when observing the non-linear P(1)-Re-P(2) axis of 176.44(6)˚, with the *trans* angles N(1)-Re-Cl(1) = 168.5(1)˚ and O(2)-Re-Cl(2) = 177.6(1)˚ also deviating from linearity.

The rhenium is situated within the mean equatorial plane formed by $ONCl_2$, with angles P(1)-Re-Cl(1) = 90.59(6)˚, P(1)-Re-Cl(2) = 89.56(6)˚, P(1)-Re-N(1) = 90.8(1)˚, and P(1)-Re-O(2) = 89.9(1)˚ close to orthoganality. The ligand forms a six-membered chelate ring with a bite angle of O(2)-Re-N(1) = 85.8(2)˚. The pyridinolate and benzoxazole rings are almost coplanar forming a dihedral angle of 7.61˚. The bond angle C(1)-N(1)-C(12) = 105.1(5)˚ is less than the ideal 120˚ angle for sp^2 hybridized nitrogen atoms and is similar to the corresponding bond angle found in the free ligand [C(1)-N(1)-C(12) = 105.21(1)˚]. However, the bond angle Re-N(1)-C(1) = 122.5(4)˚ indicates that N(1) is an sp^2 hybridized nitrogen atom.

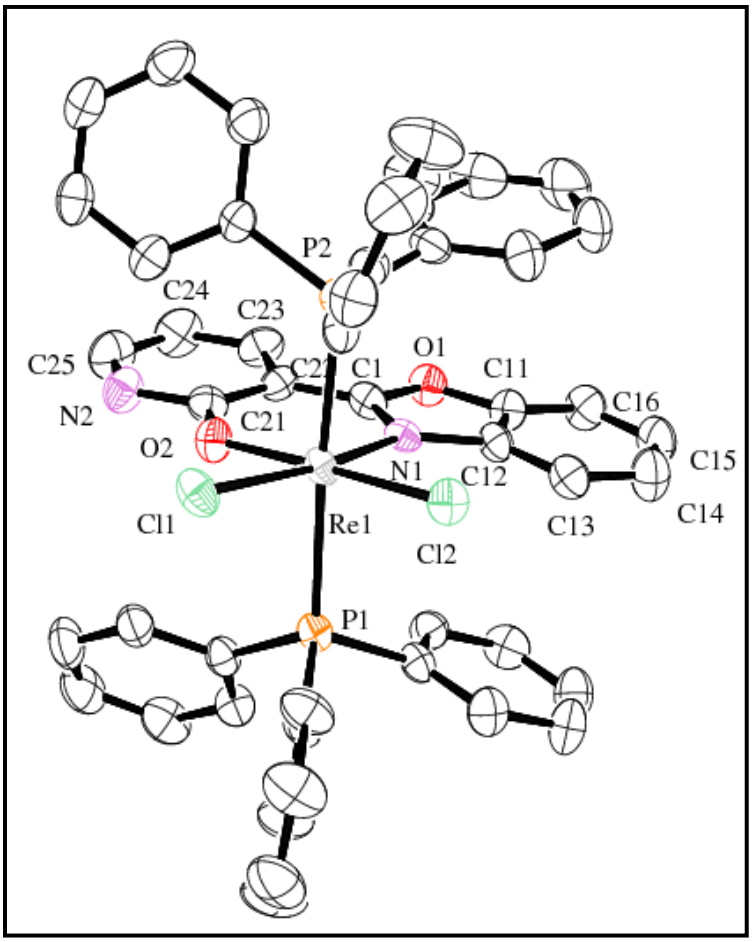

Figure 6.12: ORTEP view of **1** showing 50% probability displacement ellipsoids and the atom labeling. Hydrogen atoms were omitted for clarity.

The Re-P bond lengths are similar [Re-P(1) = 2.482(2) Å and Re-P(2) = 2.492(2) Å] and fall within the range found for Re(III)-P bond distances [23, 25]. The two chlorides are in *cis* positions with Re-Cl bond lengths of 2.403(2) and 2.331(2) Å for Re-Cl(1) and Re-Cl(2) respectively. The Re-O(2) bond distance [2.024(5) Å] is typical of rhenium(III)-phenolate single bonds [26]. The Re-N(1) bond length of 2.152(5) Å is comparable to similar bonds found in rhenium(III) complexes containing a coordinated benzoxazole nitrogen [27]. The structural data confirms that the rhenium is in the +III oxidation state with the bop chelate coordinated as a bidentate monoanionic chelate. Two intermolecular hydrogen-bonds exists in the molecule; C(23)H(23)•••O(1) and C(62)H(62)•••O(2) (Table 6.2). All other hydrogen-bonds in the molecule involve C-H bonds

Table 6.2: Hydrogen-bond distances (Å) and angles (˚) in **1**.

D-H•••A	D-H	H•••A	D•••A	D-H•••A
C(23)H(23)•••O(1)	0.9500	2.4100	2.738(9)	100.00
C(62)H(62)•••O(2)	0.9500	2.3100	3.053(9)	134.00

6.3.3 Synthesis and characterization of $[ReO(abo)I(PPh_3)_2]ReO_4$ (2)

The reaction of *cis*-$[ReO_2I(PPh_3)_2]$ with two molar equivalents of Habo in refluxing methanol gave the product $[ReO(abo)I(PPh_3)_2]ReO_4$ (**2**). The ligand coordinates as a bidentate chelate through the phenolate oxygen and imine nitrogen.

Compound **2** is diamagnetic and a 1:1 electrolyte in methanol. It is soluble in polar solvents and is stable for weeks in the solid state, and for days in solution.

The infrared spectrum of **2** (Figure 6.13) is characterized by an intense peak at 959 cm^{-1} due to the Re=O stretching frequency, and is within the range (890-1020 cm^{-1}) found for this vibration [28]. The *ν*(C=N) of the coordinated abo ligand is observed at 1603 cm^{-1}

and is at an identical position as the free ligand. The medium intensity peaks at 486 and 507 cm^{-1} are assigned to the Re-O and Re-N stretches respectively.

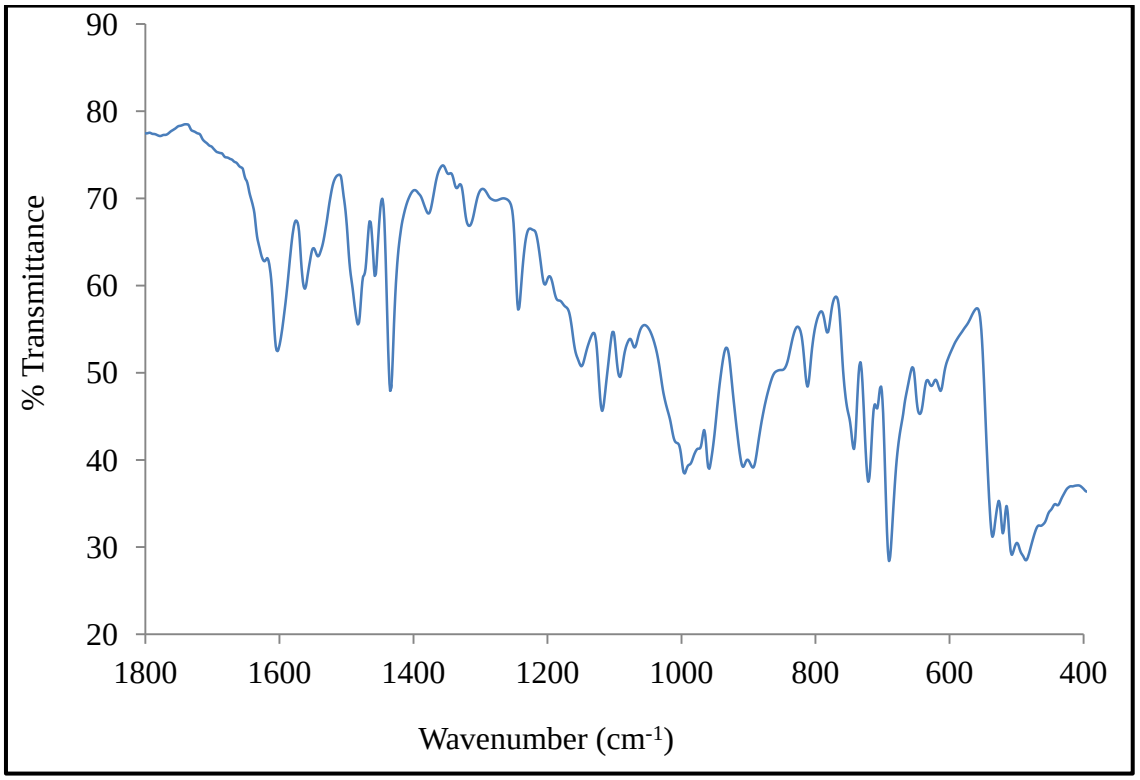

Figure 6.13: IR spectrum of **2**.

The ^{1}H NMR spectrum (Figure 6.14) of **2** consists of three multiplets in the aromatic region. The multiplet in the 7.53-7.68 ppm region is ascribed to the thirty protons of the triphenylphosphine groups. The two multiplets in the 7.35-7.52 ppm region integrates for the seven protons of the aromatic rings of the abo chelate. The two-proton signal due to the amine protons appear as a broad singlet at 3.82 ppm. The UV-Vis spectrum of **2** (Figure 6.15) displays a single intense absorption at 336 nm. This band is due to an intraligand transition occurring within the coordinated ligand. The free ligand Habo displays a similar absorption at 335 nm. For **2**, no ligand-to-metal or d-d transitions were observed.

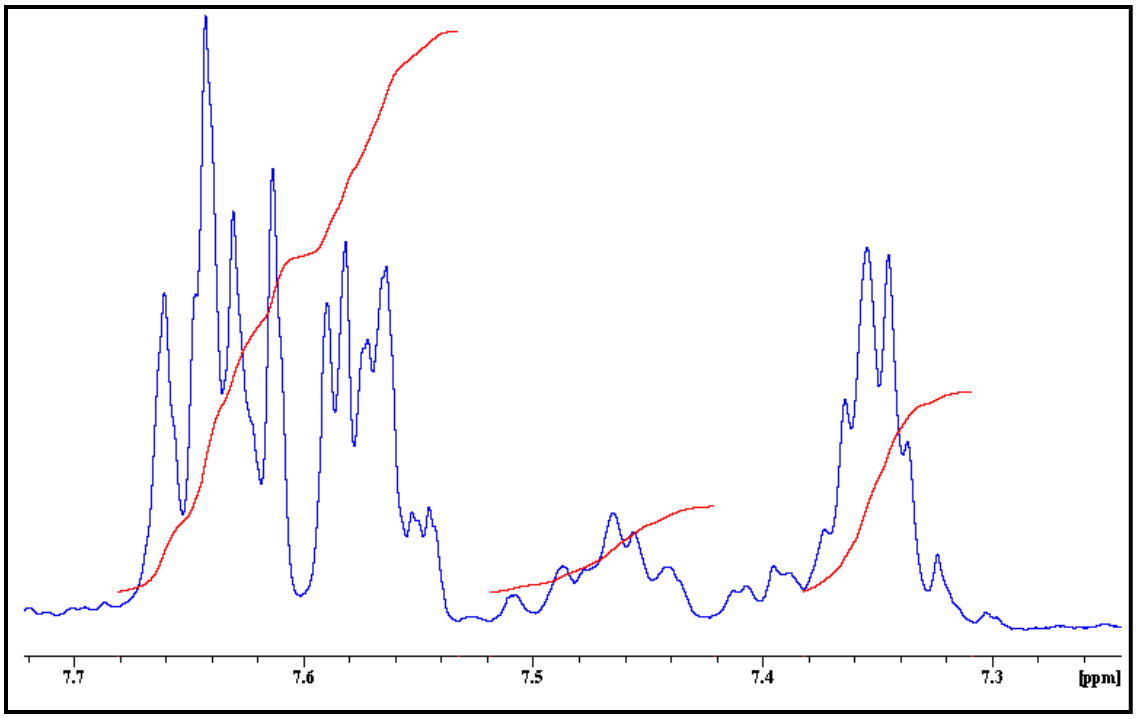

Figure 6.14: ^{1}H NMR spectrum of the aromatic region for **2**.

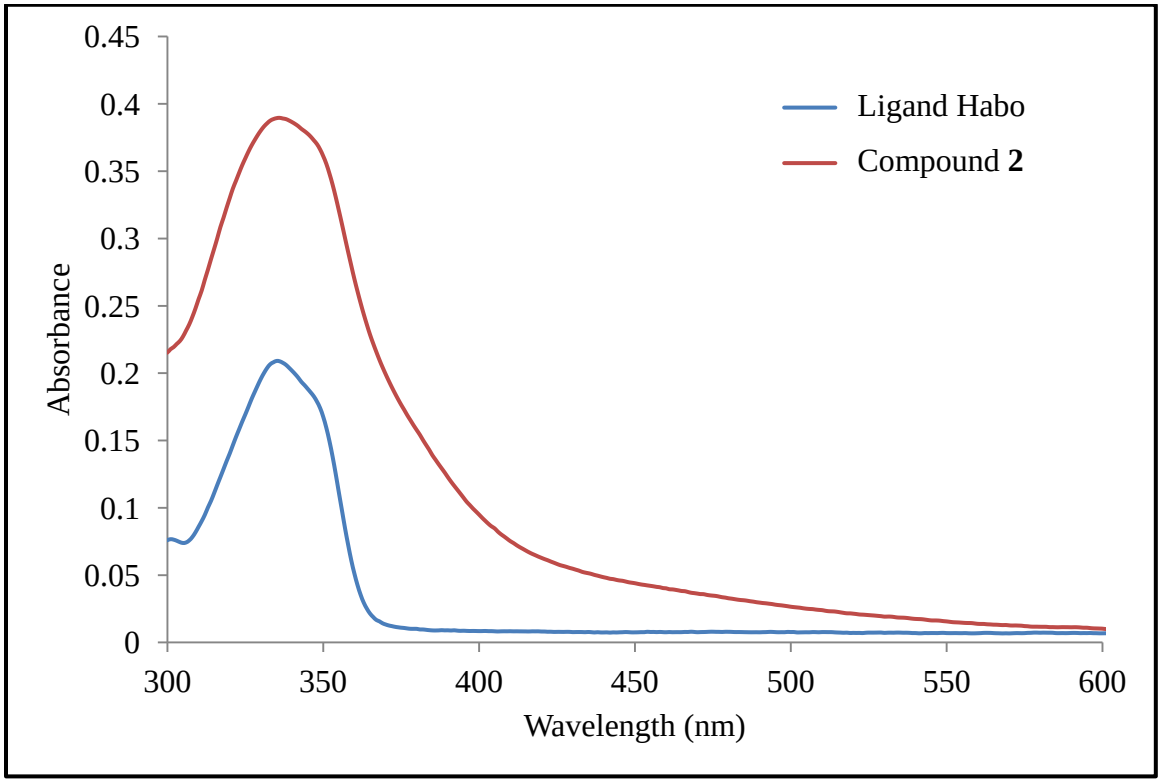

Figure 6.15: Overlay absorption spectra of ligand Habo and compound **2**.

The X-ray structure determination of **2** reveals that the rhenium atom lies at the centre of a distorted octahedron (Figure 6.16). The equatorial plane of the octahedron is formed by two phosphorus atoms in *trans* arrangement, an imino nitrogen atom N(1), and an iodide ion. The phenolate oxygen atom O(2) and the oxo group O(3) are in *trans* axial positions. Distortion from an ideal octahedral environment results in a non-linear O(2)-Re-O(3) axis of 168.6(3)˚ with the *trans* angles N(1)-Re-I(1) = 175.4(2)˚ and P(1)-Re-P(2) = 170.89(7)˚, deviating considerably from linearity.

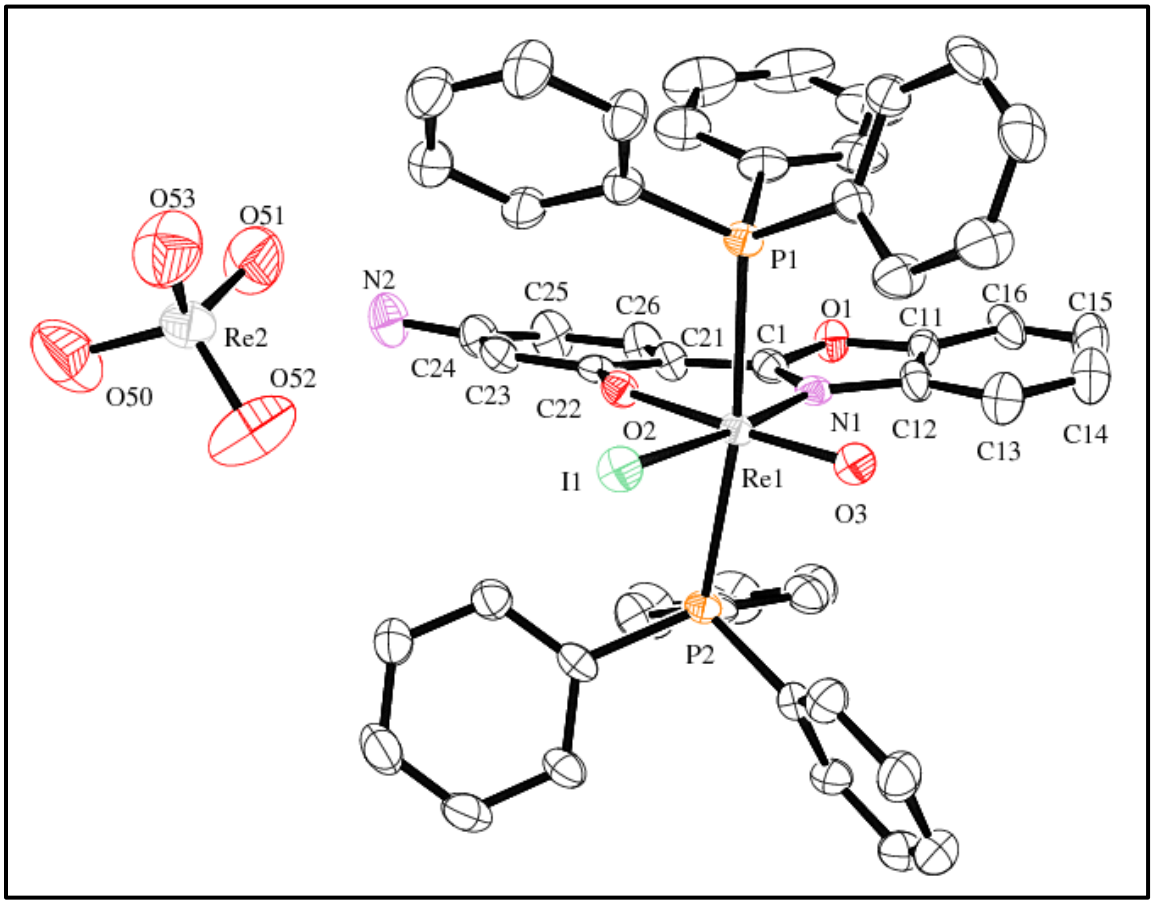

Figure 6.16: ORTEP view of **2** showing 50% probability displacement ellipsoids and the atom labeling. Hydrogen atoms were omitted for clarity.

The rhenium atom lies only slightly out of the mean equatorial plane by 0.015 Å towards P(2), with the angles P(2)-Re-I(1) = 91.04(5)˚, P(2)-Re-O(2) = 86.2(2)˚, P(2)-Re-N(1) = 91.40(2)˚ and P(2)-Re-O(3) = 92.2(2)˚. The bite angle formed by the bop chelate [O(2)-Re-N(1) = 81.6(2)˚] is smaller than the corresponding bite angle **[**85.8(2)˚] of the six-

membered metallocycle in complex **1**. This difference in the bite angles of **1** and **2** are attributed to the presence of the doubly bonded oxo group and the bulky iodide ion coordinated to rhenium in **2**. The aminophenol and benzoxazole rings of **2** do not lie in the same plane, and the least-squares planes defined by the ring atoms of these two moieties intersect at an angle of 14.38˚.

The Re-P distances of Re-P(1) = 2.509(2) Å and Re-P(2) = 2.522(2) Å are similar to those found for oxorhenium(V) complexes in the literature [29]. The Re-N(1) bond length of 2.183(6) Å is slightly longer than the corresponding Re-$N_{oxazole}$ distance in **1** [Re-N(1) = 2.152(5) Å] due to the difference in oxidation state of the rhenium and the cationic nature of $[ReO(abo)I(PPh_3)_2]^+$. The Re-O(3) bond length of 1.690(6) Å is typical of Re=O bond lengths found in octahedral monooxorhenium(V) complexes, which usually occurs in the 1.68-1.72 Å range [30, 31]. The Re-O(2) bond length of 1.944(5) Å falls in the range [1.93-2.03 Å] observed for a phenolate oxygen coordinated *trans* to an oxo group in rhenium(V) complexes [30-32]. The structural information of **2** indicates that the abo ligand acts as a bidentate monoanionic chelate.

As with complex **1**, the bond angle C(1)-N(1)-C(12) = 105.9˚ is smaller than expected for an sp^2 hybridized nitrogen atom, but the bond angle Re-N(1)-C(1) = 125.4(2)˚ is close to 120˚, suggesting that N(1) is an sp^2 hybridized atom. The perrhenate counter-ion is involved in a series of intermolecular hydrogen-bonds (Table 6.3). The phenolate oxygen atom is involved in intramolecular hydrogen-bonding with two triphenylphosphine hydrogens H(46) and H(66). The oxygen atom O(3) forms intramolecular hydrogen-bonds with the phenyl proton H(13) and the triphenylphosphine hydrogen H(56) (Figure 6.17).

Table 6.3: Hydrogen-bond distances (Å) and angles (˚) in **2**.

D-H•••A	D-H	H•••A	D•••A	D-H•••A
C(13)H(13)•••O(3)	0.9500	2.2800	2.922(11)	125.00
C(46)H(46)•••O(2)	0.9500	2.4400	3.227(11)	140.00
C(56)H(56)•••O(3)	0.9500	2.4200	3.099(11)	128.00
C(66)H(66)•••O(2)	0.9500	2.4600	3.285(11)	145.00
N(2)H(2A)•••O(51)	0.8800	2.1400	2.952(13)	153.00
O(90)H(90)•••O(51)	0.8400	2.1400	2.828(17)	139.00
C(66)H(66)•••O(2)	0.9500	2.4600	3.285(11)	145.00
C(33)H(33)•••O(96)	0.9500	2.5200	3.408(17)	155.00
C(35)H(35)•••O(50)	0.9500	2.5100	3.310(16)	141.00
C(52)H(52)•••O(50)	0.9500	2.5900	3.151(14)	118.00
C(65)H(65)•••O(52)	0.9500	2.4700	3.330(14)	151.00
C(75)H(75)•••O(95)	0.9500	2.465700	3.35(2)	140.00
C(85)H(85)•••O(52)	0.9500	2.5900	3.327(14)	135.00

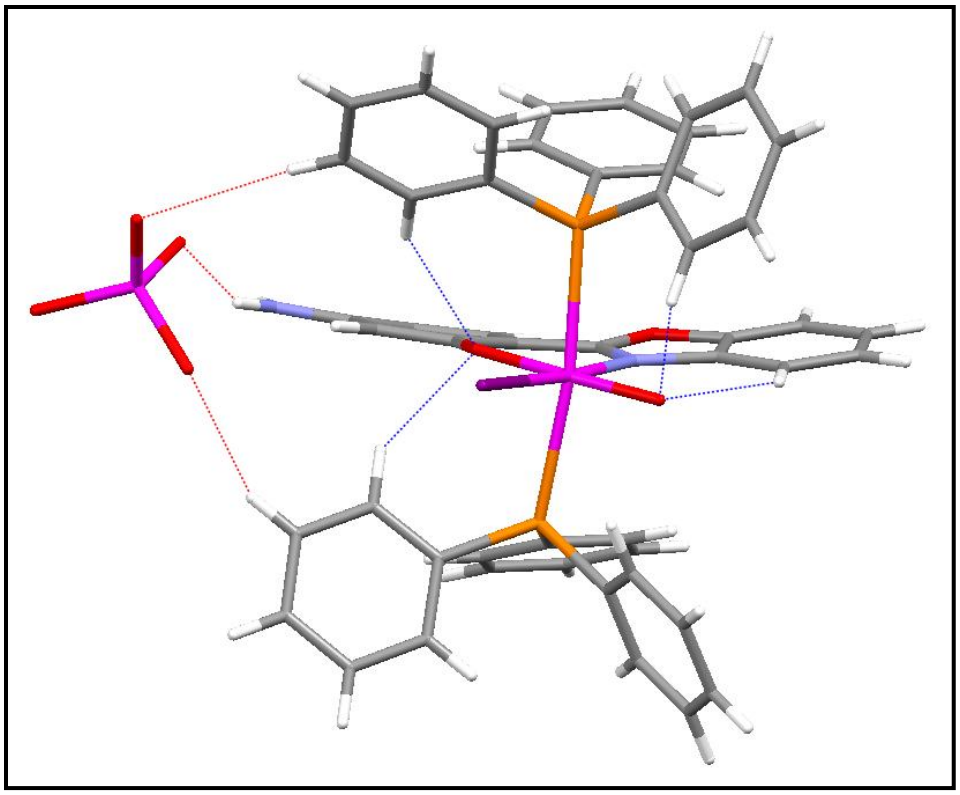

Figure 6.17: A perspective view of **2** illustrating the intramolecular hydrogen-bonding and selected intermolecular hydrogen-bonds involving the perrhenate counter-ion.

6.4 References

[1] J. Giglio, G. Patsis, I. Pirmettis, M. Papadopoulos, C. Raptopoulou, M. Pelecanou, E. Leon, M. Gonzalez, H. Cerecetto, A. Rey, *Eur. J. Med. Chem*., 2008, **43**, 741.

[2] Y. Junfeng, Y. Duanzhi, M. Xiaofeng, G. Zili, Z. Jiong, W. Yongxian, F.F. Knapp, *Nucl. Med. Biol*., 1999, **26**, 573.

[3] F. Demaimay, L. Dazord, A. Roucoux, N. Noiret, H. Patin, A. Moisan, *Nucl. Med. Biol*., 1997, **24**, 701.

[4] C. Müller, C. Dumas, U. Hoffmann, P.A. Schubiger, R. Schibli, *J. Organomet. Chem*., 2004, **689**, 4712.

[5] J.J. Kennedy-Smith, K.A. Nolin, H.P. Gunterman, F.D. Toste, *J. Am. Chem. Soc*., 2003, **125**, 4056.

[6] U.G. Hong, H.W. Park, J. Lee, S. Hwang, J. Yi, I.K. Song, *Appl. Catal. A*, 2012, **415- 416**, 141.

[7] G.S. Owens, J. Arias, M.M. Abu-Omar, *Catal. Today*, 2000, **55**, 317.

[8] C.C. Romao, F.E. Kuhn, W.A. Herrmann, *Chem. Rev*., 1997, **97**, 3197.

[9] H. Luo, S. Liu, S.J. Rettig, C. Orvig, *Can. J. Chem*., 1995, **73**, 2272.

[10] M. Gomez, G. Muller, M. Rocamora, *Coord. Chem. Rev*., 1999, **193–195**, 769.

[11] E. Shuter, H.R. Hoveyda, V. Karunaratne, S.J. Rettig, C. Orvig, *Inorg. Chem.*, 1996, **35**, 368.

[12] J. Gangopadhyay, S. Sengupta, S. Bhattacharyya, I. Chakraborty, A. Chakravorty, *Inorg. Chem*., 2002, **41**, 2616.

[13] APEX2, SADABS and SAINT, Bruker AXS Inc., Madison, Wisconsin, USA, 2010.

[14] G.M. Sheldrick, *Acta Cryst*., 2008, **A64**, 112.

[15] A. Altomare, M.C. Burla, G. Cascarano, C. Giacovazzo, A. Guagliardi, A.G.G. Moliterni, G. Polidori, *J. Appl. Cryst*., 1995, **28**, 842.

[16] C.B. Hübschle, G.M. Sheldrick, B. Dittrich. *J. Appl. Cryst.*, 2011, **44**, 1281.

[17] M. Zhang, R. Gao, X. Hao, W.-H. Sun, *J. Organomet. Chem*., 2008, **693**, 3867; F. Yang, Y. Wu, Z. Zhu, J. Zhang, Y. Li, *Tetrahedron*, 2008, **64**, 6782.

[18] H. Asanda, M. Ozeki, M. Fujiwara, T. Matsushita, *Polyhedron*, 2002, **21**, 1139.

[19] F. Wiesbrock, H. Schmidbaur, *J. Inorg. Biochem*., 2004, **98**, 473; C.A. Jimenez, J.B. Belmar, J. Alderete, F.S. Delgado, M. Lopez-Rodriguez, O. Pena, M. Julvee, C. Ruiz-Perez, *Dalton Trans*., 2007, 2135.

[20] Y.-P. Tong, S.-L. Zheng, X.-M. Chen, *J. Mol. Struct*., 2007, **826,** 104; X. Quezada-Buendia, A. Esparza-Ruiz, A. Pena-Hueso, N. Barba-Behrens, R. Contreras, A. Flores-Parra, S. Bernes, S.E. Castillo-Blum, *Inorg. Chim. Acta*, 2008, **361**, 2759.

[21] H. Spies, M. Glaser, F.E. Hahn, T. Lugger, D. Scheller, *Inorg. Chim. Acta*, 1995, **232**, 235.

[22] B. Machura, R. Kruszynski, M. Jaworska, J. Klak, J. Mrozinski, *Polyhedron*, 2006, **25**, 2537

[23] T.I.A. Gerber, P. Mayer, Z.R. Tshentu, *J. Coord. Chem*., 2006, **59**, 1509.

[24] S.A.S. Anaya, A. Hagenbach, U. Abram, *Inorg. Chem. Commun*., 2009, **12**, 128.

[25] E. Marchesi, A. Marchi, L. Marvelli, M. Peruzzini, M. Brugnati, V. Bertolasi, *Inorg. Chim. Acta*, 2005, **358**, 352.

[26] H. Pietzch, H. Spies, P. Leibnitz, G. Reck, *Polyhedron*, 1995, **14**, 1849; U. Witten, J. Strahle, U. Abram, *Z. Anorg. Allg. Chem*., 1995, **621**, 1338; T.I.A. Gerber, D. Luzipo, P. Mayer, *J. Coord. Chem.*, 2003, **56**, 1549.

[27] S. Sengupta, J. Gangopadhyay, A. Chakravorty, *Dalton Trans*., 2003, 4635.

[28] T.I.A. Gerber, D. Luzipo, P. Mayer, *Inorg. Chim. Acta*, 2004, **357**, 429.

[29] G. Bandoli, A. Dolmella, T.I.A. Gerber, J. Perils, J.G.H. du Preez, *Inorg. Chim. Acta*, 1999, **294**, 114.

[30] X. Chen, F.J. Femia, J.W. Babich, J. Zubieta, *Inorg. Chim. Acta*, 2001, **316**, 33.

[31] A. Mondal, S. Sarkar, D. Chopra, T.N.G Row, K.K. Rajak, *Dalton Trans*., 2004, 3244.

[32] J.Y. Kim, Y.J. Ji, H.-J. Ha, H.K. Chae, *Bull. Korean Chem. Soc*., 2003, **24**, 504.

Table 6.4: Crystal and structure refinement data for [Hbop.Hppc].

Chemical formula	$C_{12}H_{10}N_2O_3.C_{12}H_8N_2O_2$
Formula weight	442.42
Crystal system	Monoclinic
Space group	$P2_1/c$
a (Å)	12.4695(5)
b (Å)	10.7901(4)
c (Å)	17.2574(5)
β (˚)	117.153(2)
Volume ($Å^3$)	2066.0 (1)
Z	4
Density (Calcd.) (gcm^{-3})	1.422
Absorption coefficient (mm^{-1})	0.102
F (000)	920
θ range	3.1-28.3
Index ranges *h*	-16/16
k	-14/14
l	-22/23
Reflections measured	19548
Independent/observed reflections	5114/3633
Data/parameters	5114/304
Goodness-of-fit on F^2	1.06
Final *R* indices [$I > 2\ \sigma(I)$]	0.0580
	(*wR2* = 0.1712)
Largest diff. peak/hole ($eÅ^{-3}$)	0.54/-0.61

Table 6.5: Crystal and structure refinement data for **1**.

Chemical formula	$C_{48}H_{37}C_{l2}N_2O_2P_2Re.3H_2O$
Formula weight	1040.85
Crystal system	Monoclinic
Space group	$P2_1/c$
a (Å)	16.400 (2)
b (Å)	25.353(3)
c (Å)	11.149(1)
β (˚)	103.420(4)
Volume ($Å^3$)	4508.9(9)
Z	4
Density (Calcd.) (gcm^{-3})	1.533
Absorption coefficient (mm^{-1})	2.932
F (000)	2072
θ range	3.1-28.4
Index ranges *h*	-20/21
k	-33/33
l	-14/14
Reflections measured	42839
Independent/observed reflections	11213/6524
Data/parameters	11213/541
Goodness-of-fit on F^2	0.95
Final *R* indices [$I > 2\ \sigma(I)$]	0.0526
	(*wR2* = 0.1292)
Largest diff. peak/hole ($eÅ^{-3}$)	3.82/-2.53

Table 6.6: Crystal and structure refinement data for **2**.

Chemical formula	$C_{49}H_{39}IN_2O_7P_2Re_2.CH_3OH.2H_2O$
Formula weight	1393.13
Crystal system	Monoclinic
Space group	$P2_1/c$
a (Å)	17.0430(6)
b (Å)	15.4740(6)
c (Å)	18.7360(7)
β (°)	99.198(2)
Volume ($Å^3$)	4877.6(3)
Z	4
Density (Calcd.) (gcm^{-3})	1.897
Absorption coefficient (mm^{-1})	5.717
F (000)	2680
θ range	1.8-28.4
Index ranges *h*	-22/22
k	-17/20
l	-25/24
Reflections measured	44587
Independent/observed reflections	12166/9789
Data/parameters	12166/606
Goodness-of-fit on F^2	1.14
Final *R* indices [$I > 2\sigma(I)$]	0.0584
	(*wR2* = 0.1258)
Largest diff. peak/hole ($eÅ^{-3}$)	3.52/-4.03

Table 6.7: Selected bond lengths (Å) and angles (˚) for [Hbop.Hppc].

Bond lengths			
O(3)-C(2)	1.2321(1)	N(3)-C(2)	1.3387(1)
O(4)-C(31)	1.2473(1)	N(4)-C(35)	1.3498(1)
O(5)-C(42)	1.3578(1)	N(4)-C(31)	1.3733(1)
O(1)-C(1)	1.3747(1)	N(1)-C(1)	1.2875(1)
O(1)-C(11)	1.3788(1)	N(1)-C(12)	1.3974(1)
O(2)-C(21)	1.2352(1)	N(2)-C(25)	1.3496(1)
N(3)-C(41)	1.4106(1)	N(2)-C(21)	1.3806(1)
Bond angles			
O(2)-C(21)-C(22)	125.96(1)	O(3)-C(2)-N(3)	124.57(1)
C(2)-N(3)-C(41)	128.08(1)	N(3)-C(2)-C(32)	115.26(1)
C(31)-N(4)-C(35)	124.11(1)	O(4)-C(31)-C(32)	125.45(1)
C(1)-N(1)-C(12)	105.21(1)	O(1)-C(1)-C(22)	116.27(1)
C(21)-N(2)-C(25)	124.64(1)	N(1)-C(1)-C(22)	129.09(1)

Table 6.8: Selected bond lengths (Å) and angles (˚) for **1**.

Bond lengths			
Re(1)-Cl(1)	2.403(2)	N(1)-C(1)	1.345(9)
Re(1)-Cl(2)	2.331(2)	N(2)-C(25)	1.34(1)
Re(1)-P(1)	2.482(2)	N(2)-C(21)	1.365(9)
Re(1)-P(2)	2.492(2)	N(1)-C(12)	1.408(9)
Re(1)-O(2)	2.024(5)	C(1)-O(1)	1.347(8)
Re(1)-N(1)	2.152(5)	C(11)-O(1)	1.388(8)
O(2)-C(21)	1.294(8)	C(1)-C(22)	1.43(1)
Bond angles			
Cl(1)-Re(1)-Cl(2)	94.92(6)	C(1)-N(1)-C(12)	105.1(5)
P(1)-Re(1)-P(2)	176.44(6)	P(1)-Re-Cl(1)	90.59(6)
O(2)-Re(1)-N(1)	85.8(2)	P(1)-Re-Cl(2)	89.56(6)
N(1)-Re(1)-Cl(1)	168.5(1)	P(1)-Re-N(1)	90.8(1)
O(2)-Re(1)-Cl(2)	177.6(1)	P(1)-Re-O(2)	89.9(1)
Cl(1)-Re(1)-O(2)	82.8(1)	P(2)-Re-Cl(1)	90.75(6)
Cl(2)-Re(1)-N(1)	96.5(1)	Re-N(1)-C(1)	122.5(4)

Table 6.9: Selected bond lengths (Å) and angles (˚) for **2**.

Bond lengths			
Re(1)-I(1)	2.7066(7)	O(2)-C(22)	1.348(9)
Re(1)-P(1)	2.509(2)	N(1)-C(1)	1.32(1)
Re(1)-P(2)	2.522(2)	C(24)-N(2)	1.35(1)
Re(1)-O(2)	1.944(5)	N(1)-C(12)	1.32(1)
Re(1)-O(3)	1.690(6)	C(1)-O(1)	1.350(9)
Re(1)-N(1)	2.183(6)	C(21)-C(1)	1.43(1)
Bond angles			
P(1)-Re(1)-P(2)	170.89(7)	I(1)-Re(1)-O(3)	96.7(2)
I(1)-Re(1)-N(1)	175.4(2)	P(2)-Re-I(1)	91.04(5)
O(2)-Re(1)-O(3)	168.6(3)	P(2)-Re-O(2)	86.2(2)
O(2)-Re(1)-N(1)	81.6(2)	P(2)-Re-N(1)	91.4(2)
O(3)-Re(1)-N(1)	87.1(3)	P(2)-Re-O(3)	92.2(2)
I(1)-Re(1)-P(1)	88.46(5)	C(1)-N(1)-C(12)	105.9(6)
P(1)-Re(1)-O(2)	84.7(2)	Re-N(1)-C(1)	125.4(5)

Chapter 7

Rhenium Complexes with Multidentate Benzo(thiazole/imidazole) Ligands

7.1 Introduction

Interest in benzothiazoles (Figure 7.1(a)) has increased dramatically since the discovery that the compound 2-(4-aminophenyl)benzothiazole is active against a range of breast carcinoma cell lines *in vitro* [1]. It was found that manipulation of the substituents on the phenyl rings of the benzothiazole results in the alteration of the cytostatic activity against a series of ovarian, cervical, lung, colon and renal malignant cell lines [2]. Furthermore, it has been discovered that the compound 2-(4-methylaminophenyl)-6-hydroxybenzothiazole (termed *Pittsburg Compound B*, Figure 7.2) has diagnostic applications for amyloid deposits in patients suffering from Alzheimer's disease [3]. Another analogue of heterocyclic compounds, benzimidazoles (Figure 7.1(b)), have received considerable interest due to their numerous biological applications and have shown to exhibit antifungal, antiviral, anticancer, antimitotic, anti-inflammatory and antiparasitic activities [4].

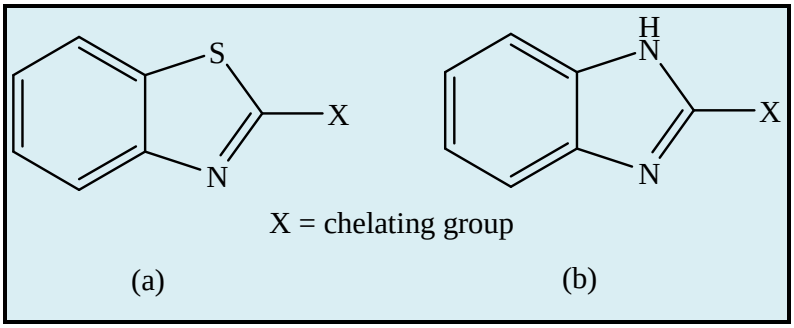

Figure 7.1: Structures of the (a) benzothiazole and the (b) benzimidazole moieties.

Derivatives of benzothiazoles and benzimidazoles are therefore an interesting class of ligands for transition metals, and especially for the synthesis of new rhenium and technetium radiopharmaceuticals for radiotherapy and tumour imaging, respectively. It was established that benzothiazole rhenium compounds may be useful for the *in vivo* diagnosis of Alzheimer's disease [5], while rhenium complexes containing benzimidazole derivatives exhibit optimal biological activities [6].

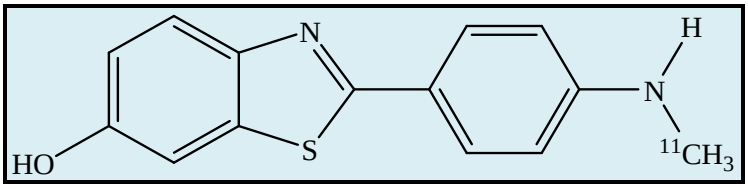

Figure 7.2: Structure of 2-(4-methylaminophenyl)-6-hydroxybenzothiazole.

The ligand system 2-(2-aminophenyl)benzothiazole (Habt) and 2-(2-hydroxyphenyl) benzothiazole (Hhpd) has previously been used as bidentate ligands in their reactions with $[Re(CO)_5Br]$ and *trans*-$[ReOBr_3(PPh_3)_2]$ respectively [7]. In the respective products *fac*-$[Re(Habt)(CO)_3Br]$ and *cis*-$[ReOBr_2(hpd)(PPh_3)]$, Habt acts as a neutral bidentate NN-donor ligand, with hpd coordinated as a monoanionic NO-donor chelate. The reaction of a benzimidazole ligand, H_2apb = 2-(2-aminophenyl)-1-benzimidazole, with *trans*-$[ReO_2(py)_4]Cl$ led to the formation of the neutral oxorhenium(V) complex [ReO(Hapb)(apb)], containing two bidentate imido-coordinated benzimidazole ligands [8].

This chapter describes the synthesis of potentially tridentate benzothiazole and benzimidazole ligands (Scheme 7.1 and 7.2) and their coordination behaviour with the $[ReO]^{3+}$ and *fac*-$[Re(CO)_3]^+$ moieties. The reaction of the potentially tridentate *bis*(benzimidazol-2-ylethyl)sulfide (btn) with *trans*-$[ReOCl_3(PPh_3)_2]$ led to the formation of the dioxo-bridged cationic complex salt, $(\mu\text{-}O)_2[Re_2O_2(btn)_2]I_2$ (**1**). From the reaction of the corresponding benzothiazole analogue, *bis*(benzothiazol-2-ylethyl)sulfide (bts) with $[Re(CO)_5Br]$, the neutral complex, *fac*-$[Re(CO)_3(bts)Br]$ (**2**) was obtained. The dimeric compound, $(\mu\text{-dbt})_2[Re(CO)_3]_2$ (**3**) was isolated by reacting $[Re(CO)_5Cl]$ with Hdbt = 1,3-*bis*(benzothiazol-2-yl)thiourea. The neutral complex, $(\mu\text{-mbt})_2[Re(CO)_3]_2$ (**4**)

was prepared by the heating of $[Re(CO)_5Cl]$ with a twofold molar excess of 1-(benzothiazol-2-ylidene)-3-methylthiourea (Hmbt) in refluxing toluene. When Hmbt was reacted with *trans*-$[ReOCl_3(PPh_3)_2]$, the cationic complex salt, $[ReCl_2(bte)(PPh_3)_2]Cl$ (**5**) (bte = (benzothiazole-2-yl)-*N*-ethylidenemethanamine) was formed. The reaction of 2,2'-(oxy*bis*(methylene))*bis*(benzimidazole) (bmb) with $[Re(CO)_5Cl]$, resulted in the rhenium(I) complex salt (**6**), *fac*-$[Re(CO)_3(bmb)]^+$ with the *tri*-μ-chlorohexacarbonyldirhenate, $[Re_2(CO)_6Cl_3]^-$ as the counter anion. A rhenium(I) complex, $[Re(CO)_3(btp)Cl]$ (**7**) was isolated from the reaction of the bidentate 2,9-*bis*(benzothiazol-2-yl)-1,10-phenanthroline (btp) ligand and $[Re(CO)_5Cl]$.

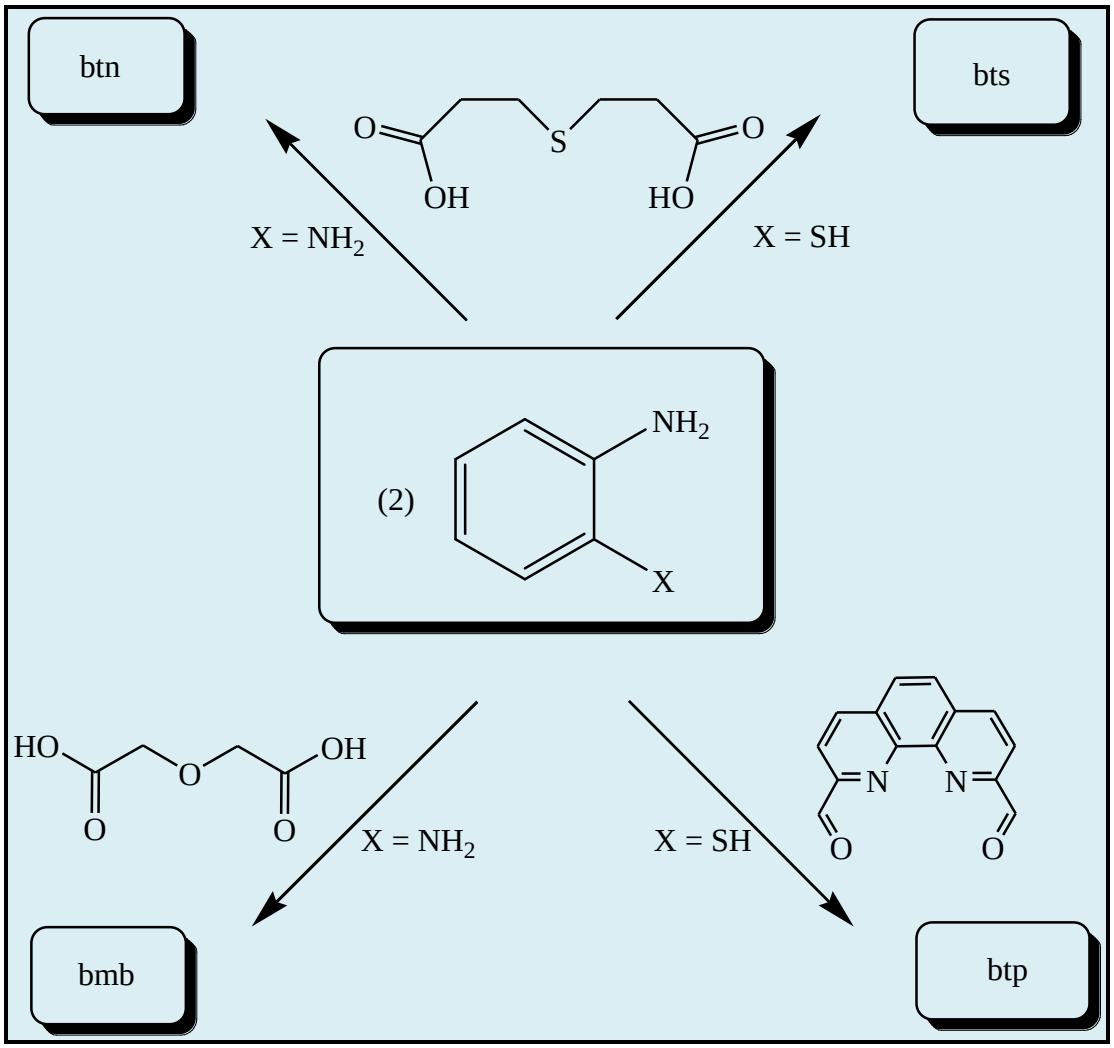

Scheme 7.1: Reaction pathway for the formation of *bis*(benzothiazole/benzimidazole) derivatives.

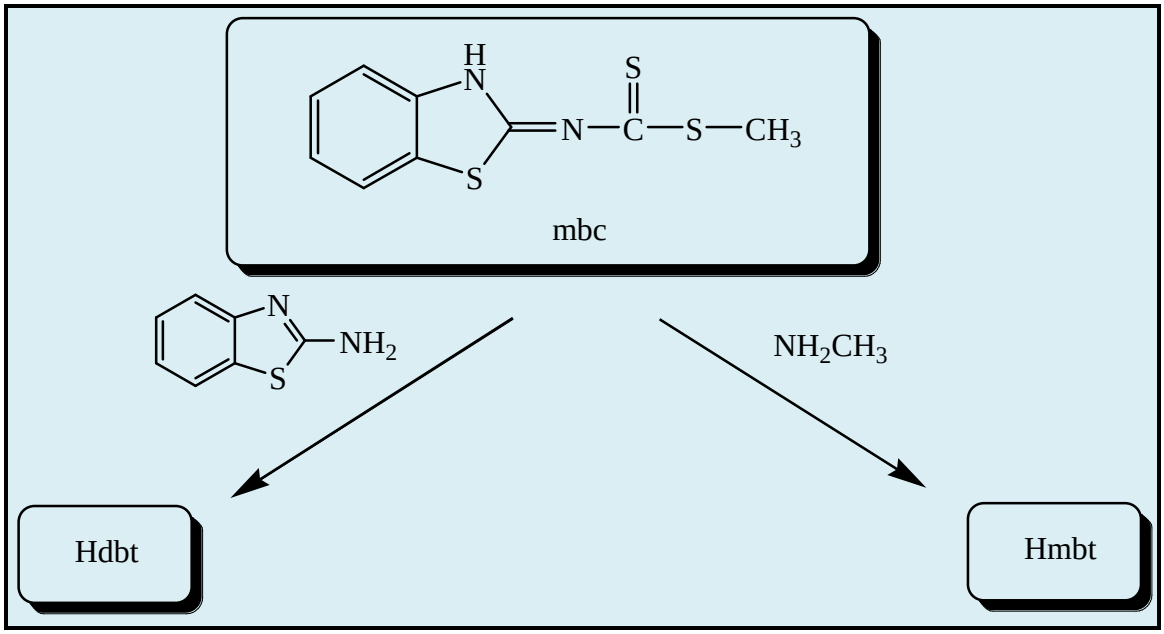

Scheme 7.2: Reaction pathway for the formation of 1,3-*bis*(benzothiazol-2-yl)thiourea (Hdbt) and 1-(benzothiazol-2-ylidene)-3-methylthiourea (Hmbt).

7.2 Experimental

7.2.1 Synthesis of *bis*(benzimidazol-2-ylethyl)sulfide (btn)

A mixture of 0.84 g of 3,3'-thiodipropionic acid (4.72 mmol) and 1.00 g of 1,2-diaminobenzene (9.25 mmol) was dissolved in 50 cm^3 of 4 M HCl. The solution was heated under reflux for 24 hours, and then filtered while hot. The filtrate was placed in a cold room at 0 °C overnight, and the blue crystals which formed were collected by filtration and dried under vacuum. Yield = 82 %, m.p. = 137 °C. Anal. Calcd. (%) for $C_{18}H_{18}N_4S$: C, 67.1; H, 5.6; N, 17.4; S, 9.9. Found: C, 65.9; H, 5.9; N, 17.0; S, 9.3. IR (ν_{max}/cm^{-1}): *v*(N-H) 3403; *v*(C=N) 1623. ^{1}H NMR (295K, ppm): 7.81 (q, 4H, *H*(1), *H*(4), *H*(9), *H*(12)); 7.55 (q, 4H, *H*(2), *H*(3), *H*(10), *H*(11)); 3.57 (t, 4H, C(5)H_2, C(8)H_2); 3.29 (t, 4H, C(6)H_2, C(7)H_2); 2.48 (s, 2H, N*H*(13), N*H*(14)).

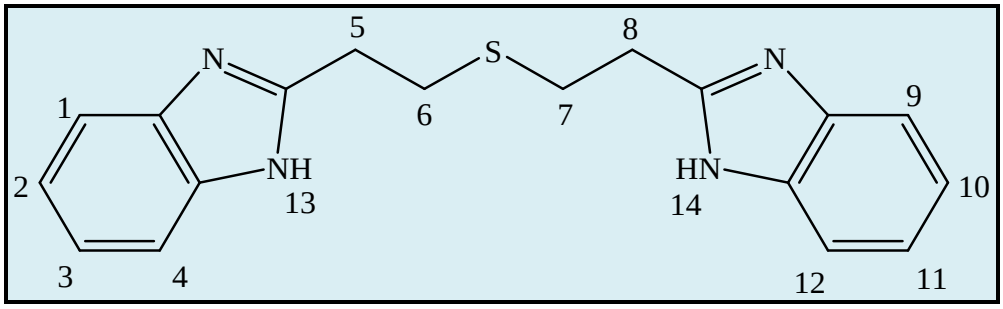

Figure 7.3: Structure of btn.

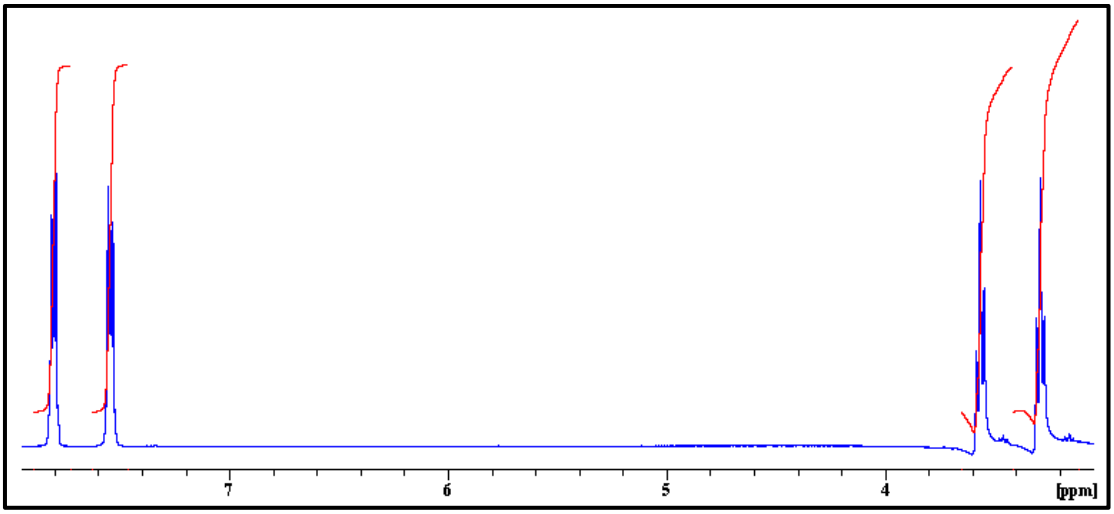

Figure 7.4: ^{1}H NMR spectrum of btn in the 3.00-8.00 ppm region.

7.2.2 Synthesis of *bis*(benzothiazol-2-ylethyl)sulfide (bts)

A mixture of 1.00 g of 3,3'-thiodipropionic acid (5.62 mmol) and 1.40 g of 2-aminothiophenol (11.20 mmol) was added to hot polyphosphoric acid. The solution was stirred at 220 °C for 4 hours. After cooling the reaction mixture to room temperature, it was poured into ice-cold water. A brown precipitate formed which was filtered and recrystallized from ethanol. Yield = 57 %, m.p. = 151 °C. Anal. Calcd. (%) for $C_{18}H_{16}N_2S_3$: C, 60.6; H, 4.5; N, 7.9; S, 27.0. Found: C, 62.1; H, 4.9; N, 7.2; S, 26.2. IR (ν_{max}/cm^{-1}): ν(C=N) 1517. ^{1}H NMR (295K, ppm): 8.06 (d, 2H, *H*(1), *H*(9)); 7.96 (d, 2H, *H*(4), *H*(12)); 7.51 (t, 2H, *H*(2), *H*(10)); 7.42 (t, 2H, *H*(3), *H*(11)); 3.42 (t, 4H, C(5)H_2, C(8)H_2); 3.14 (t, 4H, C(6)H_2, C(7)H_2).

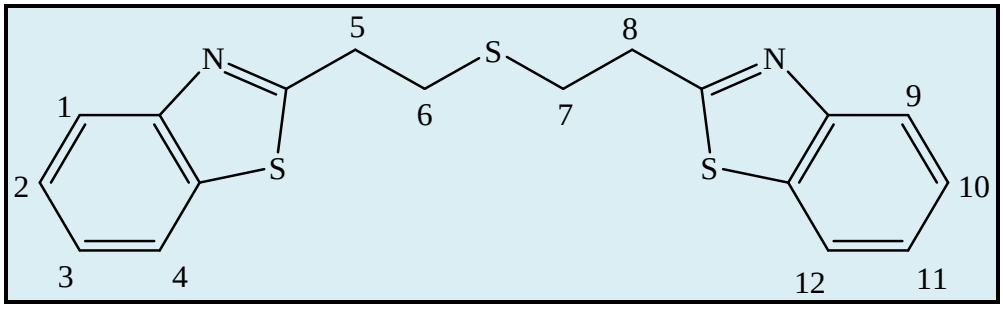

Figure 7.5: Structure of bts.

7.2.3 Synthesis of methylbenzothiazol-2-ylidenecarbamodithioate (mbc)

A mass of 3.00 g of 2-aminobenzothiazole (20 mmol) was dissolved in 50 cm^3 of DMF in an ice-water bath. To this mixture an aqueous 20 M NaOH solution (3 cm^3) was slowly added, and the solution was stirred for 30 min. Then, 2.4 cm^3 of carbon disulfide was slowly added and the resultant yellow solution was stirred for a further 30 min. Aqueous 20 M NaOH (3 cm^3) was added dropwise and after 30 min, 2.84 g of methyl iodide (20 mmol) was added to the solution which was stirred for a further two hours. The product was poured into 500 cm^3 of water and neutralized with 2 M hydrochloric acid. A yellow precipitate formed and was filtered under vacuum, washed with water and recrystalized from ethanol to yield yellow crystals. Yield = 81 %, m.p. = 183 °C. Anal. Calcd. (%) for $C_9H_8N_2S_3$: C, 45.0; H, 3.4; N, 11.7; S, 40.0. Found: C, 44.0; H, 3.1; N, 11.2; S, 40.2. IR (ν_{max}/cm^{-1}): *ν*(N-H) 3172; *ν*(C=N) 1603; *ν*(C=S) 1210. ^{1}H NMR (295K, ppm): 7.83 (d, 1H, *H*(4)); 7.77 (d, 1H, *H*(1)); 7.55 (t, 1H, *H*(3)); 7.45 (t, 1H, *H*(2)); 5.38 (s, br, 1H, N*H*); 2.75 (s, 3H, CH_3).

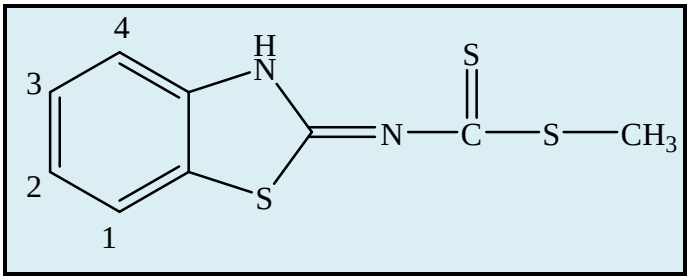

Figure 7.6: Structure of mbc.

7.2.4 Synthesis of 1,3-*bis*(benzothiazol-2-yl)thiourea (Hdbt)

A mixture of 1.00 g of 2-aminobenzothiazole (66 mmol) and 1.50 g of methylbenzothiazol-2-ylidenecarbamodithioate (63 mmol) was heated at 60 °C for three hours in a glass vial. The yellow solid was recrystallized from chloroform to produce a yellow powder. Yield = 48 %, m.p. = 255 °C. Anal. Calcd. (%) for $C_{15}H_{10}N_4O_3$: C, 52.6; H, 2.9; N, 16.4; S, 28.1. Found: C, 53.7; H, 2.8; N, 17.0; S, 27.2. IR (ν_{max}/cm^{-1}): *ν*(C=N) 1644(s); *ν*(C=S) 1238. ^{1}H NMR (295K, ppm): 7.94 (d, 2H, *H*(4), *H*(8)); 7.66 (d, 2H, *H*(1), *H*(5)); 7.45 (t, 2H, *H*(3), *H*(7)); 7.32 (t, 2H, *H*(2), *H*(6)); 3.38 (s, br, 2H, N*H*(9), N*H*(10)). UV-Vis (CH_3CN, λ_{max} (ε, M^{-1}cm^{-1})): 325 (47700), 340 (39300), 359 (41100), 375 (37100), 397sh (17400).

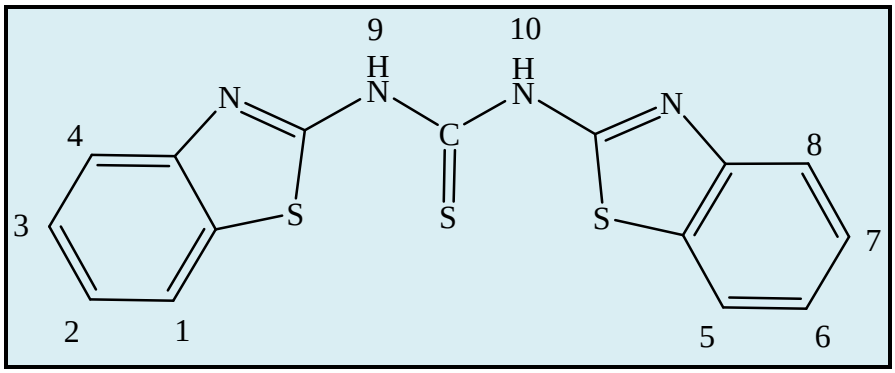

Figure 7.7: Structure of Hdbt.

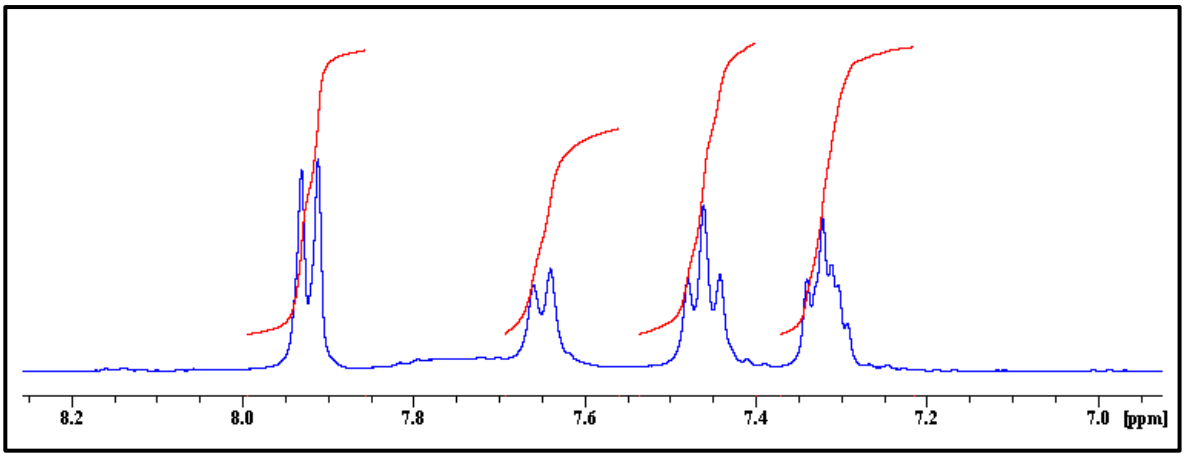

Figure 7.8: ^{1}H NMR spectrum of Hdbt in the 6.90-8.25 ppm region.

7.2.5 Synthesis of 1-(benzothiazol-2-ylidene)-3-methylthiourea (Hmbt)

An aqueous solution of NH_2CH_3 (40%, 0.430 cm^3, 0.0063 mol) was added to a solution of methylbenzothiazol-2-ylidenecarbamodithioate (1.2 g, 0.0063 mol) in ethanol (40 cm^3) at room temperature. The mixture was heated at reflux for 6 hours. The yellow solution was cooled to room temperature and light yellow crystals formed which was filtered and washed with ethanol. Yield = 68 %, m.p. = 216 °C. Anal. Calcd. (%) for $C_9H_9N_3S_2$: C, 48.4; H, 4.1; N, 18.8; S, 28.7. Found: C, 49.3; H, 4.4; N, 18.6; S, 27.3. IR (ν_{max}/cm^{-1}): *ν*(N-H) 3176, 3044; *ν*(C=N) 1556; *ν*(C=S) 1214. ^{1}H NMR (295K, ppm): 9.90 (s, br, 1H, N(5)*H*); 7.87 (d, 2H, *H*(1), *H*(4)); 7.64 (s, br, 1H, N(6)*H*); 7.39 (t, 1H, *H*(2)); 7.25 (t, 1H, *H*(3)); 3.34 (s, 3H, CH_3).

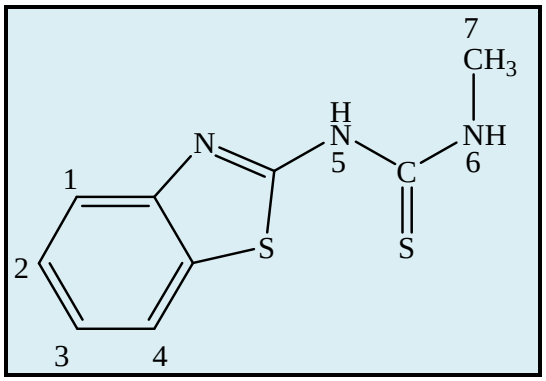

Figure 7.9: Structure of Hmbt.

7.2.6 Synthesis of 2,2'-(oxy*bis*(methylene))*bis*(benzimidazole) (bmb)

A mixture of 2.00 g (15 mmol) of diglycolic acid and 3.23 g (30 mmol) of 1,2-diaminobenzene was added to 50 cm^3 of hot polyphosphoric acid. The solution was stirred at 200 °C for 5 hours, after which it was allowed to cool to room temperature. The solution was slowly added to a 10 % aqueous potassium carbonate solution to produce a milky green precipitate which was filtered and dried under vacuum. Yield = 67 %, m.p. = 212 °C. Anal. Calcd. (%) for $C_{16}H_{14}N_4O$: C, 69.1; H, 5.1; N, 20.1. Found: C, 69.8; H, 4.7; N, 19.5. IR (ν_{max}/cm^{-1}): *ν*(C=N) 1628. ^{1}H NMR (295K, ppm): 7.58 (q, 4H, *H*(1), *H*(4), *H*(7), *H*(10)); 7.22 (q, 4H, *H*(2), *H*(3), *H*(8), *H*(9)); 6.00 (s, br, 2H, N*H*(11), N*H*(12)); 4.93 (s, 4H, C(5)H_2, C(6)H_2).

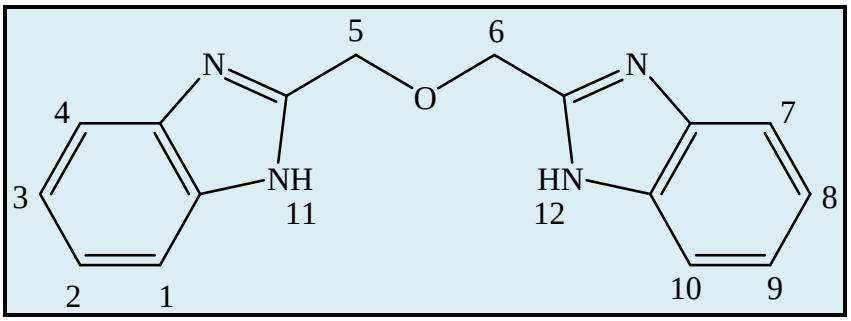

Figure 7.10: Structure of bmb.

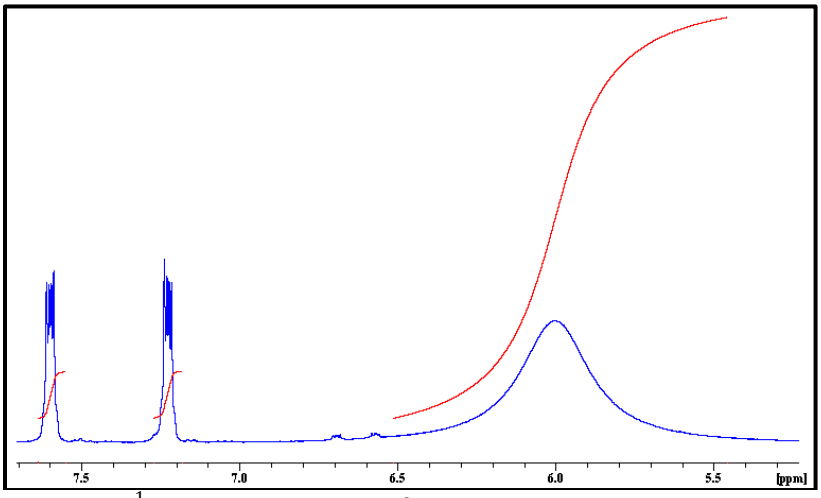

Figure 7.11: ^{1}H NMR spectrum of bmb in the 5.20-7.70 ppm region.

7.2.7 Synthesis of 1,10-phenanthroline-2,9-dicarbaldehyde (pdc)

Neocruproine hydrate (3.00 g, 14.4 mmol) and selenium dioxide (11.29 g, 100.8 mmol) were dissolved in 210 cm^3 of 1,4-dioxane. The solution was heated at reflux temperature for 3 hours after which a clear yellow solution formed. The solution was filtered while hot and upon cooling a light pink solid was obtained which was recrystallized from acetone/hexane. Yield = 88 %, m.p. = 242 °C. Anal. Calcd. (%) for $C_{14}H_8N_2O_2$: C, 71.2; H, 3.4; N, 11.9. Found: C, 73.1; H, 3.6; N, 12.7. IR (ν_{max}/cm^{-1}): ν(C=O) 1700s. ^{1}H NMR (295K, ppm): 10.36 (s, 2H, *H*(1), *H*(8)); 8.82 (d, 2H, *H*(2), *H*(7)); 8.34 (d, 2H, *H*(3), *H*(6)); 8.30 (d, 2H, *H*(4), *H*(5)).

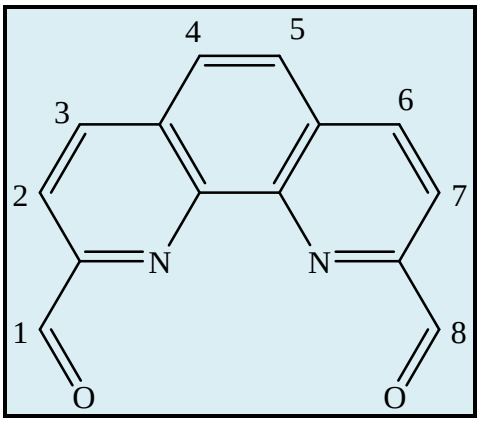

Figure 7.12: Structure of pdc.

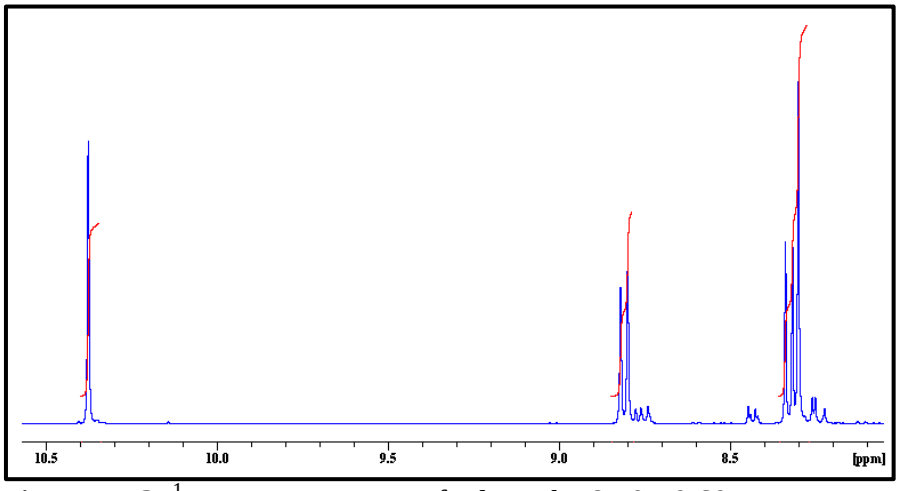

Figure 7.13: ^{1}H NMR spectrum of pdc in the 8.10-10.60 ppm region.

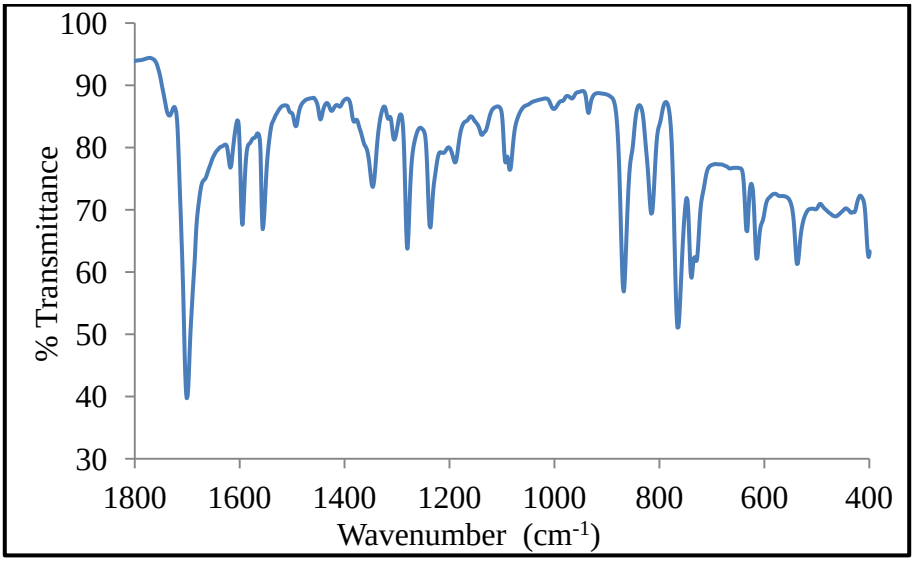

Figure 7.14: IR spectrum of pdc.

7.2.8 Synthesis of 2,9-*bis*(benzothiazol-2-yl)-1,10-phenanthroline (btp)

A mixture of 1.00 g (4.23 mmol) of 1,10-phenanthroline-2,9-dicarbaldehyde and 1.05 g (8.40 mmol) of 2-aminothiophenol was added to 50 cm^3 of polyphosphoric acid. The solution was stirred for 5 hours at 200 °C, after which it was cooled to room temperature. A brown precipitate formed on the addition of a 10 % aqueous potassium carbonate solution. The precipitate was filtered and recrystallized from acetonitrile to produce brown crystals suitable for X-ray diffraction analysis. Yield = 70 %, m.p. = 290 °C. Anal. Calcd. (%) for $C_{26}H_{14}N_4S_2$: C, 69.9; H, 3.2; N, 12.6; S, 14.4. Found: C, 68.8; H, 3.7; N, 12.2; S, 15.2. IR (ν_{max}/cm^{-1}): ν(C=N) 1510. ^{1}H NMR (295K, ppm): 8.77 (dd, 4H, *H*(5), *H*(6), *H*(9), *H*(10)); 8.35 (d, 2H, *H*(7), *H*(8)); 8.22 (d, 4H, *H*(1), *H*(4), *H*(11), *H*(14)); 7.66 (t, 2H, *H*(2), *H*(13)); 7.60 (t, 2H, *H*(3), *H*(12)). UV-Vis (CH_2Cl_2, λ_{max} (ε, $M^{-1}cm^{-1}$)): 305 (23000), 351 (15600), 365 (15500), 378 (12700).

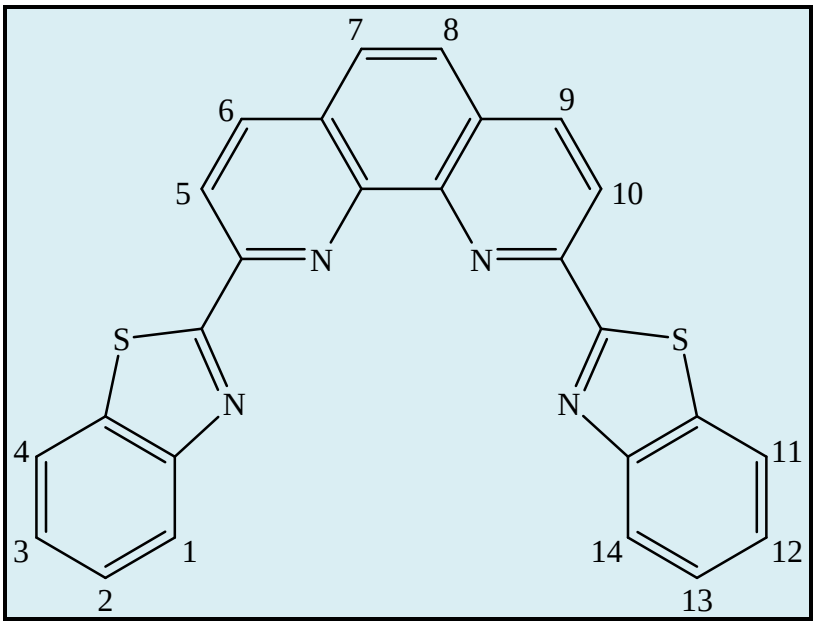

Figure 7.15: Structure of btp.

7.2.9 Synthesis of $(\mu\text{-}O)_2[Re_2O_2(btn)_2]I_2$ (1)

A mixture of btn (75 mg, 233 μmol) and *cis*-$[ReO_2I(PPh_3)_2]$ (100 mg, 115 μmol) in 20 cm^3 of methanol was heated under reflux for 2 hours. After cooling to room temperature, a brown precipitate was removed by filtration. The slow evaporation of the mother liquor over two days produced brown crystals. Yield = 72 %, m.p. = 195 °C. Anal. Calcd. (%) $C_{36}H_{36}N_8O_4S_2I_2Re_2$: C, 32.4; H, 2.7; N, 8.4; S, 4.8. Found: C, 32.6; H, 2.9; N, 8.3; S, 4.3. IR (ν_{max}/cm^{-1}): *ν*(N-H) 3050; *ν*(C=N) 1626; *ν*(Re=O) 940; *ν*(Re-O-Re) 692; *ν*(Re-N) 467; *ν*(Re-S) 429. ^{1}H NMR (295K, ppm): 7.77-7.84 (m, 4H); 7.61-7.68 (m, 4H); 7.51-7.60 (m, 8H); 3.72 (s, br, 4H, N(2)*H*, N(2^i)*H*, N(4)*H*, N(4^i)*H*); 3.50 (t, 8H, C(2)H_2, C(2^i)H_2, C(11^i)H_2, C(11^i)H_2,); 3.21 (t, 8H, C(1)H_2, C(1^i)H_2, C(10)H_2, C(10^i)H_2). Conductivity (10^{-3} M, CH_3CN): 256 $ohm^{-1}cm^2mol^{-1}$. UV-Vis (CH_3CN, λ_{max} (ε, $M^{-1}cm^{-1}$)): 510 (860).

7.2.10 Synthesis of *fac*-$[Re(CO)_3(bts)Br]$ (2)

$[Re(CO)_5Br]$ (100 mg, 246 μmol) and bts (175 mg, 490 μmol) in 20 cm^3 of toluene were heated under reflux for 3 hours under nitrogen. After cooling to room temperature, the reaction mixture was allowed to evaporate slowly at room temperature. After 2 days brown needles were collected. Yield = 66 %, m.p. = 182 °C. Anal. Calcd. (%) for $C_{21}H_{16}N_2O_3S_3BrRe$: C, 35.7; H, 2.3; N, 4.0; S, 13.6. Found: C, 35.8; H, 2.5; N, 3.9; S, 13.9. IR (ν_{max}/cm^{-1}): *ν*(C≡O) 2027, 1920, 1886; *ν*(Re-N) 475. ^{1}H NMR (295K, ppm): 8.55 (d, 1H, *H*(9)); 8.18 (d, 1H, *H*(12)); 8.07 (d, 1H, *H*(18)); 7.96 (d, 1H, *H*(21)); 7.73 (t, 1H, *H*(10)); 7.61 (t, 1H, *H*(11)); 7.53 (t, 1H, *H*(19)); 7.44 (t, 1H, *H*(20)); 2.54 (m, 4H, C(5)H_2, C(14)H_2); 2.01 (m, 4H, C(4)H_2, C(13)H_2). Conductivity (10^{-3} M, MeOH): 39 $ohm^{-1}cm^2mol^{-1}$. UV-Vis (MeOH, λ_{max} (ε, $M^{-1}cm^{-1}$)): 428 (170).

7.2.11 Synthesis of (μ-dbt)$_2$[Re(CO)$_3$]$_2$ (3)

A mass of 190 mg (555 μmol) of Hdbt was added to 105 mg (290 μmol) of [Re(CO)$_5$Cl] in 20 cm^3 of toluene, and the mixture was heated under reflux for 3 hours under nitrogen. After cooling to room temperature the solution was filtered, and the filtrate was left to evaporate slowly at room temperature over a period of 3 days. Yellow needles were collected, which were washed with diethyl ether and dried under vacuum. Yield = 65 %, m.p. = 262 °C. Anal. Calcd. (%) for $C_{36}H_{18}N_8O_6Re_2S_6$: C, 35.3; H, 1.5; N, 9.2. Found: C, 35.2; H, 1.7; N, 9.0. IR (ν_{max}/cm^{-1}): *ν*(C≡O) 2017, 1909, 1873; *ν*(NH) 3169; *ν*(C=N) 1633; ν(C-S) 751; *ν*(Re-N) 519, 498; *ν*(Re-S) 395. ^{1}H NMR (295K, ppm): 8.27 (d, 2H); 7.92 (t, 2H); 7.70 (d, 2H); 7.65 (d, 2H); 7.54 (t, 2H); 7.46 (t, 2H); 7.40 (t, 2H); 7.26 (d, 2H); 3.34 (s, br, 2H, N(23)*H*, N(13)*H*). Conductivity (10^{-3} M, DMF): 16 ohm^{-1}cm^{2}mol^{-1}. UV-Vis (DMF, λ_{max} (ε, M^{-1}cm^{-1})): 326 (7100), 357 (83700), 376 (78200), 396sh (50300).

7.2.12 Synthesis of (μ-mbt)$_2$[Re(CO)$_3$]$_2$ (4)

A mixture of 117 mg (525 μmol) of Hmbt and 107 mg (296 μmol) of [Re(CO)$_5$Cl] was dissolved in 20 cm^3 of toluene. The solution was heated under reflux for 3 hours under nitrogen. After cooling to room temperature, a white precipitate was collected by filtration, washed with diethyl ether and dried under vacuum. Crystals suitable for X-ray diffraction studies were obtained by recrystallization from a methanol/dichloromethane (1:1 v/v) mixture. Yield: 71 %, m.p. = 291 °C. Anal. Calcd. (%) for $C_{24}H_{16}N_6O_6Re_2S_4.2CH_3OH$: C, 29.8; H, 2.3; N, 8.0. Found: C, 29.5; H, 2.4; N, 7.7. IR (ν_{max}/cm^{-1}): *ν*(C≡O) 2018, 1894; *ν*(NH) 3069; *ν*(C=N) 1612; *ν*(C-S) 758; *ν*(Re-N) 519, 532; *ν*(Re-S) 401. ^{1}H NMR (295K, ppm): 9.78 (s, br, 1H, N(23)*H*); 9.18 (s, br, 1H, N(13)*H*); 7.98 (d, 1H, *H*(16)); 7.93 (d, 1H, *H*(13)); 7.87 (d, 1H, *H*(26)); 7.78 (d, 1H, *H*(15)); 7.56-7.67 (m, 2H, *H*(14), *H*(23)); 7.35-7.53 (m, 2H, *H*(24), *H*(25)); 3.12 (s, 3H, C(29)*H*$_3$); 2.88 (s, 3H, C(19)*H*$_3$). Conductivity (10^{-3} M, DMF): 4 ohm^{-1}cm^{2}mol^{-1}. UV-Vis (DMF, λ_{max} (ε, M^{-1}cm^{-1})): 308 (41800), 378 (8900).

7.2.13 Synthesis of $[ReCl_2(bte)(PPh_3)_2]Cl$ (5)

A mass of 51 mg (228 μmol) of Hmbt was added to 103 mg (124 μmol) of *trans*-$[ReOCl_3(PPh_3)_2]$ in 20 cm^3 of methanol. The mixture was heated under reflux for three hours after which the light brown solution was left to cool to room temperature and then filtered. The mother liquor was left to evaporate at room temperature to give brown crystals. Yield = 46 %, m.p. = 258 °C. Anal. Calcd. (%) for $C_{46}H_{40}Cl_3N_2P_2ReS$: C, 54.8; H, 4.0; N, 10.6; S, 3.2. Found: C, 55.3; H, 4.6; N, 10.8; S, 2.8. IR (ν_{max}/cm^{-1}): *ν*(C=N) 1584, 1491; *ν*(Re-N) 430, 395. ^{1}H NMR (295K, ppm): 9.78 (s, 1H, C(3)*H*); 8.53 (d, 1H, *H*(12)); 8.19 (d, 1H, *H*(15)); 7.78-7.92 (m, 2H, *H*(13), *H*(14)); 7.10-7.69 (m, 30H, 2 x PP*h*$_3$); 2.77 (s, 3H, C*H*$_3$). Conductivity (10^{-3} M, DMF): 65 $ohm^{-1}cm^2mol^{-1}$. UV-Vis (DMF, λ_{max} (ε, $M^{-1}cm^{-1}$)): 310 (77500), 328sh (51200), 384 (7750).

7.2.14 Synthesis of $[Re(CO)_3(bmb)][Re_2(CO)_6Cl_3]$ (6)

A mixture of $[Re(CO)_5Cl]$ (108 mg, 298 μmol) and bmb (155 mg, 557 μmol) was heated under reflux in 20 cm^3 of toluene for three hours in a nitrogen atmosphere. The resultant light brown solution was cooled to room temperature, and the solution was left overnight to evaporate slowly at room temperature. Transparent crystals formed which was filtered and dried under vacuum. Yield = 63 %, m.p. = 222 °C. Anal. Calcd. (%) for $C_{19}H_{14}N_4O_4Re.C_6Cl_3O_6Re_2$: C, 21.1; H, 2.2; N, 4.7. Found: C, 20.6; H, 2.6; N, 4.7. IR (ν_{max}/cm^{-1}): *ν*(C≡O) 2120, 2020, 1998, 1965, 1930, 1887; *ν*(C=N) 1628; *ν*(Re-N) 483. ^{1}H NMR (295K, ppm): 7.57 (q, 4H, *H*(13), *H*(16), *H*(23), *H*(26)); 7.21 (q, 4H, *H*(14), *H*(15), *H*(24), *H*(25)); 4.85 (s, 4H, C(1)*H*$_2$, C(2)*H*$_2$); 4.10 (s, br, 2H, N(4)*H*, N(2)*H*). Conductivity (10^{-3} M, DMF): 75 $ohm^{-1}cm^2mol^{-1}$. UV-Vis (DMF, λ_{max} (ε, $M^{-1}cm^{-1}$)): 324 (8460), 359 (5420).

7.2.15 Synthesis of *fac*-[Re(CO)$_3$(btp)Cl] (7)

A mass of 245 mg (549 μmol) of btp was added to 109 mg (301 μmol) of [Re(CO)$_5$Cl] in 20 cm^3 of toluene. The mixture was heated at reflux conditions for 3 hours under nitrogen. The resultant orange solution was cooled to room temperature then filtered. The precipitate was dissolved in CH_2Cl_2 and layered with hexane. Orange crystals were produced after three days. Yield = 66 %, m.p. > 300 °C. Anal. Calcd. (%) for $C_{29}H_{14}ClN_4O_3ReS_2$: C, 46.3; H, 1.9; N, 7.4; S, 8.5. Found: C, 46.2; H, 2.1; N, 7.1; S, 8.3. IR (ν_{max}/cm^{-1}): ν(C≡O) 2011, 1927, 1885; ν(C=N) 1579; ν(Re-N) 486. ^{1}H NMR (295K, ppm): 9.22 (d, 2H, *H*(32), *H*(32^i)); 8.58 (d, 2H, *H*(33), *H*(33^i)); 8.52 (s, 2H, *H*(36), *H*(36^i)); 8.39 (d, 2H, *H*(13), *H*(13^i)); 8.26 (d, 2H, *H*(16), *H*(16^i)); 7.73 (t, 2H, *H*(14), *H*(14^i)); 7.65 (t, 2H, *H*(15), *H*(15^i)). Conductivity (10^{-3} M, DMF): 26 ohm^{-1}cm^{2}mol^{-1}. UV-Vis (DMF, λ_{max} (ε, M^{-1}cm^{-1})): 306 (28000), 328 (28050).

7.2.16 X-ray Crystallography

X-ray diffraction studies were performed at 200(2) K using a Nonius Kappa CCD (for **1**), an Oxford Xcalibur (for **2**) and a Bruker Kappa Apex II (for mbc, Hmbt, btp.CH_3CN, **3**, **4**.CH_3OH, **5**, **6** and **7**) diffractometers with graphite monochromated Mo Kα radiation (λ = 0.71073 Å). SAINT was used for cell refinement and data reduction [9]. The structures were solved by direct methods using SHELXS-97 [10] or SIR97 [11], and refined by least-squares procedures using SHELXL-97 [10] with SHELXLE [12] as a graphical interface. All non-hydrogen atoms were refined anisotropically, and the hydrogen atoms were calculated in idealised geometrical positions. Data were corrected for absorption effects by the numerical method using SADABS [9].

7.3 Results and Discussion

7.3.1 Synthesis and characterization of methylbenzothiazol-2-ylidenecarbamodithioate (mbc)

The benzothiazole compound, methylbenzothiazol-2-ylidenecarbamodithioate (mbc), was formed *via* a two-step reaction from 2-aminobenzothiazole according to a literature method [13]. The reaction of carbon disulfide and 2-aminobenzothiazole in DMF in the presence of concentrated sodium hydroxide results in the formation of the dithiocarbonimidic acid derivative (Scheme 7.3). Alkylation of this product with methyl iodide, followed by acidification of the solution gave the compound mbc.

This compound can act as a bidentate ligand for transition metals [14]. It can also be further derivatized by the substitution of the thiomethyl group to form thioureas and thiocarbamic esters [15]. Yellow crystals of the compound were obtained by recrystallization from ethanol. It is soluble in a variety of solvents including ethanol, dichloromethane, acetone, acetonitrile and DMF, and is insoluble in methanol and toluene.

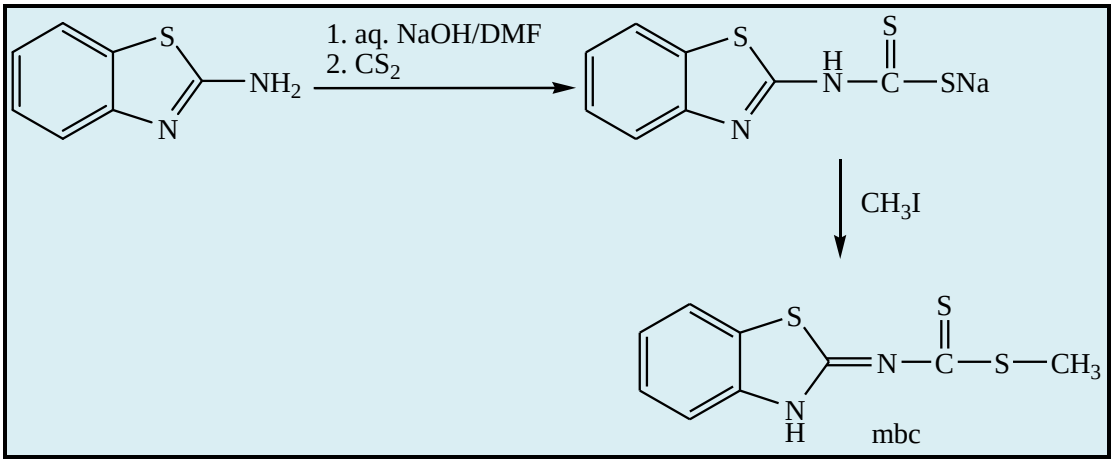

Scheme 7.3: Reaction pathway for the formation of mbc.

The IR spectrum of mbc (Figure 7.16) contains absorptions at 1603 and 1210 cm^{-1} due to the imine [ν(C=N)] and thiocarbonyl [ν(C=S)] stretching frequencies respectively. The

peak at 3172 cm^{-1} is due to the N-H stretch. The ^{1}H NMR spectrum (Figure 7.17) displays four one-proton signals in the aromatic region. The two doublets appearing at 7.77 and 7.83 ppm are ascribed to protons H(13) and H(16) of the benzothiazole ring (see Figure 7.18 for the atom labeling). The triplets at 7.45 and 7.55 ppm are due to protons H(14) and H(15). The proton of the amine group appears as a broad singlet at 5.38 ppm, and the singlet at 2.75 ppm integrates for the three protons of the thiomethyl moiety.

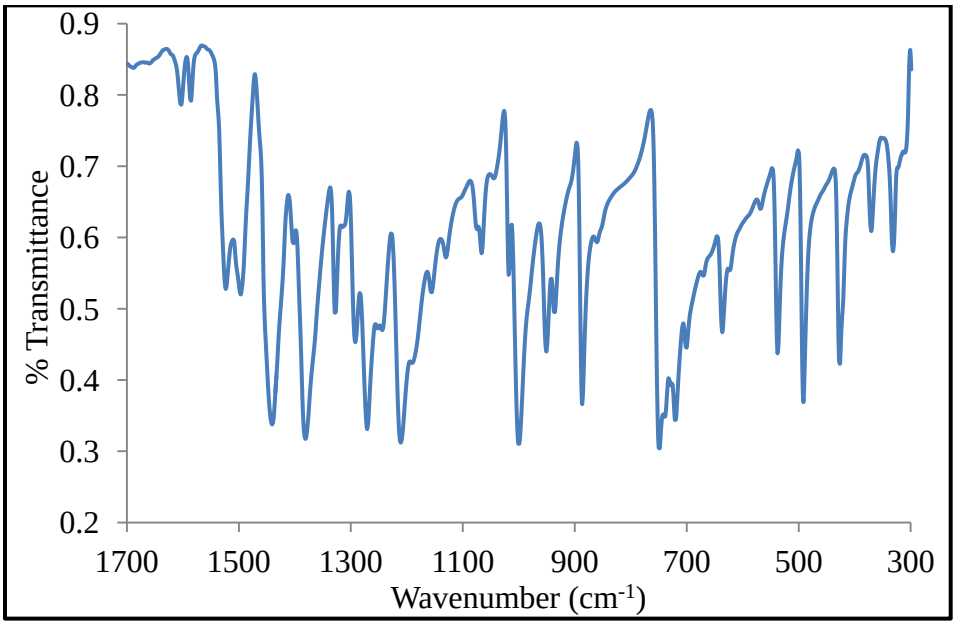

Figure 7.16: IR spectrum of mbc.

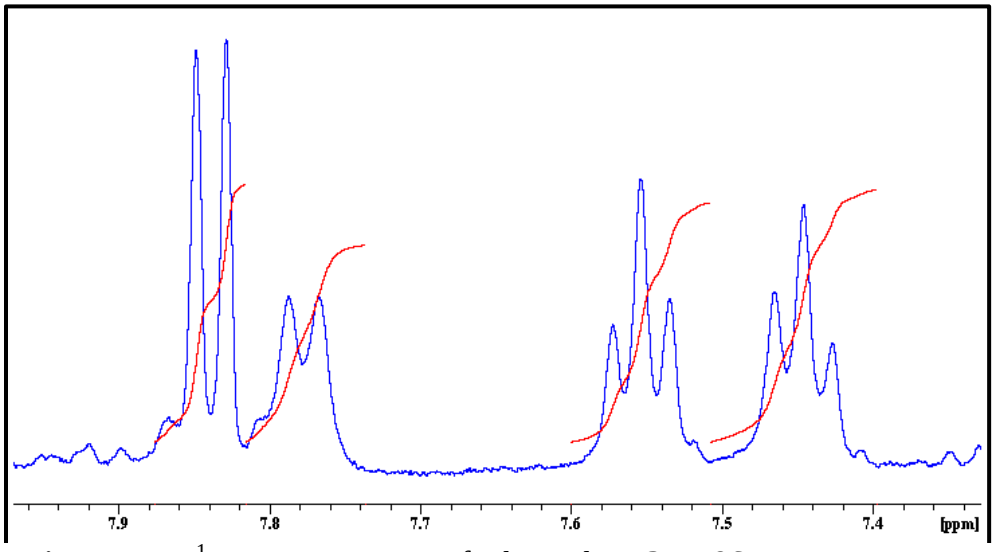

Figure 7.17: ^{1}H NMR spectrum of mbc in the 7.32-7.96 ppm region.

An ORTEP perspective view of mbc is shown in Figure 7.18. It consists of a benzothiazole moiety and a dithiocarbamate group. The X-ray structure analysis reveals that the nitrogen of the benzothiazole moiety is in its protonated form with the C(1)-N(1) single bond of 1.340(2) Å slightly shorter than typical C-N single bonds found in protonated benzothiazole compounds [16]. The C(1)-N(2) bond distance [1.337(3) Å] is surprisingly longer than expected for a C-N double bonds [~1.28 Å] found in the literature [17].

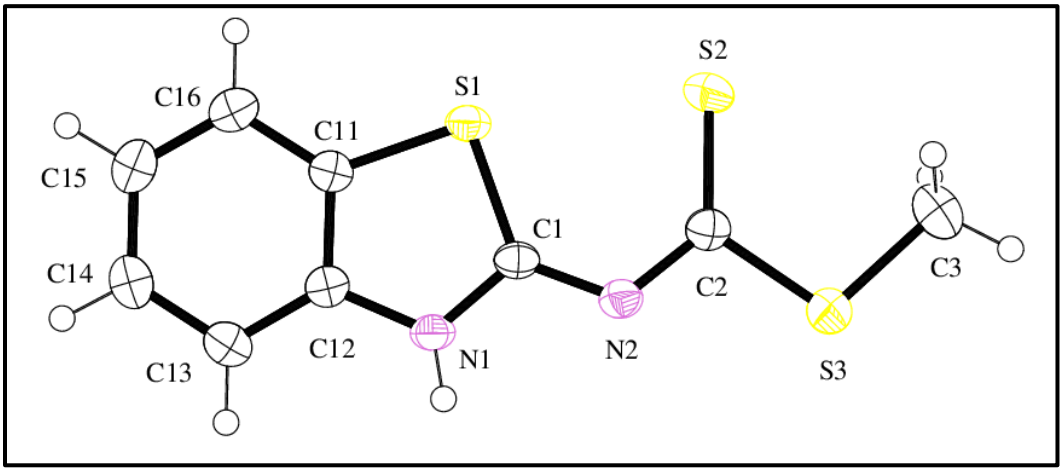

Figure 7.18: An ORTEP view of mbc showing 50% probability displacement ellipsoids and the atom labeling.

The bond angle around N(2) [C(1)-N(2)-C(2) = 121.1(2)˚] is close to the expected 120˚ angle for a sp^2 hybridized atom. The C(2)-S(2) [1.654(2) Å] bond length is considerably shorter than the C(2)-S(3) bond [1.764(2) Å], and can be considered as a double bond while the latter is regarded as single. The C-C bond lengths in the phenyl ring C(11)-C(16) [average = 1.389(3) Å] show that the π electron density is delocalized in this aromatic ring.

The molecular packing and intermolecular interactions in the crystal structure of mbc are shown in Figure 7.19. There are two intermolecular hydrogen-bonds in the packing of mbc: N(1)H(1)•••N(2) and C(13)H(13)•••S(3) (Table 7.1). Each mbc molecule (molecule **A** in Figure 7.20) is connected to four separate neighbouring mbc molecules. The four neighbouring mbc molecules are parallel to one another and orthogonal to molecule **A**.

The shortest distance between two parallel molecules is 3.414 Å, observed for the planes through the phenyl rings of neighbouring molecules.

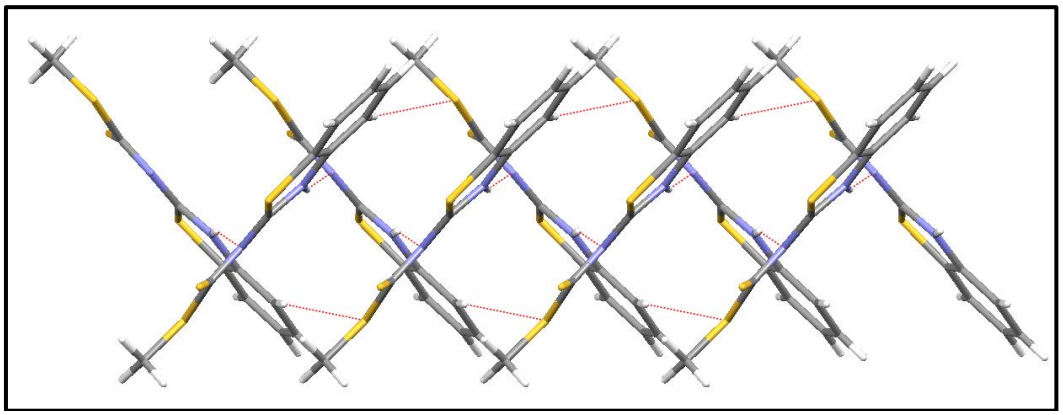

Figure 7.19: Molecular packing and intermolecular interactions in the crystal structure of mbc.

Table 7.1: Hydrogen-bond distances (Å) and angles (˚) in mbc.

D-H•••A	D-H	H•••A	D•••A	D-H•••A
N(1)H(1)•••N(2)	0.81	2.28	3.056(2)	161
C(13)H(13)•••S(3)	0.95	2.82	3.627(2)	144

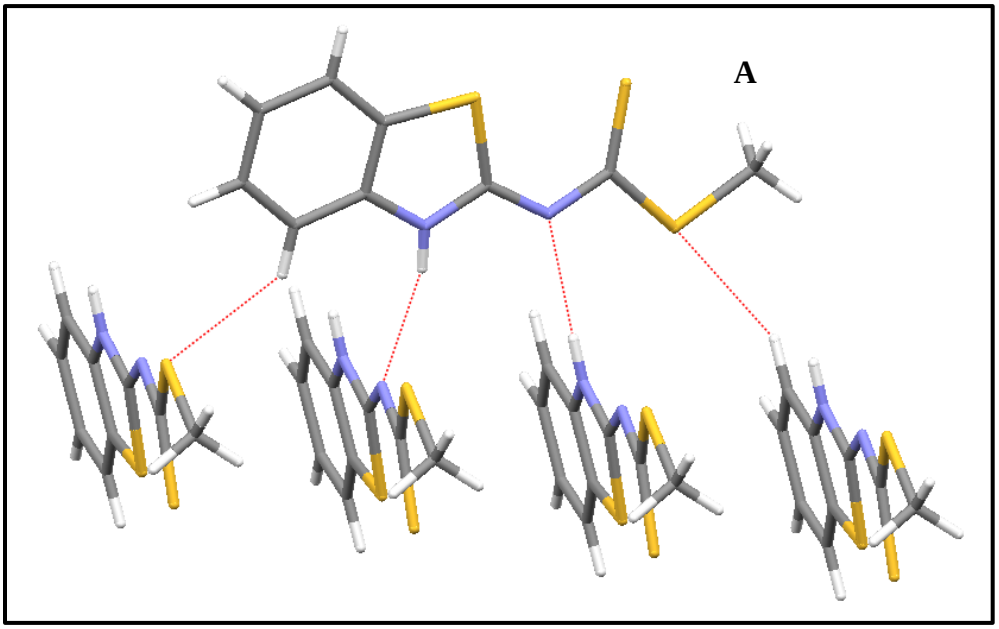

Figure 7.20: Intermolecular interactions between neighbouring mbc molecules.

7.3.2 Synthesis and characterization of 1-(benzothiazol-2-ylidene)-3-methylthiourea (Hmbt)

The potentially bidentate ligand 1-(benzothiazol-2-ylidene)-3-methylthiourea (Hmbt) was synthesized according to a literature method [15] by the reaction of methylbenzothiazol-2-ylidenecarbamodithioate (mbc) with an aqueous solution of methylamine in refluxing ethanol. Hmbt is soluble in dichloromethane and acetone, and insoluble in toluene, alcohols and acetonitrile.

In the infrared spectrum of Hmbt two peaks are observed at 3176 and 3044 cm^{-1}, due to *v*(N-H) of the amino nitrogens N(2) and N(3) (see Figure 7.22 for the atom labeling). The imine [*v*(C=N)] and thiocarbonyl [*v*(C=S)] stretches appear as sharp peaks at 1556 and 1214 cm^{-1} respectively. The amine protons, N(2)H and N(3)H, appear as broad singlets at 7.64 and 9.90 ppm respectively in the ^{1}H NMR spectrum of the compound (Figure 7.21). The signals of the four protons of the phenyl ring appear as a two-proton doublet (at 7.87 ppm) and two one-proton triplets (at 7.25 and 7.39 ppm). The three-proton singlet at 3.34 ppm is ascribed to the methyl protons.

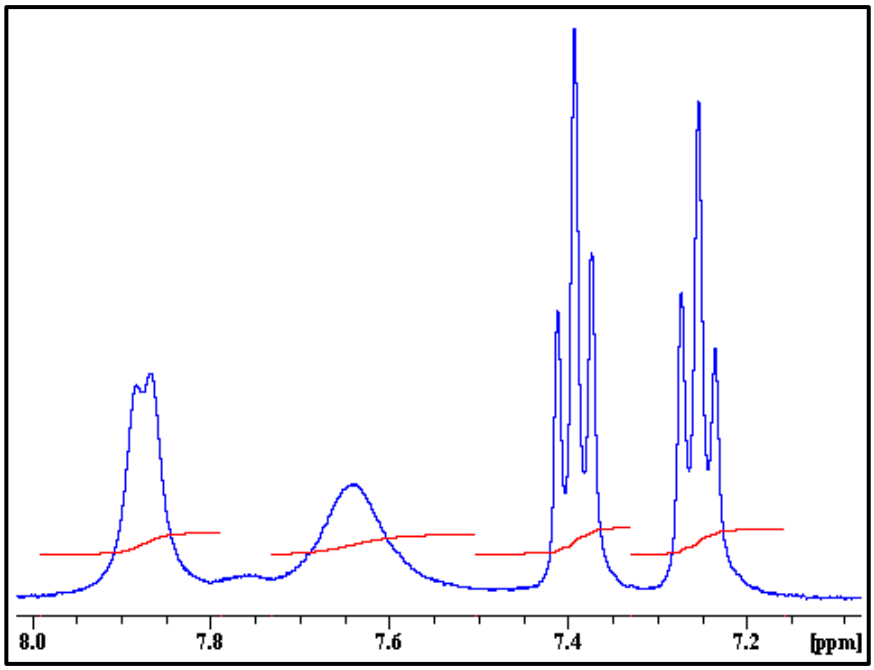

Figure 7.21: ^{1}H NMR spectrum of Hmbt.

An ORTEP view of the asymmetric unit of Hmbt is shown in Figure 7.22. It consists of a benzothiazole component and a methylthiourea moiety. The C(1)-N(1)-C(16) = 109.8(1)˚ angle is significantly shorter than expected for sp^2 hybridized atoms. The N(1)-C(1) bond length of 1.296(2) Å is indicative of an imine double bond [18]. The longer N(2)-C(2) and N(3)-C(2) bond lengths are similar [average = 1.35(2) Å], and can be regarded as single. The C(2)-S(2) bond length [1.685(1) Å] is typical of C=S bonds [19].

The delocalization of π electrons in the aromatic ring is evident in the bond lengths of the C(11)-C(16) [average = 1.392(2) Å] phenyl ring. Hmbt contains intramolecular hydrogen-bonding between the imidazole nitrogen [N(1)] and the amine proton [N(3)-H(3)] (Figure 6.23). Intermolecular hydrogen-bonding exists between the thiocarbonyl sulfur [S(2)] and the amine proton [N(2)-H(2)] of an adjacent molecule of Hmbt (Table 7.2).

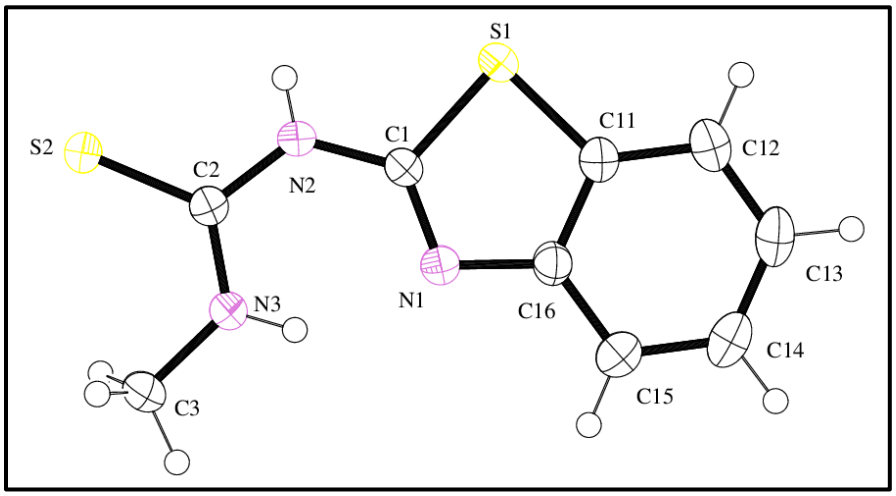

Figure 7.22: An ORTEP view of Hmbt showing 50% probability displacement ellipsoids and the atom labeling.

Table 7.2: Hydrogen-bond distances (Å) and angles (˚) in Hmbt.

D-H•••A	D-H	H•••A	D•••A	D-H•••A
N(2)H(2)•••S(2)	0.77	2.56	3.317(1)	165
N(3)H(3)•••N(1)	0.86	1.98	2.690(2)	140

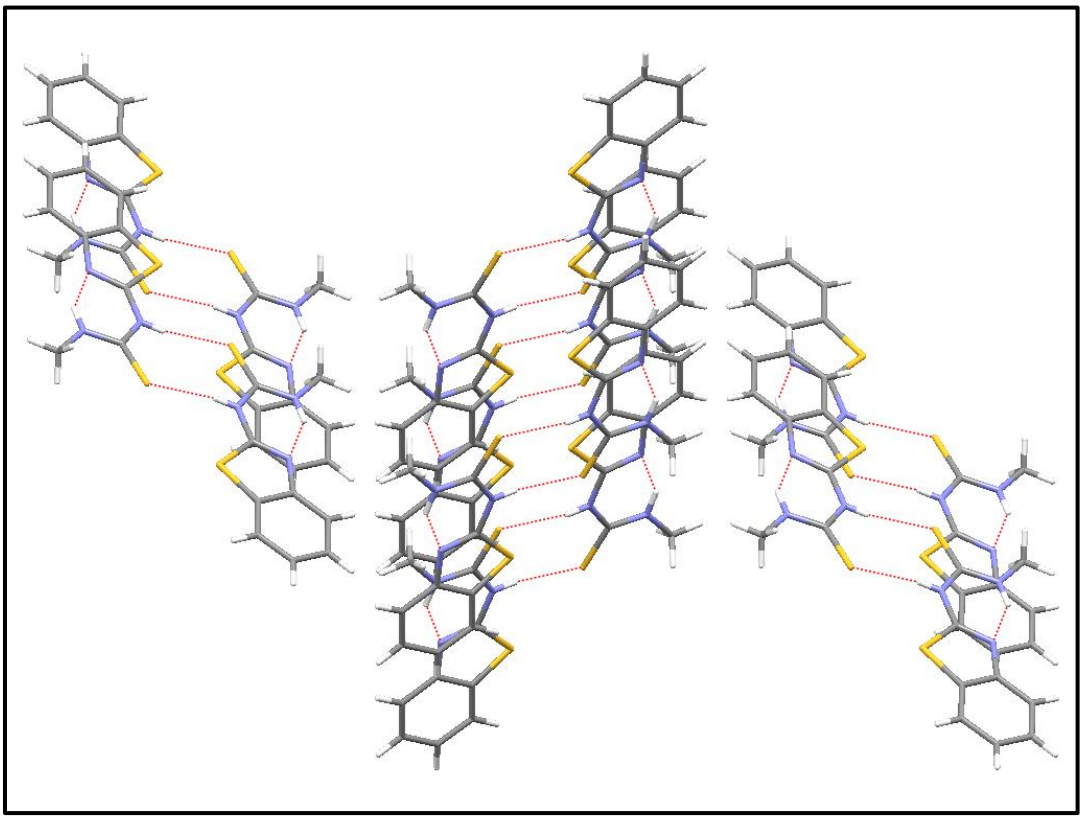

Figure 7.23: Molecular packing of Hmbt, showing the intra- and intermolecular hydrogen-bonding.

7.3.3 Synthesis and characterization of 2,9-*bis*(benzothiazol-2-yl)-1,10-phenanthroline (btp)

The compound 2,9-*bis*(benzothiazol-2-yl)-1,10-phenanthroline (btp) was synthesized *via* a two-step reaction from neocruproine hydrate according to Scheme 7.4. The first step involves the oxidation of the methyl groups of neocruproine using selenium dioxide in 1,4-dioxane to form the symmetrical dialdehyde, 1,10-phenanthroline-2,9-dicarbaldehyde. The condensation reaction of 1,10-phenanthroline-2,9-dicarbaldehyde with two mole equivalents of 2-aminothiophenol produced 2,9-*bis*(benzothiazol-2-yl)-1,10-phenanthroline (btp).

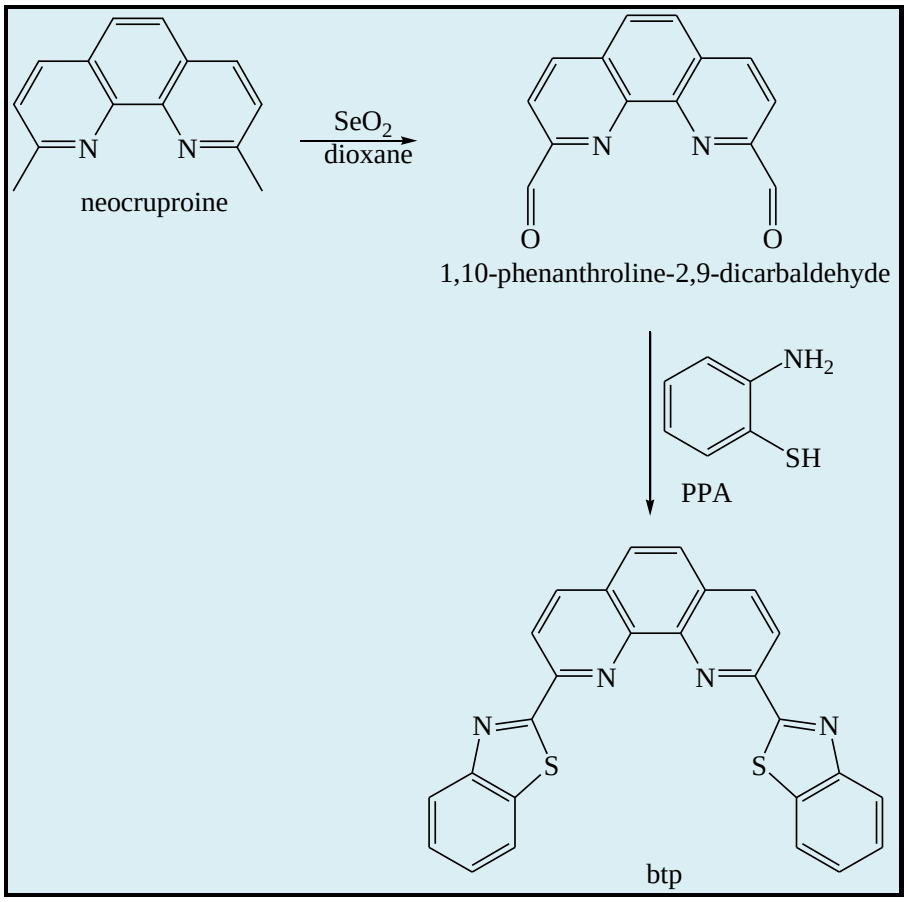

Scheme 7.4: Reaction pathway for the formation of ligand btp.

Brown crystals of btp were obtained by recrystallization from an acetonitrile solution of the product. The compound is a potentially tetradentate ligand containing the 1,10-phenanthroline group and two benzothiazole moieties. The compound is insoluble in most organic solvents and only dissolves in dichloromethane and acetonitrile upon heating.

The infrared spectrum of btp displays the C=N stretching frequency as a medium intensity peak at 1510 cm^{-1}. The symmetry within the molecule is emphasized by the ^{1}H NMR spectrum of btp. The signals of four phenanthroline protons appear as a doublet of doublets at 8.77 ppm. The two-proton doublet at 8.35 ppm is ascribed to the remaining two phenanthroline protons. The phenyl protons of the benzothiazole units appear further upfield as a four-proton doublet (at 8.22 ppm), and two two-proton triplets (at 7.60 and 7.66 ppm). The electronic spectrum of btp in dichloromethane displays four high energy

bands in the 300-400 nm region. These bands are assigned to intraligand transitions occurring within the highly conjugated π system.

The compound btp is symmetrical with a central 1,10-phenanthroline ring joined to two benzothiazole moieties (Figure 7.24). The molecule is close to planarity with the S(1) and S(2) thiazole rings forming a dihedral angle of 15.42˚ and dihedral angles of 9.37˚ and 7.31˚ respectively with the central phenanthroline ring. The N(4)-C(20) [1.297(2) Å] and N(1)-C(7) [1.299(2) Å] bond lengths are similar and typical of C=N bonds found in benzothiazole compounds [18]. The phenanthroline C-N bond lengths are however longer than that of the benzothiazole C=N bond lengths [N(3)-C(19) = 1.327(2) Å, N(3)-C(13) = 1.353(2) Å, N(2)-C(8) = 1.331 Å and N(2)-C(12) = 1.354(2) Å] due to the delocalization of the π electrons in the aromatic rings of the phenanthroline moiety. There is only one intermolecular hydrogen-bond, between the nitrogen atom of the acetonitrile molecule of crystallization and a phenanthroline proton [C(17)-H(17)•••N(5)] (Figure 7.24).

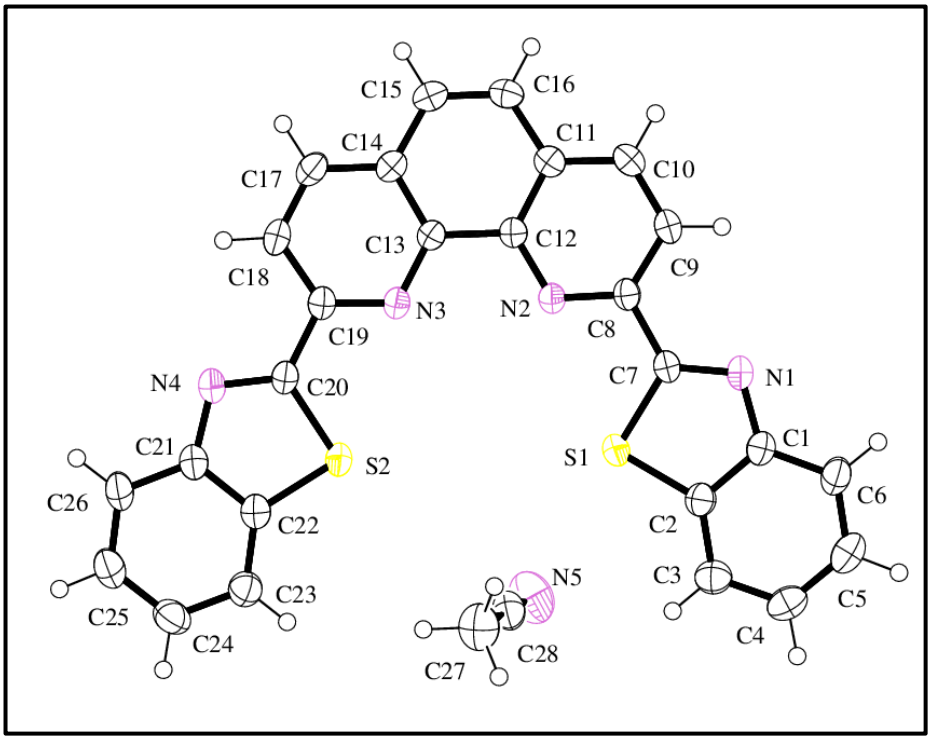

Figure 7.24: An ORTEP view of btp showing 50% probability displacement ellipsoids and the atom labeling.

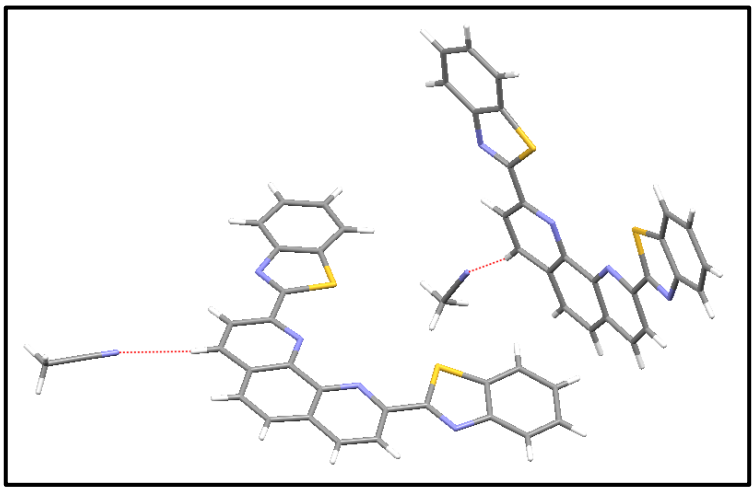

Figure 7.25: Perspective view of btp, showing the intermolecular hydrogen-bonding.

7.3.4 Synthesis and characterization of $(\mu\text{-}O)_2[Re_2O_2(btn)_2]I_2$ (1)

Compound **1** was prepared in good yield by heating *bis*(benzimidazol-2-ylethyl)sulfide (btn) and *cis*-$[ReO_2I(PPh_3)_2]$ in methanol for two hours. The slow evaporation of the mother liquor over two days led to the isolation of brown platelets. The synthesis of **1** is described by the following equation:

$$2[ReO_2I(PPh_3)_2] + 2btn \longrightarrow (\mu\text{-}O)_2[Re_2O_2(btn)_2]I_2 + 4PPh_3$$

The compound is stable in air for months and is a 2:1 electrolyte in acetonitrile (Λ_M = 256 $ohm^{-1}cm^2mol^{-1}$). It is insoluble in alcohols and acetone and soluble in acetonitrile, dichloromethane, DMF and dimethylsulfoxide.

The infra-red spectrum shows the presence of both terminal and bridging oxo groups (Figure 7.26). The band around 940 cm^{-1} is assigned to the terminal Re=O stretching vibration [20]. A strong absorption at about 692 cm^{-1} indicates the presence of bridging oxo groups in the solid state [20]. The medium intensity peak at 467 and 429 cm^{-1} is assigned to *v*(Re-N) and *v*(Re-S) respectively. The peak at 1626 cm^{-1} is due to *v*(C=N) of the coordinated benzimidazole moieties. The proton NMR spectrum (Figure 7.27) of **1** is not informative, with three complicated multiplets in the 7.50-7.85 ppm region

integrating for the 16 aromatic protons of the two btn ligands. The signal of the four imidazole protons appears as a broad four-proton singlet at 3.72 ppm. The triplets at 3.21 and 3.50 ppm each integrate for eight ethyl protons. The electronic spectrum of **1** displays a broad absorption band at 510 nm assigned to metal-to-ligand charge transfer transitions.

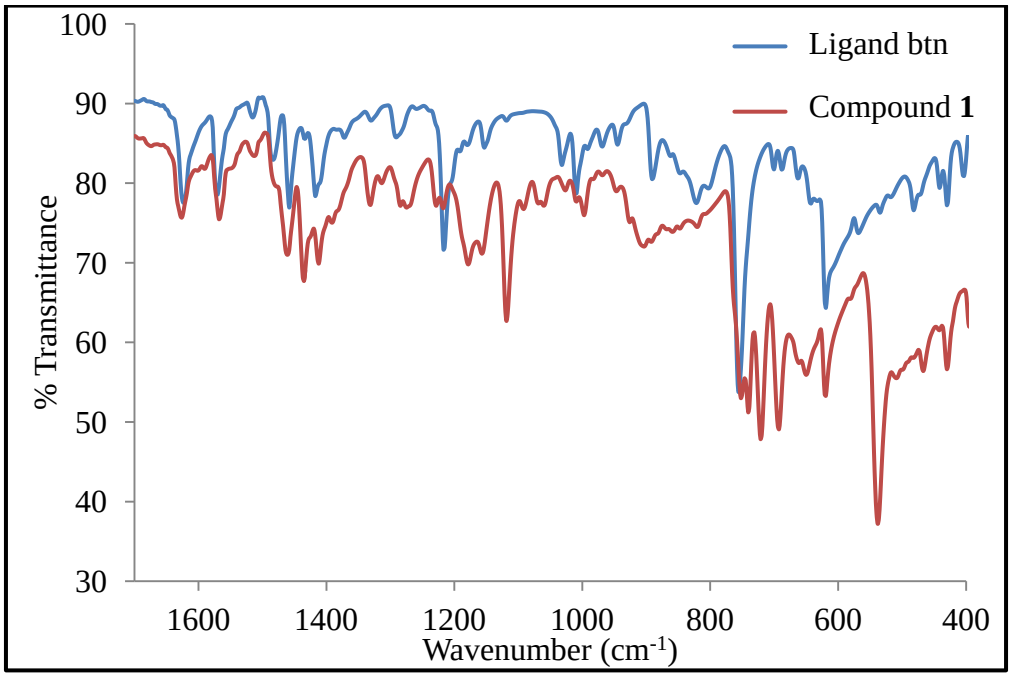

Figure 7.26: IR spectra of ligand btn and compound **1**.

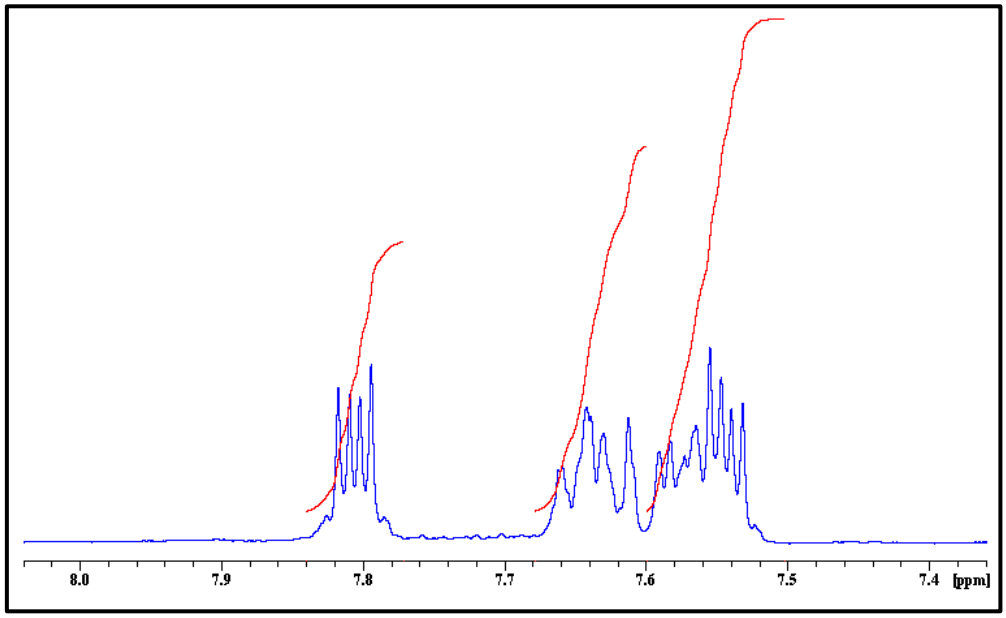

Figure 7.27: ^{1}H NMR spectrum of **1**.

The structure of **1** is shown in Figure 7.28. The dinuclear molecule is centrosymmetric, with a rhombic $(\mu\text{-}O)_2Re_2$ unit at the centre. Each oxo-bridge is unsymmetrical, with unequal Re-O distances of 1.859(2) [Re(1)-O(2)] and 2.109(3) Å [Re(1)-O(2^i)]. These distances fall in the range normally observed for oxo groups coordinated *trans* and *cis* respectively to an oxo group in oxorhenium(V) complexes [21-23], with O(2) being coordinated *trans* to the oxo group O(1), but *cis* to O(1^i). The Re–Re distance across the rhombus is 3.129(1) Å, implying no Re-Re bonding.

The asymmetric unit of **1** consists of half of the dimer $(\mu\text{-}O)_2[Re_2O_2(btn)_2]^{2+}$. Each rhenium is in a distorted octahedral environment. The basal plane is defined by the two bridging and terminal oxo groups and the sulfur atom S(1). The neutral imino nitrogen atoms N(1) and N(3) are coordinated in *trans* axial positions. Distortion from an ideal rhenium-centred octahedron results in a non-linear O(1)-Re-O(2) axis of 170.2(1)˚, and N(1)-Re-N(3) and S(1)-Re-O(2^i) angles of 176.4(1)˚ and 170.39(7)˚ respectively. The O(1)-Re-N(1) [89.1(1)˚] and O(1)-Re-N(3) [89.8(1)˚] angles are remarkably close to orthogonality, with the O(1)-Re-S(1) [95.34(9)˚] and O(1)-Re-O(2^i) [94.1(1)˚] angles very similar. Surprisingly, there is a considerable difference in the two bite angles of the tridentate ligand btn [N(1)-Re-S(1) = 85.62(9)˚; S(1)-Re-N(3) = 91.07(7)˚], which is consistent with the different Re-N bonding distances [Re-N(1) = 2.133(3) Å, Re-N(3) = 2.106(3) Å]. This phenomenon is probably due to different non-bonding interactions of the hydrogen atoms bonded to C(1) and C(10), with one hydrogen on C(1) and one on C(10) interacting with O(2) and an iodide counter-ion respectively. The Re=O(1) bond length of 1.721(2) Å is longer than those normally found for a linear monooxo-bridged O=Re-O-Re=O framework [21], but falls in the observed range for similar compounds containing a bent bridge [22]. The five-membered imidazole rings around Re(1) are π-stacked with the corresponding imidazole rings around Re(1^i), with a distance of 3.326 Å between the imidazole ring centroids (Figure 7.29).

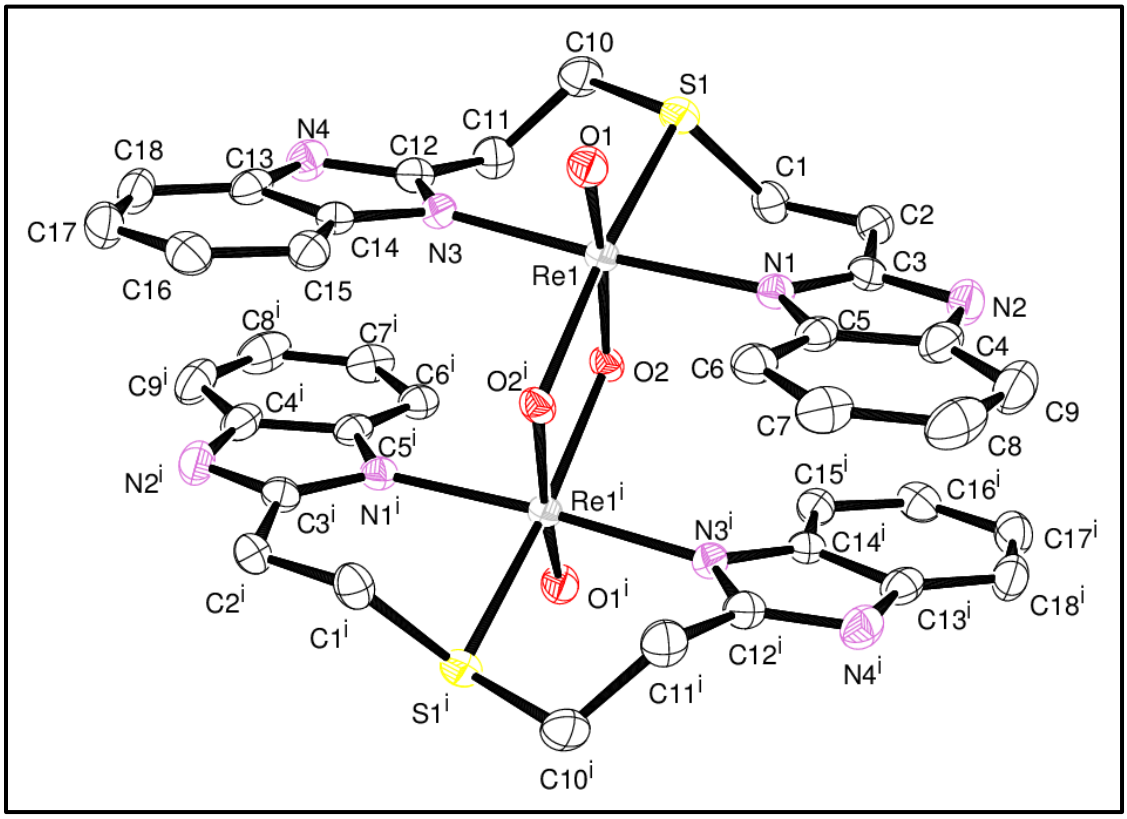

Figure 7.28: An ORTEP view of **1** showing 50% probability displacement ellipsoids and the atom labeling. Hydrogen atoms and the iodide counter-ions were omitted for clarity.

A search of the literature has revealed that **1** is the first example of a complex cation containing the $[(\mu\text{-}O)_2\{Re_2O_2\}]^{2+}$ core without a metal-metal bond. Bent dioxo-bridged oxorhenium(V) complexes are not new, but the few examples in the literature are all neutral [23]. Compound **1** would have been neutral if one of the nitrogen atoms N(2) or N(4) was deprotonated and coordinated to the metal. Deprotonation of an imidazole amino nitrogen of the bidentate chelate apb was observed in the neutral complex [ReO(Hapb)(apb)] (H_2apb = 2-(2-aminophenyl)-1-benzimidazole) [8]. Studies of oxorhenium(V) with neutral tridentate ligands only, are rare in the literature. Interestingly, it was found that the reaction of the neutral tetradentate ligand *tris*(2-pyridylmethyl)amine and its derivatives (tpa) with *trans*-$[ReOCl_3(PPh_3)_2]$ gave the products $[(\mu\text{-}O)_2\{Re_2(tpa)_2\}](PF_6)_3$, with the two rhenium atoms in the oxidation states +III and +IV [24].

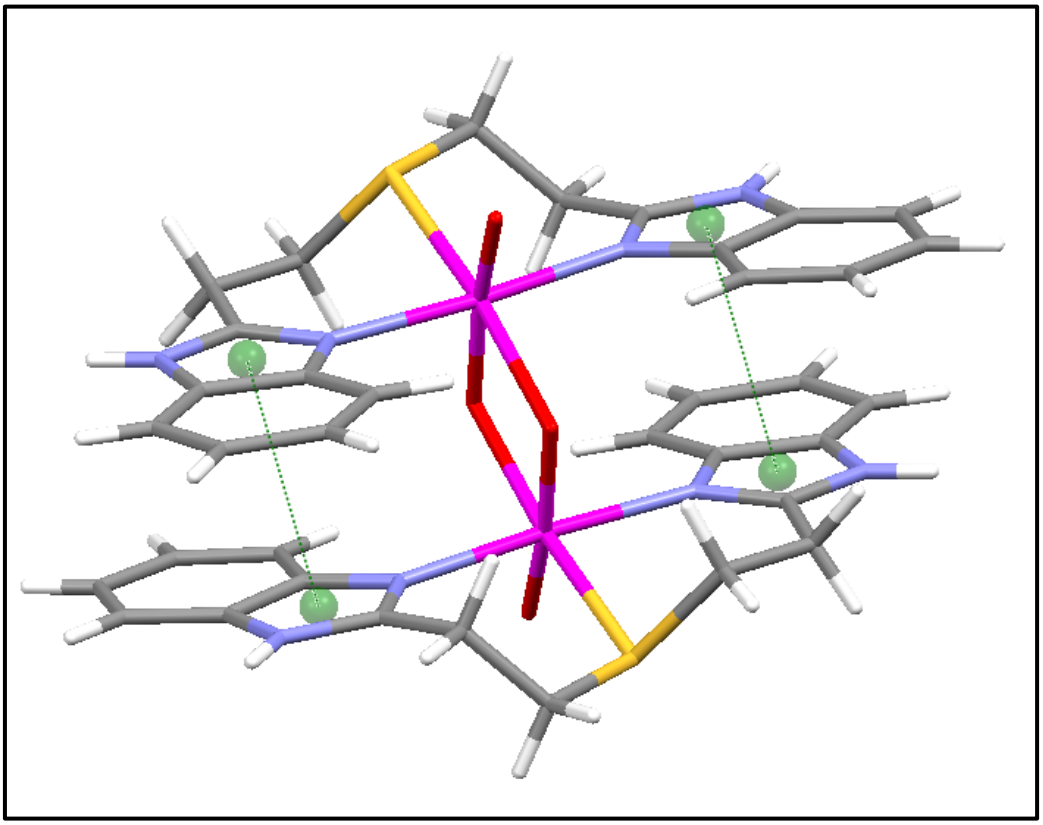

Figure 7.29: Perspective view of **1** illustrating the π-π stacking between the imidazole rings.

7.3.5 Synthesis and characterization of *fac*-[Re(CO)$_3$(bts)Br] (2)

The *fac*-[Re(CO)$_3$(bts)Br] complex was prepared by the heating of [Re(CO)$_5$Br] with two equivalents of bts in refluxing toluene under nitrogen. The reaction is described by the following equation:

$$[Re(CO)_5Br] + bts \longrightarrow \textit{fac}\text{-}[Re(CO)_3(bts)Br] + 2CO$$

The complex is soluble in a variety of solvents including acetone, acetonitrile, dichloromethane, DMF and DMSO. It is stable for months in the solid state and only for days in solution and the low molar conductivity in methanol (Λ_M = 39 ohm^{-1}cm^{2}mol^{-1}) confirms that it is a non-electrolyte.

The dominant feature of the infrared spectrum of $[Re(CO)_3(bts)Br]$ (**2**) is the presence of three intense absorption bands at 1886, 1920 and 2027 cm^{-1} ascribed to the three carbonyls of **2** in the *facial* isomer arrangement (Figure 7.30). The ^1H NMR spectra of **2** (Figure 7.31) is characterized by eight individual one-proton signals (4 doublets and 4 triplets) in the aromatic region due to the phenyl protons of the benzothiazole moieties. Unlike the free bts ligand, the proton spectrum of **2** does not display magnetic equivalence, demonstrating the unsymmetrical nature of **2** due to the bidentate coordination of bts in the complex. In addition, two four-proton multiplets are found around 2.00 ppm, ascribed to the ethyl protons. Complex **2** displays a broad low energy absorption band at 428 nm. Similar bands in this region have previously been assigned to metal-to-ligand charge transfer (MLCT) $d_\pi(Re) \rightarrow \pi^*$ transitions [25].

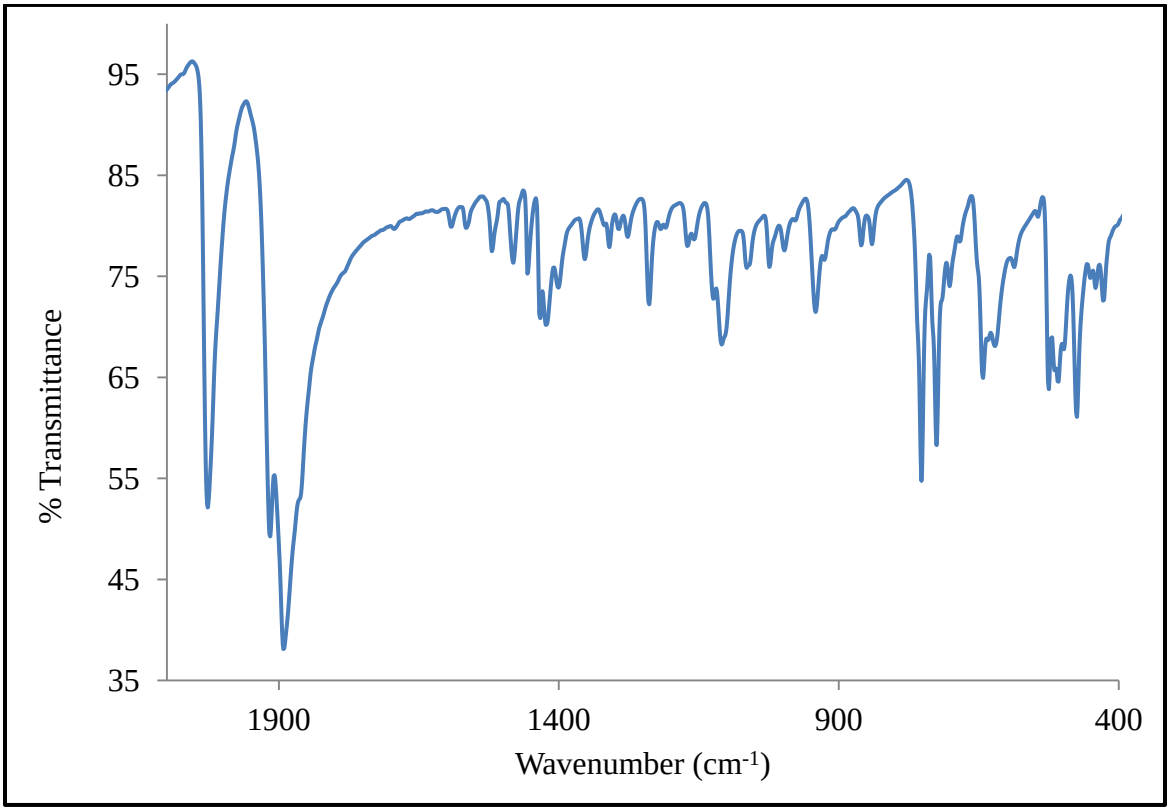

Figure 7.30: IR spectrum of complex **2**.

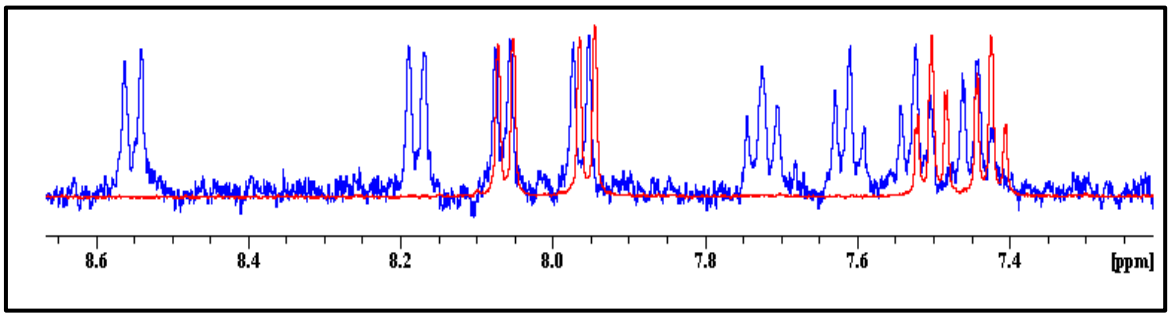

Figure 7.31: Overlay ^{1}H NMR spectra of ligand bts (red) and complex **2** (blue).

Brown needles of **2**, suitable for X-ray crystallography, were obtained from the slow evaporation of the reaction mixture. The packing in the unit cell shows discrete, monomeric and neutral [Re(CO)$_3$(bts)Br] units, with no intermolecular contacts shorter than the Van der Waals' radii sum. The rhenium(I) atom lies in a distorted octahedral environment, with the bromide, thiazole imino nitrogen and sulfur donor atoms of bts in a *facial* arrangement, imposed by the *fac*-[Re(CO)$_3$]$^+$ core (Figure 7.32). The ligand bts therefore acts as a neutral bidentate chelate. The Re-C(carbonyl) bond distances [1.896(5)-1.960(5) Å] fall in the range observed [1.890(2)-1.928(2) Å] for similar complexes [26]. The Re-N(1) bond length of 2.222(3) Å is typical for Re-N(imino) bonds of coordinated thiazoles and imidazoles [27].

The distortion from octahedral ideality mainly results from the *trans* angles, which fall in the range 175.1(1)-177.2(1)˚. These distortions are the result of the constraints imposed by the bidentate coordination of the ligand bts, which has a bite angle of 88.66(9)˚ [N(1)-Re-S(1)]. The steric repulsion between the bromide and the equatorially coordinated sulfur atom [Br(1)-Re-S(1) = 93.24(3)˚] is substantially larger than between the bromide and the axial nitrogen [Br(1)-Re-N(1) = 86.96(8)˚]. The C(4)-S(1)-C(13) bond angle of 101.7(2)˚ is markedly smaller than would be expected for a sp^3 hybridized sulfur atom, with the Re-N(1)-C(8) angle of 123.7(3)˚ close to expectation for a sp^2 hybridized imine nitrogen.

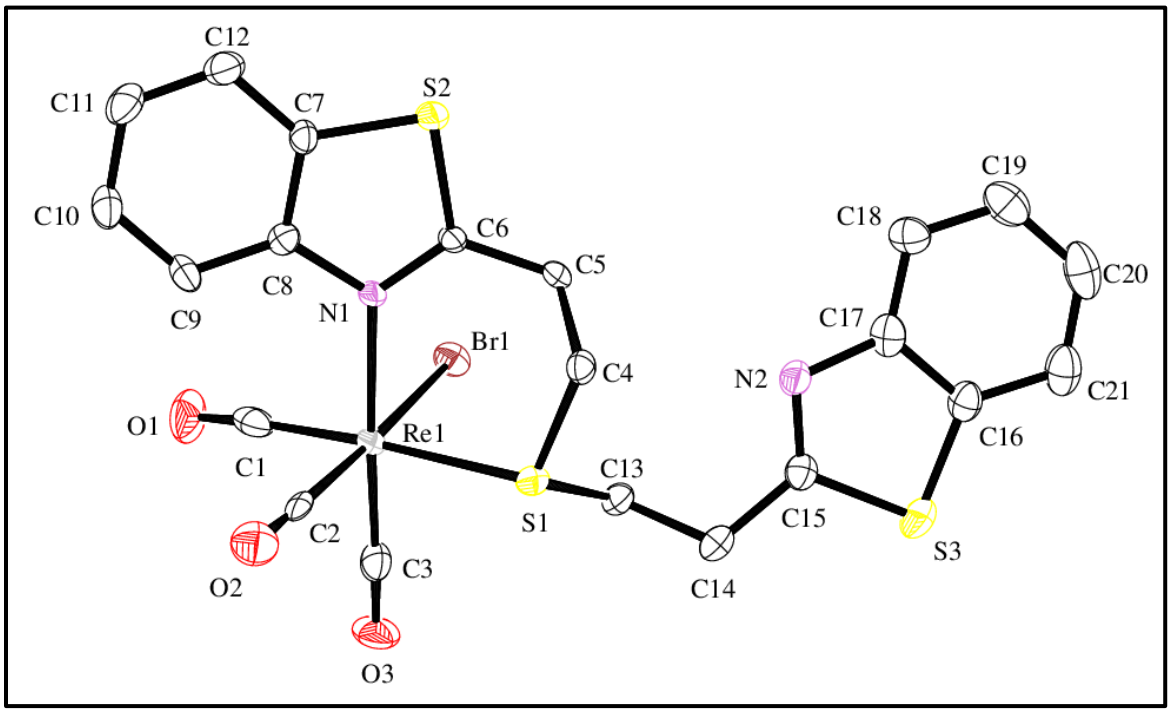

Figure 7.32: An ORTEP view of **2** showing 50% probability displacement ellipsoids and the atom labeling. Hydrogen atoms were omitted for clarity.

Complex **2** is unique in the sense that it contains both a coordinated and a free benzothiazole group. This result may have implications in the design of rhenium(I) and technetium(I) radiopharmaceuticals, with the uncoordinated thiazole likely to have a different biological activity than the coordinated one. Coordination of bts as a tridentate chelate would have led to the formation of the complex salt *fac*-[$Re(CO)_3$(bts)]Br.

7.3.6 Synthesis and characterization of (μ-dbt)$_2$[$Re(CO)_3$]$_2$ (3)

The reaction of Hdbt with [$Re(CO)_5Cl$] in toluene gave a yellow product of formulation (μ-dbt)$_2$[$Re(CO)_3$]$_2$ in good yield. Each ligand in the dimeric molecule of **3** coordinates as a bidentate monoanionic chelate to one rhenium atom and monodentately to the second rhenium atom.

$$2[Re(CO)_5Cl] + 2Hdbt \longrightarrow (\mu\text{-dbt})_2[Re(CO)_3]_2 + 2HCl + 4CO$$

Complex **3** is soluble in dichloromethane, acetone and DMF and only partially soluble in alcohols, acetonitrile and toluene. It is stable for days in solution and for months in the solid state.

The IR spectrum of **3** (Figure 7.33) displays three peaks at 1873, 1909 and 2017 cm^{-1} due to *ν*(C=O). The Re-N stretches are found at 498 and 519 cm^{-1}. The peak at 395 cm^{-1} is due to the Re-S stretch. The *ν*(C=N) of the coordinated benzothiazole ligand is found at 1633 cm^{-1} and is at a lower frequency relative to that of the free Hdbt ligand which occurs at 1644 cm^{-1}. The ^{1}H NMR spectrum of **3** (Figure 7.34) emphasizes the symmetry within the molecule. The aromatic region consists of four two-proton doublets and four two-proton triplets. A broad two-proton singlet is observed at 3.34 ppm due to the protons of the amine nitrogens.

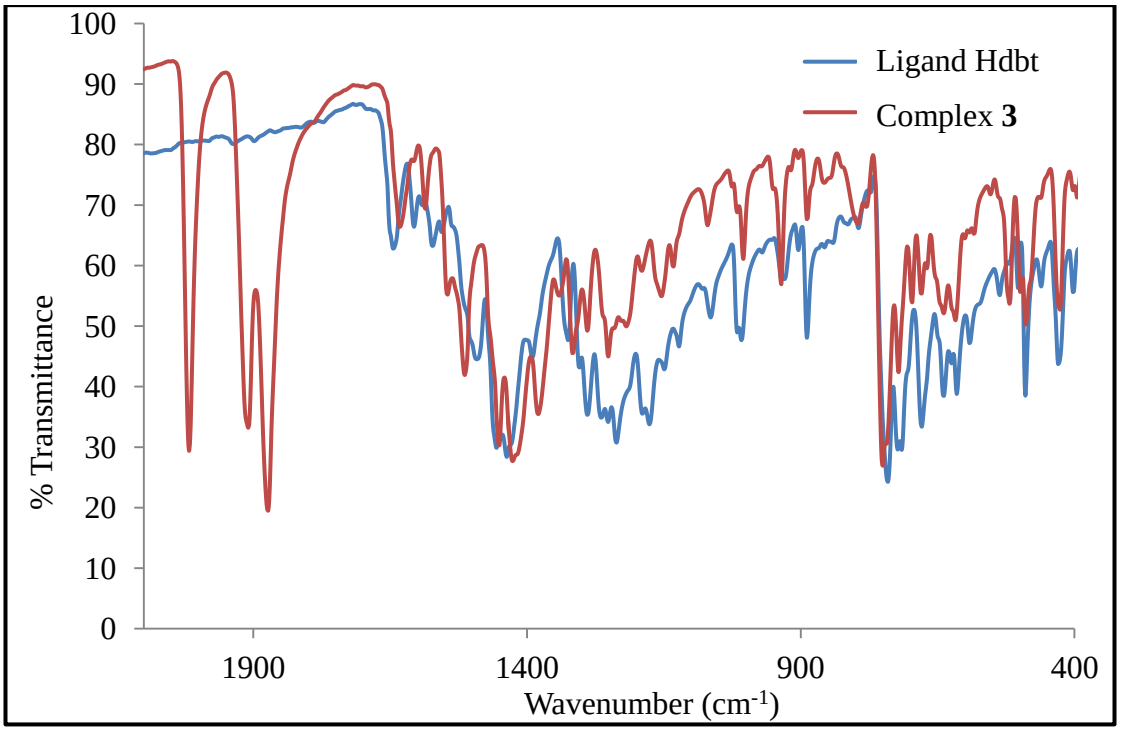

Figure 7.33: Overlay IR spectra of ligand Hdbt and complex **3**.

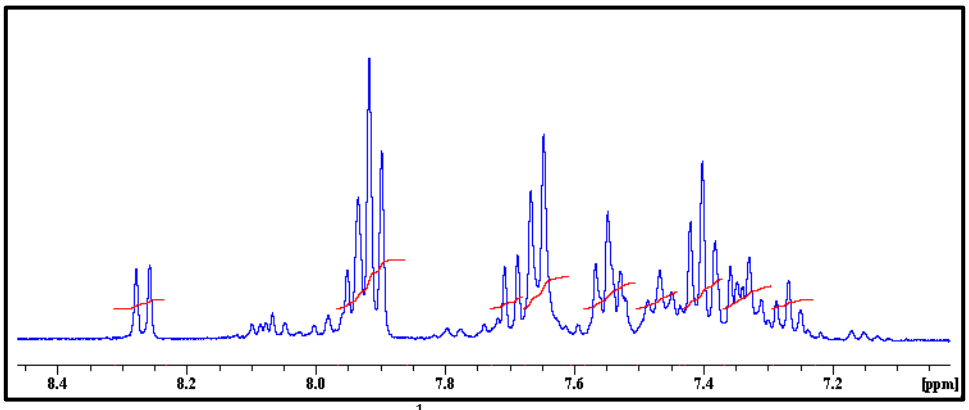

Figure 7.34: ^{1}H NMR spectrum of **3**.

The UV-Vis spectrum of **3** (Figure 7.35) in DMF displays several high energy bands in the 300-400 nm region. These bands are assigned to intraligand ($\pi \rightarrow \pi^{*}$) transitions of the coordinated dbt moeity and are similar to the bands observed for the free Hdbt ligand. No metal-to-ligand or d-d transitions were observed. The emission spectrum (λ_{ex} = 350 nm) of an ethanol solution of **3** at room temperature shows a broad band at 529 nm (Figure 7.34). This emission results from ligand-centred $\pi^* \rightarrow \pi$ relaxations [28-30].

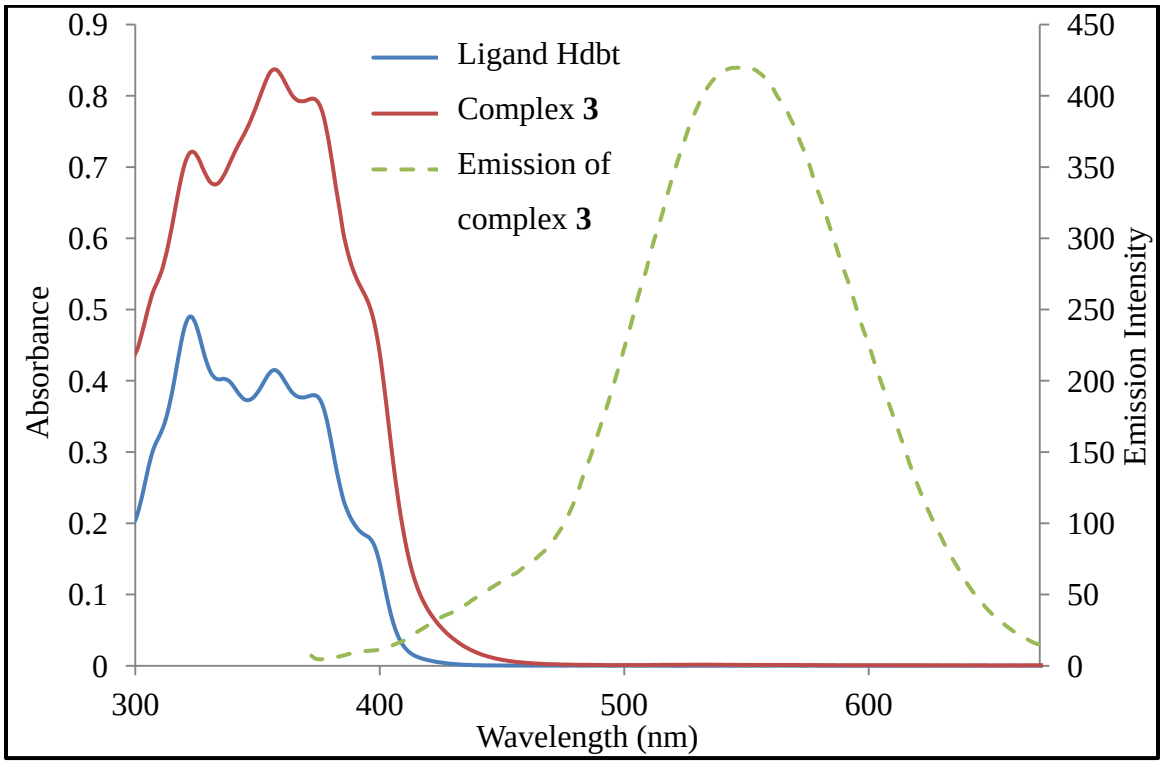

Figure 7.35: Overlay UV-Vis spectra of ligand Hdbt (blue) and complex **3** (red) and emission spectrum of complex **3** (green dashed line).

The structure of **3** is shown in Figure 7.36. The dimeric molecule consists of two *fac*-$[Re(CO)_3]^+$ units bridged by two dbt chelates. Each dbt molecule acts as a tridentate ligand, with bidentate N,S-coordination to one Re(I) centre and monodentate coordination to the second metal *via* a benzothiazole nitrogen. Each Re(I) atom is at the centre of a distorted octahedron, and is coordinated to three carbonyls in a *facial* arrangement, two benzothiazole imino nitrogen atoms and a thiolic sulfur atom. The distortion from octahedral ideality around each metal centre is reduced considerably by the bite angles N(11)-Re(1)-S(12) = 81.9(2)˚ and N(21)-Re(2)-S(22) = 80.8(2)˚, brought about by the six-membered chelate rings, and the S(12)-Re(1)-N(24) [92.0(2)˚] and S(22)-Re(2)-N(14) [91.8(2)˚] angles.

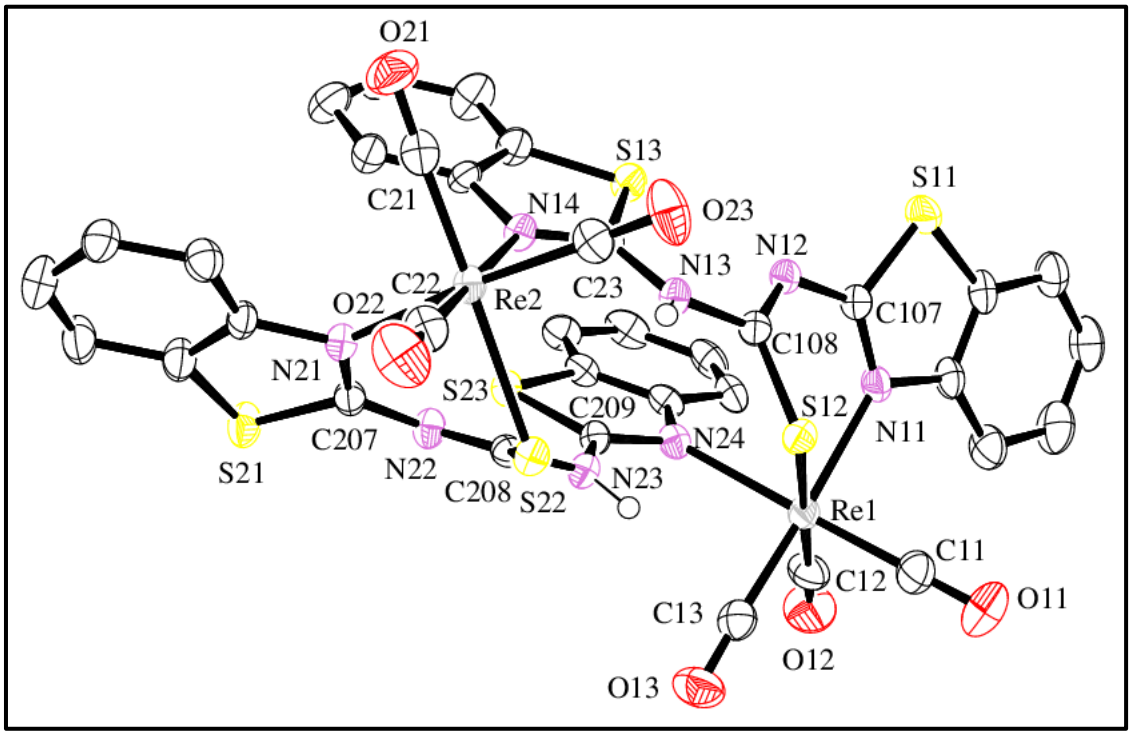

Figure 7.36: An ORTEP view of **3** showing 50% probability displacement ellipsoids and the atom labeling. Aromatic hydrogen atoms were omitted for clarity.

Each dbt ligand is monoanionic, with a thiolate sulfur atom. The N(12)-C(108) [1.29(1) Å] and N(22)-C(208) [1.29(1) Å] bonds are double, the N(13)-C(108) [1.37(1) Å] and N(23)-C(208) [1.39(1) Å] bonds are single, and the S(12)-C(108) [1.735(8) Å] and S(22)-C(208) [1.737(9) Å] bonds are single. The six Re-(carbonyl) bond distances fall in the

range 1.89(1)-1.92(1) Å and are similar to the Re-C bonds for similar complexes [26, 31]. The Re(1)-N(11) and Re(2)-N(21) bond lengths [2.225(6) Å average] are noticeably shorter than the Re(1)-N(24) and Re(2)-N(14) ones [2.253(7) Å average].

7.3.7 Synthesis and characterization of (μ-mbt)$_2$[Re(CO)$_3$]$_2$ (4)

The neutral complex (μ-mbt)$_2$[Re(CO)$_3$]$_2$ (**4**) was prepared by heating [Re(CO)$_5$Cl] and a twofold molar excess of 1-(benzothiazol-2-ylidene)-3-methylthiourea **(**Hmbt) under reflux in toluene. The X-ray crystal structure of (μ-mbt)$_2$[Re(CO)$_3$]$_2$ shows that bridging between the two metal centres occurs *via* the two thiolic sulfur atoms of the two mbt ligands. One mbt ligand is also coordinated *via* a benzothiazole nitrogen atom to a rhenium(I) atom, with the second mbt ligand attached to the metal *via* a thiourea imino nitrogen.

$$2[Re(CO)_5Cl] + 2Hmbt \longrightarrow (\mu\text{-}mbt)_2[Re(CO)_3]_2 + 4CO + 2HCl$$

Complex **4** is stable in air and a non-electrolyte in DMF. It is soluble in a variety of solvents including alcohols, DMF and dichloromethane and is insoluble in acetonitrile.

The IR spectrum of **4** (Figure 7.37) displays two intense peaks in the carbonyl stretching region at 1894 cm^{-1} and 2018 cm^{-1}. The presence of an imine entity (CH=N) in the complex is intimated by a strong peak at 1612 cm^{-1}. Peaks at 758 and 401 cm^{-1} are indicative of *ν*(C-S) and *ν*(Re-S) respectively.

The ^{1}H NMR spectrum of **4** displays the signals of the nitrogen protons [N(13)H and N(23)H] of the coordinated mbt ligands as broad singlets at 9.78 and 9.18 ppm respectively. The aromatic protons of the mbt chelates appear in the 7.30-8.00 ppm region as four one-proton doublets and two two-proton multiplets. The two three-proton singlets at 2.88 and 3.12 ppm are ascribed to the methyl protons C(29)H$_3$ and C(19)H$_3$ respectively. The electronic spectrum of **4** is dominated by an intense band at 308 nm

accompanied by a less intense shoulder at 378 nm. The excitation of an ethanol solution of **4** at various excitation wavelengths produced no emission transitions.

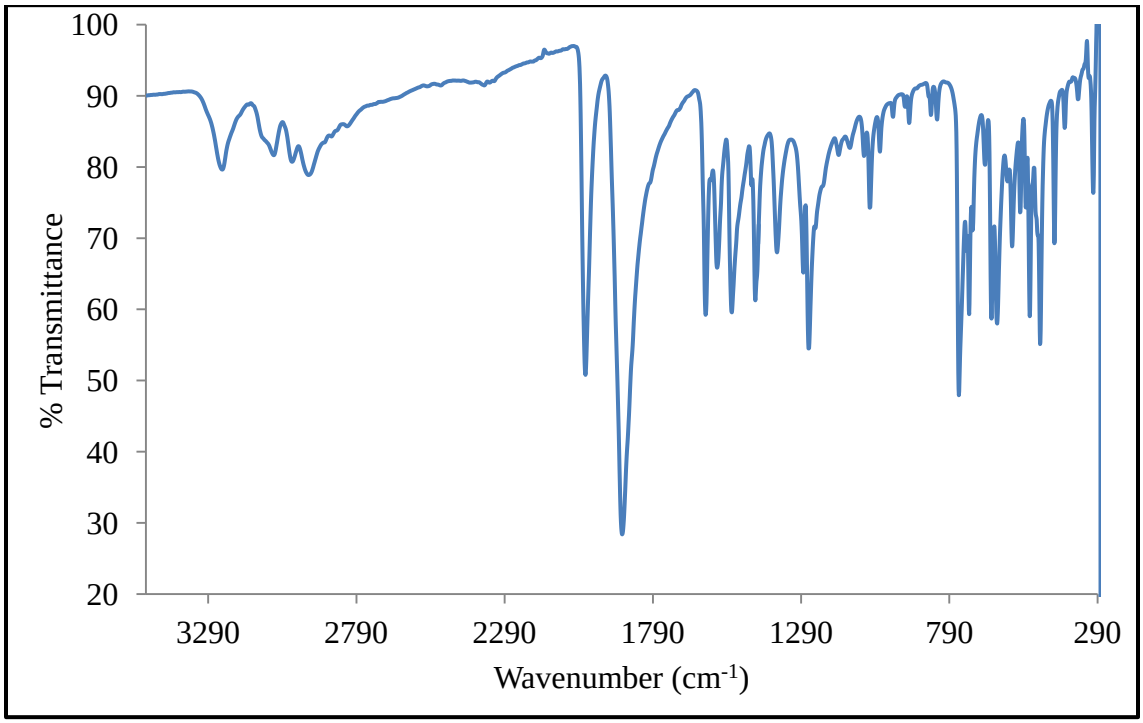

Figure 7.37: IR spectrum of complex **4**.

Colourless crystals with the formulation of **4.**2MeOH were obtained from the recrystallization with a 1:1 (*v/v*) methanol/dichloromethane mixture. The packing in the unit cell shows discrete, dimeric and neutral $[Re(CO)_3(mbt)]_2$ units. Each rhenium(I) atom lies in a distorted octahedral environment, with a nitrogen and two bridging thiolic sulfur atoms in a *facial* arrangement, imposed by the *fac*-$[Re(CO)_3]^+$ core (Figure 7.38). Both mbt ligands act as monoanionic tridentate ligands with coordination to the metals through a nitrogen and a bridging sulfur atom. However, different nitrogen atoms of the two chelates are used for coordination. The Re(I) is coordinated to the benzothiazole nitrogen N(11), forming a six-membered metallocycle, and Re(2) is bonded to the imine nitrogen N(22), giving a four-membered chelate ring.

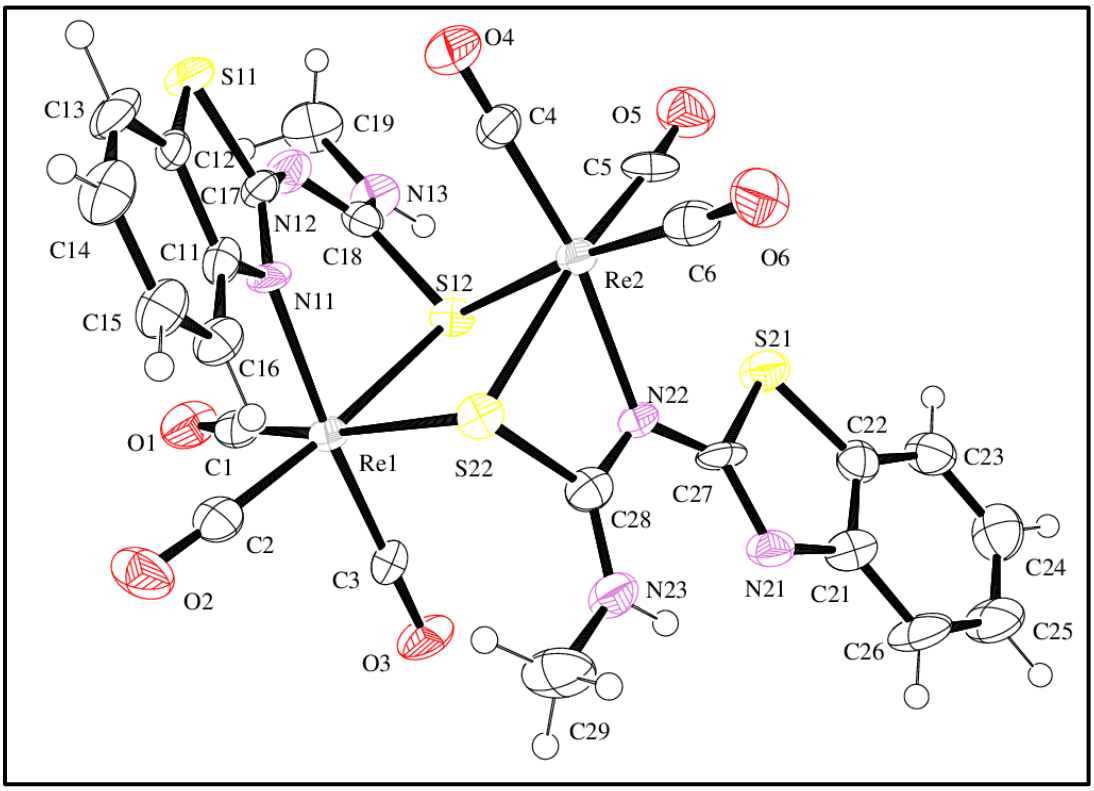

Figure 7.38: An ORTEP view of **4** showing 50% probability displacement ellipsoids and the atom labeling.

The dinuclear molecule is characterised by a rhombic $(\mu\text{-}S)_2Re_2$ at the centre. Each sulfur-bridge is unsymmetrical, with unequal Re-S distances [Re(1)-S(12) = 2.481(2), Re(1)-S(22) = 2.572(3), Re(2)-S(12) = 2.516(2), Re(2)-S(22) = 2.550(2) Å]. These distances fall in the range normally observed for thiolic sulfur atoms coordinated to a *fac*-$[Re(CO)_3]^+$ core [31]. The Re-Re distance across the rhombus is 3.785 Å, implying no Re-Re bonding. The Re-C(carbonyl) bond distances [1.90(1)-1.93(1) Å] fall in the range observed [1.890(2)-1.928(2) Å] for similar complexes [26, 31]. The Re-N bond lengths [Re(1)-N(11) = 2.205(9) Å, Re(2)-N(22) = 2.19(1) Å] are typical for Re(I)-N(imino) bonds [27]. The distortion from octahedral ideality is more severe around Re(2) [*trans* angles S(12)-Re(2)-C(6) = 172.8(4)˚, N(22)-Re(2)-C(4) = 166.6(4)˚, S(22)-Re(2)-C(5) = 167.9(3)˚] than around Re(1) [*trans* angles N(11)-Re(1)-C(3) = 175.0(4)˚; S(12)-Re(1)-C(2) = 175.2(4)˚; S(22)-Re(1)-C(1) = 170.8(3)˚]. This is mainly the result of the constraints imposed by the smaller bite angle S(22)-Re(2)-N(22) of 65.1(3)˚ compared to N(11)-Re(1)-S(12) of 83.7(2)˚.

The packing of the molecules in the unit cell is complemented by intramolecular hydrogen-bonds [N(23)-H(23A)•••N(21) and C(29)-H(29C)•••S(22)] (Figure 7.39). The methanol solvent of crystallization is involved in three intermolecular hydrogen-bonds with a molecule of **4** (Table 7.3).

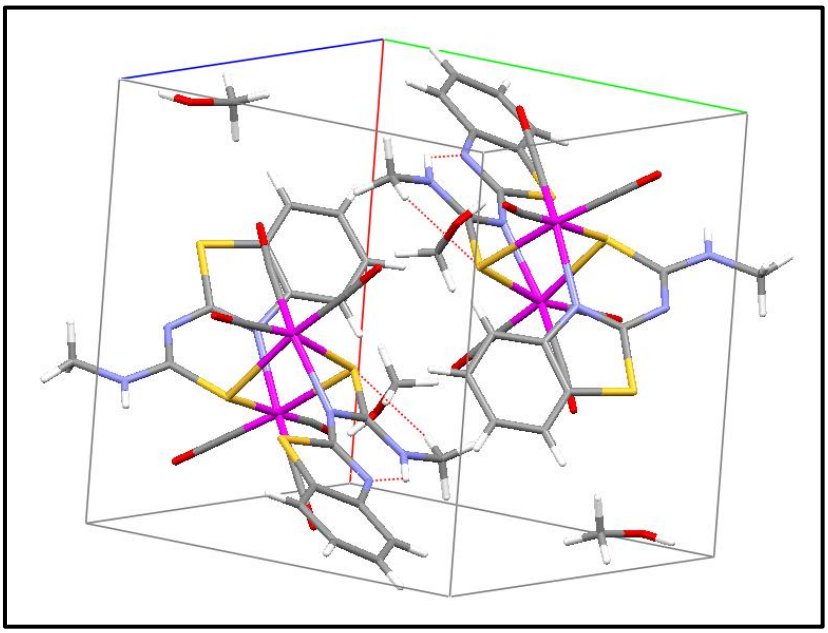

Figure 7.39: Packing diagram in the unit cell of **4**, showing the intramolecular hydrogen-bonds (red dashed lines).

Table 7.3: Hydrogen-bond distances (Å) and angles (˚) in **4**.

D-H•••A	D-H	H•••A	D•••A	D-H•••A
N(23)H(23A)•••N(21)	0.88	2.04	2.70(1)	131
C(29)H(29C)•••S(22)	0.98	2.66	3.14(2)	111
N(13)H(13A)•••O(32)	0.88	1.98	2.84(2)	167
C(32)H(32A)•••S(21)	0.98	2.87	3.81(2)	159
C(32)H(32B)•••S(2)	0.98	2.51	3.44(2)	159

The different coordination modes of the two mbt chelates in the structure are surprising and unusual. The formation of a four membered chelate ring is rare in the coordination

chemistry of transition metals, especially with the logical option available to Re(2) to coordinate to N(21), rather than N(22), in order to reduce angular strain and distortion around the metal. No similar examples could be found in the literature. The major difference in the coordination behaviour of the ligands mbt (in **4**) and dbt (in **3**) is that the thiolic sulfur atom does not act as a bridge between the two metal centres in the latter.

7.3.8 Synthesis and characterization of $[ReCl_2(bte)(PPh_3)_2]Cl$ (5)

The coordination behaviour of 1-(benzothiazol-2-ylidene)-3-methylthiourea (Hmbt) with the $[Re^{V}O]^{3+}$ core was investigated by reacting a twofold molar excess of Hmbt with *trans*-$[ReOCl_3(PPh_3)_2]$ in ethanol. The reaction unexpectedly led to the formation of the rhenium(III) complex salt $[ReCl_2(bte)(PPh_3)_2]Cl$ (bte = (benzothiazole-2-yl)-*N*-ethylidenemethanamine). The low reaction yield of the product seems to indicate that **5** may be the result of a disproportionation reaction.

The formation of bte from Hmbt is surprising and an explanation for a plausible reaction pathway would be highly speculative. However, it is thought that a methanol solvent molecule, as well as an oxygen atom (dissociated from the $[Re^{V}O]^{3+}$ starting material) could have played a role in the transformation of the Hmbt ligand to form bte. The bte ligand acts as a bidentate neutral chelate forming a five-membered chelate ring.

Compound **5** is stable in air and in solution. It has poor solubility in most organic solvents and is only soluble in dichloromethane and DMF. It is a 1:1 electrolyte in DMF. The microanalytical data of **5** is in good agreement with its formulation.

In the infrared spectrum of **5** (Figure 7.40), the benzothiazole and imine stretching frequencies [ν(C=N)] appear at 1491 and 1584 cm^{-1} respectively. There is no intense peak in the 890-1020 cm^{-1} region that can be ascribed to ν(Re=O). The medium intensity peaks at 393 and 430 cm^{-1} are assigned to the Re-N stretching frequencies.

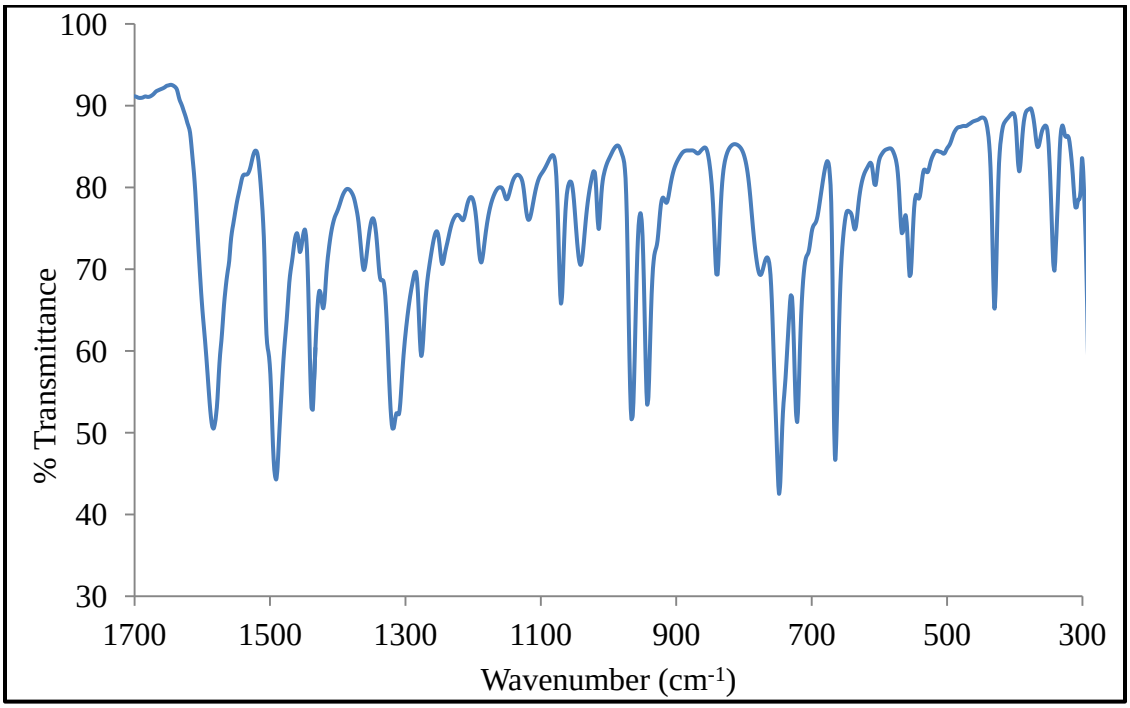

Figure 7.40: IR spectrum of complex **5**.

The ^{1}H NMR spectrum of **5** consists of poorly resolved peaks with paramagnetic shifts and line broadening of the signals. The signal furthest downfield at 9.78 ppm is assigned to the methine proton. The signals of the aromatic protons of the bte chelate occur as two one-proton doublets (at 8.19 and 8.53 ppm) and a two-proton multiplet (in the 7.78-7.92 ppm region). The multiplet in the 7.10-7.69 ppm region integrates for the 30 protons of the two triphenylphosphines. The UV-Vis spectrum of **5** in DMF shows intraligand charge transfer bands at 310 and 328 nm. A ligand-to-metal charge transition is observed at 384 nm.

The molecular structure of the complex cation of **5** is illustrated in Figure 7.41. The rhenium(III) atom lies at the centre of a distorted octahedron. The basal plane is defined by the two chloride atoms and two imino nitrogen atoms. The two phosphorus atoms are in *trans* axial positions. Distortions from octahedral environment results in a non-linear P(1)-Re-P(2) axis of 176.87(8)˚, with the *trans* angles Cl(1)-Re-N(2) = 170.8(5)˚ and Cl(2)-Re-N(1) = 171.5(3)˚ also deviating from linearity. The rhenium atom lies 0.028 Å out of the mean equatorial plane towards P(2). The bte ligand forms a five-membered chelate ring with the N(1)-Re(1)-N(2) bite angle of 76.8(6)˚. The two chlorides are in *cis*

sites relative to each other [Cl(1)-Re-Cl(2) = 94.2(1)˚]. The Re-Cl bond distances are different [Re-Cl(1) = 2.435(3) Å and Re-Cl(2) = 2.341(3) Å] and within the range [2.34(2)-2.44(2) Å] found for rhenium complexes containing phoshine ligands [32].

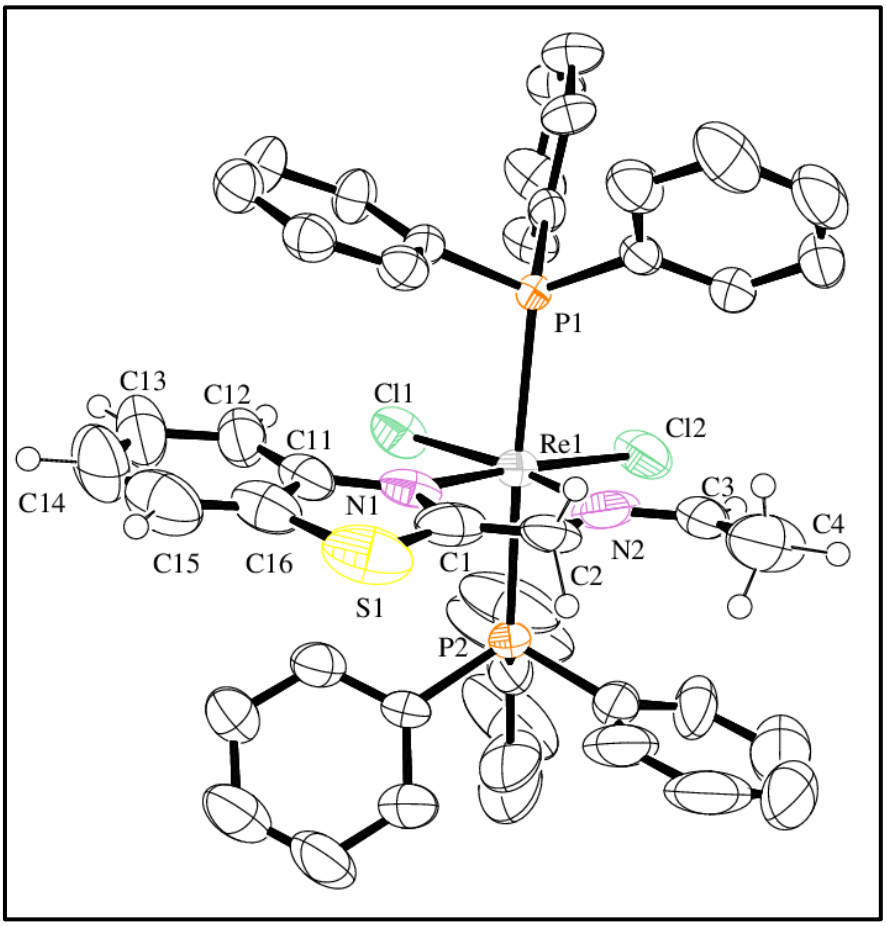

Figure 7.41: An ORTEP view of **5** showing 50% probability displacement ellipsoids and the atom labeling. Aromatic hydrogens of the triphenylphoshine rings are omitted for clarity.

The Re-N(2) = 2.09(1) Å bond length falls within the range observed [2.05-2.12 Å] for the Re-N(imine) bonds [33], while the Re-N(1) bond length is slightly longer at 2.149(9) Å. The N(2)-C(3) bond length of 1.29(2) Å (a double bond) and the C(2)-N(2)-C(3) = 120(1)˚ leave no doubt that N(2) is an sp^2-hybridized imino coordinated nitrogen. The C-C bond lengths in the C(11)-C(16) ring [average = 1.38(2) Å] are typical for aromatic

systems. All the hydrogen-bonds in the molecules involve C-H bonds, and as such will not be discussed.

7.3.9 Synthesis and characterization of $[Re(CO)_3(bmb)][Re_2(CO)_6Cl_3]$ (6)

The reaction of the potentially tridentate ligand 2,2'-(oxy*bis*(methylene)) *bis*(benzimidazole) (bmb) with $[Re(CO)_5Cl]$ in toluene under nitrogen produced $[Re(CO)_3(bmb)][Re_2(CO)_6Cl_3]$ (**6**), as described by the equation:

$$3[Re(CO)_5Cl] + bmb \longrightarrow [Re(CO)_3(bmb)][Re_2(CO)_6Cl_3] + 6CO$$

The complex salt **6** exhibits poor solubility in polar and non-polar organic solvents and only dissolves in DMF and dimethylsulfoxide upon heating. It is air stable, diamagnetic, and is a 1:1 electrolyte in DMF (Λ_M = 75 $ohm^{-1}cm^2mol^{-1}$). Transparent crystals of **6** were produced by allowing a toluene solution of the compound to slowly evaporate at room temperature.

The infra-red spectrum of **6** displays peaks in the 1880-2130 cm^{-1} region due to ν(C=O) of the nine carbonyl groups present in the compound. The ν(C=N) peak observed at 1628 cm^{-1} is at an identical position as that of the free ligand. The Re-N stretch occurs as a medium intensity peak at 483 cm^{-1}. The ^{1}H NMR spectrum of **6** displays two quartets at 7.57 and 7.21 ppm integrating for four protons each (Figure 7.42). The ethyl protons [C(1)H_3 and C(2)H_3] appear as a singlet at 4.85 ppm and the broad two-proton singlet at 4.10 ppm is due to the protons of the imidazole nitrogens N(2) and N(4).

The electronic absorption and emission spectra of **6** is shown in Figure 7.43. Two bands are visible in the UV-Vis spectrum at 324 and 359 nm. These high energy bands are due to intraligand transitions occurring in the coordinated ligand. Upon excitation (λ_{ex} = 300 nm) of an ethanol solution of **6** at room temperature, an emission band was observed at 375 nm due to ligand centred $\pi^* \rightarrow \pi$ relaxations.

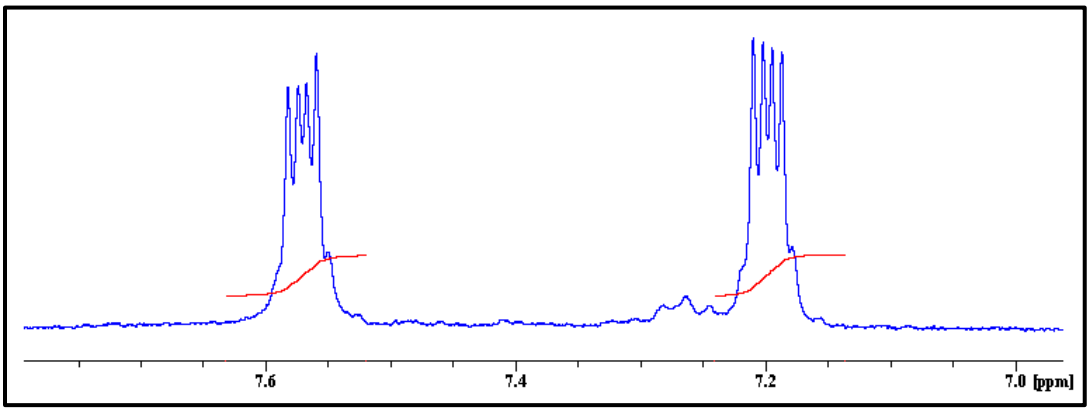

Figure 7.42: ^{1}H NMR spectrum of **6**.

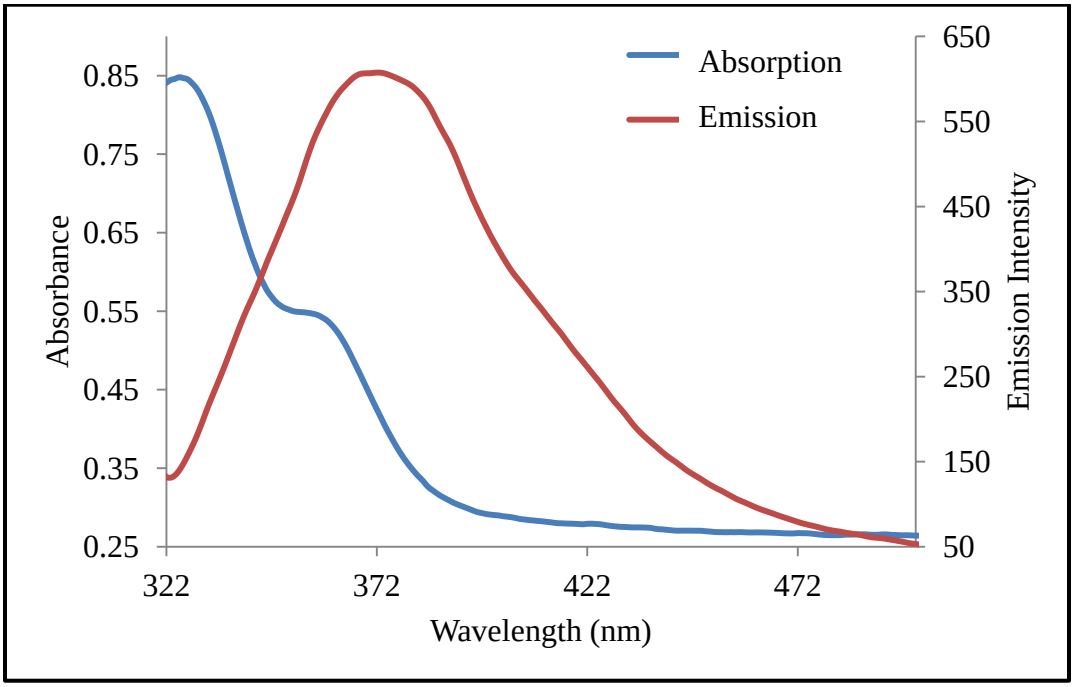

Figure 7.43: UV-Vis and emission spectra of **6**.

The X-ray results show that the tridentate bmb ligand is coordinated to the metal *via* two benzimidazole nitrogen atoms N(1) and N(3) and the ether oxygen O(1) (Figure 7.44). The rhenium atom lies in a distorted octahedral environment with the three carbonyl donors in a *facial* orientation. The distortion from an ideal octahedral geometry is due to the *trans* angles N(3)-Re(1)-C(50) = 172.7(2)˚, N(1)-Re(1)-C(52) = 169.8(2)˚ and O(1)-Re(1)-C(51) = 174.6(1)˚ deviating from linearity. This deviation is caused by the constraints produced by the tridentate chelation of the bmb ligand which forms two 5-

membered chelate rings with bite angles of N(1)-Re(1)-O(1) = 75.1(1)˚ and N(3)-Re(1)-O(1) = 74.9(1)˚. In order for the ligand to be tridentately coordinated to the metal in a *facial* orientation, the two benzimidazole moieties twists towards one another, with the ligand folded at the central oxygen atom. The benzimidazole rings form a dihedral angle of 65.64˚ with each other (Figure 7.45).

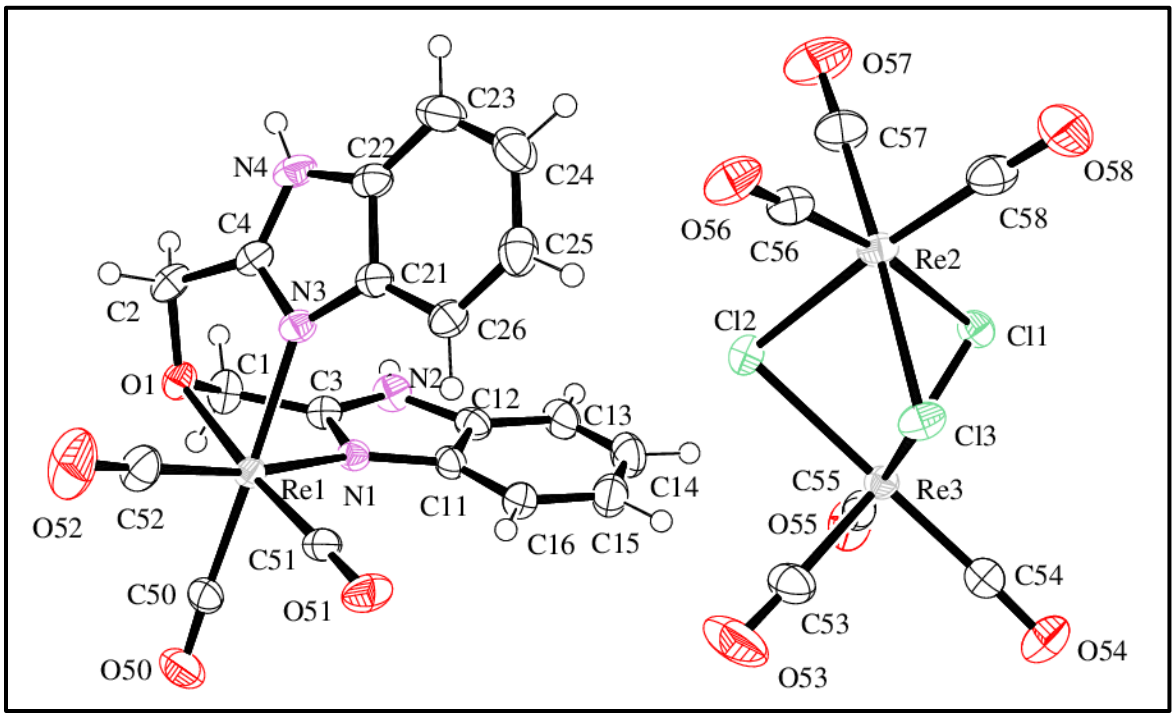

Figure 7.44: An ORTEP view of **6** showing 50% probability displacement ellipsoids and the atom labeling.

The two Re(1)-N bond lengths are similar [average = 2.158(3) Å] and are typical of Re^{I}-$N_{(imidazole)}$ bonds [34], while the Re(1)-O bond length is longer [Re-O(1) = 2.266(3) Å]. Two Re(1)-C bond lengths are similar (Re(1)-C(50) = 1.933(4) Å, Re(1)-C(52) = 1.929(4) Å) with the third being shorter (Re(1)-C(51) = 1.873(4) Å), due to the smaller *trans* effect of the oxygen O(1) atom compared to the nitrogen atoms N(1) and N(3). The C(1)-O(1)-C(2) bond angle of 114.3(3)˚ is larger than would be expected for a sp^3 hybridized oxygen atom. The Re-N(1)-C(11) and Re-N(3)-C(21) angles of 136.4(3)˚ and 137.1(3)˚ respectively are larger than that expected for sp^2 hybridized imine nitrogens.

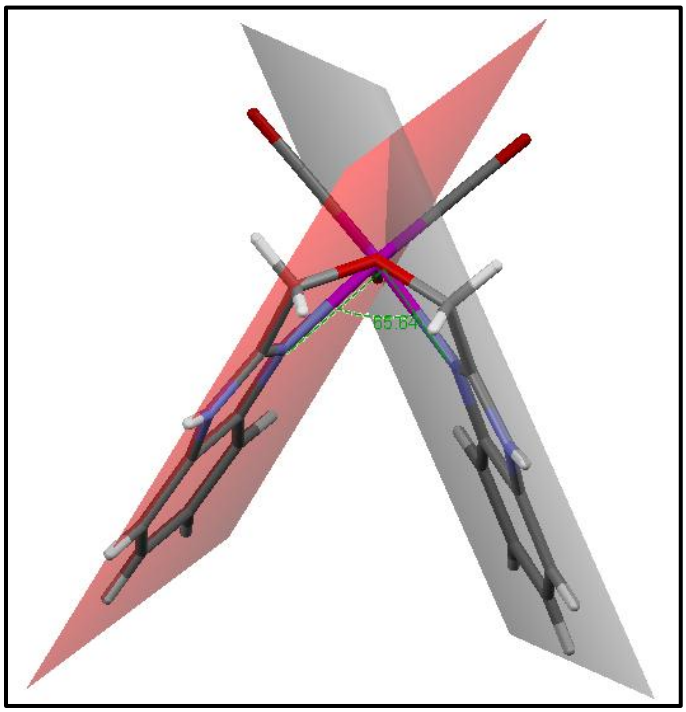

Figure 7.45: Perspective view of $[Re(bmb)(CO)_3]^+$ depicting the intersection of the planes through the benzimidazole rings.

Surprisingly, the $[Re(bmb)(CO)_3]^+$ cation in the complex salt **6** is accompanied by the trichloro bridged $[Re_2Cl_3(CO)_6]^-$ as the counter-anion, instead of the expected chloride ion. The presence of the $[Re_2Cl_3(CO)_6]^-$ anion as a counter-ion to rhenium complexes is rare with only a few known examples in the literature. For example, the reaction of *hexakis*(3,5-dimethylpyrazolyl)cyclotriphosphazene $[P_3N_3(3,5\text{-}Me_2Pz)_6]$ with $[Re(CO)_5Cl]$ in toluene led to the formation of *fac*-$[Re(CO)_3\{P_3N_3(3,5\text{-}Me_2Pz)_6\}][Re_2Cl_3(CO)_6]$ [35]. $[Re(CO)_5Cl]$ is known to undergo dimerization in aromatic solvents like hexamethylbenzene $[C_6Me_6]$ resulting in $[Re(CO)_3(C_6Me_6)][Re_2Cl_3(CO)_6]$ [36] being formed. The presence of $[Re_2Cl_3(CO)_6]^-$ as the counter-ion instead of chloride may therefore be attributed to the reaction being conducted in an aromatic solvent (toluene). All six Re-C(carbonyl) bond lengths [average = 1.898(5) Å] of $[Re_2Cl_3(CO)_6]^-$ fall in the range observed for rhenium(I) complexes [26, 31].

7.3.10 Synthesis and characterization of *fac*-[Re(CO)$_3$(btp)Cl] (7)

The 2,9-*bis*(benzothiazol-2-yl)-1,10-phenanthroline (btp) ligand contains the 1,10-phenanthroline moiety which is ideal to coordinate as a NN-donor chelate to the Re(I) core, with the uncoordinated benzothiazole groups free to function as a possible biological agent. The reaction of btp with [Re(CO)$_5$Cl] resulted in the ligand substitution of two carbonyls to produce *fac*-[Re(CO)$_3$(btp)Cl], according to the following equation:

$$[Re(CO)_5Cl] + btp \longrightarrow \textit{fac}\text{-}[Re(CO)_3(btp)Cl] + 2CO$$

Orange platelets of complex **7** were obtained by the slow diffusion of hexane into a dichloromethane solution of the compound. The complex is stable in air and is a non-electrolyte in DMF. It has poor solubility in most organic solvents and is only soluble in ethanol, DMF and dimethylsulfoxide.

The infrared spectrum of **7** is characterized by three intense peaks in the 1880-2020 cm^{-1} region, typical of ν(C=O) of the *fac*-[Re(CO)$_3$]$^+$ unit. The strong peak at 1579 cm^{-1} is due to the ν(C=N) of the benzothiazole units and the medium intensity peak at 486 cm^{-1} is attributed to ν(Re-N). The aromatic region of the ^{1}H NMR spectrum of **7** displays seven two-proton signals corresponding to the 14 protons of the coordinated btn ligand (Figure 7.46). These signals show magnetic equivalence of the protons, emphasizing the symmetry of the complex. The signals of the six protons of the phenanthroline moiety appear as two doublets (at 8.58 and 9.22 ppm) and a singlet (at 8.52 ppm) and are shifted relative to the free ligand, implying that coordination occurs through the two phenanthroline nitrogen atoms only, with the benzothiazole groups remaining uncoordinated. The two two-proton doublets (at 8.26 and 8.39 ppm) and two two-proton triplets (at 7.73 and 7.65 ppm) are due to the eight protons of the two benzothiazole units.

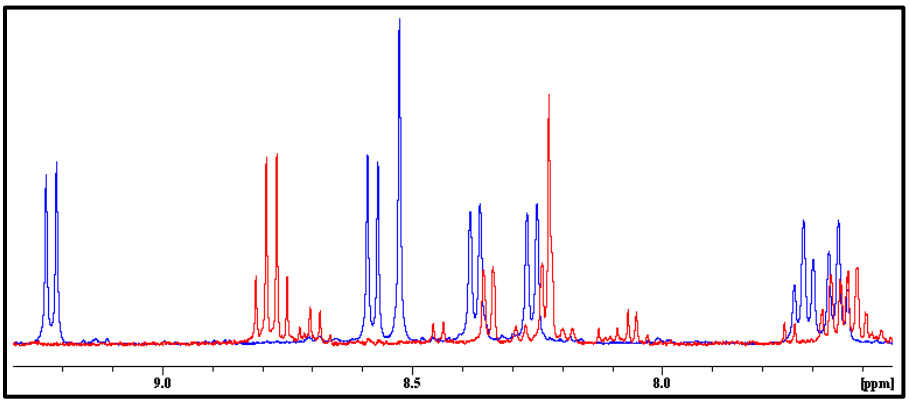

Figure 7.46: Overlay ^{1}H NMR spectra of ligand btp (red) and complex **7** (blue).

The UV-Vis spectrum of **7** in DMF shows a broad intra-ligand charge transfer transition ($\pi \rightarrow \pi^{*}$) in the 300-400 nm region (Figure 7.47). This transition appears as four separate bands in the UV-Vis spectrum of the free ligand. The photoexcitation of an ethanol solution of **3** at room temperature (λ_{ex} = 350 nm) gives rise to blue emissions (416 nm), which may be attributed to ligand-centred $\pi^* \rightarrow \pi$ relaxations [28-30].

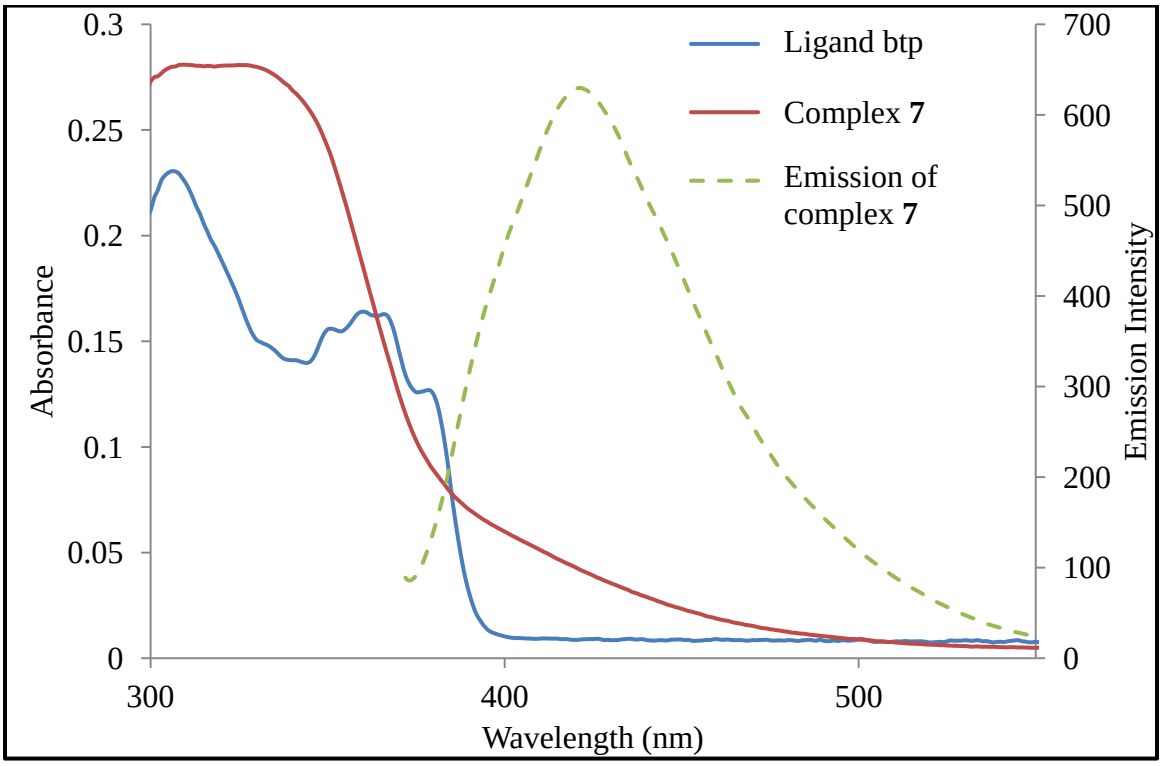

Figure 7.47: Overlay UV-Vis spectra of ligand btp (blue) and complex **7** (red) and emission spectrum of complex **7** (green dashed line).

A perspective view of the asymmetric unit of **7** is shown in Figure 7.48. The basal plane is defined by the phenanthroline nitrogens [N(2) and N(2^{i})] and two carbon atoms [C(90) and C(90^{i})]. The rhenium atom is lifted out of this plane by 0.13 Å towards Cl(1). Complex **7** is totally symmetric around the Cl(1)-Re-C(91) axis [Cl(1)-Re-C(91) = 179.3(2)˚]. The two Re-N bonds are identical [2.212(3) Å], as are the two Re-C(90) bond lengths [1.910(5) Å]. The N(2)-Re-N(2^{i}) bite angle equals 75.1(1)˚, with the *trans* angle N(2)-Re-C(90) = 169.9(2)˚. It is noticeable that the repulsion between Cl(1) and the two nitrogen atoms are more severe [Cl(1)-Re-N(2) = 81.06(9)˚] than with the carbon atoms C(90) [Cl(1)-Re-C(90) = 90.5(1)˚]. In the thiazole rings, the N(1)-C(1) bond is a distinct double bond [1.291(5) Å]. The two five-membered thiazole rings [C(1)N(1)C(12)C(11)S(1)] each form a dihedral angle of 42.64˚ with the C(31)C(32)C(33)C(34)C(35)N(2) plane of the phenanthroline ring. The least-square planes of the two thiazole rings intersect at an angle of 61.21˚.

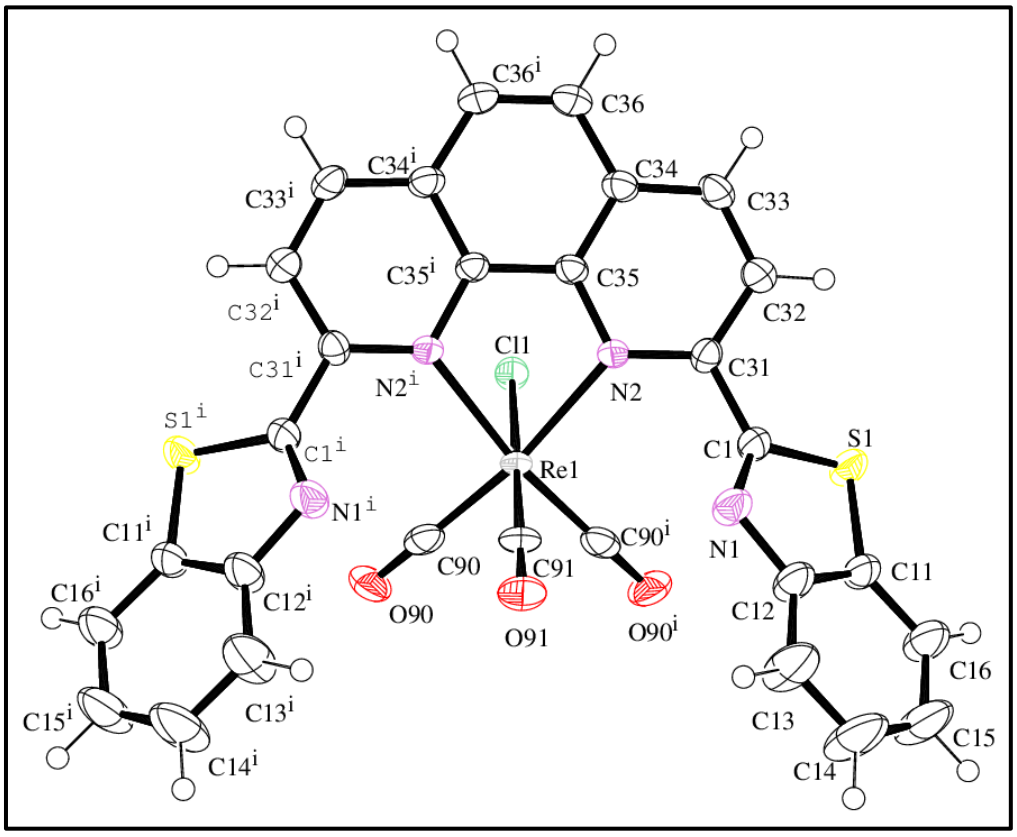

Figure 7.48: An ORTEP view of **7** showing 50% probability displacement ellipsoids and the atom labeling.

The packing of complex **7** in the unit cell is complemented by a network of intra- and intermolecular hydrogen-bonds and π-π stacking (Figure 7.50, Table 7.4). The chloride atom connects to two adjacent molecules *via* intermolecular bonds with the phenyl protons C(16)H(16). A second intermolecular hydrogen-bond exists between a carbonyl oxygen O(90) and a phenyl proton C(14)H(14). The sulfur atom S(1) of the benzothiazole moieties are involved in intramolecular hydrogen-bonds with the phenanthroline proton C(32)H(32). The phenanthroline rings are π-π stacked with centroid to centroid distances of 3.445 Å.

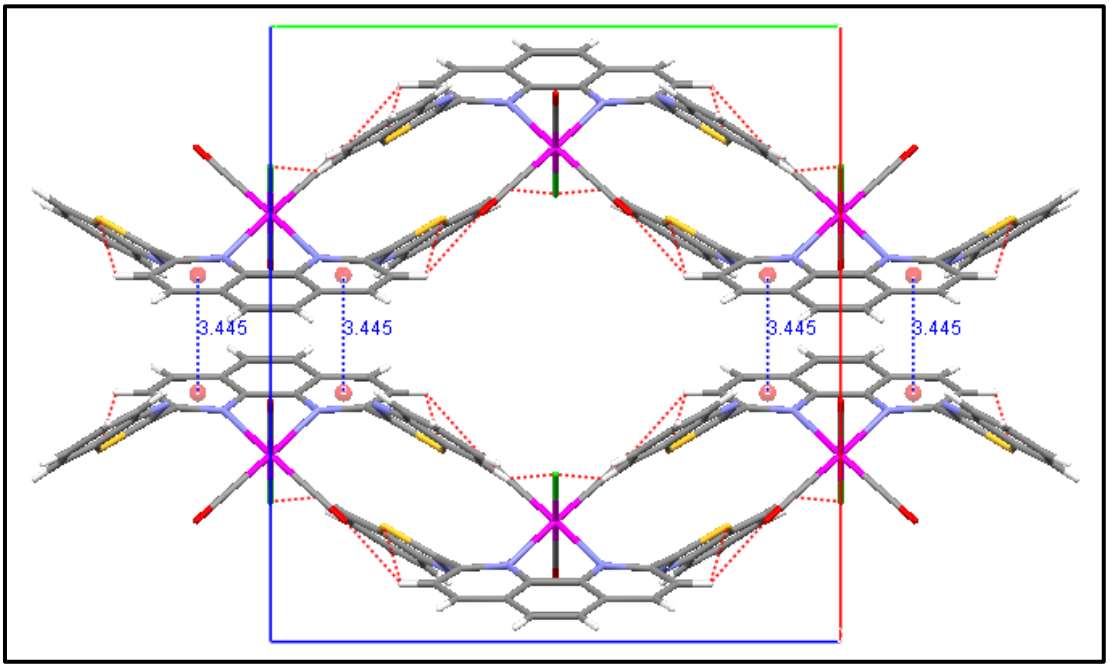

Figure 7.50: Packing diagram of **7** in the unit cell illustrating hydrogen-bonds (red dashed lines) and π-π interactions (blue dashed lines).

Table 7.4: Hydrogen-bond distances (Å) and angles (˚) in mbc.

D-H•••A	D-H	H•••A	D•••A	D-H•••A
C(16)H(16)•••Cl(1)	0.95	2.81	3.514(5)	132
C(14)H(14)•••O(90)	0.95	2.56	3.259(7)	131
C(32)H(32)•••S(1)	0.95	2.84	3.177(4)	102

The electrochemical processes of the rhenium(I) complexes were studied *via* cyclic voltammetry in the -1.50 to 1.50 V region. Complexes **2** and **7** revealed similar oxidation peaks at 1.35 and 1.32 V respectively. There is no cathode counter peak associated with these oxidative waves indicating that the processes are irreversible. The process is ascribed to the Re(I)/Re(II) redox couple and is slightly outside the range observed [0.80 to 1.30 V] for Re(I) based oxidative processes under similar conditions [28, 30, 37]. For complex **3**, the oxidative peak was observed at 1.06 V. The cyclic voltammograms of **4** and **6** displayed no redox processes in the potential window scanned (1.50 to -1.50 V) under identical conditions.

7.4 References

[1] D.F. Shi, T.D. Bradshaw, S. Wrigley, C.J. McCall, P. Lelieveld, I. Fichtner, M.F.G. Stevens, *J. Med. Chem*., 1996, **39**, 3375.

[2] T.D. Bradshaw, A.D. Westwell, *Curr. Med. Chem.*, 2004, **11**, 1009.

[3] W.E. Klunk, H. Engler, A. Nordberg, Y. Wang, G. Blomqvist, D.P. Holt, M. Bergström, I. Savitcheva, G. Hung, E. Estrada, B. Ausen, M.L. Debnath, J. Barletta, J.C. Price, J. Sandell, B.J. Lopresti, A. Wall, P. Koivisto, G. Antoni, C.A. Mathis, B. Längström, *Ann. Neurol*., 2004, **55**, 306.

[4] K. Bacharaju, S.R. Jambula, S. Sivan, S.J. Tangeda, V. Manga, *Bioorg. Med. Chem. Lett*., 2012, **22**, 3274; F. Hernández-Luis, A. Hernández-Campos, R. Castillo, G. Navarrete-Vázquez, O. Soria-Arteche, M. Hernández-Hernández, L. Yépez-Mulia, *Eur. J. Med. Chem*., 2010, **45**, 3135; G. Mariappan, R. Hazarika, F. Alam, R. Karki, U. Patangia, S. Nath, *Arabian J. Chem*., 2011, doi:10.1016/j.arabjc.2011.11.008; A.K. Tiwari, A.K. Mishra, A. Bajpai, P. Mishra, S. Singh, D. Sinhab, V.K. Singha, *Bioorg. Med. Chem. Lett*., 2007, **17**, 2749; R. Kore, R. Srivastava, *J. Mol. Catal. A: Chem*., 2011, **345**, 117.

[5] K. Lin, M.L. Debnath, C.A. Mathis, W.E. Klunk, *Bioorg. Med. Chem. Lett.*, 2009, **19**, 2258.

[6] M.M. Mashaly, H.F. El-Shafiy, S.B. El-Maraghy, H.A. Habib, *Spectrochim. Acta, Part A*, 2005, **61**, 1853.

[7] I.N. Booysen, T.I.A. Gerber, P. Mayer, *Inorg. Chim. Acta*, 2010, **363**, 1292.

[8] I. Booysen, T.I.A. Gerber, P. Mayer, *J. Coord. Chem*., 2008, **61**, 1525.

[9] APEX2, SADABS and SAINT, Bruker AXS Inc., Madison, Wisconsin, USA, 2010.

[10] G.M. Sheldrick, *Acta Cryst*., 2008, **A64**, 112.

[11] A. Altomare, M.C. Burla, G. Cascarano, C. Giacovazzo, A. Guagliardi, A.G.G. Moliterni, G. Polidori, *J. Appl. Cryst*., 1995, **28**, 842.

[12] C.B. Hübschle, G.M. Sheldrick, B. Dittrich. *J. Appl. Cryst.*, 2011, **44**, 1281.

[13] F. Merchan, J. Garin, E. Melendez, *Synthesis*, 1982, **7**, 590.

[14] F. Tellez, A. Flores-Parra, N. Barba-Behrens, R. Contreras, *Polyhedron*, 2004, **23**, 2481.

[15] F. Tellez, A. Cruz, H. Lopez-Sandoval, I. Ramos-Garcia, M. Gayosso, R.N. Castillo-Sierra, B. Paz-Michel, H. Noth, A. Flores-Parra, R. Contreras, *Eur. J. Org. Chem*., 2004, 4203.

[16] A. Castineiras, M.C. Gomez, P. Sevillano, *J. Mol. Struct*., 2000, **554**, 301; M.A. Lynn, L.J. Carlson, H. Hwangbo, J.M. Tanski, L.A. Tyler, *J. Mol. Struct.*, 2012, **1011**, 81.

[17] T. Tunc, H. Tezcan, M. Sari, O. Buyukgungor, R. Yagbasan, *Acta Crystallogr.*, 2003, **C59**, o528; D.X. West, J.K. Swearingen, J. Valdez-Martinez, S. Hernandez-Ortega, A.K. El-Sawaf, F. Meurs, A. Castineiras, I. Garcia, E. Bermejo, *Polyhedron*, 1999, **18**, 2919.

[18] C. Rodriguez, N.S. de Groot, A. Rimola, A. Alvarez-Larena, V. Lloveras, J. Vidal-Gancedo, S. Ventura, J. Vendrell, M. Sodupe, P. Gonzalez-Duarte, *J. Am.*

Chem. Soc., 2009, **131**, 1436; D. Lakshmanan, R.M. Raj, R. Selvakuma, M. Bakthadoss, S. Murugavel, *Acta Cryst*., 2001, **E67**, o2259; Y. Zang, Z.H. Su, Q.Z. Wang, L. Teng, *Acta Cryst*., 2008, **E64**, o2065.

[19] H.Y. Wang, P.S. Zhao, J. Song, R.Q. Li, *J. Chem. Crystallogr*., 2011, **41**, 379; P.P. Sun, F.F. Jian, X. Wang, *J. Chem. Crystallogr*., 2010, **40**, 4; J. Valdes-Martinez, S. Hernandez-Ortega, M. Rubio, D.T. Li, J.K. Swearingen, W. Kaminsky, D.R. Kelman, D.X. West, *J. Chem. Crystallogr*., 2004, **34**, 533.

[20] V. Saboonchian, A.A. Danopoulos, A. Guiterrez, G. Wilkinson, D.J. Williams, *Polyhedron*, 1991, **10**, 2241.

[21] B. Machura, R. Kruszynski, J. Kusz, *Polyhedron*, 2007, **26**, 3054; B. Machura, *Coord. Chem. Rev*., 2005, **249**, 591; N.H. Huy, U. Abram, *Inorg. Chem*., 2007, **46,** 5310.

[22] M. Ganesan, P.N. Kapoor, P.E. Fanwick, R.A. Walton, *Inorg. Chem. Commun*., 2002, **5**, 1073; K.-Y. Shih, P.E. Fanwick, R.A. Walton, *Inorg. Chim. Acta*, 1993, **213**, 247.

[23] S. Cai, D.M. Hoffman, J.C. Huffman, D.A. Wierda, H. Woo, *Inorg. Chem*., 1987, **26**, 3693.

[24] H. Sugimoto, M. Kamei, K. Umakoshi, Y. Sasaki, M. Suzuki, *Inorg. Chem*., 1996, **35**, 7082.

[25] A. Vogler, H. Kunkely, *Coord. Chem. Rev*., 2000, **200–202**, 991.

[26] L. Maria, C. Moura, A. Paulo, I.C. Santos, *J. Organomet. Chem*., 2006, **691**, 4773; L. Wei, S.R. Banerjee, M.K. Levadala, J. Babich, J. Zubieta, *Inorg. Chim. Acta*, 2004, **357**, 1499.

[27] C. Melian, C. Kremer, L. Suescun, A. Mombru, R. Mariezcurrena, E. Kremer, *Inorg. Chim. Acta*., 2000, **306**, 70; M. Chatterjee, B. Achari, S. Das, R. Banerjee, C. Chakrabarti, J.K. Dattagupta, S. Banerjee, *Inorg. Chem*., 1998, **37**, 5424.

[28] K. Wang, L. Huang, L. Gao, L. Jin, *Inorg. Chem*., 2002, **41**, 3353.

[29] S.-S. Sun, A.J. Lees, *Organometallics*, 2001, **20**, 2353.

[30] Z. Si, J. Li, B. Li, F. Zhao, S. Liu, W. Li, *Inorg. Chem*., 2007, **46**, 6155.

[31] S.R. Banerjee, M.K. Levadala, L. Wei, J.F. Valliant, K.A. Stephenson, J.W. Babich, K.P. Maresca, J. Zubieta, *Inorg. Chem*., 2002, **41**, 6417.

[32] G. Bandoli, A. Dolmella, T.I.A. Gerber, J. Perils, J.G.H. Du Preez, *Bull. Chem. Soc. Ethiop*., *2002*, **16**, 149; H. Spies, M. Glaser, F.E. Hahn, T. Lugger, D. Scheller, *Inorg. Chim. Acta*, 1995, **232**, 235; S. Das, I. Chakraborty, A. Chakravorty, *Polyhedron*, 2003, **22**, 901.

[33] U. Mazzi, E. Roncari, R. Rossi, V. Bertolasi, O. Traverso, L. Magon, *Transition Met. Chem.*, 1980, **5**, 289; W.A. Hermann, M.U. Rauch, G.R. Artus, *Inorg. Chem*., 1996, **35**, 1988.

[34] T. Tsotakos, C. Tsoukalas, G. Patsis, A. Panagiotopoulou, N. Nikolic, D. Jankovic, D. Djokic, C.P. Raptopoulou, A. Terzis, D. Papagiannopoulou, M. Pelecanou, M. Papadopoulos, I. Pirmettis, *Inorg. Chim. Acta*, 2011, **377**, 62; B. Machura, M. Wolff, I. Gryca, A. Palion, K. Michalik, *Polyhedron*, **30**, 2011, 2275; A. Albertino, C. Garino, S. Ghiani, R. Gobetto, C. Nervi, L. Salassa, E. Rosenberg, A. Sharmin, G. Viscardi, R. Buscaino, G. Croce, M. Milanesio, *J. Organomet. Chem*., 2007, **692**, 1377.

[35] M. Harmjanz, B.L. Scott, C.J. Burns, *Chem. Commun*., 2002, 1386.

[36] R.L. Davis, N.C. Baenziger, *Inorg. Nucl. Chem. Lett*., 1977, **13**, 475.

[37] Y. Chen, W. Liu, J.S. Jin, B. Liu, Z.G. Zou, J.L. Zuo, X.Z. You, *J.Organomet. Chem.*, 2009, **694**, 763; H. Tsubaki, A. Sekine, Y. Ohashi, K. Koike, H. Takeda, O. Ishitani, *J. Am. Chem. Soc*., 2005, **127**, 15544; V.W.-W. Yam, S.H.-F. Chong, C.-C. Ko, K.-K. Cheung, *Organometallics*, 2000**, 19**, 5092.

Table 7.5: Crystal and structure refinement data for mbc.

Chemical formula	$C_9H_8N_2S_3$
Formula weight	240.38
Crystal system	Monoclinic
Space group	$P2_1/c$
a (Å)	10.6891(3)
b (Å)	4.8085(1)
c (Å)	22.2726(5)
β (˚)	116.195(1)
Volume ($Å^3$)	1027.21(4)
Z	4
Density (Calcd.) (gcm^{-3})	1.554
Absorption coefficient (mm^{-1})	0.679
F (000)	496
Crystal size (mm)	0.06 x 0.18 x 0.26
θ range	2.1-28.3
Index ranges *h*	-14/14
k	-6/4
l	-29/29
Reflections measured	9757
Independent/observed reflections	2566/2177
Data/parameters	2566/132
Goodness-of-fit on F^2	1.06
Final *R* indices [$I > 2\ \sigma(I)$]	0.0330
	(*wR2* =0.0958)
Largest diff. peak/hole ($eÅ^{-3}$)	0.58 /-0.30

Table 7.6: Crystal and structure refinement data for Hmbt.

Chemical formula	$C_9H_9N_3S_2$
Formula weight	223.33
Crystal system	Monoclinic
Space group	*C*2/c
a (Å)	15.6060(8)
b (Å)	5.8282(3)
c (Å)	22.510 (1)
β (˚)	96.903(2)
Volume ($Å^3$)	2032.6(2)
Z	8
Density (Calcd.) (gcm^{-3})	1.460
Absorption coefficient (mm^{-1})	0.485
F (000)	928
Crystal size (mm)	0.06 x 0.18 x 0.56
θ range	2.6-28.3
Index ranges *h*	-20/20
k	-7/5
l	-29/29
Reflections measured	8754
Independent/observed reflections	2497/1970
Data/parameters	2497/136
Goodness-of-fit on F^2	1.04
Final *R* indices [$I > 2\ \sigma(I)$]	0.0314
	(*wR2* = 0.0890)
Largest diff. peak/hole ($eÅ^{-3}$)	0.24/-0.26

Table 7.7: Crystal and structure refinement data for btp.

Chemical formula	$C_{26}H_{14}N_4S_2.C_2H_3N$
Formula weight	487.61
Crystal system	Monoclinic
Space group	$P2_1/c$
a (Å)	22.1345(6)
b (Å)	4.9925(1)
c (Å)	20.5273(5)
β (˚)	90.767(1)
Volume ($Å^3$)	2268.20(9)
Z	4
Density (Calcd.) (gcm^{-3})	1.428
Absorption coefficient (mm^{-1})	0.264
F (000)	1008
Crystal size (mm)	0.10 x 0.45 x 0.68
θ range	2.2-28.3
Index ranges *h*	-27/29
k	-6/6
l	27/27
Reflections measured	20787
Independent/observed reflections	5582/4330
Data/parameters	5582/317
Goodness-of-fit on F^2	1.03
Final *R* indices [$I > 2\ \sigma(I)$]	0.0429
	(*wR2* = 0.1238)
Largest diff. peak/hole ($eÅ^{-3}$)	0.37/-0.27

Table 7.8: Crystal and structure refinement data for **1**.

Chemical formula	$C_{36}H_{36}N_8O_4I_2S_2Re_2$
Formula weight	1335.08
Crystal system	Monoclinic
Space group	$P2_1/c$
a (Å)	13.7528(4)
b (Å)	11.3835(3)
c (Å)	14.0391(3)
β (˚)	118.451(2)
Volume ($Å^3$)	1932.43(9)
Z	2
Density (Calcd.) (gcm^{-3})	2.295
Absorption coefficient (mm^{-1})	8.016
F (000)	1256
Crystal size (mm)	0.01 x 0.06 x 0.06
θ range	3.3-27.6
Index ranges *h*	-17/17
k	-14/14
l	-18/18
Reflections measured	31213
Independent/observed reflections	4452/3908
Data/parameters	4452/244
Goodness-of-fit on F^2	1.09
Final *R* indices [$I > 2\ \sigma(I)$]	0.0231
	(*wR2* = 0.0489)
Largest diff. peak/hole ($eÅ^{-3}$)	1.43 /-1.17

Table 7.9: Crystal and structure refinement data for **2**.

Chemical formula	$C_{21}H_{16}BrN_2O_3S_3Re$
Formula weight	706.67
Crystal system	Monoclinic
Space group	$P2_1/n$
a (Å)	7.4762(2)
b (Å)	10.6438(3)
c (Å)	28.180(1)
β (˚)	92.975(3)
Volume ($Å^3$)	2239.4(1)
Z	4
Density (Calcd.) (gcm^{-3})	2.096
Absorption coefficient (mm^{-1})	7.517
F (000)	1352
Crystal size (mm)	0.05 x 0.12 x 0.25
θ range	4.3-26.3
Index ranges *h*	-9/5
k	-13/12
l	-28/35
Reflections measured	8858
Independent/observed reflections	4524/3514
Data/parameters	4524/280
Goodness-of-fit on F^2	0.88
Final *R* indices [$I > 2\sigma(I)$]	0.0270
	(*wR2* = 0.0477)
Largest diff. peak/hole ($eÅ^{-3}$)	0.99/-0.96

Table 7.10: Crystal and structure refinement data for **3**.

Chemical formula	$C_{36}H_{18}N_8O_6S_6Re_2$
Formula weight	1223.43
Crystal system	Triclinic
Space group	*P*-1
a (Å)	15.9808(3)
b (Å)	17.3856(3)
c (Å)	19.0582(4)
α (˚)	76.456(1)
β (˚)	89.527(1)
γ (˚)	64.318(1)
Volume ($Å^3$)	4612.9 (2)
Z	4
Density (Calcd.) (gcm^{-3})	1.762
Absorption coefficient (mm^{-1})	5.564
F (000)	2336
Crystal size (mm)	0.07 x 0.11 x 0.28
θ range	1.1-28.4
Index ranges *h*	-18/21
k	-23/23
l	-25/25
Reflections measured	84106
Independent/observed reflections	23007/17638
Data/parameters	23007/1045
Goodness-of-fit on F^2	1.08
Final *R* indices [$I > 2\ \sigma(I)$]	0.0482
	(*wR2* = 0.1644)
Largest diff. peak/hole ($eÅ^{-3}$)	7.50/-6.34

Table 7.11: Crystal and structure refinement data for **4**.

Chemical formula	$C_{24}H_{16}N_6O_6S_4Re_2.2CH_3OH$
Formula weight	1049.21
Crystal system	Triclinic
Space group	*P*-1
a (Å)	11.3173(5)
b (Å)	12.2880(5)
c (Å)	12.6402(5)
α (˚)	79.325(2)
β (˚)	74.109(2)
γ (˚)	77.634(2)
Volume ($Å^3$)	1636.4(1)
Z	2
Density (Calcd.) (gcm^{-3})	2.129
Absorption coefficient (mm^{-1})	7.702
F (000)	1000
Crystal size (mm)	0.08 x 0.16 x 0.29
θ range	1.7-28.3
Index ranges *h*	-14/14
k	-16/13
l	-15/16
Reflections measured	26244
Independent/observed reflections	7773/5683
Data/parameters	7773/421
Goodness-of-fit on F^2	1.14
Final *R* indices [$I > 2\ \sigma(I)$]	0.0536
	(*wR2* = 0.1382)
Largest diff. peak/hole ($eÅ^{-3}$)	5.91/-2.97

Table 7.12: Crystal and structure refinement data for **5**.

Chemical formula	$C_{46}H_{40}C_{l2}N_2P_2SClRe$
Formula weight	1007.37
Crystal system	Orthorhombic
Space group	*P*bca
a (Å)	10.554(5)
b (Å)	22.945(5)
c (Å)	37.314(5)
Volume ($Å^3$)	9036(5)
Z	8
Density (Calcd.) (gcm^{-3})	1.481
Absorption coefficient (mm^{-1})	3.017
F (000)	4016
Crystal size (mm)	0.14 x 0.16 x 0.51
θ range	2.2-28.3
Index ranges *h*	-14/13
k	-30/30
l	-49/33
Reflections measured	48227
Independent/observed reflections	11227/7759
Data/parameters	11227/473
Goodness-of-fit on F^2	1.12
Final *R* indices [$I > 2\ \sigma(I)$]	0.0735
	(*wR2* = 0.2135)
Largest diff. peak/hole ($eÅ^{-3}$)	2.87/-1.89

Table 7.13: Crystal and structure refinement data for **6**.

Chemical formula	$C_{19}H_{14}N_4O_4Re.C_6Cl_3O_6Re_2$
Formula weight	1195.38
Crystal system	Triclinic
Space group	*P*-1
a (Å)	9.1780(3)
b (Å)	13.4840(5)
c (Å)	14.4030(5)
α (˚)	100.571(1)
β (˚)	108.448(1)
γ (˚)	107.189(1)
Volume ($Å^3$)	1538.1(1)
Z	2
Density (Calcd.) (gcm^{-3})	2.581
Absorption coefficient (mm^{-1})	12.098
F (000)	1096
θ range	1.9-28.0
Index ranges *h*	-11/12
k	-17/16
l	-19/19
Reflections measured	26382
Independent/observed reflections	7326/6878
Data/parameters	7326/414
Goodness-of-fit on F^2	1.16
Final *R* indices [$I > 2\ \sigma(I)$]	0.0208
	(*wR2* = 0.0531)
Largest diff. peak/hole ($eÅ^{-3}$)	0.86/-1.63

Table 7.14: Crystal and structure refinement data for **7**.

Chemical formula	$C_{29}H_{14}ClN_4O_3S_2Re$
Formula weight	752.24
Crystal system	Monoclinic
Space group	*C*2/m
a (Å)	17.8280(3)
b (Å)	16.2170(3)
c (Å)	10.7570(2)
β (˚)	100.471(1)
Volume ($Å^3$)	3058.2 (1)
Z	4
Density (Calcd.) (gcm^{-3})	1.634
Absorption coefficient (mm^{-1})	4.233
F (000)	1456
θ range	1.7-28.4
Index ranges *h*	-21/23
k	-21/21
l	-14/14
Reflections measured	24559
Independent/observed reflections	3186/3186
Data/parameters	3940/187
Goodness-of-fit on F^2	0.97
Final *R* indices [$I > 2\ \sigma(I)$]	0.0337
	(*wR2* = 0.0713)
Largest diff. peak/hole ($eÅ^{-3}$)	1.40/-1.10

Table 7.15: Selected bond lengths (Å) and angles (˚) for mbc.

Bond lengths			
S(1)-C(1)	1.75(2)	C(13)-C(14)	1.387(3)
S(1)-C(11)	1.752(2)	C(14)-C(15)	1.396(3)
S(2)-C(2)	1.654(2)	C(15)-C(16)	1.383(3)
S(3)-C(2)	1.764(2)	S(3)-C(3)	1.781(2)
C(11)-C(16)	1.389(3)	N(1)-C(1)	1.340(2)
C(11)-C(12)	1.388(2)	N(2)-C(1)	1.337(3)
C(12)-C(13)	1.392(3)	N(2)-C(2)	1.350(2)
Bond angles			
C(2)-S(3)-C(3)	103.7(1)	N(1)-C(1)-N(2)	119.1(2)
C(1)-N(2)-C(2)	121.1(2)	S(2)-C(2)-N(2)	129.1(2)
S(1)-C(1)-N(1)	111.0(1)	S(2)-C(2)-S(3)	123.3(1)
C(1)-N(1)-C(12)	115.8(2)	N(1)-C(12)-C(11)	111.6(2)
C(1)-S(1)-C(11)	90.31(9)	S(1)-C(11)-C(12)	111.3(2)

Table 7.16: Selected bond lengths (Å) and angles (˚) for Hmbt.

Bond lengths			
S(1)-C(1)	1.752 (2)	C(13)-C(14)	1.391(3)
S(2)-C(2)	1.685(1)	C(14)-C(15)	1.382(2)
N(1)-C(1)	1.296(2)	C(15)-C(16)	1.395(2)
C(11)-C(16)	1.409(2)	N(2)-C(1)	1.373(2)
C(11)-C(12)	1.388(2)	N(2)-C(2)	1.372 (2)
C(12)-C(13)	1.384(3)	N(3)-C(2)	1.32(2)
Bond angles			
C(1)-S(1)-C(11)	88.32(8)	S(1)-C(1)-N(1)	117.1(1)
C(1)-N(1)-C(16)	109.8(1)	N(1)-C(1)-N(2)	125.7(1)
C(1)-N(2)-C(2)	127.5(1)	N(2)-C(2)-N(3)	116.8(1)
C(2)-N(3)-C(3)	123.1(1)	S(2)-C(2)-N(3)	123.5(1)
S(1)-C(11)-C(16)	109.7(1)	N(1)-C(16)-C(11)	115.1(1)

Table 7.17: Selected bond lengths (Å) and angles (˚) for btp.

Bond lengths			
N(3)-C(13)	1.353(2)	N(2)-C(12)	1.354(2)
N(3)-C(19)	1.327(2)	N(2)-C(8)	1.331(2)
N(4)-C(20)	1.297(2)	N(1)-C(7)	1.299(2)
N(4)-C(21)	1.387(3)	N(1)-C(1)	1.382(2)
S(2)-C(20)	1.747(2)	S(1)-C(7)	1.745(2)
S(2)-C(22)	1.734(2)	S(1)-C(2)	1.735(2)
C(20)-C(19)	1.471(3)	C(7)-C(8)	1.464(3)
Bond angles			
N(3)-C(13)-C(12)	119.0(2)	N(2)-C(12)-C(13)	118.7(2)
N(3)-C(19)-C(20)	116.5(2)	N(2)-C(8)-C(7)	116.2(2)
C(20)-S(2)-C(22)	88.76(9)	C(2)-S(1)-C(7)	88.70(8)
C(20)-N(4)-C(21)	110.1(2)	C(1)-N(1)-C(7)	110.3(2)
C(13)-N(3)-C(19)	117.3(2)	C(8)-N(2)-C(12)	117.7(2)
N(4)-C(21)-C(22)	115.4(2)	N(1)-C(1)-C(2)	115.3(2)
S(2)-C(22)-C(21)	109.2(1)	S(1)-C(2)-C(1)	109.3(1)

Table 7.18: Selected bond lengths (Å) and angles (˚) for **1**.

Bond lengths			
Re(1)-S(1)	2.388(1)	Re(1)-O(2^{i})	2.109(3)
Re(1)-O(1)	1.721(2)	S(1)-C(1)	1.819(4)
Re(1)-O(2)	1.859(2)	S(1)-C(10)	1.821(4)
Re(1)-N(1)	2.133(3)	N(1)-C(3)	1.333(5)
Re(1)-N(3)	2.106(3)	N(3)-C(12)	1.328(5)
Bond angles			
S(1)-Re(1)-O(1)	95.34(9)	O(1)-Re(1)-N(3)	89.8(1)
S(1)-Re(1)-O(2)	94.50(8)	S(1)-C(1)-C(2)	109.5(3)
S(1)-Re(1)-N(1)	85.62(9)	N(1)-Re(1)-N(3)	176.4(1)
S(1)-Re(1)-N(3)	91.07(7)	Re(1)-S(1)-C(1)	98.5(1)
O(1)-Re(1)-O(2)	170.2(1)	Re(1)-S(1)-C(10)	110.3(1)
O(1)-Re(1)-N(1)	89.1(1)	C(10)-C(11)-C(12)	114.2(3)
S(1)-Re(1)-O(2^{i})	170.39(7)	O(1)-Re(1)-O(2^{i})	94.1(1)

Table 7.19: Selected bond lengths (Å) and angles (˚) for **2**.

Bond lengths			
Re(1)-Br(1)	2.6327(5)	Re(1)-C(3)	1.896(5)
Re(1)-S(1)	2.491(1)	S(1)-C(4)	1.798(4)
Re(1)-N(1)	2.222(3)	S(1)-C(13)	1.809(4)
Re(1)-C(1)	1.922(5)	N(1)-C(6)	1.315(5)
Re(1)-C(2)	1.960(5)	C(4)-C(5)	1.521(6)
Bond angles			
S(1)-Re(1)-N(1)	88.66(9)	S(1)-Re(1)-C(1)	175.1(1)
C(4)-S(1)-C(13)	101.7(2)	S(1)-Re(1)-C(2)	89.5(1)
N(1)-Re(1)-C(3)	177.0(2)	C(6)-N(1)-C(8)	110.8(3)
Br(1)-Re(1)-S(1)	93.24(3)	S(1)-C(4)-C(5)	113.4(3)
Br(1)-Re(1)-N(1)	86.96(8)	Re(1)-N(1)-C(8)	123.7(3)
Br(1)-Re(1)-C(2)	177.2(1)	C(4)-C(5)-C(6)	112.2(3)

Table 7.20: Selected bond lengths (Å) and angles (˚) for **3**.

Bond lengths			
Re(1**)**-S(12**)**	2.510(2)	Re**(**2)-N**(**21)	2.214(6)
Re(1)-N(11)	2.235(6)	Re(2)-C(21)	1.92(1)
Re(1)-N(24)	2.263(6)	Re(2)-C(22)	1.908(9)
Re(1)-C(11)	1.89 (1)	Re(2)-C(23)	1.915(8)
S(22)-C(208)	1.737(9)	S(12)-C(108)	1.735(8)
Re(1)-C(12)	1.92(1)	N(12)-C(108)	1.29(1)
Re(1)-C(13)	1.912(9)	N(13)-C(108)	1.37(1)
Re(2)-S(22)	2.519(2)	N(22)-C(208)	1.29(1)
Re(2)-N(14)	2.243(7)	N(23)-C(208)	1.39(1)
Bond angles			
S(12)-Re(1)-N(11)	81.9(2)	S(22)-Re(2)-N(14)	91.8(2)
S(12)-Re(1)-C(12)	177.8(3)	S(22)-Re(2)-N(21)	80.8(2)
S(12)-Re(1)-C(13)	92.4(3)	S(22)-Re(2)-C(21)	179.0(2)
N(11)-Re(1)-N(24)	86.7(2)	S(22)-Re(2)-C(23)	94.3(3)
N(11)-Re(1)-C(13)	174.2(3)	N(14)-Re(2)-C(22)	178.1(3)
N(24)-Re(1)-C(11)	178.7(3)	N(21)-Re(2)-C(23)	173.9(3)
S(12)-Re(1)-N(24)	92.0(2)	N(14)-Re(2)-N(21)	86.0(2)

Table 7.21: Selected bond lengths (Å) and angles (˚) for **4**.

Bond lengths			
Re(1)-S(12)	2.481(2)	Re(2)-C(5)	1.92(1)
Re(1)-S(22)	2.572(3)	Re(2)-C(6)	1.92(1)
Re(1)-N(11)	2.205(9)	N(12)-C(18)	1.30(2)
Re(1)-C(1)	1.92(1)	N(22)-C(28)	1.36(2)
Re(1)-C(3)	1.92(1)	N(13)-C(18)	1.32(2)
Re(2)-S(12)	2.516(2)	N(23)-C(28)	1.31(2)
Re(2)-N(22)	2.19(1)	S(12)-C(18)	1.79(1)
Re(2)-C(4)	1.93(1)	S(22)-C(28)	1.77(1)
Bond angles			
S(12)-Re(1)-S(22)	81.74(8)	S(12)-Re(2)-S(22)	81.50(8)
S(12)-Re(1)-N(11)	83.7(2)	C(17)-N(12)-C(18)	125(1)
S(12)-Re(1)-C(1)	89.1(3)	S(12)-Re(2)-N(22)	78.3(3)
S(12)-Re(1)-C(2)	175.2(4)	S(12)-Re(2)-C(5)	91.1(4)
Re(1)-S(12)-Re(2)	98.45(9)	S(12)-Re(2)-C(6)	172.8(4)
S(22)-Re(1)-C(1)	170.8(3)	S(22)-Re(2)-N(22)	65.1(3)
Re(1)-S(22)-Re(2)	95.29(8)	S(22)-Re(2)-C(4)	101.5(4)
S(22)-Re(1)-C(3)	92.8(3)	S(22)-Re(2)-C(5)	167.9(3)
N(11)-Re(1)-C(2)	92.6(4)	N(22)-Re(2)-C(4)	166.6(4)
N(11)-Re(1)-C(3)	175.0(4)	N(22)-Re(2)-C(6)	94.6(5)

Table 7.22: Selected bond lengths (Å) and angles (˚) for **5**.

Bond lengths			
Re(1)-Cl(1)	2.435(3)	N(2)-C(3)	1.29(2)
Re(1)-Cl(2)	2.341(3)	C(1)-C(2)	1.32(2)
Re(1)-P(1)	2.486(2)	C(11)-C(12)	1.40(2)
Re(1)-P(2)	2.489(3)	C(12)-C(13)	1.38(2)
Re(1)-N(1)	2.149(9)	C(13)-C(14)	1.37(2)
Re(1)-N(2)	2.09(1)	C(14)-C(15)	1.38(3)
N(2)-C(2)	1.42(2)	C(15)-C(16)	1.36(2)
N(1)-C(1)	1.32(2)	C(11)-C(16)	1.37(2)
Bond angles			
P(1)-Re(1)-P(2)	176.87(8)	Cl(2)-Re(1)-N(2)	94.6(5)
N(1)-Re(1)-N(2)	76.8(6)	Cl(1)-Re(1)-N(1)	94.3(2)
Cl(1)-Re(1)-Cl(2)	94.2(1)	N(2)-C(2)-C(1)	116(1)
Cl(2)-Re(1)-N(1)	171.5(3)	C(2)-N(2)-C(3)	120(1)
Cl(1)-Re(1)-N(2)	170.8(5)	C(1)-N(1)-C(11)	108.9(9)

Table 7.23: Selected bond lengths (Å) and angles (˚) for **6**.

Bond lengths			
Re(1)-O(1)	2.266(3)	O(1)-C(1)	1.455(5)
Re(1)-N(1)	2.159(3)	O(1)-C(2)	1.456(5)
Re(1)-N(3)	2.157(3)	N(4)-C(4)	1.339(6)
Re(1)-C(50)	1.933(4)	N(3)-C(4)	1.322(6)
Re(1)-C(51)	1.873(4)	N(2)-C(3)	1.345(6)
Re(1)-C(52)	1.929(4)	N(1)-C(3)	1.319(5)
Bond angles			
O(1)-Re(1)-N(1)	75.1(1)	N(1)-Re(1)-C(52)	169.8(2)
O(1)-Re(1)-N(3)	74. 9(1)	N(3)-Re(1)-C(50)	172.7(2)
O(1)-Re(1)-C(51)	174.6(1)	N(1)-C(3)-N(2)	112.3(3)
O(1)-Re(1)-C(52)	95.2(2)	N(3)-C(4)-N(4)	112.6(4)
N(1)-Re(1)-N(3)	80.6(1)	Re(1)-N(1)-C(11)	136.4(3)
N(1)-Re(1)-C(51)	101.1(2)	Re(1)-N(3)-C(21)	137.1(3)

Table 7.24: Selected bond lengths (Å) and angles (˚) for **7**.

Bond lengths			
Re(1)-Cl(1)	2.479(1)	Re(1)-N(2^{i})	2.212(3)
Re(1)-N(2)	2.212(3)	Re(1)-C(90^{i})	1.910(5)
Re(1)-C(90)	1.910(5)	S(1)-C(1)	1.742(4)
Re(1)-C(91)	1.916(6)	N(1)-C(1)	1.291(5)
Bond angles			
Cl(1)-Re(1)-N(2)	81.06(9)	N(2)-Re(1)-C(90^{i})	98.3(2)
Cl(1)-Re(1)-C(91)	179.3(2)	N(2^{i})-Re(1)-C(90^{i})	169.9(2)
Cl(1)-Re(1)-N(2^{i})	81.06(9)	C(1)-S(1)-C(11)	88.7(2)
N(2)-Re(1)-C(90)	169.9(2)	C(31)-N(2)-C(35)	117.4(3)
N(2)-Re(1)-N(2a)	75.1(1)	S(1)-C(1)-N(1)	116.7(3)
Cl(1)-Re(1)-C(90)	90.5(1)	Cl(1)-Re(1)-C(90^{i})	90.5(1)

Chapter 8

Conclusion and Future Work

This study presents the successful synthesis of a variety of rhenium complexes containing bidentate aromatic ligands and derivatives of heterocyclic ligands. The complexes were spectrally and structurally characterized.

The biologically active compound 4-aminoantipyrine and its derivatives proved to be suitable ligands for coordination to rhenium. This work can be extended to include other derivatives of pyrazolone, which is an active moiety in pharmacological activity. For example, acyl pyrazolone compounds (Figure 8.1) has been extensively studied as chelating ligands towards main group and transition metals [1, 2]. However, very few rhenium complexes containing this class of ligands are known.

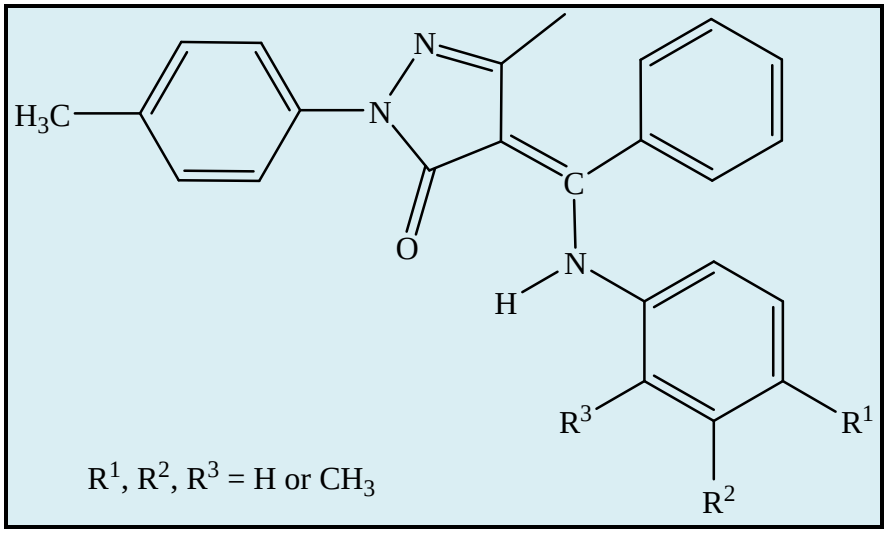

Figure 8.1: Structural drawing of acyl pyrazolone derivatives.

Chapters 4 and 5 report the reactions of bidentate aromatic ligands towards the *fac*-$[Re^{I}(CO)_3]^+$ and $[Re^{V}O]^{3+}$ cores. Novel rhenium complexes were isolated and found to have unusual structural and chemical properties. These bidentate ligands can be derivatized to incorporate amine and carboxylic acid fragments for potential use as a bifunctional chelator to the metal center. Therefore, the discovery of rhenium complexes incorporating this class of ligand systems has synthetic significance in radiopharmacy.

A variety of 1,3-benzothiazole, benzimidazole and benzoxazole derivatives were synthesized and characterized in Chapters 6 and 7. These heterocyclic compounds were reacted with rhenium(I) and (V) precursors to produce novel complexes. This study can be expanded by synthesizing heterocyclic ligands from compounds like the bioactive 2,5-diamino-1,3,4-thiadiazole (Figure 8.2), which contains more than two heteroatoms [3], and investigating the coordination chemistry of these derivatives towards rhenium.

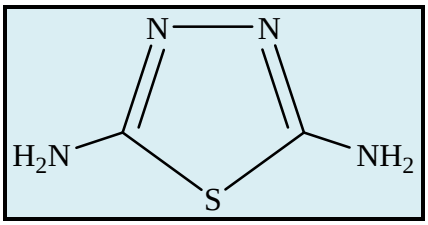

Figure 8.2: Structure of 2,5-diamino-1,3,4-thiadiazole.

References

[1] R.N. Jadeja, J.R. Shah, *Polyhedron*, 2007, **26**, 1677.

[2] F. Marchetti, C. Pettinari, R. Pettinari, *Coord. Chem. Rev.*, 2005, **249**, 2909.

[3] J.A. Obaleye, J.F. Adediji, M.A. Adebayo, *Molecules*, 2011, **16**, 5861.